Stiff-Person Syndrom - Pathophysiologische Mechanismen von Glyzinrezeptor Autoantikörpern

Stiff-person syndrome - Pathophysiological mechanisms of glycine receptor autoantibodies

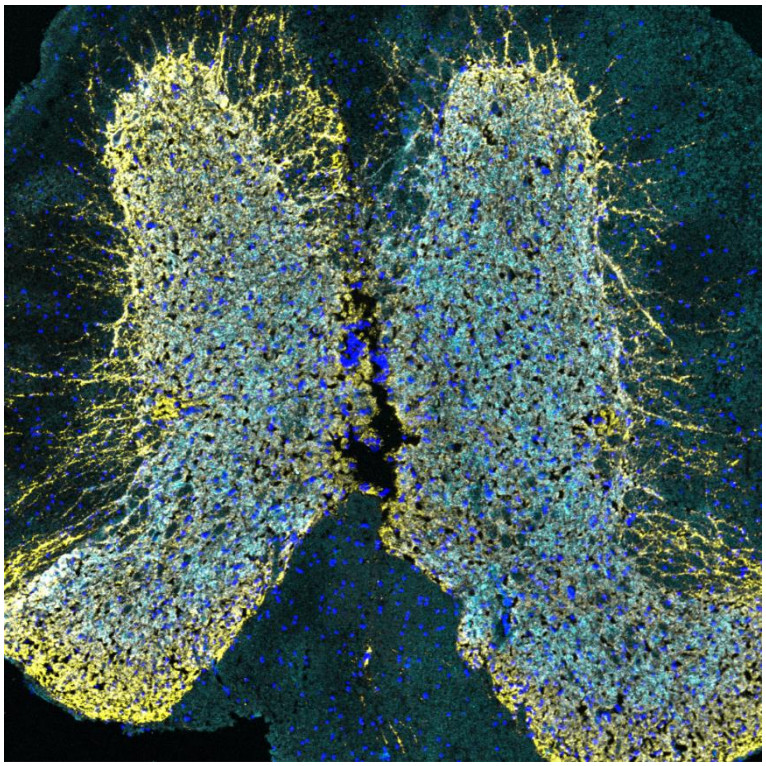

Doctoral thesis for a doctoral degree
at the Graduate School of Life Sciences,
Julius-Maximilians-Universität Würzburg,
Section Neuroscience

submitted by

Vera Rauschenberger

from

Saarbrücken

Würzburg 2020

Submitted on: .....

Office stamp

Members of the Thesis Committee

Chairperson: Prof. Dr. Paul Pauli .....

Primary Supervisor: Prof. Dr. Carmen Villmann .....

Supervisor (Second): Prof. Dr. Claudia Sommer .....

Supervisor (Third): Prof. Dr. Christian Geis .....

Supervisor (Fourth): .....

(If applicable)

Date of Public Defence: .....

Date of Receipt of Certificates: .....

Cover picture: Immunohistochemical staining of spinal cord from a mouse with catheter injections of disease control IgG (magenta), co-stained with mAb4a (cyan), synaptophysin (yellow) and DAPI (blue).

Index of contents

Index of figures and tables

Summary

The Stiff-person syndrome (SPS) is a rare autoimmune disease that is characterized by symptoms including stiffness in axial and limb muscles as well as painful spasms. Different variants of SPS are known ranging from moderate forms like the stiff-limb syndrome to the most severe form progressive encephalomyelitis with rigidity and myoclonus (PERM). SPS is elicited by autoantibodies that target different pre- or postsynaptic proteins. The focus of the present work is on autoantibodies against the glycine receptor (GlyR). At start of the present thesis, as main characteristic of the GlyR autoantibody pathology, receptor cross-linking followed by enhanced receptor internalization and degradation via the lysosomal pathway was described. If binding of autoantibodies modulates GlyR function and therefore contributes to the GlyR autoantibody pathology has not yet been investigated. Moreover, not all patients respond well to plasmapheresis or other treatments used in the clinic. Relapses with even higher autoantibody titers regularly occur.

In the present work, further insights into the disease pathology of GlyRα autoantibodies were achieved. We identified a common GlyRα1 autoantibody epitope located in the far N-terminus including amino acids A^{1}-G^{34} which at least represent a part of the autoantibody epitope. This part of the receptor is easily accessible for autoantibodies due to its location at the outermost surface of the GlyRα1 extracellular domain. It was further investigated if the glycosylation status of the GlyR interferes with autoantibody binding. Using a GlyRα1 de-glycosylation mutant exhibited that patient autoantibodies are able to detect the de-glycosylated GlyRα1 variant as well. The direct modulation of the GlyR analyzed by electrophysiological recordings demonstrated functional alterations of the GlyR upon autoantibody binding. Whole cell patch clamp recordings revealed that autoantibodies decreased the glycine potency, shown by increased EC_{50} values. Furthermore, an influence on the desensitization behavior of the receptor was shown. The GlyR autoantibodies, however, had no impact on the binding affinity of glycine. These issues can be explained by the localization of the GlyR autoantibody epitope. The determined epitope has been exhibited to influence GlyR desensitization upon binding of allosteric modulators and differs from the orthosteric binding site for glycine, which is localized much deeper in the structure at the interface between two adjacent subunits. To neutralize GlyR autoantibodies, two different methods have been carried out. Transfected HEK293 cells expressing GlyRα1 and ELISA plates coated with the GlyRα1 extracellular domain were used to efficiently neutralize the autoantibodies. Finally, the successful passive transfer of GlyRα1 autoantibodies into zebrafish larvae and mice was shown. The autoantibodies detected their target in spinal cord and brain regions rich in GlyRs of zebrafish and mice. A passive transfer of human GlyRα autoantibodies to zebrafish larvae generated an impaired escape behavior in the animals compatible with the abnormal startle response in SPS or PERM patients.

Zusammenfassung

Das Stiff-person Syndrom (SPS) ist eine seltene Autoimmunerkrankung, die sich durch Symptome wie Steifheit in Muskeln des Rumpfes und der Gliedmaßen sowie schmerzhafte Spasmen auszeichnet. Vom SPS sind verschiedene Varianten bekannt, die von mäßigen Formen, wie dem Stiff-limb Syndrom (limb von engl. Extremitäten), bis zur schwersten Variante, der progressiven Enzephalomyelitis mit Steifheit und Myoklonus (PERM, vom engl. progressive encephalomyelitis with rigidity and myoclonus), reichen. Ausgelöst wird das SPS durch Autoantikörper, die an verschiedene prä- und postsynaptische Proteine binden. Der Fokus in dieser Arbeit liegt dabei auf Autoantikörpern, die gegen den Glyzinrezeptor (GlyR) gerichtet sind. Zu Beginn dieser Thesis galten als Hauptcharakteristika der Pathologie von Autoantikörpern die Quervernetzung von Rezeptoren gefolgt von einer verstärkten Rezeptor Internalisierung und dem Abbau über das Lysosom. Allerdings wurde bisher noch nicht untersucht, ob die GlyR Funktion durch eine Autoantikörperbindung verändert wird. Darüber hinaus sprechen nicht alle Patienten gut auf Plasmapheresen oder andere Therapien an. Rückfälle mit noch viel höheren Autoantikörpertitern treten regelmäßig auf.

Die vorliegende Arbeit erweitert die Kenntnisse der pathophysiologischen Mechanismen, die durch GlyRα Autoantikörper ausgelöst werden. Wir konnten ein Epitop der GlyRα1 Autoantikörper im N-terminalen Bereich ausfindig machen, wobei die Aminosäuren A^{1}-G^{34} zumindest einen Teil des Epitops bilden. Dieser GlyR Bereich kann durch die Autoantikörper sehr leicht erreicht werden, weil er sich an der Oberfläche der extrazellulären Domäne des GlyRs befindet. Weiterhin wurde untersucht, ob die Glykosylierung des GlyRs die Autoantikörperbindung beeinflusst. Mit Hilfe von Mutanten, bei denen die Glykosylierungsstelle entfernt wurde, konnte gezeigt werden, dass Patientenautoantikörper die nicht-glykosylierte Variante des GlyRα1 ebenfalls detektieren können. Elektrophysiologische Messungen ergaben, dass die Funktionalität des GlyRs durch die Bindung von Autoantikörpern beeinträchtigt wird. Erhöhte EC_{50} Werte zeigen, dass Autoantikörper die Wirksamkeit von Glyzin in niedrigeren Konzentrationen auf den Rezeptor verringern. Außerdem beeinflussen die Autoantikörper die Desensitisierung des Rezeptors. Allerdings waren die Glyzin-Wirksamkeit in sättigenden Konzentrationen und die Affinität von Glyzin zum Rezeptor unverändert. Diese Ergebnisse können durch die Lokalisierung des GlyR Autoantikörper-Epitops erklärt werden. Das ermittelte Epitop ist bekannt dafür, dass dort allosterische Modulatoren binden können und dadurch die Desensitisierung beeinflusst wird. Außerdem unterscheidet sich das Epitop von der orthosterischen Bindestelle von Glyzin, welche viel tiefer in der Struktur an der Grenze zweier benachbarter Untereinheiten liegt. Um die GlyR Autoantikörper zu neutralisieren, wurden zwei verschiedene Methoden entwickelt. Transfizierte HEK293 Zellen, die den GlyRα1 exprimieren, und ELISA Platten, die mit der

extrazellulären Domäne des GlyRα1 beschichtet waren, wurden zur effizienten Neutralisation der Autoantikörper verwendet. Abschließend konnte in der vorliegenden Arbeit die erfolgreiche passive Übertragung von GlyRα1 Autoantikörpern in Zebrafischlarven und Mäusen gezeigt werden. In Zebrafischen und Mäusen detektierten die Autoantikörper ihr Antigen im Rückenmark und in Gehirnregionen, in denen der GlyR zahlreich exprimiert ist. Ein passiver Transfer von menschlichen GlyRα Autoantikörpern in Zebrafischlarven beeinträchtigte das Fluchtverhalten der Tiere, welches kompatibel mit dem krankhaften Startle Reflex in SPS- oder PERM-Patienten ist.

1. Introduction

1.1 Stiff-person syndrome

Stiff-person syndrome (SPS) is a rare autoimmune disease (prevalence 1:1,000,000) that was first described by Moersch and Woltman (1956). Most patients come down with SPS at the age of around 46 years. However, disease onset ranges from 11 months to 75 years. SPS is characterized by symptoms including stiffness in axial and limb muscles, brainstem signs, hyperekplexia, seizures as well as painful spasms that can be randomly or elicited by unexpected noise, emotional stress or tactile stimuli (Meinck and Thompson, 2002; Sommer et al., 2005; Hutchinson et al., 2008; Geis et al., 2009; McKeon et al., 2013; Carvajal-Gonzalez et al., 2014; Baizabal-Carvallo and Jankovic, 2015; Martinez-Hernandez et al., 2016). Different variants of SPS are known ranging from moderate forms like the stiff-limb syndrome where symptoms are confined to the limb, to the most severe form progressive encephalomyelitis with rigidity and myoclonus (PERM) where patients additionally suffer from brainstem myoclonus, breathing problems and spinal cord involvement (Meinck and Thompson, 2002; Damasio et al., 2013).

1.2 Pathophysiological mechanisms in SPS

The symptoms of SPS patients are comparable to symptoms of patients suffering from hyperekplexia, a disease caused by mutations in the genes encoding the glycine receptor (GlyR) subunits (Villmann et al., 2009b; Atak et al., 2015; Schaefer et al., 2015; Langlhofer and Villmann, 2017; Schaefer et al., 2018b). In hyperekplexia, pathophysiological mechanisms were for instance analyzed in genetic mouse variants that phenotypically represent the patient's symptoms (Buckwalter et al., 1994; Kingsmore et al., 1994; Mulhardt et al., 1994; Ryan et al., 1994; Saul et al., 1994; Kling et al., 1997; Villmann et al., 2009b; Becker et al., 2012; Schaefer et al., 2012; Schaefer et al., 2017; Schaefer et al., 2018b). In SPS, disease pathology was shown to be elicited by autoantibodies that target different synaptic proteins such as the gamma-aminobutyric acid (GABA)-producing enzyme glutamate decarboxylase (GAD), $GABA_A$ receptor-associated protein, amphiphysin, gephyrin or GlyR (Solimena and De Camilli, 1991; De Camilli et al., 1993; Butler et al., 2000; Wessig et al., 2003; Koerner et al., 2004; Raju et al., 2006; Hutchinson et al., 2008; Irani et al., 2010; Dalmau et al., 2017). 60-80% of patients diagnosed with SPS are positive for autoantibodies against at least one protein at inhibitory synapses. Most common are GAD65 (isoform of GAD with a molecular weight of 65 kDa) autoantibodies (75% of autoantibody positive cases, Fig. 1A), followed by GlyR autoantibodies (20%) and amphiphysin autoantibodies (5%) (Dalmau et al., 2017). So far, the autoantibodies as disease triggering factors have been described but just little is known about

the pathophysiology. Some autoantibodies have been shown to be associated with tumors however the occurrence is varying from <5% in patients with GlyR autoantibodies (Thymoma, lung, Hodgkin) and up to >90% in patients with amphiphysin autoantibodies (breast cancer, small-cell lung cancer) (summarized in Dalmau et al., 2017). Associated tumors have also been described in other autoantibody mediated diseases such as in over 40% of patients with N-methyl-D-aspartate receptor (NMDAR) autoantibodies (Teratoma). Furthermore, it is believed that B cells are potentially the autoantibody-producing cells because of the positive effect of B cell depleting therapies like rituximab application (Rineer and Fretwell, 2017).

Some common aspects regarding the pathophysiological mechanism when autoantibodies reach their target have been identified. Receptor internalization upon autoantibody binding is a common mechanism of autoantibodies targeting for example NMDARs or GlyRs (Fig. 1B). Thereby, autoantibodies cross-link receptors resulting in protein internalization which furthermore changes the surface dynamics of the receptors (Carvajal-Gonzalez et al., 2014; Dalmau et al., 2017). Following internalization, receptors are degraded via the lysosomal pathway. Moreover, activation of the C1 complement system has been determined as disease pathology of GlyR autoantibodies (Carvajal-Gonzalez et al., 2014). Additionally, autoantibodies against $GABA_BR$, NMDAR as well as the GlyR can also block the receptor function (Castillo-Gomez et al., 2017; Dalmau et al., 2017; Crisp et al., 2019). It is likely that there are further so far unknown disease mechanisms. The understanding of the autoantibody pathology will help to develop novel therapeutic approaches since the patient's responses to treatments varies largely. The most common therapies include immunotherapies like intravenous immunoglobulin application, plasmapheresis or application of drugs enhancing the GABAergic inhibition like diazepines (Howard, 1963; Vicari et al., 1989; Pagano et al., 2014). Although patient's symptoms improve because of a reduced autoantibody concentration in serum or by counteracting muscle spasms through stronger GABAergic inhibition, relapses often occur and have a huge impact on daily life (Hutchinson et al., 2008; Damasio et al., 2013; McKeon et al., 2013; Carvajal-Gonzalez et al., 2014; Doppler et al., 2016; Dalmau et al., 2017). Additionally, during plasmapheresis not only 1-2 g offending material is removed from the blood but also 150 g healthy protein (Nydegger and Sturzenegger, 2001).

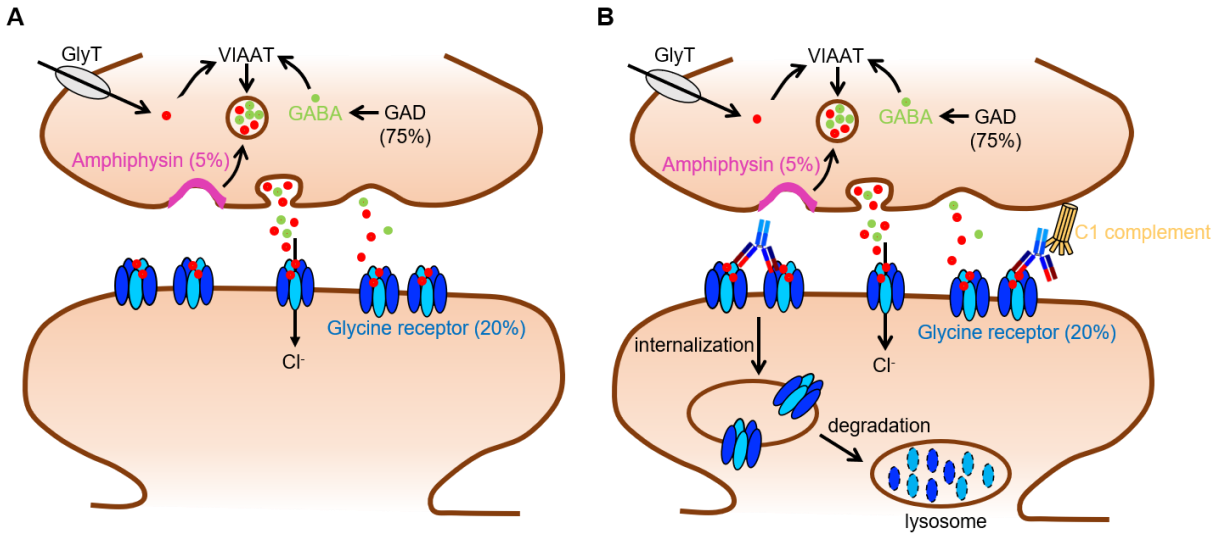

Fig. 1: Autoantibodies at inhibitory synapses. (**A**) Overview of the main targets of autoantibodies in SPS, the GABA producing enzyme GAD (present in 75% of autoantibody positive cases), the glycine receptor (20%) and amphiphysin (5%). (**B**) Pathophysiological mechanisms of GlyR autoantibodies. Autoantibodies cross-link GlyRs, leading to receptor internalization (left). As a consequence, receptors are degraded by the lysosomal pathway. Additionally, GlyR autoantibody binding activates the C1 complement system (right). GAD = glutamate decarboxylases; GlyT = glycine transporter; VIAAT = vesicular inhibitory amino acid transporter.

1.3 Autoantibody epitopes in SPS and other forms of autoantibody-associated diseases

The epitope identification of autoantibodies is important to get deeper insights into possible structural or functional changes upon autoantibody binding and to explore potential clinically relevant differences between patients. For some autoantibodies, it is unclear whether they share a common epitope or if several epitopes exist. GAD65 autoantibodies have been identified to bind to amino acids 451-585 within the C-terminal domain, thus inhibiting the enzymatic activity of GAD65 (Raju et al., 2005). The blockade of enzymatic activity by autoantibodies is probably due to a changed enzyme conformation rather than a hindrance between the binding of glutamate or the cofactor pyridoxal 5'-phosphate to GAD65. However, not all GAD autoantibodies from SPS patients recognize the C-terminal epitope nor hinder the enzymatic activity of GAD65. Thus, another linear epitope for GAD65 autoantibodies was determined within the N-terminus, covering amino acid residues 4-22. This epitope is exclusively found for GAD65 autoantibodies from SPS patients although GAD autoantibodies are also present in diabetes type 1 patients. Thus, autoantibodies from the same subtype but occurrence in different diseases depict different binding properties. Another group of autoantibodies identified in SPS target amphiphysin, a regulatory endocytic protein that modulates clathrin-mediated endocytosis (Dalmau et al., 2017). These amphiphysin autoantibodies target the SH3 domain, which is involved in the interaction with dynamin, thus inducing the generation of clathrin-coated intermediates in vesicle endocytosis. Hence, binding

of amphiphysin autoantibodies results in endocytic dysfunction (Shupliakov et al., 1997; Di Paolo et al., 2002). In GluN1 autoantibodies in NMDAR encephalitis, two specific amino acids N368/G369 within the N-terminus have been characterized to be essential for NMDAR autoantibody binding (Gleichman et al., 2012). The N-terminal domain has been shown to be involved in receptor assembly and to be a target for different allosteric modulators which alter the channel opening and closing (Meddows et al., 2001; Hansen et al., 2010; Paoletti, 2011; Gleichman et al., 2012). Structurally, the N-terminus builds a clamshell-like structure that interacts with other receptor subunits (Jin et al., 2009; Karakas et al., 2009; Sobolevsky et al., 2009; Gleichman et al., 2012). The autoantibody epitope N368/G369 is located adjacent to the hinge of the clamshell, thus also modulating the receptor dynamics in the open or closed state. Hence, autoantibody binding to N368/G369 stabilizes the open conformation of the receptor, thus increasing the open duration.

The epitope of GlyR autoantibodies has not yet been described. However, it was shown that GlyR autoantibodies bind to HEK293 cells expressing the homopentameric GlyRα1, α2 or α3 without permeabilization of the cells (Carvajal-Gonzalez et al., 2014; Doppler et al., 2016). These data point to an epitope localized in the extracellular domain (ECD) of the receptor in its native configuration. Additionally, it was shown that autoantibody binding in live stainings is more reliable due to the correct folding of the receptor in its native conformation (Vincent et al., 2012). Moreover, intracellular autoantibody epitopes are suggested to be rarely pathogenic. Binding to all α-subunits (α1, α2, α3) has been demonstrated arguing for a sequence identical in all GlyRα subunits. Similarly, binding to extracellular epitopes has been shown for α-amino-3-hydroxy-5-methyl-4-isoxazolepropionic acid receptor (AMPAR) autoantibodies present in patients suffering from autoimmune encephalitis. AMPAR autoantibodies bind to extracellular epitopes of the GluA1 or GluA2 subunit, thus disrupting receptor trafficking and turnover (Lai et al., 2009). This in turn leads to a relocation from synaptic to extrasynaptic sites and to a decrease in number of synaptically localized receptors.

The glycosylation state of the targeted protein is also discussed for different autoantibodies to be involved in autoantibody binding (Labasque et al., 2014; Miura et al., 2015; Olsen et al., 2015). Contactin-1 autoantibodies in peripheral neuropathies were shown to require N-glycosylation for binding the target (Labasque et al., 2014). This was tested by tunicamycin treatment which blocks cell surface expression of contactin-1, instead contactin-1 remains in the endoplasmic reticulum (ER). Thus, to target the intracellular de-glycosylated contactin-1, cells have to be fixed and permeabilized before immunofluorescence staining. Here, the autoantibody signal was completely abolished, thus autoantibodies only detect N-glycosylated contactin-1. Furthermore, to verify these results, the authors created de-glycosylation mutants by changing the asparagine residue to glutamine at the nine glycosylation sites independently and tested the binding ability of patient autoantibodies. Indeed, glycosylation sites N467, N473

and N494 were identified to be important for autoantibody binding. Contrariwise, another group exhibited contactin-1 autoantibody binding under tunicamycin treatment followed by immunostaining of fixed and permeabilized cells, indicating that it is independent of contactin-1 glycosylation (Miura et al., 2015). Additionally, they confirmed their experiments by de-glycosylating contactin-1 with peptide N-glycosidase F (PNGaseF), which removes N-linked glycans. Following PNGaseF treatment, the binding ability of autoantibodies was tested using Western blot analysis. Hence, the patient sera detected the de-glycosylated as well as the glycosylated contactin-1.

NMDAR1 autoantibody binding in NMDAR encephalitis was first thought to be dependent on one specific glycosylation site at N368 because de-glycosylation mutant of this specific residue was not detected by patient autoantibodies (Gleichman et al., 2012). However, a further mutation nearby N368 (T370A) decreased autoantibody binding but did not completely abolish autoantibody binding. Thus, the region surrounding the glycosylation site N368 is necessary for autoantibody binding but not the glycosylation itself. Instead, the authors suggested that mutations in this domain disrupt the NMDAR1 structure that autoantibodies are unable to bind. Hence, the folding status around residue N368 is important for autoantibody binding.

Furthermore, the necessity of glycosylation for contactin associated protein-like 2 (Caspr2) autoantibody binding in limbic encephalitis was investigated (Olsen et al., 2015). Thus, Caspr2 possess 12 N-linked glycosylation sites in the extracellular domain, the region of autoantibody binding. N-glycosylation was disabled by tunicamycin treatment of Caspr2 expressing HEK293T cells followed by fixation, permeabilization and immunofluorescence staining. Fluorescence signals of autoantibodies were detected. Thus, the de-glycosylation does not prohibit the ability of Caspr2 autoantibodies to detect their target. Additionally, Caspr2 expressed in cells was de-glycosylated by PNGaseF treatment and tested for autoantibody binding in Western blot analysis. In doing so, the patient autoantibodies were still able to bind, thus the glycosylation is not essential for Caspr2 autoantibody binding. The above stated autoantibodies were closer analyzed for the necessity of a glycosylated target protein for binding (Gleichman et al., 2012; Labasque et al., 2014; Miura et al., 2015; Olsen et al., 2015). However, the autoantibodies described above are related to other autoimmune diseases but not SPS. To my knowledge, there are no studies investigating the necessity of glycosylation for SPS autoantibody binding nor for GlyR autoantibodies.

1.4 *In vivo* animal models for SPS

Drachman (1990) developed five criteria to estimate the presence of an autoantibody-mediated disease. One of the criteria implies that after passive transfer into an animal model, the animal suffers from similar symptoms as human patients. Using such models helps to improve the

understanding of involved signaling pathways as well as to evolve novel therapeutic approaches. Such topics cannot be investigated with *in vitro* experiments. Since long time, passive transfer of anti-acetylcholine receptor autoantibodies into mice, rats and rabbits was performed to characterize pathogenic effects of *Myasthenia gravis* (Toyka et al., 1975; Toyka et al., 1980; Mantegazza et al., 2016). This method was stated to be the simplest way to study immunopathogenesis of autoantibodies and to evaluate therapeutic potentials (Mantegazza et al., 2016). Indeed, transfer of acetylcholine receptor autoantibodies via daily intraperitoneal injections over 14 days into mice resulted in reduced amplitudes of miniature endplate potentials, decreased numbers of acetylcholine receptors at the neuromuscular endplate and clinical weakness in some animals (Toyka et al., 1975; Toyka et al., 1980). Thus, the basic features of *Myasthenia gravis* were successfully transferred from humans into mice, indicating that the passive transfer of autoantibodies is also a useful method to study SPS. In transfer models for SPS, different application methods were reported depending on the autoantibody type, their localization and the pathology. For example, intraperitoneal, intrathecal or intraventricular applications were used. Usually, autoantibody IgG fractions were purified from patient sera and afterwards transferred into animals. Amphiphysin IgG could be successfully transferred via intrathecal catheters and intraperitoneally applications in rats thereby reducing the GABAergic transmission and eliciting dose-dependent symptoms such as stiffness and muscle spasms resembling the patients symptoms (Sommer et al., 2005; Geis et al., 2010; Werner et al., 2016). Furthermore, passive transfer of GAD65 IgG via intrathecal, intraventricular or intracerebellar applications in rats and mice induced symptoms equally to SPS patients including anxiety, impaired locomotor function, stiffness, increased spinal cord excitability, impaired GABAergic neurotransmission and deteriorated cognitive functions (Geis et al., 2011; Manto et al., 2011; Hampe et al., 2013; Hansen et al., 2013; Manto et al., 2015). Passive transfer of autoantibodies was also used to induce symptoms of patients suffering from NMDAR encephalitis in mice for better understanding the pathophysiology (Planaguma et al., 2015; Planaguma et al., 2016). To do so, mice have got intraventricular catheters for NMDAR autoantibody application which is nearby the hippocampus where the target proteins are localized. Mice treated with patient NMDAR autoantibodies elicited progressive memory deficits and depressive-like behavior. Additionally, the density of cell-surface and synaptic NMDARs was decreased and functionally, the long-term synaptic plasticity was impaired. In another form of autoimmune encephalitis, patients are positive for AMPAR autoantibodies which elicit symptoms including impaired formation of new memories as well as retrograde amnesia or anxiety (Lai et al., 2009; Hoftberger et al., 2015). To check whether these signs of disease can be elicited in mice, two different application methods were used (Haselmann et al., 2018). Thus, the IgG fraction of AMPAR autoantibodies were either transferred for two weeks continuously into both lateral ventricles or via stereotactic injections into the CA1 and

CA3 region as well as the dentate gyrus of the hippocampus in both hemispheres. Indeed, memory deficits proved by a decreased object recognition index, could be elicited with both application methods. Additionally, analysis of the Elevated Plus Maze and Black-And-White Maze revealed less time spent and fewer entries into the open arms or white sectors, thus showing increased anxiety levels in mice treated with patient IgG of AMPAR autoantibodies.

Passive transfer models for GlyR autoantibodies do not exist yet. The use of mice or rats seems suitable, but zebrafish larvae might also represent a model system to study changes in motor behavior. Impaired glycinergic inhibition has been demonstrated for genetic variants in zebrafish using the escape response as a functional readout for altered motor behavior. One of the genetic variants with disturbed glycinergic inhibition is the hyperekplexia model *bandoneon*, which elicits touch-induced bilateral muscle contractions upon point mutations in *glrb2* gene (Hirata et al., 2005; Ganser et al., 2013). Additionally, knock outs of GlyRα1 in zebrafish also led to strong motor dysfunction tested by touch-evoked escape behavior (Samarut et al., 2019). Glycinergic transmission is also inhibited by mutating the DEAH-box RNA helicase which controls GlyR expression, resulting in impaired escape behavior (Hirata et al., 2013). Thus, passive transfer of autoantibodies into zebrafish might lead to impaired swimming behavior and thus worthwhile to investigate for GlyR autoantibodies to create an *in vivo* model for SPS.

1.5 The glycine receptor - structural domains

The present project investigates effects of autoantibodies against the glycine receptor (GlyR). The GlyR is an inhibitory ligand-gated ion channel permeable for chloride ions (Lynch, 2004). Besides the nicotinic acetylcholine receptor, the $GABA_{A/C}$ receptor and the $5HT_3$ receptor, the GlyR belongs to the superfamily of the Cys-loop receptors. Cys-loop receptors share the pentameric conformation and a common disulfide bridge in the extracellular domain (Nemecz et al., 2016). Each subunit of the GlyR is composed of a large N-terminal extracellular domain (ECD) followed by four transmembrane domains (TM1-4) that are connected via intra- or extracellular loops, and a short extracellular C-terminus (Fig. 2A, C) (Du et al., 2015; Huang et al., 2015; Huang et al., 2017; Langlhofer and Villmann, 2017). TM1, 3 and 4 of each subunit build the interface between receptor and lipid bilayer. TM2 domains point to each other and form the inner wall of the channel pore (Lynch, 2004). Four α-subunits (α1, α2, α3 and α4) and one β-subunit are known. The assembled receptor presents either α homomers or heteromers with a stoichiometry of 3α:2β or 2α:3β subunits (Fig. 2B) (Kuhse et al., 1993; Grudzinska et al., 2005; Durisic et al., 2012; Yang et al., 2012; Patrizio et al., 2017). The majority of receptors in adults are composed of α1β and α3β heteromers (Malosio et al., 1991).

In mammals, the GlyRα1 and β subunit are mainly expressed in the brainstem and spinal cord (Malosio et al., 1991; Singer et al., 1998; Jonsson et al., 2012; Weltzien et al., 2012). During development, the α2 subunit is expressed in the spinal cord but is replaced by the α1 subunit in the first two postnatal weeks (Kuhse et al., 1990; Malosio et al., 1991). Additionally, the GlyRα2 is involved in retinal photoreceptor development and may regulate the ethanol consumption because GlyRα2 knock out mice were shown to have a reduced ethanol intake (Young and Cepko, 2004; Blednov et al., 2015; Leacock et al., 2018). The α3 subunit is abundantly expressed in the spinal cord ventral horn and dorsal horn in the superficial layer (laminae II and III), there being involved in nociceptive processing and inflammatory pain sensitization (Baer et al., 2003; Harvey et al., 2004; Zeilhofer, 2005). Furthermore, the GlyRα3 is located in the pre-Bötzinger complex of the brainstem participating in the pathway of rhythmic breathing (Manzke et al., 2010). The gene encoding for the GlyRα4 subunit is considered to be a pseudogene in humans because of an in-frame stop codon within exon 9 (Simon et al., 2004). However, in mice and zebrafish the GlyRα4 is expressed and mediates synaptic currents as demonstrated in a murine artificial synapse model (Leacock et al., 2018). Lastly, the GlyRβ is expressed throughout the embryonic and adult brain starting with expression around embryonic day 14 in mice, however the expression increases quickly after birth (Malosio et al., 1991). The β-subunit has a high affinity to the scaffold protein gephyrin which anchors the GlyR at postsynaptic sites (Kneussel and Betz, 2000).

During maturation, post-translational N-glycosylation of GlyRs occurs in the endoplasmic reticulum (Griffon et al., 1999; Schaefer et al., 2018a). A glycosylation site is determined by the amino acid motif N-X-S/T which is present once in the ECD of the GlyRα1 and α3 subunit (α1: ^{38}NVS^{40}, α3: ^{38}NVT^{40}, numbers refer to mature protein) and twice in the ECD of the GlyRα2 and β subunits (α2: ^{45}NVT^{47}, ^{76}NDS^{78}; β: ^{32}NST^{34}, ^{220}NCT^{222}) (Pult et al., 2011; Schaefer et al., 2018a). The glycosylation state of a protein can be determined by using the enzymes endoglycosidase H (EndoH) and/or peptide N-glycosidase F (PNGaseF). EndoH cuts within the chitobiose core of high mannose type-glycans and leaves one N-acetylglucosamine connected to the asparagine (Schaefer et al., 2018a). In contrast, PNGaseF cleaves nearly all mannose-chains connected to asparagine.

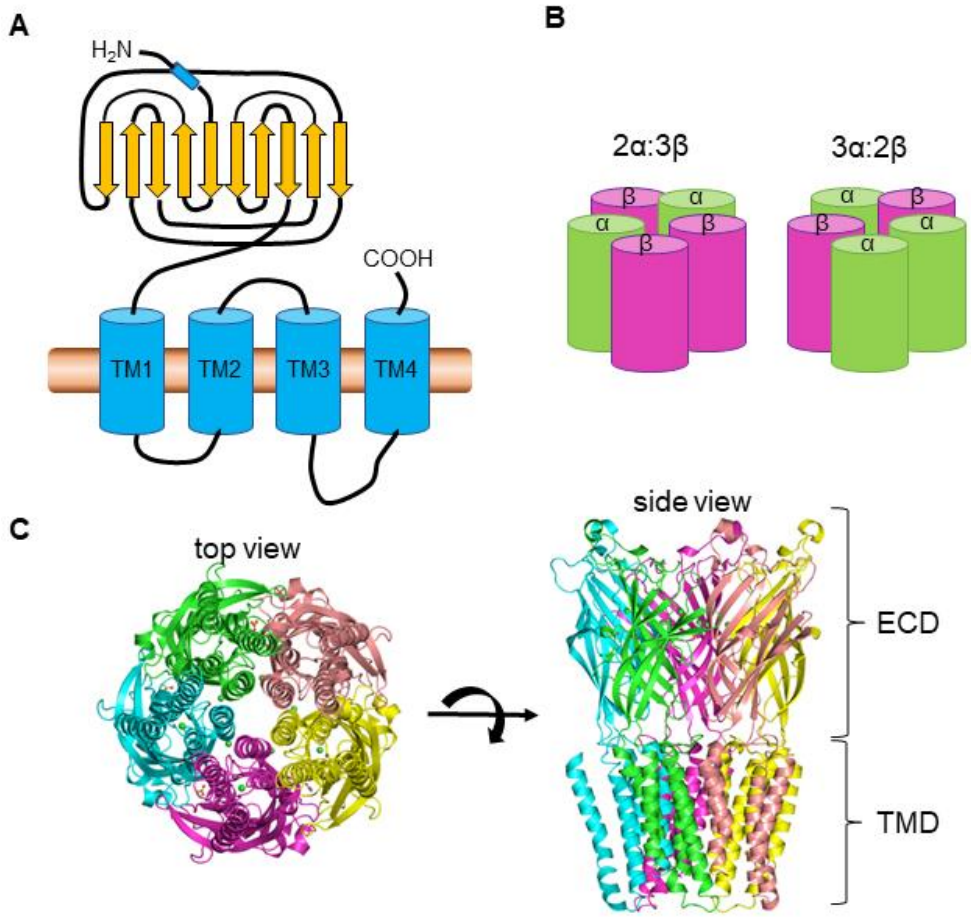

Fig. 2: Structure of the glycine receptor. (**A**) Structure of a GlyR subunit: a large N-terminal extracellular domain (ECD), four transmembrane domains (TM1-4) connected by intra- and extracellular loops, and a short extracellular C-terminus. α-helices are shown as barrels, β-sheets as arrows. (**B**) Pentameric subunit stoichiometry of GlyRs. GlyRs are either composed of 2α:3β (left) or 3α:2β (right). α subunits are shown in green, β subunits in magenta. (**C**) Top view (left) and side view (right) of homopentameric GlyRα1. The five subunits are shown in different colors. ECD = extracellular domain; TMD = transmembrane domain. Pictures in (**C**) were modified from PDBe-KB consortium, PDBe-KB: a community-driven resource for structural and functional annotations. Nucleic Acids Research, Database Issue (2020) (PDBe 4x5t).

1.6 The glycine receptor in the mammalian spinal cord and brain

GlyRs enable fast synaptic inhibition in the adult spinal cord and brainstem as well as in the retina (Lynch, 2004). In the spinal cord, GlyRs are located in motoneurons and involved in feedback control of the nerve-muscle circuit (Schaefer et al., 2012). Sensory inputs are transmitted to the motoneurons via glutamatergic neurons in the dorsal root ganglia (Fig. 3A). As a consequence, the motoneurons are excited and release acetylcholine at the neuromotor endplate which binds to nicotinic acetylcholine receptors in the muscles, leading to excitation and finally muscle contraction. Inhibitory glycinergic interneurons (IaIN or Renshaw cells) are excited by cholinergic collaterals of the motoneuron or by glutamatergic primary afferents (Siembab et al., 2010). These interneurons inhibit motoneurons by glycine release, thereby

controlling the acetylcholine release at the neuromotor endplate. This feedback control loop via glycinergic interneurons is essential for regulating the required amount of acetylcholine to reach the threshold for action potential generation and muscle contraction. In SPS patients with GlyR autoantibodies, this glycinergic feedback control is disturbed probably due to enhanced receptor internalization and therefore reduction of GlyR numbers at motoneuronal membranes (Fig. 3B). This in turn leads to the typical SPS symptoms as muscle stiffness and spasms.

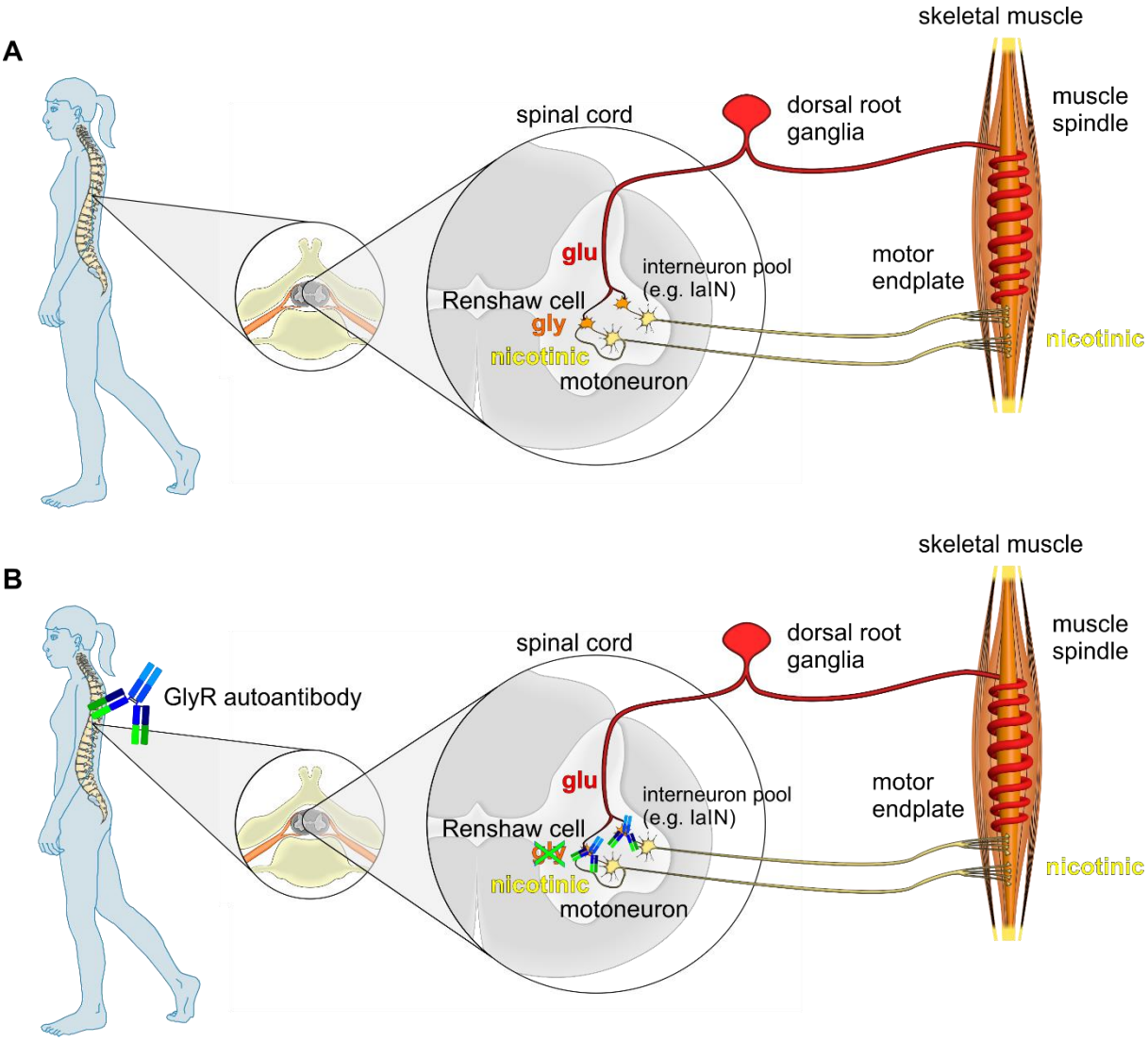

Fig. 3: Normal and morbid nerve-muscle circuit in the spinal cord. (**A**) Glutamatergic neurons in the dorsal root ganglia (red) innervate motoneurons, whereby motoneurons (yellow) transmit acetylcholine to muscles, leading to muscle contractions. Simultaneously, collaterals of the motoneurons excite inhibitory, glycinergic interneurons (IaIN or Renshaw cells, orange) by releasing acetylcholine. Glutamatergic primary afferents are also able to innervate the interneurons. Thereby, the interneurons control acetylcholine release at the neuromotor endplate to circumvent overexcitation (interneuron feedback control). (**B**) The glycinergic feedback control via interneurons described in (**A**) is disturbed in SPS patients being positive for GlyR autoantibodies. Autoantibodies (blue) bind to GlyRs localized in the motoneurons, leading to GlyR internalization. Thus, the control mechanism breaks down resulting in overexcitation in muscles. Figure was modified from Schaefer et al. (2012) and from SMART (Servier Medical Art), licensed under a Creative Common Attribution 3.0 Unported License. http://smart.sevier.com.

GlyRs in the brainstem are participating in processing of acoustic stimuli. From the inner hair cells in the cochlea, excitatory spiral ganglion neurons project to the cochlear nucleus (CN), the first station in the brainstem of the afferent auditory pathway (Reuss, 2000; Malmierca and Ryugo, 2012; Yu and Goodrich, 2014). Neurons in the CN send glutamatergic projections to the ipsilateral lateral superior olive (LSO) as well as to the contralateral medial nucleus of the trapezoid body (MNTB) (Morest, 1968; Warr, 1972; Tolbert et al., 1982; Glendenning et al., 1985; Smith et al., 1991). Furthermore, the MNTB neurons inhibit the neurons of the ipsilateral LSO via GABAergic/glycinergic projections (Kotak et al., 1998; Nabekura et al., 2004). LSO and MNTB belong to the superior olivary complex (SOC) that is important for sound localization, thereby encoding interaural time differences in the medial superior olive as well as interaural level differences in the LSO (Kotak et al., 1998; Tollin, 2003; Grothe et al., 2010; Grothe and Pecka, 2014). LSO neurons further project glycinergic to the inferior colliculus (IC), an important center of integration of the ascending and descending auditory pathway (Brunso-Bechtold et al., 1981; Grothe et al., 2010; Malmierca and Ryugo, 2012).

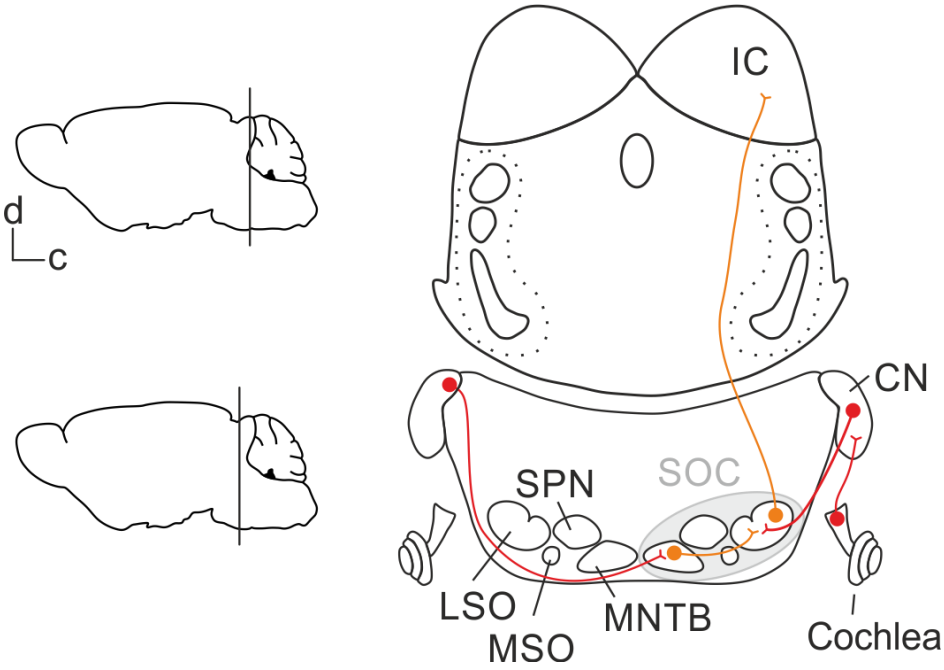

Fig. 4: Glycinergic projections in the auditory brainstem. Spiral ganglion neurons from the cochlea innervate the CN by transmitting glutamate. CN neurons project also glutamatergic to the ipsilateral LSO and contralateral MNTB. Glycinergic transmissions are present from the MNTB to the ipsilateral LSO and from the LSO to ipsilateral IC. Glutamatergic projections are depicted in red, glycinergic in orange. Sagittal views (left) show position of appropriate coronal slice scheme (right). c = caudal; CN = cochlear nucleus; d = dorsal; IC = inferior colliculus; LSO = lateral superior olive; MNTB = medial nucleus of the trapezoid body; MSO = medial superior olive; SOC = superior olivary complex; SPN = superior paraolivary nucleus. Modified from Hirtz (2012).

Besides the auditory nuclei, functional glycinergic synapses are also localized in the hypoglossal nucleus and the thalamus amongst others (Lynch, 2004). Furthermore, GlyRs are involved in controlling rhythmic breathing in the pre-Bötzinger complex as stated above, which was demonstrated in *oscillator* mice expressing non-functional GlyRα1 (Busselberg et al., 2001; Manzke et al., 2010).

1.7 The glycine receptor in zebrafish

Zebrafish express five GlyRα subunits (GlyRα1, GlyRα2, GlyRα3, GlyRα4a, GlyRα4b) and two GlyRβ subunits (GlyRβa, GlyRβb) (Hirata et al., 2009). Zebrafish GlyRα1, GlyRα3 and GlyRα4b were shown to be orthologs of the mammalian GlyRα1, GlyRα3 and GlyRα4 subunits proven by phylogenetic analysis (Imboden et al., 2001). During development, the location of expression of the various subunits differs in the organism. The *glra1* gene is expressed in the telencephalon, diencephalon, midbrain, hindbrain and spinal cord in zebrafish older than 52 hours post-fertilization (hpf) (Devignot et al., 2003). The *glra4a* gene is localized in the olfactory pit, midbrain, hindbrain and somite, whereas the *glra4b* is expressed in the retina in zebrafish at an age of 52 hpf (Ogino and Hirata, 2016). Furthermore, the *glrb2* gene was found in the hindbrain and spinal cord at 24 hpf (Hirata et al., 2005). The localization of *glra2* and *glra3* was not investigated yet.

1.8 Aim of this study

The aim of this study was to get further insights into the pathophysiological mechanisms of GlyRα autoantibodies with regard to the functional effects of autoantibodies to GlyRs. Epitope localization is one important aspect and used to determine if different epitopes exist and binding to the epitope(s) alter(s) receptor kinetics in various ways. An epitope in the ECD of the GlyRα1 has been suggested because autoantibody binding to the native configuration of the GlyRα1 was already demonstrated. Furthermore, the necessity of GlyRα1 glycosylation for autoantibody binding has to be investigated because other autoantibodies are speculated to bind their target only in its glycosylated from. In addition to the effects of GlyRα1 autoantibody binding, this study aims to develop possible therapeutic approaches by specifically neutralizing the autoantibodies from patient serum. The possibility to specifically target GlyRα1 autoantibodies would help to target only the morbid autoantibodies and not the healthy material from blood. Furthermore, the effect of passively transferred GlyRα1 autoantibodies into zebrafish larvae and mice will be studied. Thereby, the focus will be on the devolvement of patient symptoms in the animal and the changes in the behavior. The correct binding of GlyR autoantibodies after passive transfer will be verified by immunohistochemical stainings and Western Blot analysis.

2. Materials and Methods

2.1 Materials

2.1.1 Bacteria

DH5α™ derivative electrocompetent *Escherichia coli* cells (C2989K, New England BioLabs, Ipswich, Massachusetts, USA) were used for transformation of plasmid DNA during cloning experiments. The DH5α™strain has the following genotype: *fhuA2 Δ(argF-lacZ)U169 phoA glnV44 Φ80 Δ(lacZ)M15 gyrA96 recA1 relA1 endA1 thi-1 hsdR17*.

2.1.2 Cell line

Human embryonic kidney cells (HEK293, ATCC®CRL-1573™, Wesel, Germany) were grown in Minimum essential medium (MEM, Life Technologies, Darmstadt, Germany) containing 10% fetal bovine serum, 2 mM GlutaMax, 1 mM Sodium pyruvate, 50 U/ml penicillin and 50 µg/ml streptomycin. Cells were kept in an incubator at 37°C and 5% CO_2. 24 h after seeding, HEK293 cells were used for transfection.

2.1.3 Mouse strains

For cultivation of motoneurons, wildtype mice of the strain CD1 (Charles River Laboratories, Wilmington, MA, USA) were used. They were bred in the animal facility of the Institute for Clinical Neurobiology at the University Hospital Würzburg, Germany and kept at a 12 h light-dark interval with food and water *ad libitum* (reference number: FB VVL 568/300- 1869/13; approved by the District Government of Lower Franconia, Germany).

Wildtype mice of the strain C57BL6 (The Jackson Laboratory, Bar Harbor, ME, USA) were used for *in vivo* experiments with passive transfer of patient IgG. These mice were bred and hold at a 12 h light-dark interval with food and water *ad libitum* at the Neurology Department, University Hospital Jena, Germany. The *in vivo* experiments are in accordance with the assignments of the German Animal Welfare Act. All tests used were approved by the Thuringian State Office for consumer protection, Germany (reference number: UKJ-17-053).

2.1.4 Vectors and plasmids

The vectors and plasmids used for either cloning or transfections of HEK293 cells are summarized in the following table (Tab. 1).

Tab. 1: Vectors and plasmids used for cloning and transfection.

Vectors and plasmids	Insert	Origin/Manufacturer
pRK5	high copy CMV and SP6 promoter; Ampicillin resistance, used for human GlyR variants	† P. Seeburg, MPI for Medical Science
hsa1	human wildtype GlyRα1 in pRK5; parental clone for cloning GlyRα1^{N38Q}	
hsa1^{N38Q}	human GlyRα1 with amino acid exchange Asn to Gln at position 38 of mature protein; in pRK5	
hsa1^{I132L,A137S}	human GlyRα1 with amino acid exchanges I132L, A137S; in pRK5	Barbara Schleyer, AG Villmann
hsa1^{I132L,A137S,E173D,Q174E,G175A,A176P}	human GlyRα1 with amino acid exchanges I132L, A137S, E173D, Q174E, G175A, A176P; in pRK5	Barbara Schleyer, AG Villmann
hsa1^{A4R,P5S,K6A}	human GlyRα1 with amino acid exchanges A4R, P5S, K6A; in pRK5	Barbara Schleyer, AG Villmann
hsa1^{N76S}	human GlyRα1 with amino acid exchange N76S; in pRK5	Barbara Schleyer, AG Villmann
hsa1^{H107N}	human GlyRα1 with amino acid exchange H107N; in pRK5	Barbara Schleyer, AG Villmann
hsa1^{S121F,R122K}	human GlyRα1 with amino acid exchanges S121F, R122K; in pRK5	Barbara Schleyer, AG Villmann
hsa1^{A212V}	human GlyRα1 with amino acid exchange A212V; in pRK5	Barbara Schleyer, AG Villmann
mma2	mouse wildtype GlyRα2 in pRK7	
hsa3	human wildtype GlyRα3 in pRK5	
hsa3^{L132I,S137A}	human GlyRα3 with amino acid exchanges L132I, S137A; in pRK5	Barbara Schleyer, AG Villmann
hsa3^{L138I,S143A,D178E,E179Q,A180G,P181A}	human GlyRα3 with amino acid exchanges L138I, S143A, D178E, E179Q, A180G, P181A; in pRK5	Barbara Schleyer, AG Villmann
hsa3^{R4A,S5P,A6K}	human GlyRα3 with amino acid exchanges R4A, S5P, A6; in pRK5K	Barbara Schleyer, AG Villmann
drGlyRα1	zebrafish wildtype GlyRα1 in pCS2	Hiromi Hirata, Department of Chemistry and Biological

		Science, Sagamihara, Japan
drGlyRα2	zebrafish wildtype GlyRα2 in pCS2	Hiromi Hirata, Department of Chemistry and Biological Science, Sagamihara, Japan
drGlyRα3	zebrafish wildtype GlyRα3 in pCS2	Hiromi Hirata, Department of Chemistry and Biological Science, Sagamihara, Japan
drGlyRα4a	zebrafish wildtype GlyRα4a in pCS2	Hiromi Hirata, Department of Chemistry and Biological Science, Sagamihara, Japan
drGlyRα4b	zebrafish wildtype GlyRα4b in pCS2	Hiromi Hirata, Department of Chemistry and Biological Science, Sagamihara, Japan
drGlyRβa	zebrafish wildtype GlyRβa in pCS2	Hiromi Hirata, Department of Chemistry and Biological Science, Sagamihara, Japan
drGlyRβb	zebrafish wildtype GlyRβb in pCS2	Hiromi Hirata, Department of Chemistry and Biological Science, Sagamihara, Japan
pEGFPN1	enhanced green fluorescent protein (EGFP)	Clontech, St-Germain-en-Laye, France

Plasmids were fabricated at AG Villmann from University Hospital Würzburg, Germany or as otherwise stated. dr = *danio rerio*; hs = *homo sapiens*; mm = *mus musculus*. Numbers in mutations refer to mature protein. Wildtype implies the native full-length protein.

2.1.5 Enzymes

The enzymes used in different experiments are summarized below (Tab. 2).

Tab. 2: Enzymes used in the experiments. Manufacturers as well as the experiments are stated.

Enzymes	Manufacturer	Used for
GoTaq polymerase with GoTaq Green buffer (5x) and $MgCl_2$	Promega	Polymerase chain reaction (PCR)
Restriction endonucleases with supplied buffers	NEB	DNA-Digestion
DNAse	Roche	Protein preparation and neuron cultivation
RNase	Carl Roth	Plasmid DNA purification

2.1.6 Chemicals

All chemicals used for experiments in the present study were ordered from AppliChem (Darmstadt, Germany), BioRad (Munich, Germany), Calbiochem Merck (Darmstadt, Germany), Carl Roth (Karlsruhe, Germany), Merck (Darmstadt, Germany), New England Biolabs (Ipswich, MA, USA), Sigma-Aldrich (Munich, Germany) or as otherwise stated. Additional products stated below were obtained from Abgent (San Diego, CA, USA), Cell Signalling Technology (Cambridge, United Kingdom), Dianova (Barcelona, Spain), Gibco Live Technologies (Carlsbad, CA, USA), Invitrogen by Thermo Fisher Scientific (Waltham, MA, USA), Macherey Nagel (Düren, Germany), PAN-Biotech (Aidenbach, Germany), Promega (Fitchburg, WI, USA), Qiagen (Venlo, Netherlands), Roche Diagnostics (Mannheim, Germany), Santa Cruz Biotechnology (Dallas, TX, USA), Synaptic Systems (Göttingen, Germany) and Thermo Fisher Scientific (Waltham, MA, USA).

2.1.7 Kits

The different kits used are summarized in the following list (Tab. 3).

Tab. 3: Kits that were used in the experiments.

Kits	Manufacturer	Used for
SuperSignal West Pico or Femto	Thermo Fisher Scientific	Western blot detection
Gel Extraction Kit	Qiagen	Gel extraction
NucleoBond Xtra Maxi	Macherey-Nagel	Plasmid DNA purification
Mini DNA preparation	AG Villmann	Plasmid DNA purification
Gel and PCR Clean-up	Macherey-Nagel	DNA purification from PCR or agarose gels

2.1.8 Patient sera

The permission for using patient sera in experiments has been exhibited by the Ethics Committee of the Medical Faculty of the University of Würzburg, Germany with the project on "Autoantibodies and glycinergic dysfunction - pathophysiology of associated motor disorders".

Information of patient sera and IgG used in this study are summarized in the following table (Tab. 4). For evaluation of GlyRα1 positive patient sera, GlyRα1 and green fluorescent protein (GFP) co-transfected HEK293 cells were incubated with the sera and stained with the live staining protocol (see 2.2.5.1 Immunocytochemical stainings of GlyR autoantibodies). In total, 28 sera were tested and 20 were identified as positive. In this study, 9 positive patient sera and IgG samples of patient 1, 2 and 8 were included. Because of a low amount of some patient sera, not each serum could be tested in all experiments. As controls, serum from a healthy patient (healthy control), a patient suffering from multiple sclerosis (disease control) and a patient suffering from GAD autoantibodies (GAD^+) were used.

Tab. 4: Clinical data of patients.

	Sex	Age	Diagnosis	Material
patient 1	female	54	SPS	serum, CSF, IgG
patient 2	male	37	SPS	serum, IgG
patient 3	male	34	PERM	serum
patient 4	male	52	SPS	serum
patient 5	male	63	PERM	serum
patient 6	female	33	SPS	serum
patient 7	female	14	SPS	serum
patient 8	male	76	PERM	serum, IgG
patient 9	male	n. a.	SPS	serum

CSF = cerebrospinal fluid; n. a. = not available.

2.1.9 Antibodies

Primary (Tab. 5) and secondary antibodies (Tab. 6) used in the experiments are collected in the following lists.

Tab. 5: List and details of primary antibodies.

Antibody/antigen	Cat.no.	Company	Host	Dilution
mAb2b/glycine receptor α1	146 111	Synaptic Systems	mouse monoclonal, purified IgG	1:500
mAb4a/glycine receptor	146 011	Synaptic Systems	mouse monoclonal, purified IgG	1:500
Synaptophysin	AB 9272	Calbiochem	rabbit	1:500
GFP	SC 8334	Santa Cruz	rabbit	1:5000
GAPDH	CB1001	Calbiochem	mouse	1:1000
Gephyrin	147111	Synaptic Systems	monoclonal mouse	1:1000
Pan-cadherin	40685	Cell Signalling	rabbit	1:1000
Anti-his tag	AM1010a	Abgent	monoclonal mouse	1:1000
MAP2	MAB 3418	Merck Millipore	monoclonal mouse	1:500
VGAT	131003	Synaptic Systems	polyclonal rabbit	1:500

GAPDH = glyceraldehyde-3-phosphate dehydrogenase; MAP2 = microtubule associated protein 2; VGAT = vesicular GABA transporter.

Tab. 6: List and details of secondary antibodies.

Antibody	Conjugate	Cat.no.	Company	Dilution
goat anti-human	Cy3	109-165-003	Dianova	1:500
goat anti-human	Alexa 488	109-545-098	Dianova	1:500
goat anti-mouse	Cy3	115-165-003	Dianova	1:500
goat anti-mouse	Alexa 488	115-546-004	Dianova	1:500
goat anti-rabbit	Cy3	111-165-003	Dianova	1:500
goat anti-rabbit	Cy5	111-175-006	Dianova	1:500
DAPI		D3571	Invitrogen	1:2000-1:5000
goat anti-human	HRP	109-035-088	Dianova	1:15000-1:20000
goat anti-mouse	HRP	114-035-146	Dianova	1:15000-1:20000
goat anti-rabbit	HRP	111-036-003	Dianova	1:15000-1:20000

HRP = horseradish peroxidase.

2.1.10 Cell culture solutions, media and transfection reagents

Cell culture solutions and cell culture media (Tab. 7) as well as the reagents for the transfection of HEK293 cells (Tab. 8) are listed below.

Tab. 7: Composition of solutions used for cell culture.

Solution/Medium	Manufacturer/Composition
Dulbecco's phosphate buffered saline (PBS) (1x)	Gibco, Live Technologies
FBS (fetal bovine serum)	Gibco, Live Technologies
MEM (Minimum essential medium)	Gibco, Live Technologies
Neurobasal medium (NB medium)	Gibco, Live Technologies
Hank's balanced salt solution (HBSS)	Gibco, Live Technologies
GlutaMax	Gibco, Live Technologies
Penicillin/Streptomycin (Pen/Strep)	Gibco, Live Technologies
Trypsin 0.05%	PAN-Biotech
B-27 supplement	Gibco, Live Technologies
Silane solution	Stock: 10% (v/v) 3-aminopropyltriethoxysilane from Roth in H_2O dest.; working concentration: 1:10 in H_2O dest.
Poly-L-lysine hydrobromide	Stock: 5 mg/ml from Sigma in H_2O dest.; for use dilute 1:100 in H_2O dest.
Cell media:	
HEK293 cell medium	10% fetal bovine serum, 2 mM GlutaMax, 1 mM Sodium pyruvate, 50 U/ml penicillin, 50 µg/ml streptomycin, 90%MEM
Neuronal medium	2 mM GlutaMax, 50 ml 50x B27, 95% Neurobasal medium
Freezing medium	10% Dimethylsulfoxide (DMSO), 30% FCS, 60% cell medium

Tab. 8: Composition of solutions used for HEK293 transfection.

Transfection reagents	Manufacturer/Composition
2x HBS (HEPES buffered saline)	50 mM Hepes, 12 mM Dextrose, 10 mM KCl, 28 mM NaCl, 1.5 mM Na_2HPO_4, pH 6.95
TE Buffer (Tris-EDTA)	Applichem (A0973,0500)
Lipofectamine 2000	Invitrogen (11668-030)
Opti-Mem	Gibco, Live Technologies

2.1.11 Culture medium for bacteria

The composition of the culture medium for bacteria is specified in the following table (Tab. 9).

Tab. 9: Composition of culture medium for bacteria.

Medium	Composition per liter
2x YT medium	15 g/l tryptone, 10 g/l yeast extract, 5 g/l NaCl; for 2x YT agar plates: add 5 g agar
For bacterial selection following antibiotic was added:	
ampicillin	50 µg/ml

2.1.12 Solutions for biotinylation assay

The composition of quenching and lysis buffer used in biotinylation assays is summarized in the following table (Tab. 10).

Tab. 10: Composition of buffers used in biotinylation assays.

Buffer	Composition
Quenching buffer	192 mM glycine, 25 mM Tris in PBS, pH 8.0
Lysis Buffer	Tris buffered saline (TBS) with 1% Triton-X 100, one protease inhibitor mixture tablet (Roche Diagnostics)

2.1.13 Solutions and polyacrylamide gels for Western blot

The solutions for Western blots (Tab. 11) as well as the ingredients for polyacrylamide gels (Tab. 12) are listed below.

Tab. 11: Composition of solutions used in Western blot experiments.

Solution	Composition
TBS	50 mM Tris, 150 mM NaCl
TBST buffer (Tris buffered saline with 0.05% Tween)	50 mM Tris, 150 mM NaCl, 0.05% Tween-20
SDS buffer	25 mM Tris, 192 mM glycine, 0.1% (w/v) sodium dodecyl sulfate (SDS), pH 8.3
10x Towbin buffer	1.9 M glycine, 250 mM Tris
Blocking solution	5% bovine serum albumin (BSA) or 5% milk powder in TBST
Transfer buffer	10% (v/v) 10x Towbin buffer, 20% (v/v) EtOH, 70% (v/v) H_2O dest.
2x SDS loading dye	25% (v/v) stacking gel buffer, 20% (v/v) glycerol, 4% (w/v) SDS, 0.1 M dithiothreitol (DTT), 1% (w/v) bromphenol blue
Stacking gel buffer	0.5 M Tris/HCl, 0.4% (w/v) SDS, pH 6.8
Separating gel buffer	1.5 M Tris HCl, 0.4% (w/v) SDS, pH 8.8
Coomassie staining solution	0.1% Coomassie brilliant blue R250, 25% methanol, 7.5% acetic acid
Coomassie color stripping	40% Methanol, 10% acetic acid

Tab. 12: Composition of 13% Polyacrylamide gels.

Composition 13% Polyacrylamide gel (volumina per gel)	
Stacking gel	325 µl polyacrylamide (PAA), 625 µl stacking gel buffer, 1.55 ml H_2O dest., 12.5 µl 10% APS, 2.5 µl Tetramethylethylendiamin (TEMED)
13% Separating gel	3.9 ml polyacrylamide (PAA), 2.25 ml separating gel buffer, 2.85 ml H_2O dest., 30 µl 10% APS, 10 µl TEMED

2.1.14 Solutions for Enzyme-linked Immunosorbent Assay (ELISA)

The buffers and solutions that were used in ELISA experiments are mentioned in the following table (Tab. 13).

Tab. 13: Composition of solutions in ELISA experiments.

Solution	Composition
0.1 M carbonate buffer	prepare 0.1 M $NaHCO_3$ and 0.1 M Na_2CO_3. Adjust to pH 9.7 by mixing both solutions (~70% 0.1 M $NaHCO_3$ and 30% 0.1 M Na_2CO_3).
blocking solution	10% FBS and 0.05% Tween-20 in PBS
solution for antibody dilution	10% FBS in PBS

2.1.15 Solutions for immunocytochemistry and immunohistochemistry

Solutions and buffers that were used in immunocytochemical stainings as well as their ingredients are listed below (Tab. 14).

Tab. 14: Composition of buffers and solutions used in immunocytochemical and immunohistochemical stainings.

Solution	Composition
2-4% paraformaldehyde (PFA)	solve 2-4 g PFA in 50 ml H_2O dest., add few drops of 1 N NaOH and heat at 55°C while stirring. Add 10 ml 10x PBS and fill up to 100 ml with H_2O dest.
phosphate buffered saline (PBS)	137 mM NaCl, 3 mM KCl, 6.5 mM Na_2HPO_4 x H_2O, 1.5 mM KH_2PO_4 x $3H_2O$ pH 7.4
blocking immunocytochemistry	5% normal goat serum in PBS
blocking immunohistochemistry	10% normal goat serum in PBS
permeabilization immunocytochemistry	0.2% Triton-X-100 in PBS
permeabilization immunohistochemistry	0.3% Triton-X-100, 4% normal goat serum in PBS
quenching	50 mM NH_4Cl in PBS and 0.1 mM glycine in H_2O dest.
10 mM sodium citrate buffer	1.47 g sodium citrate and 250 µl Tween-20 solved in 500 ml PBS, pH 8
Mowiol	10% (w/v) Mowiol, 25% (w/v) glycerol, 0.1 M Tris (pH 8.5), heating at 50°C for 10 min and centrifuge at 1000 rpm for 5 min

2.1.16 Solutions and devices for electrophysiological recordings

The solutions that were used in electrophysiological measurements are summarized in the following list (Tab. 15). Furthermore, the equipment of the electrophysiological setup is mentioned below (Tab. 16).

Tab. 15: Composition of extra- and intracellular solution for electrophysiological recordings of HEK293 cells.

Solution	Composition
extracellular solution (Bormann et al., 1987)	137 mM NaCl, 5.4 mM KCl, 1.8 mM $CaCl_2$, 1 mM $MgCl_2$, 5 mM Hepes, pH 7.4 with NaOH
intracellular solution (Bormann et al., 1987)	120 mM CsCl, 20 mM TEA=$N(Et)_4Cl$, 1 mM $CaCl_2$, 2 mM $MgCl_2$, 11 mM EGTA, 10 mM Hepes, pH 7.2 with CsOH

Tab. 16: Devices at the electrophysiological setup.

Device	Manufacturer
Microscope Axiovert 135 or Axio Observer D1	Zeiss
Octaflow II system	ALA Scientific Instruments
EPC-10 amplifier	HEKA
Software PatchMaster	HEKA
P-97 Horizontal Puller	Shutter Instruments
Borosilicate capillaries	World Precision Instruments

2.1.17 Solutions for radioligand binding assay

In the radioligand binding assay, the following solutions were used (Tab. 17).

Tab. 17: Solutions and their composition used in radioligand binding assays.

Solution	Composition
HBSS	137 mM CholineCl, 5.4 mM KCl, 0.34 mM K_2HPO_4, 0.44 mM KH_2PO_4, 0.41 mM $MgSO_4$, 0.49 mM $MgCl_2$, 1.07 mM $CaCl_2$, 5.6 mM D-glucose, 10 mM Hepes, pH 7.4
Buffer B	25 mM K_2HPO_4, 25 mM KH_2PO_4, 200 mM KCl

2.2 Methods

2.2.1 Cell culture methods

2.2.1.1 Culturing of HEK293 cells

A tube of frozen HEK293 cells ($2.5x10^6$ cells per tube) was quickly thawed in a water bath at 37°C and mixed with 1 ml prewarmed culture medium (Tab. 7). The tube was centrifuged for 10 min 1400 rpm and the supernatant was removed. The cell pellet was resuspended in 10 ml pre-warmed cell culture medium and transferred into 25 cm² cell culture flask.

HEK293 cells were split twice a week at a confluency of 70-90% for maintenance of the culture. Therefore, cells were washed with warm PBS and detached by adding 0.05% trypsin for 5 min at 37°C. Cells were separated by resuspending the solution and centrifuged for 10 min at 1400 rpm. The supernatant was removed, the pellet resolved in warm culture medium, and the

cells were counted in a Neubauer counting chamber. Following seeding of the appropriate cell number into dishes or flasks, cells were kept in a humid incubator at 37°C and 5% CO_2.

For long term storage, HEK293 cells were frozen at a low number of passages. Therefore, cells were washed with PBS and detached with 0.05% trypsin. Suspension was centrifuged for 10 min at 1400 rpm and resuspended in culture medium. Freezing medium was added and $2.5x10^6$ cells/ml were frozen in CryoPure tubes (Sarstedt, Nümbrecht, Germany) (Tab. 7). Tubes were placed in an isopropanol-filled cryo-container for a slower freezing process and transferred into -80°C freezer.

2.2.1.2 Cover slip preparation for HEK293 cells and neurons

Cover slips for HEK293 cells were incubated in acetone for 5 min to promote cell attachment. Acetone was removed and evaporated from cover slips. After, cover slips were heat sterilized.

For a better attachment of neurons, cover slips were incubated in 1 M HCl and 96% EtOH (1 h each) on a shaking device and washed once with H_2O dest. After drying over night at room temperature and heat sterilizing, cover slips were immersed three times in silane solution and twice in H_2O dest. and placed in 3 cm dishes (Tab. 7). Cover slips were dried for 6 h at 37°C and 5% CO_2. Afterwards, dishes were filled with poly-L-lysine solution and incubated over night at room temperature under UV-light. Poly-L-lysine was removed, and cover slips were washed three times with H_2O dest. and stored at 4°C in darkness.

2.2.1.3 Transfection of HEK293 cells

Calcium-phosphate precipitation method

HEK293 cells were seeded and transfected at a confluency of 75% by using a calcium phosphate precipitation method. The reaction mixture containing 1 µg/µl plasmid DNA, 125 mM $CaCl_2$, 0.1x TE buffer (tris-aminomethane/ethylenediaminetetraacetate = Tris/EDTA) and 2x HBS (50 mM HEPES, 12 mM glucose, 10 mM KCl, 280 mM NaCl, 1.5 mM Na_2HPO_4) was incubated for 20 min at room temperature (Tab. 8, Tab. 18). The reaction mixture was pipetted to the HEK293 cells. After 6 h, cells were washed twice with culture medium.

Usually, GFP was co-transfected or transfected into cells on a separate dish as control for successful transfection. 24-72 h post-transfection, cells were used in the experiments.

Tab. 18: Mixture for transfecting HEK293 cells with the calcium-phosphate precipitation method.

	3 cm dish	10 cm dish
DNA	0.5-2 µg	5-20 µg
$CaCl_2$ (2.5 M)	10 µl	50 µl
0.1x TE buffer pH 7.4	ad 100 µl	ad 500 µl
2x HBS buffer	100 µl	500 µl

Transfection with Lipofectamine

For ligand binding assays, HEK293 cells were seeded in 96-well plates and transfected with Lipofectamine2000 (Thermo Fisher Scientific, Waltham, MA, USA). Therefore, 0.07 µl of DNA (1 µg/µl) and 25 µl Opti-MEM (Gibco Live Technologies, Carlsbad, CA, USA) per well were mixed and incubated for 5 min at room temperature. Additionally, 0.14 µl Lipofectamine and 25 µl Opti-MEM were mixed and also incubated for 5 min at room temperature. Both mixtures were pooled and again incubated for 5 min before it was applied to the cells in the well plate.

2.2.1.4 Tunicamycin treatment

24 after transfection with GlyRα1, HEK293 cells were treated with tunicamycin (Cat.no.: T7765, Sigma-Aldrich, Munich, Germany) to prevent N-glycosylation of newly synthesized glycoproteins. Therefore, a stock solution of 10 mg/ml tunicamycin resolved in dimethyl sulfoxide (DMSO) was prepared and added to the cell culture dish in an end concentration of 5 µg/ml. DMSO alone was used as negative control. After 24 h of incubation, cells were used for immunocytochemical stainings.

2.2.1.5 Cultivation of motoneurons

Embryos at embryonic day 13 (E13) were extracted from pregnant CD1 mice that were euthanized with CO_2 and transferred into 10 cm dish filled with MEM medium. The embryos' heads were disconnected immediately. Spinal cord tissue was extracted from embryos and meninges were removed. Spinal cord tissue was digested with 5 ml trypsin and 50 µl DNase for 20 min at 37°C. Digestion was stopped by adding 500 µl FBS and tissue was triturated with a 5 ml pipette, a 1 ml pipette and a Pasteur pipette to dissociate the neurons from tissue. The suspension was left for 2-3 min to sediment tissue leftovers. The supernatant was transferred into a new tube and centrifuged for 10 min at 400 rpm. Following removal of the supernatant, the pellet was resolved in 1 ml neurobasal medium (Tab. 7). After, cells were counted and seeded onto poly-L-lysine coated glass cover slips in 3 cm dishes.

2.2.2 Cloning

2.2.2.1 Site-directed mutagenesis

The GlyRα1 de-glycosylation mutant GlyRα1^{N38Q} was produced by exchanging residue asparagine 38 to glutamine (number refers to mature protein) using overlap extension site-directed mutagenesis. As template, the human wildtype full-length GlyRα1^{WT} cDNA in pRK5 vector was used. The primers for mutagenesis were designed as follows (produced by Life Technologies, Darmstadt, Germany).

Mutagenesis primers:
Sense: 5'GT CCC CCA GTG C**A**G GTG AGC TGC AA3'
Antisense: 5'GGT GCA GCT CAC C**T**G CAC TGG GGG A3'

Parental primers:
Sense: 5' TAG GTG ACA CTA TAG AAT AAC ATC CAC TTT GCC TT3'
Antisense: 5' GTA ACC ATT ATA AGC TGC AAT AAA CAA GTT GGG CCA T3'

Ingredients for polymerase chain reaction (PCR) reaction were 100 ng/µl template DNA, 10 pmol/µl sense and antisense primer, 10 mM dNTPs, 10x Pfu buffer with BSA and Pfu polymerase.

PCR conditions:

Initial denaturation	95°C	5 min	
Denaturation	95°C	1 min	28 cycles
Annealing	64.3°C	2 min	
Elongation	72°C	3 min	
Final elongation	72°C	10 min	

This first PCR reaction generated two amplimers that were overlapping in the mutated region. The PCR product was loaded on a 1% agarose gel together with marker pRK7-Plasmid/Hinf I digest (self-made DNA standard marker 100-1500 bp) and fragments were extracted from gel by using PCR clean-up kit (Macherey Nagel, Düren, Germany) according to manufacturer's instructions. In the following overlap-PCR, the two amplimers were elongated at the 3' ends by adding 10 mM deoxyribonucleotide triphosphates (dNTPs), 10x Pfu buffer with BSA and Pfu polymerase with following PCR conditions:

Denaturation	95°C	5 min	3 cycles
Annealing	62.6°C	5 min	
Elongation	72°C	5 min	

Parental primers were added (10 pmol/µl) and PCR continued with the subsequent conditions:

Initial denaturation	95°C	5 min	
Denaturation	95°C	1 min	28 cycles
Annealing	61.6°C	2 min	
Elongation	72°C	3 min	
Final elongation	72°C	10 min	

Using restriction digest, the PCR product and the vector containing GlyRα1^{WT} were digested with restriction endonucleases Hind III and EcoR I for 1 h at 37°C. Samples were loaded on a 1% agarose gel, cut blind from the gel and extracted with the gel extraction kit (Macherey Nagel, Düren, Germany) according to manufacturer's instructions. After, vector and insert were ligated over night at 14°C.

The clones were checked by sequencing (Eurofins Genomics Germany GmbH, Ebersberg, Germany).

2.2.2.2 Transformation and selection

DH5α™ derivative electrocompetent *Escherichia coli* bacteria were thawed for 10 min on ice. After, ligation sample was added and incubated for 30 min on ice. The sample was heated for 45 s at 42°C and placed again for 2 min on ice. Pre-warmed SOC medium (New England BioLabs, Ipswich, MA, USA) was added and sample was shaken for 1 h at 37°C before plated on 2x YT agar plates containing ampicillin (1:500, Tab. 9). Agar plates were incubated over night at 37°C. Some of bacterial colonies were picked and grown by inoculating 2x YT medium containing ampicillin (1:500) and shaking the solution over night at 37°C.

Using the same picked colonies, a colony PCR containing 1.25 mM dNTPs, 25 mM $MgCl_2$, GoTag green buffer(5x), 5 pmol/µl forward and reverse primer, GoTag Flexi Polymerase and sample DNA was performed under following conditions:

Initial denaturation	95°C	5 min	
Denaturation	95°C	30 min	30 cycles
Annealing	49.3°C	30 min	
Elongation	72°C	1 min	
Final elongation	72°C	10 min	

2.2.2.3 Plasmid DNA purification

For purification of small amounts of plasmid DNA (protocol modified from Birnboim and Doly (1979)), transformed bacteria were grown in 2x YT medium with Ampicillin (1:500, Tab. 9) over night at 37°C while shaking. 1.5 ml bacterial culture was centrifuged for 1-3 min at room temperature and supernatant was removed. Afterwards, pellet was re-suspended in 200 µl ice-cold buffer P1 (Tab. 19) and 4 µl RNase (stock solution 10 mg/ml) and incubated for 5 min on ice. 400 µl buffer P2 was added and mixture again incubated for 5 min on ice. After adding 300 µl buffer P3 and incubating for 5 min on ice, solution was centrifuged for 5 min at 4°C. Subsequently, the supernatant was transferred in a new tube and DNA was precipitated by adding 800 µl isopropanol for 5 min at room temperature. Mixture was centrifuged for 5 min at room temperature and supernatant was removed. The pellet was washed with 300 µl 70% EtOH and centrifuged for 5 min at room temperature. The EtOH-supernatant was removed, and the pellet was dried at 37°C for 15 min. Finally, the pellet was re-suspended in 10-40 µl TE buffer (pH 7.4, Tab. 8) and stored at -20°C.

Tab. 19: Composition of buffers P1-P3 needed for plasmid DNA purification.

Solution	Composition
Buffer P1	50 mM glucose, 10 mM EDTA, 25 mM Tris-HCl pH 8
Buffer P2	200 mM NaOH, 1% SDS
Buffer P3	60 ml 5 M potassium acetate, 11.5 ml acetic acid, 28.5 ml H_2O dest.

Purification of larger amounts of plasmid DNA, the NucleoBond Xtra Maxi Kit (Macherey Nagel, Düren Germany) was used according to manufacturer's instructions.

2.2.3 Purification of the antibody-containing IgG fractions from patient sera

During therapeutic plasmapheresis, plasma filtrate was obtained from SPS and control patients and used to purify IgG fractions by using exchange chromatography as described earlier (Sommer et al., 2005). Afterwards, IgG fractions were dialyzed, lyophilized and stored at -20°C.

For usage, lyophilized IgG was solved and diluted in normal saline at a concentration of 100 mg/ml. IgG was stored at -80°C until usage. This procedure was executed in the Neurology Department of the University Hospital Würzburg, Germany.

2.2.4 Protein biochemical methods

2.2.4.1 Cell lysates

Cell lysates from transfected HEK293 cells were produced using the CytoBuster Protein Reagent (Merk Millipore, Billerica, MA, USA). Samples were prepared according to manufacturer's instructions. A mixture of 40 µg cell lysate, 6x sodium dodecyl sulfate (SDS) buffer (SDS buffer: 416 mM SDS, 0.9 mM bromophenol blue, 47% (v/v) glycerol, 60 mM Tris pH 6.8, 0.6 M dithiothreitol) and H_2O dest. (filled up to 24 µl) was heated for 5 min at 95°C and loaded on a 13% polyacrylamide gel (PAA gel) for Western blot analysis.

2.2.4.2 PNGaseF and EndoH digestion

Peptide N-glycosidase F (PNGaseF, cleaves between GlcNAc and asparagine residues) or endoglycosidase H (EndoH, cleaves chitobiose core of high mannose) were used to remove glycans from cell lysates of GlyRα1^{WT} and GlyRα1^{N38Q} transfected HEK293 cells (P0704S and P0702S, New England BioLabs, Ipswich, MA, USA). Samples were prepared according to manufacturer's instructions. In brief, 45 µg protein were centrifuged for 10 min at 14000 rpm and pellet was re-suspended in denaturing buffer (1:10 in H_2O dest.). Thereafter, the samples were heated for 10 min at 100°C and digested for 1 h at 37°C in one of the following mixtures:

Undigested: 13 µl sample, 2 µl 10x G5 buffer, 4 µl H_2O dest.
PNGaseF: 13 µl sample, 2 µl 10x G7 buffer, 2 µl 10% NP-40, 1 µl PNGaseF
EndoH: 13 µl sample, 2 µl 10x G5 buffer, 1 µl EndoH, 3 µl H_2O dest.

10 µl 2x SDS loading dye (Tab. 11) was added to the mixture and loaded on a 13% PAA gel for Western blot analysis.

2.2.4.3 Biotinylation assay

The biotinylation assay was performed to separately analyze proteins of the whole cell and intracellular or membrane-bound proteins. Transfected HEK293 cells were washed with ice-cold PBS (pH 8) and surface proteins were labelled by incubating and gently shaking the cells with 1 mg/ml EZ-Link Sulfo-NHS-LC-Biotin (sulfosuccinimidyl-6-[biotin-amido]hexanoate) (Thermo Fisher Scientific, Waltham, MA, USA) for 30 min at 4°C. After washing twice with PBS

and once with quenching buffer (Tab. 10), cells were incubated with quenching buffer for 10 min at 4°C. Subsequently, cells were displaced using a cell scraper with 1 ml PBS and centrifuged for 1 min at 1,000 x *g* and 4°C. The supernatant was removed, and the pellet untightened by vortexing as well as resuspended in 1 ml lysis buffer (Tab. 10). The mixture was centrifuged again for 1 min at 17,000 x *g* and a part of the supernatant was stored as whole cell fraction (WC). The remaining supernatant was mixed with 50 µl streptavidin-agarose beads (Thermo Fisher Scientific, Waltham, MA, USA) and placed in a shaking device for 2 h at 4°C to couple membrane-bound proteins labeled by biotin to the beads. Membrane-bound proteins were then separated from intracellular proteins by centrifugation for 1 min at 13,000 rpm. Thus, membrane-bound proteins were found in the pellet and intracellular proteins in the supernatant. Finally, beads with bound membrane proteins were washed three times with lysis buffer and mixed with pre-heated 2x SDS loading dye (95°C, Tab. 11). The mixture was heated again for 5 min at 95°C. For Western blot analysis, whole cell and intracellular fraction were also mixed with 2x SDS loading dye but only whole cell fraction was heated for 5 min at 95°C before loading on a 13% PAA gel (Tab. 12).

2.2.4.4 Membrane preparation of mouse tissue

For protein analyses of tissue from mice, that intrathecally received patient IgG, membrane preparations of spinal cords were performed. The tissue was extracted from mice that were deeply anesthetized with isoflurane and decapitated afterwards. Spinal cord tissues were directly frozen in liquid nitrogen and stored at -80°C until membrane preparation.

Tissues were slowly thawed on ice and hackled with 3 ml buffer H (Tab. 20) using a glass-homogenizer. After centrifuging for 30 min at 15,000 x *g* and 4°C, the supernatant was removed, the pellet re-suspended in 2 ml buffer H and again homogenized in the glass-homogenizer and additionally with an Ultra-Turrax T10 basic (IKA, Staufen im Breisgau, Germany). Subsequently, samples were centrifuged for 30 min at 15000 x *g* and 4°C. Finally, the supernatant was discarded, the pellet re-suspended in 100 µl buffer B (Tab. 20) and samples stored at -80°C until use. For loading on 13% PAA gels for Western blot analysis, 20 µg protein sample was centrifuged for 10 min at 13,000 rpm at 4°C. The supernatant was discarded, the pellet was solved in 20 µl 2x SDS loading dye, and the mixture was heated for 20 min at 56°C. Finally, the samples were centrifuged for 1 min at 13,000 rpm and supernatant was loaded on a 13% PAA gel (Tab. 12).

Tab. 20: Composition of buffer H and B used in membrane preparations of mouse tissue.

Solution	Composition
Buffer H	2 ml 250 mM K_2HPO_4, 2 ml 250 mM KH_2PO_4, 1 ml 250 mM EGTA pH 8, 1 ml 250 mM EDTA pH 8, 1 tablet Roche Complete EDTA-free Protease Inhibitor Cocktail, fill up to 50 ml with H_2O dest. Shortly before use: add 500 µl 200 mM PMSF
Buffer B	4.2 ml 3 M KCl, 5 ml 250 mM K_2HPO_4, 5 ml 250 mM KH_2PO_4, 1 tablet Roche Complete EDTA-free Protease Inhibitor Cocktail, fill up to 50 ml with H_2O dest. Shortly before use: add 50 µl DNase per 10 ml buffer B

2.2.4.5 Protein concentration determination by Bradford assay

The Bradford protein assay (Bio-Rad, Munich, Germany) was used to measure total protein concentrations. This method underlies the color change of Coomassie brilliant blue G-250 dye upon different protein concentrations. Bradford samples were prepared according to manufacturer's instructions and measured with BioPhotometer plus (Eppendorf, Hamburg, Germany).

2.2.4.6 Western blot

13% PAA gels (Tab. 12) were loaded with samples for Western blot analyses including the color pre-stained protein marker (p7712, New England BioLabs, Ipswich, MA, USA). The electrophoresis chamber was filled with SDS buffer (Tab. 11). The gels were run at 150 mV for 90 min followed by a wet-blot protein transfer to nitrocellulose membranes (GE Healthcare, Freiburg, Germany) for 1 h at 200 mA and 4°C. Large control-proteins, like pan-cadherin were transferred for 5 h at 200 mA and 4°C. After transfer, the membranes were quickly washed in TBST and blocked for 1 h at room temperature either in 5% bovine serum albumin (solved in TBST) or in 5% milk powder when patient serum or IgG was used as first antibody. Incubation with the first antibodies mAb4a (1:500 in blocking, see Tab. 5), anti-gephyrin (1:1000), anti-GFP (1:5000), anti-pan-cadherin (1:1000), patient serum (1:50) or IgG (0.2 µg/µl) was performed overnight. Membranes were washed three times for 20 min in TBST and were incubated with secondary antibodies goat anti-human, goat anti-mouse or goat anti-rabbit conjugated to horseradish peroxidase (1:15000 in blocking solution; see Tab. 6) for 1 h at room temperature. Finally, blots were washed three times for 20 min in TBST and directly detected by using the SuperSignal West Pico or Femto chemiluminescent substrate kit (Thermo Fisher Scientific, Waltham, MA, USA) according to manufacturer's instructions. Chemiluminescence

was visualized by exposure to an X-ray film (Fuji medical x-ray film, Fujifilm, Tokio, Japan) and developing the film in a Kodak X- OMAT 2000 processor (Kodak, Atlanta, USA). Western blots of samples from biotinylation assay were quantified with the software Fiji (Rasband, WS. ImageJ. U. S. National Institutes of Health, Bethesda, Maryland, USA; Schindelin et al. (2012)).

2.2.4.7 Enzyme-linked Immunosorbent Assay (ELISA)

96-wellplates with medium-binding properties (Sarstedt, Nümbrecht, Germany) were coated with the purified and refolded GlyRα1 extracellular domain (ECD) which was kindly provided by Christoph Kluck (Institute of Biochemistry, FAU Erlangen-Nürnberg) and Daniela Schneeberger (Rudolf-Virchow Center, Würzburg) (Breitinger et al., 2004). Therefore, solved ECD was diluted in carbonate buffer (Tab. 13) to a final concentration of 2 µg/ml. Incubation with the ECD was done overnight at 4°C. The plates were washed 5x with H_2O dest. After blocking with 10% FBS (diluted in PBS containing 0.05% Tween-20) for 1 h at 37°C, plate was washed again 5x with H_2O dest. and incubated with patient serum (1:100 in 10% FBS in PBS) or GlyR pan-α antibody mAb4a (1:500; cat. no. 146 011, mouse IgG_1, Synaptic Systems, Göttingen, Germany; Tab. 5) for 1 h at 37°C. Thereafter, supernatant was 3x transferred into a new coated well to bind almost all patient IgG to the ECD. Afterwards, the supernatants were used for further live staining of GlyRα1 and GFP co-transfected HEK293 cells to visualize the neutralizing effects by the ECD. 96-wellplate was 5x washed with PBS before incubating with the HRP labelled secondary antibodies, goat-anti-human or goat anti-mouse (1:20,000 in 10% FBS in PBS; Tab. 6), for 1 h at 37°C. Following five additional washing steps with PBS, TMB solution (substrate for peroxidase; Invitrogen by Thermo Fisher Scientific, Waltham, MA, USA) was applied and incubated for 15 min. The reaction was stopped by 1 M H_3PO_4. Subsequently, absorbance at 450 nm from samples in the ELISA plate were read with a Wallac 1420 Victor2 Microplate Reader (Perkin Elmer, Waltham, MA, USA).

2.2.5 Immunofluorescence staining

2.2.5.1 Immunocytochemical stainings of GlyR autoantibodies

For live stainings, GlyRα1 transfected HEK293 cells or cultured motoneurons were transferred into a humid chamber and incubated for 2 h at 4°C with patient serum (1:50 diluted in HEK293 medium), patient cerebrospinal fluid (CSF; 1:10), purified patient IgG (1:50), GlyRα1 specific antibody mAb2b or GlyR specific antibody mAb4a (Tab. 5). For neuronal cultures, neuronal markers synapsin, MAP2 or synaptophysin were additionally used. Primary antibodies were diluted in HEK293 or neuronal medium (Tab. 7). After washing with phosphate-buffered saline (PBS), cells were fixed with 4% (w/v) paraformaldehyde (PFA) with 4% sucrose for 20 min at 4°C, washed again and blocked with 5% (v/v) normal goat serum (NGS, diluted in PBS) (PAA

Laboratories, Cölbe, Germany) for 30 min at room temperature (Tab. 14). Secondary antibodies were diluted in blocking solution and incubated for 45 min at room temperature on the cells (Tab. 6). Following washing, the nuclei were stained with DAPI for 5 min at room temperature (1:5000 in PBS). Finally, cells were washed in PBS and H_2O dest. and fixed on a slide with mowiol (Tab. 14).

Fixed and permeabilized cells were used for mAb4a staining and intracellular epitope analysis. Therefore, cells were also transferred into a humid chamber, fixed with 4% PFA containing 4% sucrose for 20 min at 4°C, washed with PBS and permeabilized with 0.2% (v/v) Triton-X 100 for 5 min (Tab. 14). Cells were blocked in 5% NGS for 10 min and incubated with patient sera (1:50 in blocking) or mAb4a (1:500; Tab. 5) for 1 h at room temperature. The following steps were the same as for live stainings, including washing, secondary antibody incubation, washing in PBS, DAPI staining, washing (PBS and H_2O dest.) and mounting on a slide with mowiol.

2.2.5.2 Double staining live and fixed/permeabilized HEK293 cells

Double staining of live and fixed/permeabilized HEK293 cells were performed to investigate the binding ability of autoantibodies to target both native and denatured GlyRα1. To do so, GlyRα1 transfected HEK293 cells were incubated with patient serum (1:50) or mAb4a (1:500; diluted in HEK293 cell culture medium, Tab. 5, Tab. 7) at 4°C for 1 h and followed by washing with PBS. After, secondary antibody goat anti-human Cy3 or goat anti-mouse Cy3 was added in a dilution of 1:500 in HEK293 cell culture medium for 45 min at 4°C (Tab. 6). Subsequently, cells were washed with PBS, fixed with 4% PFA containing 4% sucrose (solved in PBS) for 20 min at room temperature and washed again with PBS (Tab. 14). Following permeabilization with 0.2% (v/v) Triton-X 100 for 5 min, HEK293 cells were incubated again with serum from the same patient (1:50; diluted in HEK293 cell culture medium) or mAb4a (1:500) for 1 h at 4°C. After, cells were washed with PBS and secondary antibody goat anti-human Alexa 488 or goat anti-mouse Alexa 488 were incubated for 45 min at 4°C. Afterwards, cells were washed in PBS, followed by DAPI staining (1:5000 diluted in PBS) for 5 min at room temperature. Lastly, HEK293 cells were washed in PBS and H_2O dest. and mounted on a slide with mowiol (Tab. 14).

2.2.5.3 Neutralization

For neutralization of patient autoantibodies from serum samples, GlyRα1 transfected HEK293 cells were incubated for 1 h at room temperature with patient serum or mAb2b (1:50 or 1:500, respectively; diluted in HEK293 medium, Tab. 5). Afterwards, the supernatant with unbound

patient antibodies was transferred to another cover slip with transfected HEK293 cells and once more incubated for 1 h. Overall, three transfers were performed. Finally, HEK293 cells were stained according to the live staining protocol (see 2.2.5.1 Immunocytochemical stainings of GlyR autoantibodies).

2.2.5.4 Competition for antibody epitope

Competition experiments were performed to analyze if patient autoantibodies and commercially available GlyRα1 antibody mAb2b share the same epitope or if the epitopes differ. Therefore, HEK293 cells were incubated at 4°C either for 2 h with a mixture of patient serum and mAb2b simultaneously or successively for 1 h with patient serum (1:50; diluted in HEK293 cell culture medium) and 1 h with mAb2b (1:50, 1:100, 1:500, 1:1000 or 1:2000; Tab. 5) and vice versa. After, HEK293 cells were washed with PBS and fixed with 4% PFA containing 4% sucrose for 20 min on ice followed by another washing step with PBS (Tab. 14). The HEK293 cells were then blocked for 30 min with 5% (v/v) normal goat serum (NGS, diluted in PBS) at room temperature. Secondary antibodies goat anti-human Cy3 and goat anti-mouse Cy5 (both 1:500 in blocking solution, Tab. 6) were incubated at room temperature for 45 min. Afterwards, cells were washed with PBS and incubated with DAPI (1:5000 in PBS) for 5 min for nuclei staining. In the end, HEK293 cells were washed with PBS and H_2O dest. and fixed on a slide with mowiol (Tab. 14).

2.2.5.5 Cryosectioning of mouse spinal cord and brain for immunohistochemical stainings

After finishing the behavioral experiments with mice that were treated with purified patient IgGs, spinal cord and brain was extracted and kept for further analysis. Therefore, the mice were deeply anesthetized with isoflurane, transcardially perfused with PBS and decapitated afterwards. The cranial bone was removed, the brain carefully extracted from the skull and directly embedded in Tissue-Tek (Sakura Finetek, Zoeterwoude, Netherlands) as well as quickly frozen on dry ice. The spinal cord was removed from spine by pushing out with a PBS-filled syringe and subsequently embedded in Tissue-Tek and frozen as well.

For immunhistochemical stainings, 9 or 12 µm thick spinal cord or brain slices were cut using a cryostat (CM1950, Leica, Wetzlar, Germany). The samples were fixed with Tissue-Tek at a cryostat holder and coronally cut with a chamber temperature of -18°C and an object temperature of -15°C. Slices were mounted on SuperFrost Plus slides (03-0060 Langenbrinck, Emmendingen, Germany) and stained at the same day.

2.2.5.6 Immunohistochemical stainings

Slides with spinal cord or brain slices were surrounded by a PAP-Pen liquid blocker (Science Services, Munich, Germany) to avoid loss of liquid from slices. Slices were placed in a humid chamber.

In stainings using the monoclonal antibody mAb4a, spinal cord or brain slices were first fixed with 2% PFA diluted in PBS for 10 min at 4°C and washed twice with PBS for 2 min. For antigen-retrieval, slices were incubated for 2 min at room temperature with sodium citrate buffer (with 0.05% Tween 20, pH 8) and for 30 min at 95°C in sodium citrate buffer afterwards (Tab. 14). Subsequently, samples were dried for 20 min at room temperature, washed twice in PBS for 2 min and permeabilized for 10 min in a solution containing 0.3% Triton-X-100 and 4% normal goat serum solved in PBS. Accordingly, slices were blocked in 10% normal goat serum diluted in PBS for 3 h and incubated in first antibodies mAb4a and synaptophysin or VGAT (each 1:500 diluted in blocking, see Tab. 5) over night at 4°C. Next day, samples were washed three times for 10 min in PBS, incubated in secondary antibodies goat anti-human Cy3, goat anti-mouse Alexa488 and goat anti-rabbit Cy5 (each 1:1000 diluted in blocking solution, see Tab. 6) for 1 h and washed again three times 10 min in PBS. Finally, slices were incubated with DAPI solution (1:2000 in PBS) for 10 min, washed three times 10 min in PBS and once in H_2O dest. and covered with Fluor Save Reagent (Calbiochem, Darmstadt, Germany) and a glass cover slip.

The use of mAb2b for immunohistochemical stainings required a different protocol. Spinal cord and brain slices were fixed for 30 s in 2% PFA at 4°C followed by a quenching step with NH_4Cl (shortly dipping, Tab. 14). Glycine at a concentration of 0.1 mM was applied and incubated for 30 min at room temperature. Subsequently, samples were blocked for 1 h with 10% normal goat serum (diluted in PBS) and in primary antibodies mAb2b and synaptophysin or VGAT (each 1:500 diluted in blocking, see Tab. 5) over night at 4°C. Following secondary antibody incubation, DAPI staining and mounting steps are similar to mAb4a staining (see above).

2.2.5.7 Microscopy

Pictures from all immunocytochemical stainings were taken with an Olympus microscope (Fluoview ix1000, Olympus, Hamburg, Germany) which was equipped with an UPLSAPO 60x oil objective (numerical aperture 1.35). The microscope settings were controlled by the software Fluoview FV 1000 (Olympus, Hamburg, Germany). The same software was used to take images. The microscope contained diode lasers of 405 nm, 495 nm and 550 nm. The following filter sets were used: DAPI (excitation: 405 nm, emission 461 nm), Alexa Fluor 488 (excitation: 473 nm, emission: 520 nm) and Cy3 (excitation: 559 nm, emission: 567 nm).

The software Fiji (Rasband, WS. ImageJ. U. S. National Institutes of Health, Bethesda, Maryland, USA; Schindelin et al. (2012)) was used for further image processing and analyses.

2.2.6 Electrophysiological recordings

Whole-cell patch clamp measurements in voltage clamp mode were performed with transfected HEK293 cells. Following a pre-incubation with mAb2b (1:500 diluted in extracellular buffer, Tab. 15), patient sera (1:10) or patient IgG (2 mg/ml) for 1 h at room temperature, recordings of GlyRα1 transfected HEK293 cells were performed. Additionally, $GlyR\alpha1^{WT}$ and $GlyR\alpha1^{N38Q}$ transfected HEK293 cells were recorded. Increasing glycine concentrations (1, 3, 10, 30, 60, 100, 300 and 1000 µM, diluted in extracellular buffer) were applied by using the Octaflow II system (ALA Scientific Instruments, Farmingdale, NY, USA, Tab. 16) and current recordings were obtained with an EPC-10 amplifier and the PatchMaster software (HEKA, Lamprecht, Germany). Patch pipettes were pulled from borosilicate capillaries (World Precision Instruments, Berlin, Germany) resulting in a pipette resistance of 3-5 MΩ when filled with intracellular buffer (Tab. 15). Cells were held at -60 mV during recordings.

To investigate the EC_{50} values, dose-response curves were fitted with a hill 1 function using Origin 9.0 (Originlab Corporation, Northampton, US). The function is as follows:

y = START + (END - START) * x^n / (k^n + x^n)
START = start value
END = end value
n = cooperative sites
k = Michaelis constant

Analyses of the desensitizing phase during the recordings were performed by fitting the decay phase of the current with the exponential function ExpDec1 in Origin 9.0 (Originlab Corporation, Northampton, US). The function is as follows:

y = A1*exp(-x/t1) + y0
y0 = y offset
A1 = amplitude
t1 = time constant

2.2.7 Radioligand binding assay

Radioligand binding assays were performed to examine effects of patient autoantibodies to the binding affinity of the agonist glycine to the GlyR. 96-wellplates were coated with 0.2% gelatin solution for 1 h, washed with PBS and incubated with 0.5% glutaraldehyde for 15 min (Tab.

17). The wellplates were washed again with PBS. One day prior to cell seeding, the 96-wellplate was filled with HEK293 culture medium and placed in the incubator at 37°C and 5% CO_2. HEK293 cells were seeded into the wells and transfected 24 h later with the GlyRα1 using Lipofectamine2000 (see 2.2.1.3 Transfection of HEK293 cells) as transfection agent. 48 h later, cells were washed with HBSS (Tab. 17) and incubated with patient serum, healthy control (1:50 in HBSS), mAb2b (1:500 in HBSS, Tab. 5) or HBSS alone as negative control for 1 h on ice. Subsequently, 30 mM glycine (diluted in buffer B; Tab. 20) was added for 30 min on ice. Glycine was then replaced by adding [^{3}H] strychnine in increasing concentrations for 30 min on ice (strychnine concentration series: 0, 1, 3, 10, 30, 100, 300 nM diluted in buffer B) (30 Ci/mmol; DuPont NEN, Waltham, MA, USA). Thereafter, the wellplate was washed with buffer B twice and cells were lysed from plate with cold H_2O dest. Rotiszint eco plus solution (Roth, Karlsruhe, Germany) was added and [^{3}H] strychnine bound to the cells was measured with a scintillation counter (Packard Tri-Carb Liquid Scintillation Counter, Perkin Elmer, Rodgau, Germany). Data were analyzed using the hill 1 fit of the software Origin 9.0 (Originlab Corporation, Northampton, US) (hill 1 fit see 2.2.6 Electrophysiological recordings).

2.2.8 *In viv*o passive transfer of purified patient IgG

2.2.8.1 Model system zebrafish

Wildtype zebrafish were bred and hold on a constant cycle of 14 h light/10 h darkness at 28°C in the animal facility of the Biocenter at the University of Würzburg, Germany. All experimental procedures as well as the animal welfare are in accordance with the German Animal Welfare Act and were approved by the District Government of Lower Franconia, Germany. Zebrafish larvae at the age of 56 hpf (hours post fertilization) were anesthetized with 0.4% tricaine before placing in a drop of 3% methylcellulose with 0.4% tricaine. A hole was poked in the skin above the 4th ventricle with a glass capillary. Methylcellulose was washed away with artificial cerebrospinal fluid (ACSF, Tab. 21) and the zebrafish were placed in ACSF containing patient serum (1:100). Another group of zebrafish were directly injected with patient serum (1:100) by using the FemtoJet 5247 (Eppendorf, Hamburg, Germany) (Fig. 5A). 20 h later, the escape responses were tested by touching the head or tail of zebrafish sitting in a 3 cm dish filled with ACSF. Videos were taken with a Samsung S7 mobile phone (Seoul, South Korea) and escape responses were categorized in normal, mild (intermediate phenotype, slow or short distance swimming, stopping during escape) or severe (no escape/swimming upon touch) as reported before (Hirata et al., 2013; Schaefer et al., 2018b) (Fig. 5B-D).

Tab. 21: Composition of artificial cerebrospinal fluid for zebrafish.

Solution	Composition
ACSF buffer	100 mM NaCl, 2.46 mM KCl, 1 mM $MgCl_2$, 0.44 mM NaH_2PO_4, 1.13 mM $CaCl_2$, 5 mM $NaHCO_3$, 10 mM glucose, pH 7.2

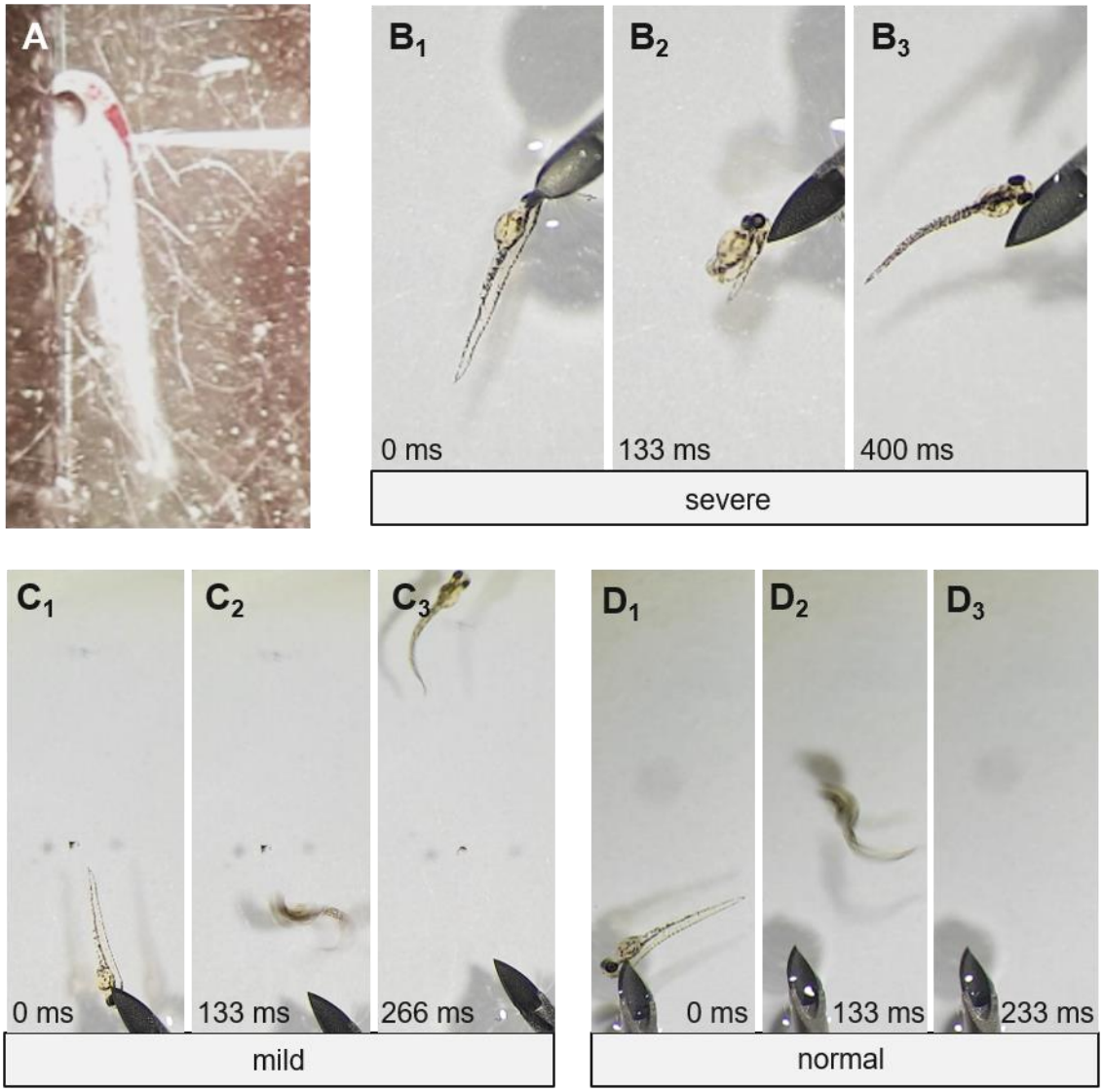

Fig. 5: Zebrafish injection and categorization of escape behavior. (**A**) Zebrafish larvae that was injected with rhodamine dextrane directly into the 4th ventricle to prove correct applications. The dye filled the whole 4th ventricle without spreading to neighboring tissue. The injecting capillary is on the right site and still sticking in the ventricle. (**B_1-B_3**) Escape behavior of zebrafish larvae with severe phenotype. Upon touch, the zebrafish larvae tries to escape but is unable to swim away. (**C_1-C_3**) Escape behavior of zebrafish larvae with mild phenotype. After touching, the zebrafish larvae is able to swim but just a short distance. (**D_1-D_3**) Zebrafish larvae with normal escape behavior. Touching the head of the zebrafish larvae results in an immediate, fast escape out of the observed area.

2.2.8.2 Surgical insertion of intrathecal catheter in mice

Lumbar intrathecal catheters were fixed in the subarachnoidal space of mice during a surgery to passively transfer patient IgG into the animals. The catheters were self-made out of polyethylene tubes (Intremedic Polyethylene Tubing Clay Adams 427401, San Jose, CA, USA) in a total length of about 9 cm with two open knots for fixation of the catheter in the animal (Fig. 6A). The surgical procedure was performed by Prof. Dr. Christian Geis (University Hospital Jena, Germany) as described earlier (Wu et al., 2004). In brief, three month old mice were anesthetized with 3% isoflurane and hair at the back were shaved. During the following surgery, isoflurane concentration was 2%. The skin at the back was disinfected with Octeniderm (Schülke, Norderstedt, Germany) and the catheter was filled with 0.9% NaCl. The skin was incised above the pelvic floor and catheter was inserted into the subarachnoidal space between lumbar 5 and 6 (Fig. $6B_1$). A wire in the catheter supported the stiffness while inserting (Fig. $6B_2$). Catheter was fixed with a thread and the open end was placed out of the skin between the eyes (Fig. $6B_3$ and B_4). 10 µl of patient IgG at a concentration of 1 mg/ml was applied daily via the opening which was closed with a wire afterwards. In the second group of mice, osmotic pumps (Micro-osmotic pump Model 1002, Alzet, Cupertino, CA, USA) filled with patient IgG at a concentration of 1 mg/ml were transplanted below the skin. After finishing all behavioral experiments, spinal cord and brain was extracted from mice. Meanwhile, the correct positioning of the catheter was proven (Fig. $6C_1$-C_2). During behavioral experiments, weight and vitality of the mice were documented daily.

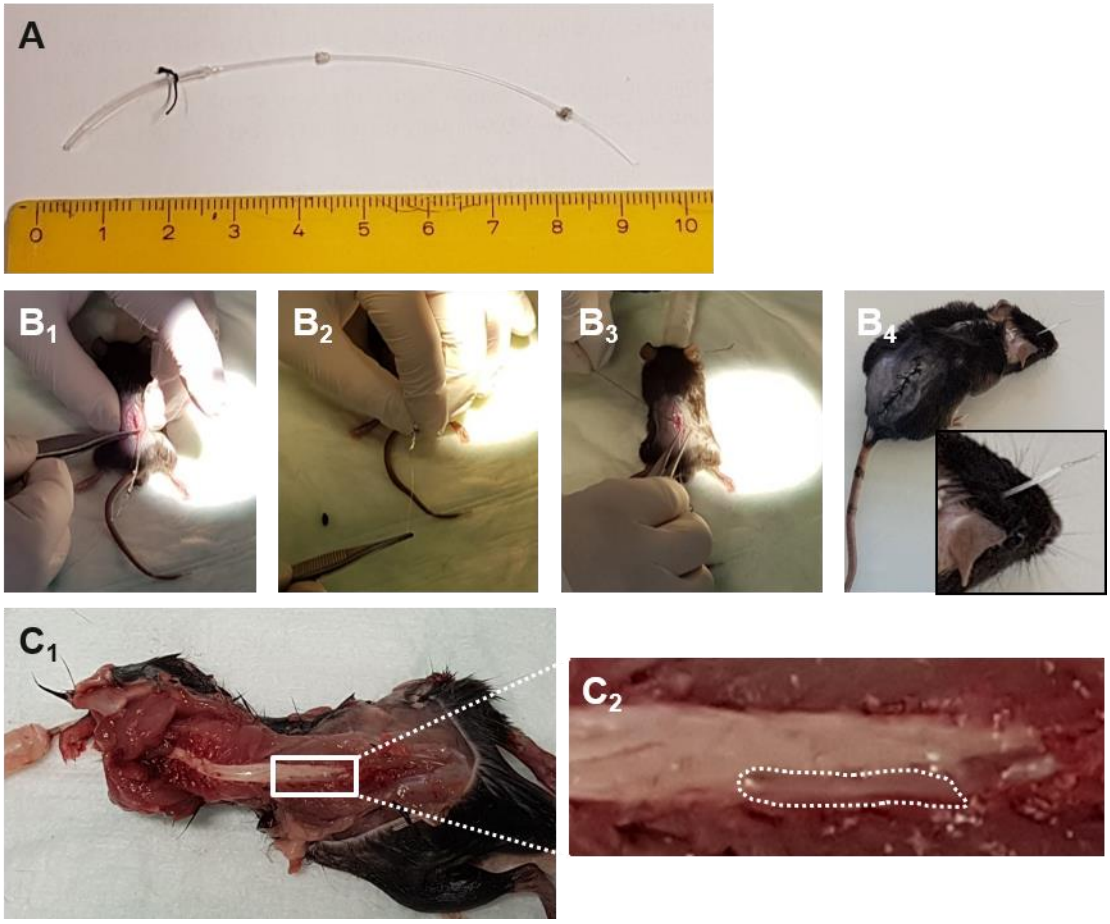

Fig. 6: Intrathecal catheterization of mice. (**A**) Composition of the intrathecal catheter. The catheter had a total length of 12 cm and consisted of two open knots. Left site was the opening coming out of the skin and right site was inserted into the subarachnoidal space of the spinal cord. Scale is in [cm]. (**B_1**) The catheter insertion was performed between lumbar 5 and 6. Surgery was executed by Prof. Dr. Christian Geis (University Hospital Jena, Germany). (**B_2**) The wire supported the stiffness of the catheter during insertion and was removed afterwards. (**B_3** and **B_4**) Catheter was fixed at the knots and the open end was placed through skin between the eyes. (**C_1**) Prove of correct placement of catheter after *in vivo* experiments. (**C_2**) Magnification of square in (**C_1**).The dotted line indicates the position of the catheter.

2.2.8.3 Behavioral experiments with mice

2.2.8.3.1 Rotarod

The Rotarod was performed to test possible changes in motor coordination as a consequence of autoantibody application. Therefore, mice were placed on motorized Rotarod-System (grooved rod Ø 3 cm; 8.5 cm-wide compartments; acceleration speed, 2–40 rpm, maximal recording 300 s, Rotarod 3375-R4, TSE-Systems, Bad Homburg, Germany) that was controlled by the software Rotarod V4.2.5 (4640) (TSE-Systems). The time was automatically stopped until the mice fall down and photo sensor was activated. In total, three rounds of Rotarod were performed with 5 min break in between. Mice were habituated to the Rotarod prior to surgery.

2.2.8.3.2 Open Field

Open Field test was performed 7 d after the surgery to analyze the exploratory behavior and locomotive performance. Therefore, mice were placed in the middle of a quadratic grey box with a size of 40 cm x 40 cm that is open at the top and that was illuminated at 30 lx. The route of the mouse was tracked by a camera (Fg3xCap, camera type VK-1316S, Eneo, Rödermark, Germany) and automatically analyzed with the software ANY-maze (Version 4.99, Stoelting Co, Dublin, Ireland). The total tracking time was 5 min.

2.2.8.3.3 Elevated Plus Maze

Elevated Plus Maze (EPM) was performed two days after the Open Field test to analyze the anxiousness level of the mice. The EPM was equipped with two open and two closed arms (same arms are oppositely positioned) in a total size of 68 cm x 68 cm and a crossover area of the arms of 4.7 cm x 4.7 cm. The illumination in the closed arms amounted 40 lx, in the open arms 140 lx and in the crossover 120 lx. The mice were tracked with the same equipment and software like the Open Field Test. The total recording time was 5 min.

2.2.8.3.4 von Frey test

The sensitivity upon mechanic stimuli was tested using the von Frey test with the up-and-down method (Chaplan et al., 1994). Therefore, the mice were placed in an acrylic glass box standing on a monitoring grid and experiment started 5 min later when the mice calmed down. Von Frey hairs were pricked in the hind paws and the presence or absence of withdrawal was noted. The starting von Frey hair had a force of 0.7 g. When the mice withdrew the paw, it was changed to a thinner filament. A thicker filament was used when there was no withdrawal. In total, six tests were performed on each hind paw.

2.2.9 Statistical analyses

Data sets were tested for statistical significance using the unpaired t-test or otherwise stated in the text. The statistical tests were performed in Excel 2016 (Microsoft Corporation, Redmond, WA, USA) or Origin 9.0 (Originlab Corporation, Northampton, US). Following significance levels were exerted: *p-value<0.05; **p-value<0.01; ***p-value<0.001.
Figures were prepared with the software Origin 9.0, CorelDraw 2017 (CorelCorporation, Ottawa, Canada), Excel 2016 and PowerPoint 2016 (Microsoft Corporation, Redmond, WA, USA). Mean values are shown as bars and error bars depict standard error of the mean (SEM) or otherwise stated.

3. Results

The present study investigates the pathology of GlyR autoantibodies. GlyR autoantibodies have been shown to bind to GlyRα subunits (Doppler et al., 2016), however, the pathology at the molecular level is not yet understood. Following GlyR autoantibody binding and cross-linking of receptors at the cellular surface, GlyRs are internalized and degraded (Carvajal-Gonzalez et al., 2014). As a consequence of autoantibody binding, patients suffer from SPS and elicit massive muscle stiffness and painful spasms (Meinck and Thompson, 2002; Hutchinson et al., 2008; McKeon et al., 2013; Carvajal-Gonzalez et al., 2014; Baizabal-Carvallo and Jankovic, 2015; Martinez-Hernandez et al., 2016). Although therapies exist, relapses often occur for unknown reason (Hutchinson et al., 2008; Damasio et al., 2013; McKeon et al., 2013; Carvajal-Gonzalez et al., 2014; Doppler et al., 2016; Dalmau et al., 2017). Thus, it is necessary to understand the autoantibody pathology in more detail to make it possible to develop further therapeutic options.

3.1 Epitope characterization of GlyRα1 autoantibodies

3.1.1 General binding properties of GlyRα1 autoantibodies

It is known that GlyR autoantibodies bind to GlyRα1, α2 and α3 subunits in a native receptor configuration indicating that the epitope is accessible from the extracellular site to the GlyR. (Carvajal-Gonzalez et al., 2014; Doppler et al., 2016). However, a further detailed analysis of the epitope of GlyR autoantibodies was so far not performed. Within the extracellular domain, most of the amino acid differences between the three α subunits are localized in the far N-terminal region (Fig. 7A). In the present study 9 sera from patients (pat1-9) diagnosed with SPS were investigated. Not all tests were done with all sera as the amount of some sera available for the study was rather limited. First, the patient sera used in this study were tested if the GlyR autoantibodies share the same properties of binding GlyRα1, α2 and α3 homopentameric receptors. Therefore, HEK293 cells were transfected with plasmids encoding GlyRα1, α2 or α3 in combination with GFP as transfection control. Living, non-fixed cells were incubated with patient serum followed by secondary anti-human antibody labeling. The GlyRα1 specific antibody mAb2b (epitope: A^{1}-S^{9} of mature GlyRα1) was used as positive control in GlyRα1 transfected HEK293 cells whereas the pan-α antibody mAb4a (P^{96}-G^{105}, numbers refer to mature GlyRα1 but is conserved between all GlyRα subunits) was used to detect GlyRα2 and α3. All GlyR autoantibody containing patient sera as well as the GlyRα1 specific antibody mAb2b were able to bind the GlyRα1 homopentamers whereas the healthy control serum and the disease control serum showed no fluorescent signal (Fig. 7B). Minor differences among the patient autoantibodies were detected in the binding of GlyRα2. GlyRα2 was strongly bound by patient 1-4, 7 and 9 autoantibodies as well as mAb4a whereas autoantibodies from patient

6 and 8 exhibited weak binding (Fig. 7C). For patient 5 serum as well as healthy and disease control serum, no fluorescent signal was detectable. Patient 2-4 serum containing autoantibodies were able to bind to GlyRα3 subunits in addition, whereas patient 1 and 5 as well as healthy control serum were not attaching to the GlyRα3 (Fig. 7D). The homopentameric GlyRα3 was strongly bound by the pan-α antibody mab4a.

All patient sera recognized the GlyRα1 subunit under native conditions. Commercial tests for the identification of the autoantibody target mainly use fixed cells and work under denatured conditions. Moreover, it was shown before that patient sera were negatively evaluated by commercial tests but positively evaluated using native conditions as also used in our lab. Therefore, it was analyzed if patient GlyR autoantibodies are able to bind the GlyR in fixed and permeabilized cells. Incubation with patient serum 2-5 resulted in a strong fluorescent signal whereas no signal was detectable when patient 1 serum or healthy control serum was applied to the cells (Fig. 8A). The mAb4a control showed, however, a brighter signal compared to the positive patient sera. MAb4a was used here because mAb2b cannot bind the GlyR in its denatured conformation.

Most of the patient samples that are available in our lab are serum samples. From patient 1 we possess serum, purified IgG as well as cerebrospinal fluid (CSF). Immunocytochemical stainings were performed to test whether these three samples of the same patient are able to bind GlyRα1. Indeed, incubation of GlyRα1 transfected HEK293 cells with patient 1 serum, purified IgG and CSF resulted in a dotted fluorescent signal surrounding the HEK293 cells in all samples (Fig. 8B). Beyond the binding ability to GlyRs following overexpression in HEK293 cells, patient autoantibodies were able to bind to GlyRs expressed in cultured motoneurons (21 days *in vitro*) (Fig. 8C, Supplementary fig. 1). The staining pattern is comparable to the mAb2b control. In comparison, the healthy control serum was unable to label motoneurons. MAP2 or synaptophysin were co-stained for identification of neurons in the cultures.

A

```
GlyRα1WT   01 •••••MYSFNTLRLYLWETIVFFSLAASKEAEAARSAPKP•••MSPSDFLDKLMGRTSGY  52
GlyRα2WT   01 •MNRQLVNILTALFAFFLETNHFRTAFCKDHDS•RSGKQPSQTLSPSDFLDKLMGRTSGY  58
GlyRα3WT   01 MAHVRHFRTLVSGFYFWEAALLLSLVATKETDSARSRSAP•••MSPSDFLDKLMGRTSGY  57

GlyRα1WT   53 DARIRPNFKGPPVNVSCNIFINSFGSIAETTMDYRVNIFLRQQWNDPRLAYNEYPDDSLD 112
GlyRα2WT   59 DARIRPNFKGPPVNVTCNIFINSFGSVTETTMDYRVNIFLRQQWNDSRLAYSEYPDDSLD 118
GlyRα3WT   58 DARIRPNFKGPPVNVTCNIFINSFGSIAETTMDYRVNIFLRQKWNDPRLAYSEYPDDSLD 117

GlyRα1WT  113 LDPSMLDSIWKPDLFFANEKGAHFHEITTDNKLLRISRNGNVLYSIRITLTLACPMDLKN 172
GlyRα2WT  119 LDPSMLDSIWKPDLFFANEKGANFHDVTTDNKLLRISKNGKVLYSIRLTLTLSCPMDLKN 178
GlyRα3WT  118 LDPSMLDSIWKPDLFFANEKGANFHEVTTDNKLLRIFKNGNVLYSIRLTLTLSCPMDLKN 177

GlyRα1WT  173 FPMDVQTCIMQLESFGYTMNDLIFEWQEQGAVQVADGLTLPQFILKEEKDL......HNQ 421
GlyRα2WT  179 FPMDVQTCTMQLESFGYTMNDLIFEWLSDGPVQVAEGLTLPQFILKEEKEL......HKK 452
GlyRα3WT  178 FPMDVQTCIMQLESFGYTMNDLIFEWQDEAPVQVAEGLTLPQFLLKEEKDL......QQD 421
```

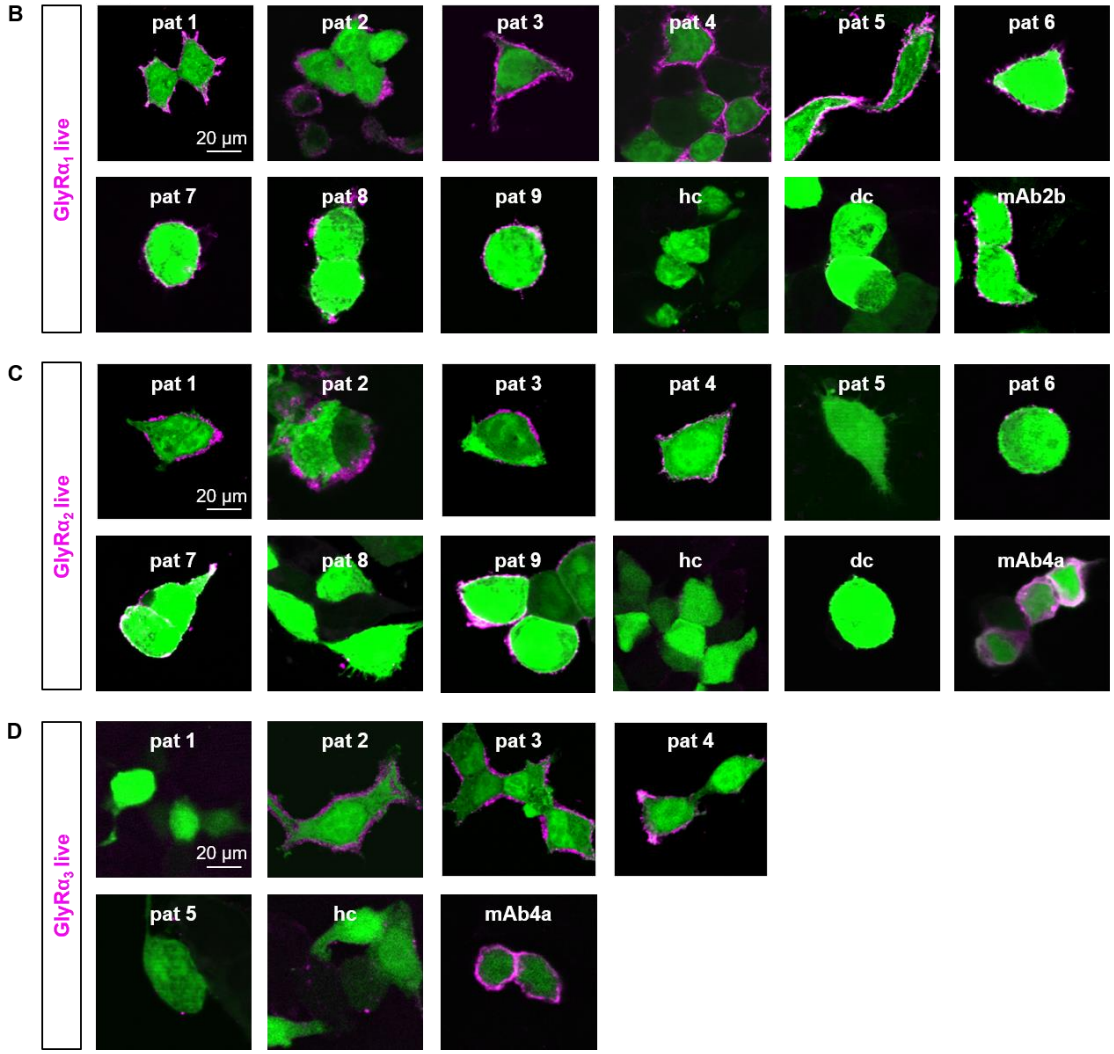

Fig. 7: GlyR autoantibodies bind to different GlyRα subunits. (**A**) Amino acid alignment of human GlyR subunits α1-α3. Start of mature protein is indicated by yellow mark and amino acid deviations are shown in bold letters. The epitope of the pan-α antibody mAb4a is depicted in blue and underlined letters (α1 and α3: residues 96-105, α2: residues 103-112 of mature protein), whereas the epitope of the GlyRα1 specific antibody mAb2b is indicated by black underline (residues 1-10 of mature protein). (**B**) Immunocytochemical stainings of GlyRα1 and GFP (green) co-transfected HEK293 cells that were incubated with patient autoantibodies or mAb2b (magenta). (**C**) Same like in (**B**) but HEK293 cells were transfected with GlyRα2 and GFP. (**D**) Same like in (**B**) or (**C**) but staining of HEK293 cells transfected with GlyRα3 and GFP. dc = disease control; hc = healthy control; pat = patient; WT = wildtype.

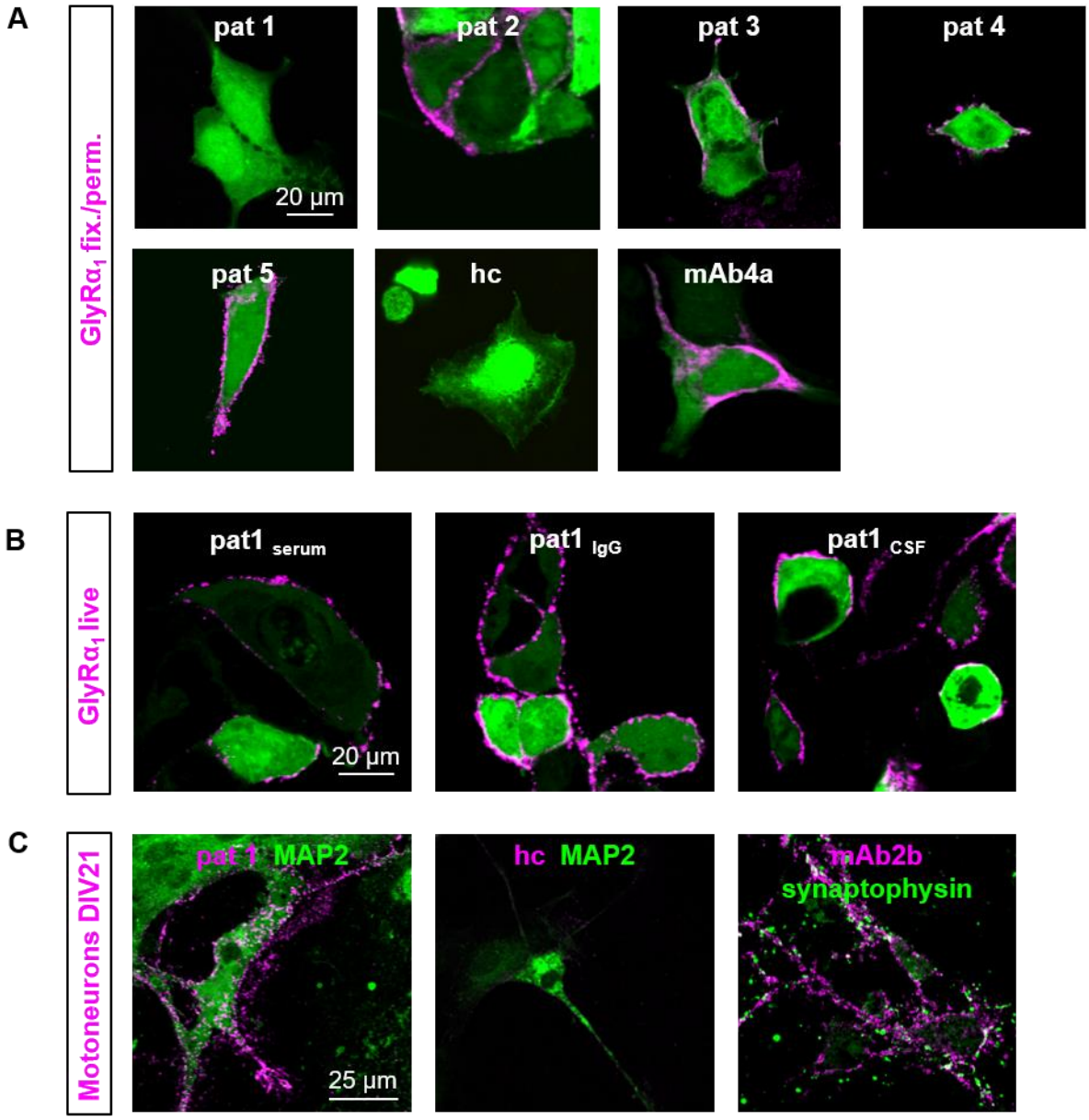

Fig. 8: GlyRα1 autoantibodies in serum and CSF as well as purified IgG bind to cell lines and primary neurons. (**A**) Immunocytochemical staining of fixed and permeabilized HEK293 cells that were transfected with GlyRα1 and GFP (green). Cells were incubated with patient sera, healthy control serum or mAb4a (magenta). (**B**) Serum, IgG and CSF of patient 1 (magenta) were applied to GlyRα1 and GFP (green) co-transfected HEK293 cells and stained with the live staining method. (**C**) Cultivated mixed motoneuron cultures at an age of 21 days *in vitro* (DIV) were stained with patient autoantibodies or mAb2b (magenta) and neuronal markers MAP2 or synaptophysin (green). CSF = cerebrospinal fluid; hc = healthy control; pat = patient.

Additionally to single staining of living cells or fixed and permeabilized cells, double staining of GlyRα1 transfected HEK293 cells was performed by first incubating the living cells with patient autoantibodies followed by fixation and permeabilization of the cells. Then, patient autoantibodies were incubated again thereby using a different secondary antibody. Thus, this method allowed staining of both cell surface (native GlyRα1) and intracellular GlyR protein

(denatured GlyRα1). The tested patient sera 1-5 and 8 showed surface and intracellular binding ability (Fig. 9). A similar staining pattern was identified with control antibody mAb4a. These results suggest that the autoantibodies are able to detect both the native and denatured GlyRα1.

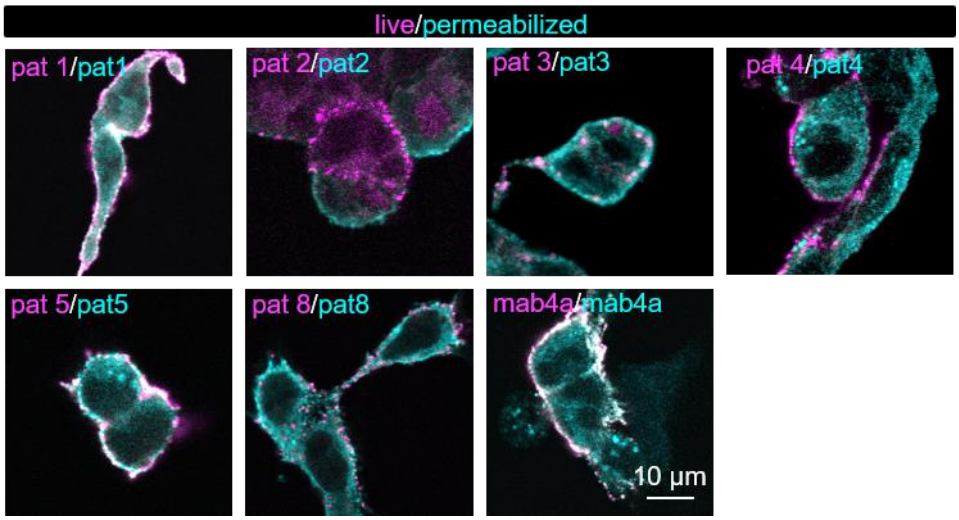

Fig. 9: Staining of native and denatured GlyRα1 with autoantibodies. Patient serum or mAb4a (magenta) was first applied to living GlyRα1 transfected HEK293 cells to target the native GlyRα1. Cells were fixed, permeabilized and incubated with patient serum or mAb4a again (cyan) to target the denatured GlyRα1. pat = patient. Due to a lack of sufficient serum, patient 6 and 7 were skipped in this experiment.

The conditions for the autoantibody binding were clarified. The first staining in this study showed that all of the tested patient autoantibodies bind to native GlyRα1 in live staining conditions whereas there are some sera that do not contain autoantibodies against the GlyRα2 or α3 (Fig. 7B-D). Main amino acid differences of these subunits are located in the far N-terminal region (Fig. 7A) including the epitope of the GlyRα1 specific antibody mAb2b. Competition analyses of patient autoantibodies with mAb2b were performed to investigate if the autoantibody epitope differs from the mAb2b epitope and if the autoantibodies are able to replace mAb2b from its binding site and vice versa. Therefore, patient 1 serum was simultaneously incubated with mAb2b for 2 h whereas patient 1 serum was diluted 1:50 and mAb2b dilution varied from 1:50 to 1:2000 (1:50 and 1:100, Fig. 10A upper row; 1:500, 1:1000 and 1:2000, Fig. 10B upper row). Both fluorescent signals were strongly colocalized regardless of mAb2b concentration. Additionally, possible antibody replacements were tested by first incubating with patient 1 serum for 1 h followed by 1 h incubation with mAb2b (Fig. 10A, B middle row) and vice versa (Fig. 10A, B lower row). Same mAb2b dilutions like for simultaneous incubations were used. The successive incubation of patient 1 autoantibodies and mAb2b in both orders resulted in a similar staining pattern like simultaneous incubation.

These results demonstrate that patient 1 autoantibodies and mAb2b do not compete for the same epitope. The data are in line with the binding of patient autoantibodies to GlyRα1 but also to other α subunits of the GlyR. For verification of saturating conditions during competition experiments, GlyRα1 transfected HEK293 cells were twice incubated with patient autoantibodies or twice with mAb2b. The first but not the second incubation of patient 1 serum resulted in fluorescent signal (Fig. 11A). MAb2b was tested in a 1:50 and 1:500 dilution resulting in a weak signal in the second incubation using the 1:50 dilution whereas in 1:500 dilution, no signal from the second incubation was detectable (Fig. 11B). These results verified that the assay was performed under saturating antibody concentrations.

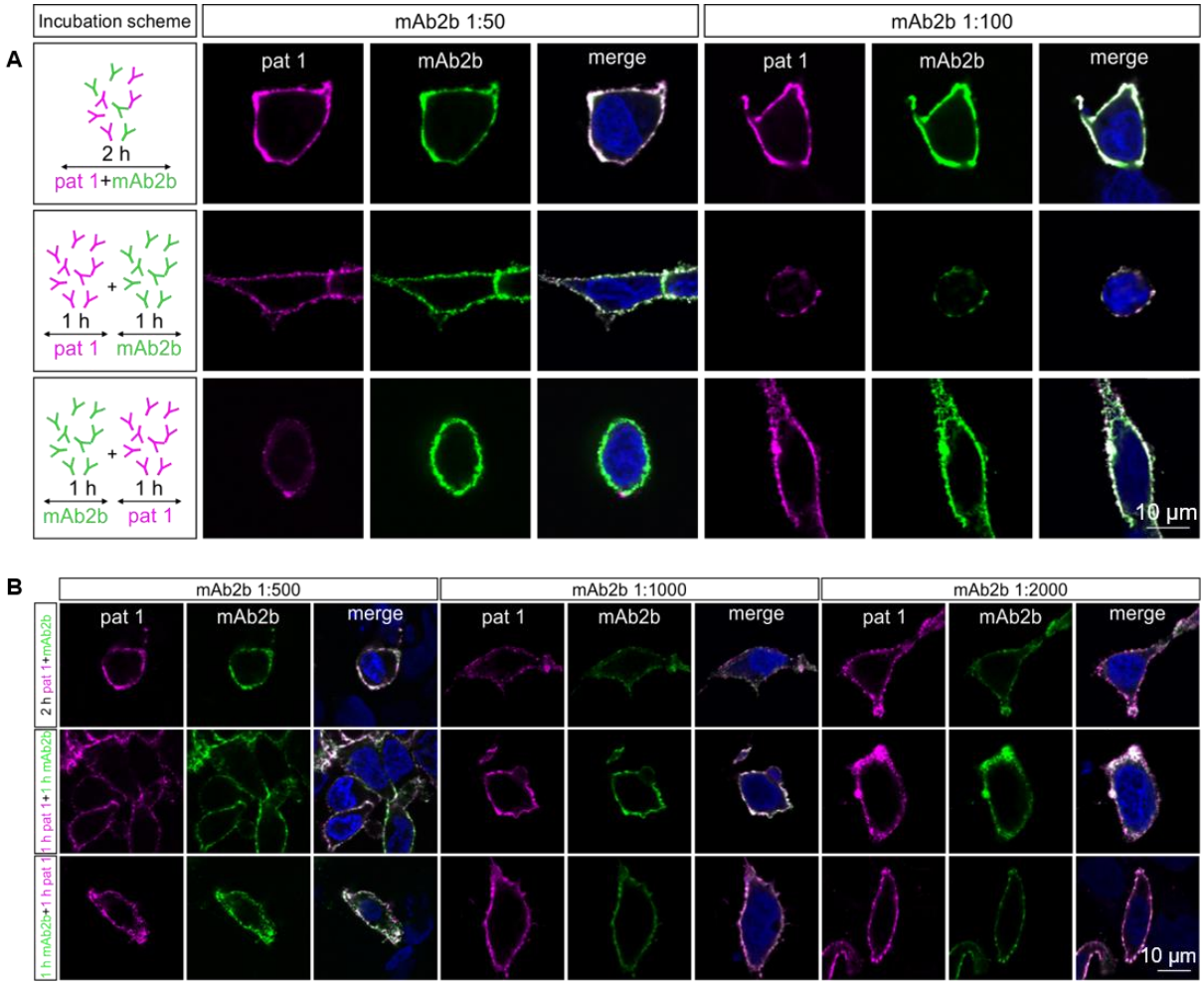

Fig. 10: Epitope competition of patient 1 autoantibodies and mAb2b. (**A**) GlyRα1 transfected HEK293 cells were incubated with patient 1 serum (magenta) and mAb2b (green) simultaneously for 2 h (upper row) or consecutively for 1 h each (middle and lower row). DAPI staining (blue) was included and shown in the merged picture. Incubation scheme is presented on the left and staining on the right. MAb2b antibody was used in different concentrations (1:50 and 1:100). (**B**) Same like in (**A**) but mAb2b concentrations of 1:500, 1:1000 and 1:2000 were used. pat = patient.

In summary, patient GlyRα1 autoantibodies are able to bind native and denatured GlyRα1 and some recognize the GlyRα2 and α3 subunit using live staining procedures. Furthermore, GlyRα autoantibodies in patient sera bind to cultured motoneurons. In addition, autoantibodies are not only present in serum of SPS patients but also in CSF. Purified IgG from patient serum provides strong binding to GlyRα1. Competition experiments showed that patient autoantibodies do not compete with mAb2b for the same epitope, but the epitopes might be located in the same region.

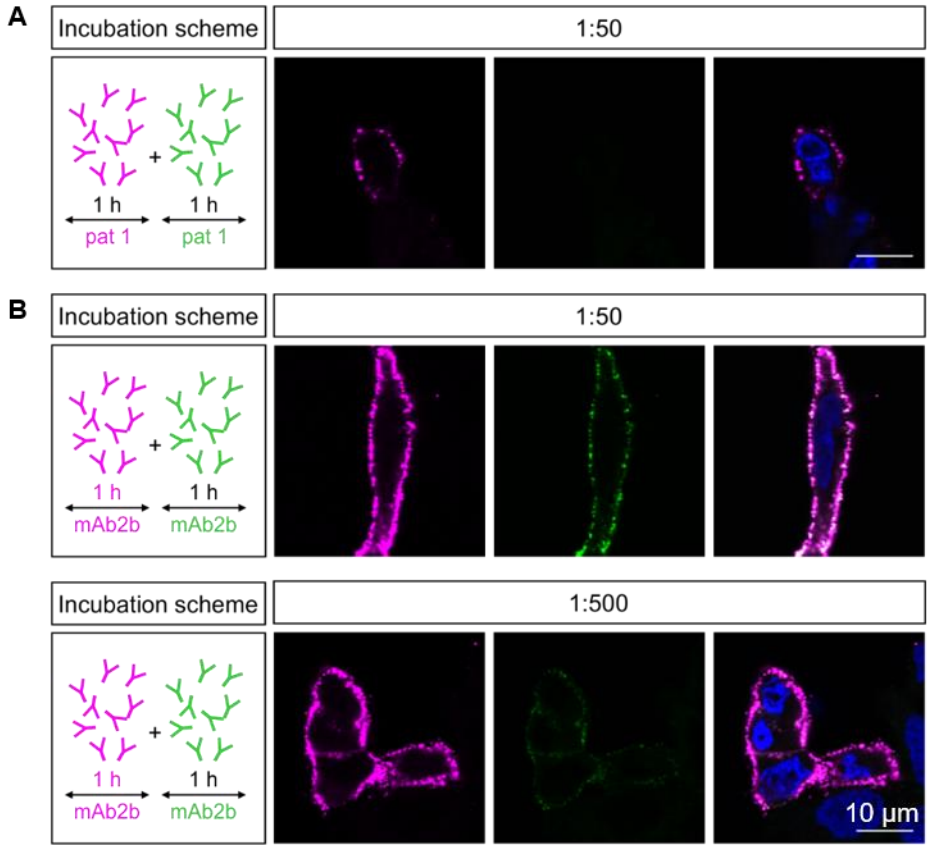

Fig. 11: Epitope saturation by patient 1 autoantibodies and mAb2b. (**A**) GlyRα1 transfected HEK293 cells were incubated twice with patient 1 serum for 1 h and stained with two different secondary antibodies (magenta and green). Patient 1 serum was diluted 1:50. (**B**) Same like in (**A**) but double-staining with mAb2b in a concentration of 1:50 (top) and 1:500 (bottom). pat = patient.

3.1.2 Autoantibody epitope characterization by GlyR mutants

Mutations in the GlyRα1 lead to the human disease hyperekplexia (Startle disease) which causes similar symptoms in human patients like the SPS. Similarly, rodents carrying a mutation in the GlyR suffer from startle disease. Two murine startle disease mutations are located in the far N-terminus of the GlyRα1, namely the *spasmodic* mutation (GlyRα1^{A52S}, Fig. 12A, magenta)

and the *shaky* mutation (GlyRα1^{Q177K}, Fig. 12A, cyan) (Ryan et al., 1994; Saul et al., 1994; Schaefer et al., 2017; Schaefer et al., 2018b). HEK293 cells were transfected with the plasmids encoding the murine mutated receptor variants GlyRα1^{A52S} or GlyRα1^{Q177K} and incubated with patient autoantibodies to test whether the amino acid changes influence the binding properties of autoantibodies. It was shown before that patient autoantibodies bind to human as well as murine GlyRα1 subunits (unpublished). Patient 1 and 4 autoantibodies were used exemplarily for this experiment because both showed strong binding in normal GlyRα1 live stainings and we possess sufficient amount of the sera. Both the patient 1 and patient 4 autoantibodies exhibited binding capability like the GlyRα1 specific antibody mAb2b when HEK293 cells were co-transfected with GFP and the GlyRα1^{A52S} carrying the *spasmodic* mutation (Fig. 12B). In comparison, no fluorescent signal was visible when cells were incubated with healthy control serum. Same observations were made when HEK293 cells were transfected with GlyRα1^{Q177K} harboring the *shaky* mutation. Patient 1 and 4 autoantibodies as well as mAb2b were able to bind to GlyRα1^{Q177K} but healthy control was not able to bind (Fig. 12C).

A

```
GlyRα1WT     01 MYSFNTLRLYLWETIVFFSLAASKEAEAARSAPKPMSPSDFLDKLMGRTSGYDAR  55
GlyRα1A52S   01 MYSFNTLRLYLWETIVFFSLAASKEAEAARSAPKPMSPSDFLDKLMGRTSGYDAR  55
GlyRα1Q177K  01 MYSFNTLRLYLWETIVFFSLAASKEAEAARSAPKPMSPSDFLDKLMGRTSGYDAR  55

GlyRα1WT     56 IRPNFKGPPVNVSCNIFINSFGSIAETTMDYRVNIFLRQQWNDPRLAYNEYPDDS 110
GlyRα1A52S   56 IRPNFKGPPVNVSCNIFINSFGSISETTMDYRVNIFLRQQWNDPRLAYNEYPDDS 110
GlyRα1Q177K  56 IRPNFKGPPVNVSCNIFINSFGSIAETTMDYRVNIFLRQQWNDPRLAYNEYPDDS 110

GlyRα1WT    111 LDLDPSMLDSIWKPDLFFANEKGAHFHEITTDNKLLRISRNGNVLYSIRITLTLA 165
GlyRα1A52S  111 LDLDPSMLDSIWKPDLFFANEKGAHFHEITTDNKLLRISRNGNVLYSIRITLTLA 165
GlyRα1Q177K 111 LDLDPSMLDSIWKPDLFFANEKGAHFHEITTDNKLLRISRNGNVLYSIRITLTLA 165

GlyRα1WT    166 CPMDLKNFPMDVQTCIMQLESFGYTMNDLIFEWQEQGAVQVADGLTL.....HNQ 421
GlyRα1A52S  166 CPMDLKNFPMDVQTCIMQLESFGYTMNDLIFEWQEQGAVQVADGLTL.....HNQ 421
GlyRα1Q177K 166 CPMDLKNFPMDVQTCIMQLESFGYTMNDLIFEWQEQGAVKVADGLTL.....HNQ 421
```

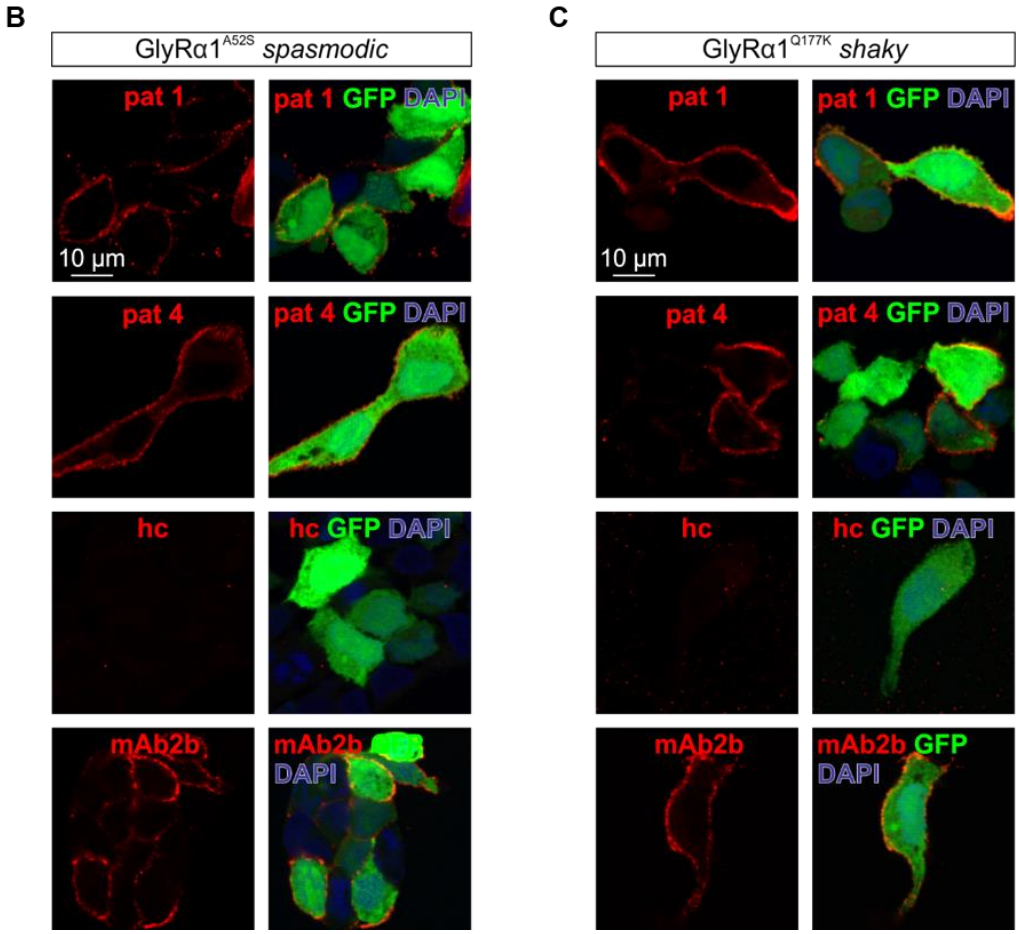

Fig. 12: Autoantibody binding to hyperekplexia mutants *spasmodic* and *shaky*. (**A**) Amino acid alignment of wildtype GlyRα1, startle disease mutants *spasmodic* (GlyRα1^{A52S}) and *shaky* (GlyRα1^{Q177K}). Start of mature protein is marked in yellow. MAb2b epitope is indicated by black line and mAb4a epitope is shown in blue underlined. The *spasmodic* mutation A52S (number refers to mature protein) is displayed in magenta and the *shaky* mutation Q177K in cyan. (**B**) GlyRα1^{A52S} and GFP (green) co-transfected HEK293 cells were incubated with patient serum, healthy control serum or mAb2b (red). DAPI staining (blue) was included in merged picture (right). (**C**) Immunostaining of GlyRα1^{Q177K} and GFP (green) co-transfected HEK293 cells with patient serum, healthy control or mAb2b (red). DAPI staining (blue) is shown in merged picture (right). hc = healthy control; pat = patient; WT = wildtype.

As some but not all patient sera bound to α2 and/or α3 GlyRs, the amino acid sequence of the whole extracellular domain (ECD) of GlyRα1 was compared with GlyRα2 and α3. The comparison yield that there are further but only single amino acid changes beside the differences in the N-terminal region (Fig. 7A). To test if mutations in the more conserved region in the ECD influence the binding ability of GlyRα1 autoantibodies, several further single and multiple amino acid exchanges were integrated into GlyRα1 and α3 (Tab. 22, Fig. 13). HEK293 cells were transfected with these different GlyRα1 or GlyRα3 variants and incubated exemplarily with patient 1 serum to test if the autoantibodies are able to bind to the mutated GlyRs. Patient 1 autoantibodies bound GlyRα1^{WT} as well as mutated clones 1-2 and 4-7 deviated from GlyRα1^{WT} (Fig. 14). No fluorescent signal was visible when clone 3 transfected HEK293 cells were incubated with patient 1 serum. Incubation of GlyRα3^{WT} transfected HEK293 cells with patient 1 serum resulted in no fluorescent signal compared to clone 8 where a fluorescent signal was detectable. In addition, autoantibodies were not able to bind HEK293 cells transfected with clone 9 and 10. The GlyRα1 specific antibody mAb2b was able to bind GlyRα1^{WT} and all clones deviated from GlyRα1^{WT} (clone 1-7) except clone 3 (Fig. 15A). Neither GlyRα3^{WT} nor clone 8-10 were bound by mAb2b. In comparison, wildtype GlyRα1 and α3 as well as clones 1-10 were strongly bound by the pan-α antibody mAb4a (Fig. 15B).These data provide some hints that the autoantibody epitope could be in the far N-terminus of the GlyRα1. Interestingly, the sequence of clone 8 seems to play an important role in autoantibody binding since clone 8 was bound by patient 1 autoantibodies but GlyRα3^{WT} not. For verification that these are general binding characteristics of GlyRα autoantibodies, other patient samples have to be tested in the future.

Tab. 22: Summary of tested GlyRα1 and GlyRα3 clones.

Clone number	Clone
1	**GlyRα$_1^{I132L,A137S}$**
2	**GlyRα$_1^{I132L,A137S,E173D,Q174E,G175A,A176P}$**
3	**GlyRα$_1^{A4R,P5S,K6A}$**
4	**GlyRα$_1^{N76S}$**
5	**GlyRα$_1^{H107N}$**
6	**GlyRα$_1^{S121F,R122K}$**
7	**GlyRα$_1^{A212V}$**
8	**GlyRα$_3^{L132I,S137A}$**
9	**GlyRα$_3^{L132I,S137A,D172E,E173Q,A174G,P175A}$**
10	**GlyRα$_3^{R4A,S5P,A6K}$**

Numbers refer to mature protein. Clones were made by Barbara Schleyer, AG Villmann.

```
GlyRα1WT    01 •••••MYSFNTLRLYLWETIVFFSLAASKEAEAARSAPKPMSPSDFLDKLMGRTSGYDARIRP  58
Clone 1     01 •••••MYSFNTLRLYLWETIVFFSLAASKEAEAARSAPKPMSPSDFLDKLMGRTSGYDARIRP  58
Clone 2     01 •••••MYSFNTLRLYLWETIVFFSLAASKEAEAARSAPKPMSPSDFLDKLMGRTSGYDARIRP  58
Clone 3     01 •••••MYSFNTLRLYLWETIVFFSLAASKEAEAARSRSAPMSPSDFLDKLMGRTSGYDARIRP  58
Clone 4     01 •••••MYSFNTLRLYLWETIVFFSLAASKEAEAARSAPKPMSPSDFLDKLMGRTSGYDARIRP  58
Clone 5     01 •••••MYSFNTLRLYLWETIVFFSLAASKEAEAARSAPKPMSPSDFLDKLMGRTSGYDARIRP  58
Clone 6     01 •••••MYSFNTLRLYLWETIVFFSLAASKEAEAARSAPKPMSPSDFLDKLMGRTSGYDARIRP  58
Clone 7     01 •••••MYSFNTLRLYLWETIVFFSLAASKEAEAARSAPKPMSPSDFLDKLMGRTSGYDARIRP  58
GlyRα3WT    01 MAHVRHFRTLVSGFYFWEAALLLSLVATKETDSARSRSAPMSPSDFLDKLMGRTSGYDARIRP  63
Clone 8     01 MAHVRHFRTLVSGFYFWEAALLLSLVATKETDSARSRSAPMSPSDFLDKLMGRTSGYDARIRP  63
Clone 9     01 MAHVRHFRTLVSGFYFWEAALLLSLVATKETDSARSRSAPMSPSDFLDKLMGRTSGYDARIRP  63
Clone 10    01 MAHVRHFRTLVSGFYFWEAALLLSLVATKETDSARSAPKPMSPSDFLDKLMGRTSGYDARIRP  63

GlyRα1WT    59 NFKGPPVNVSCNIFINSFGSIAETTMDYRVNIFLRQQWNDPRLAYNEYPDDSLDLDPSMLDSI 121
Clone 1     59 NFKGPPVNVSCNIFINSFGSIAETTMDYRVNIFLRQQWNDPRLAYNEYPDDSLDLDPSMLDSI 121
Clone 2     59 NFKGPPVNVSCNIFINSFGSIAETTMDYRVNIFLRQQWNDPRLAYNEYPDDSLDLDPSMLDSI 121
Clone 3     59 NFKGPPVNVSCNIFINSFGSIAETTMDYRVNIFLRQQWNDPRLAYNEYPDDSLDLDPSMLDSI 121
Clone 4     59 NFKGPPVNVSCNIFINSFGSIAETTMDYRVNIFLRQQWNDPRLAYSEYPDDSLDLDPSMLDSI 121
Clone 5     59 NFKGPPVNVSCNIFINSFGSIAETTMDYRVNIFLRQQWNDPRLAYNEYPDDSLDLDPSMLDSI 121
Clone 6     59 NFKGPPVNVSCNIFINSFGSIAETTMDYRVNIFLRQQWNDPRLAYNEYPDDSLDLDPSMLDSI 121
Clone 7     59 NFKGPPVNVSCNIFINSFGSIAETTMDYRVNIFLRQQWNDPRLAYNEYPDDSLDLDPSMLDSI 121
GlyRα3WT    64 NFKGPPVNVTCNIFINSFGSIAETTMDYRVNIFLRQKWNDPRLAYSEYPDDSLDLDPSMLDSI 126
Clone 8     64 NFKGPPVNVTCNIFINSFGSIAETTMDYRVNIFLRQKWNDPRLAYSEYPDDSLDLDPSMLDSI 126
Clone 9     64 NFKGPPVNVTCNIFINSFGSIAETTMDYRVNIFLRQKWNDPRLAYSEYPDDSLDLDPSMLDSI 126
Clone 10    64 NFKGPPVNVTCNIFINSFGSIAETTMDYRVNIFLRQKWNDPRLAYSEYPDDSLDLDPSMLDSI 126

GlyRα1WT   122 WKPDLFFANEKGAHFHEITTDNKLLRISRNGNVLYSIRITLTLACPMDLKNFPMDVQTCIMQL 184
Clone 1    122 WKPDLFFANEKGAHFHEITTDNKLLRISRNGNVLYSIRLTLTLSCPMDLKNFPMDVQTCIMQL 184
Clone 2    122 WKPDLFFANEKGAHFHEITTDNKLLRISRNGNVLYSIRLTLTLSCPMDLKNFPMDVQTCIMQL 184
Clone 3    122 WKPDLFFANEKGAHFHEITTDNKLLRISRNGNVLYSIRITLTLACPMDLKNFPMDVQTCIMQL 184
Clone 4    122 WKPDLFFANEKGAHFHEITTDNKLLRISRNGNVLYSIRITLTLACPMDLKNFPMDVQTCIMQL 184
Clone 5    122 WKPDLFFANEKGANFHEITTDNKLLRISRNGNVLYSIRITLTLACPMDLKNFPMDVQTCIMQL 184
Clone 6    122 WKPDLFFANEKGAHFHEITTDNKLLRIFKNGNVLYSIRITLTLACPMDLKNFPMDVQTCIMQL 184
Clone 7    122 WKPDLFFANEKGAHFHEITTDNKLLRIFKNGNVLYSIRITLTLACPMDLKNFPMDVQTCIMQL 184
GlyRα3WT   127 WKPDLFFANEKGANFHEVTTDNKLLRIFKNGNVLYSIRLTLTLSCPMDLKNFPMDVQTCIMQL 189
Clone 8    127 WKPDLFFANEKGANFHEVTTDNKLLRIFKNGNVLYSIRITLTLACPMDLKNFPMDVQTCIMQL 189
Clone 9    127 WKPDLFFANEKGANFHEVTTDNKLLRIFKNGNVLYSIRITLTLACPMDLKNFPMDVQTCIMQL 189
Clone 10   127 WKPDLFFANEKGANFHEVTTDNKLLRIFKNGNVLYSIRLTLTLSCPMDLKNFPMDVQTCIMQL 189

GlyRα1WT   185 ESFGYTMNDLIFEWQEQGAVQVADGLTLPQFILKEEKDLRYCTKHYNTGKFTCIEAR...HNQ 421
Clone 1    185 ESFGYTMNDLIFEWQEQGAVQVADGLTLPQFILKEEKDLRYCTKHYNTGKFTCIEAR...HNQ 421
Clone 2    185 ESFGYTMNDLIFEWQDEAPVQVADGLTLPQFILKEEKDLRYCTKHYNTGKFTCIEAR...HNQ 421
Clone 3    185 ESFGYTMNDLIFEWQEQGAVQVADGLTLPQFILKEEKDLRYCTKHYNTGKFTCIEAR...HNQ 421
Clone 4    185 ESFGYTMNDLIFEWQEQGAVQVADGLTLPQFILKEEKDLRYCTKHYNTGKFTCIEAR...HNQ 421
Clone 5    185 ESFGYTMNDLIFEWQEQGAVQVADGLTLPQFILKEEKDLRYCTKHYNTGKFTCIEAR...HNQ 421
Clone 6    185 ESFGYTMNDLIFEWQEQGAVQVADGLTLPQFILKEEKDLRYCTKHYNTGKFTCIEAR...HNQ 421
Clone 7    185 ESFGYTMNDLIFEWQEQGAVQVADGLTLPQFILKEEKDLRYCTKHYNTGKFTCIEVR...HNQ 421
GlyRα3WT   190 ESFGYTMNDLIFEWQDEAPVQVAEGLTLPQFLLKEEKDLRYCTKHYNTGKFTCIEVR...QQD 421
Clone 8    190 ESFGYTMNDLIFEWQDEAPVQVAEGLTLPQFLLKEEKDLRYCTKHYNTGKFTCIEVR...QQD 421
Clone 9    190 ESFGYTMNDLIFEWQEQGAVQVAEGLTLPQFLLKEEKDLRYCTKHYNTGKFTCIEVR...QQD 421
Clone 10   190 ESFGYTMNDLIFEWQDEAPVQVAEGLTLPQFLLKEEKDLRYCTKHYNTGKFTCIEVR...QQD 421
```

Fig. 13: Alignment of GlyRα1 and GlyRα3 clones containing different mutations. Clones and GlyRα3^{WT} were compared to GlyRα1^{WT}. Start of mature protein is indicated by yellow mark and mutations were shown in red. Amino acid deviations are depicted in bold letters. Epitope of mAb2b is indicated by underlined amino acids and mAb4a epitope is presented in blue underlined letters. Clone numbers and referring mutations are summarized in Tab. 22. WT = wildtype.

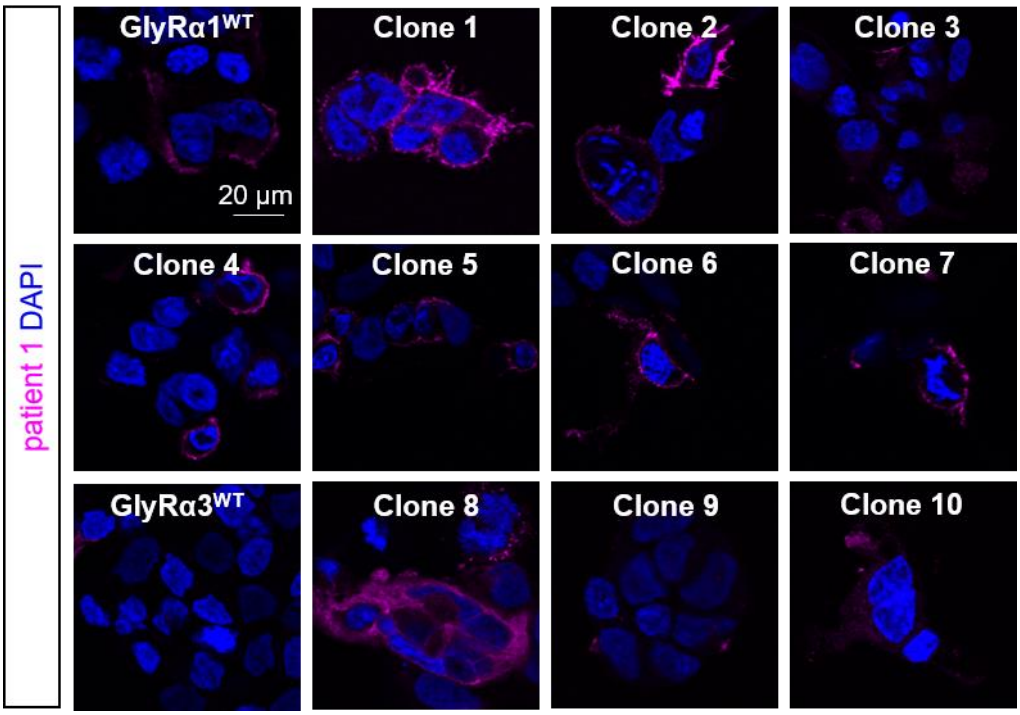

Fig. 14: Epitope characterization of autoantibodies with different GlyRα1 and GlyRα3 mutations. Immunocytochemical stainings of HEK293 cells transfected with GlyRα1^{WT}, GlyRα3^{WT} or one of the different clones (clones 1-10). Cells were stained with patient 1 serum (magenta) and DAPI (blue). Clone numbers and referring mutations are summarized in Tab. 22. WT = wildtype.

The zebrafish GlyRα1^{dr} subunit differs from human GlyRα1^{hs} mainly in the N-terminal part (Fig. 16A). Therefore, the zebrafish GlyRα1 was used as model to test the hypothesis of the far N-terminus as part of the autoantibody binding epitope. In addition, a chimera containing the N-terminus of human GlyRα1^{hs} followed by zebrafish GlyRα1^{dr} (edge at glycine residue at position 34 of mature GlyRα1^{hs}) was created and used for verification (Fig. 16A, B). Initial tests for this experiment were done by Niels v. Wardenburg (AG Villmann). HEK293 cells transfected with GlyRα1^{hs} were bound by autoantibodies from all tested patients (pat1-5 and 8) as well as mAb2b and mAb4a (Fig. 16C). Solely the healthy control serum showed no signal when incubated with GlyRα1^{hs} transfected HEK293 cells. However, when cells were transfected with GlyRα1^{dr}, exclusively mA4a and patient 4 autoantibodies were able to bind. Additionally, patient 8 incubated cells exhibited a weak fluorescent signal. All other patient sera, patient 1-3 and 5 were not able to bind GlyRα1^{dr}. When the N-terminal region of GlyRα1^{dr} was exchanged to GlyRα1^{hs} (chimera, GlyRα1^{ch}), these patient autoantibodies were able to bind the chimera GlyRα1^{ch} again. All patient sera as well as mAb2b and mAb4a controls showed fluorescent signals when incubated with GlyRα1^{ch}. Only in the negative control with serum from a healthy patient, no fluorescent signal was detectable. These data provided hints that the N-terminal region of GlyRα1^{hs} plays an important role in autoantibody binding.

For deeper insights in the area of autoantibody binding, the N-terminus of the chimera GlyRα1^{ch} was structurally investigated (Fig. 17A). This part of the receptor harbors the first α-

helical element and is located at the outermost part of the extracellular domain in a 3D model based on the zebrafish GlyRα1 cryo-EM structure (Fig. 17B) (Du et al., 2015). This position is easily accessible to GlyRα1 autoantibodies. In comparison, the mAb4a binding site is located deeper in the ion channel structure at the interface of two adjacent subunits within the extracellular domain.

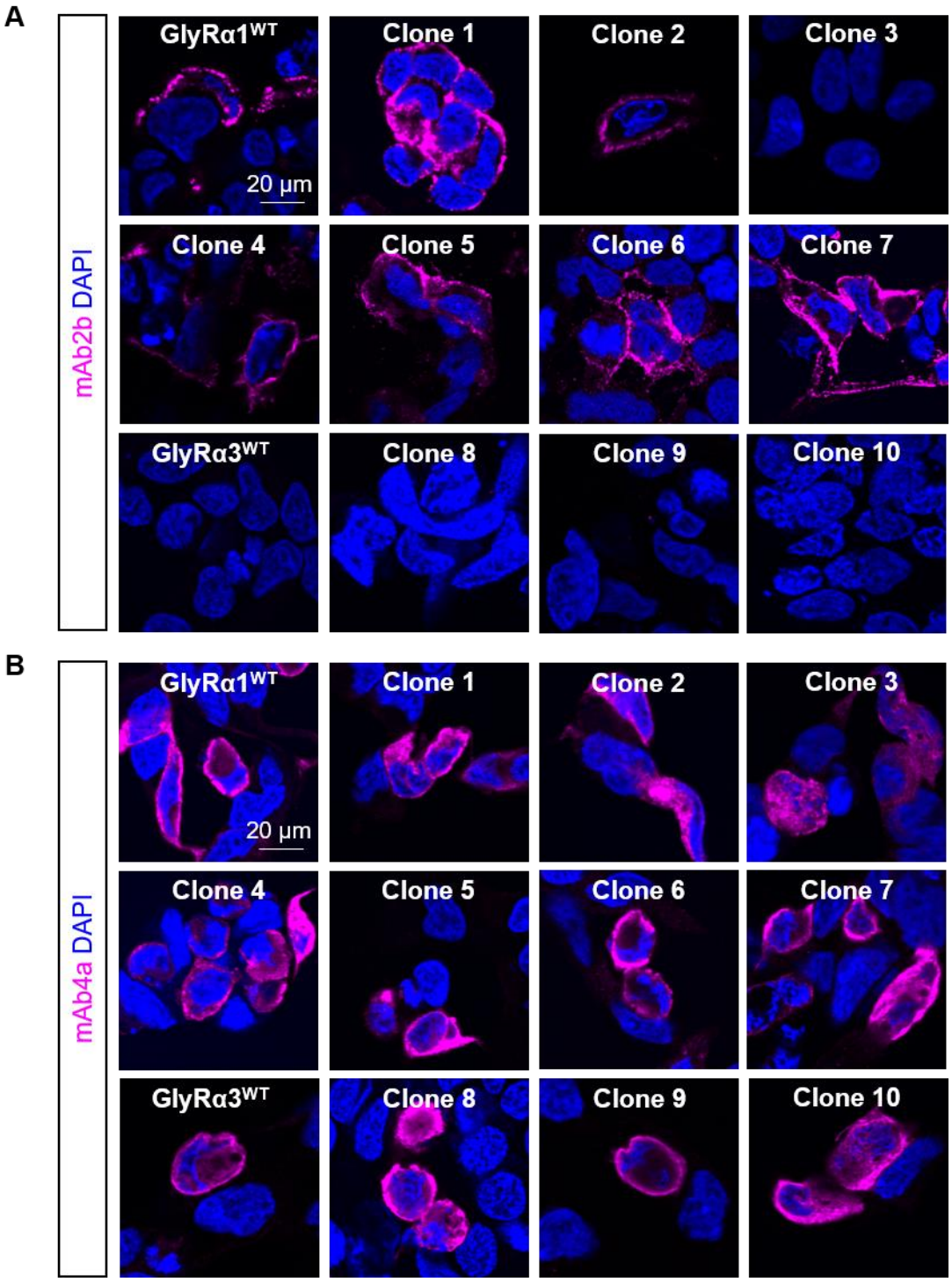

Fig. 15: MAb2b and mAb4a control staining of different GlyRα1 and GlyRα3 mutants. (**A**) MAb2b immunostaining (magenta) of HEK293 cells that were transfected with wildtype GlyRα1 and GlyRα3 or mutated forms of the receptors. Additionally, DAPI staining (blue) was included. (**B**) Same like in (**A**) but staining with mAb4a. Clone numbers and referring mutations are summarized in Tab. 22. WT = wildtype.

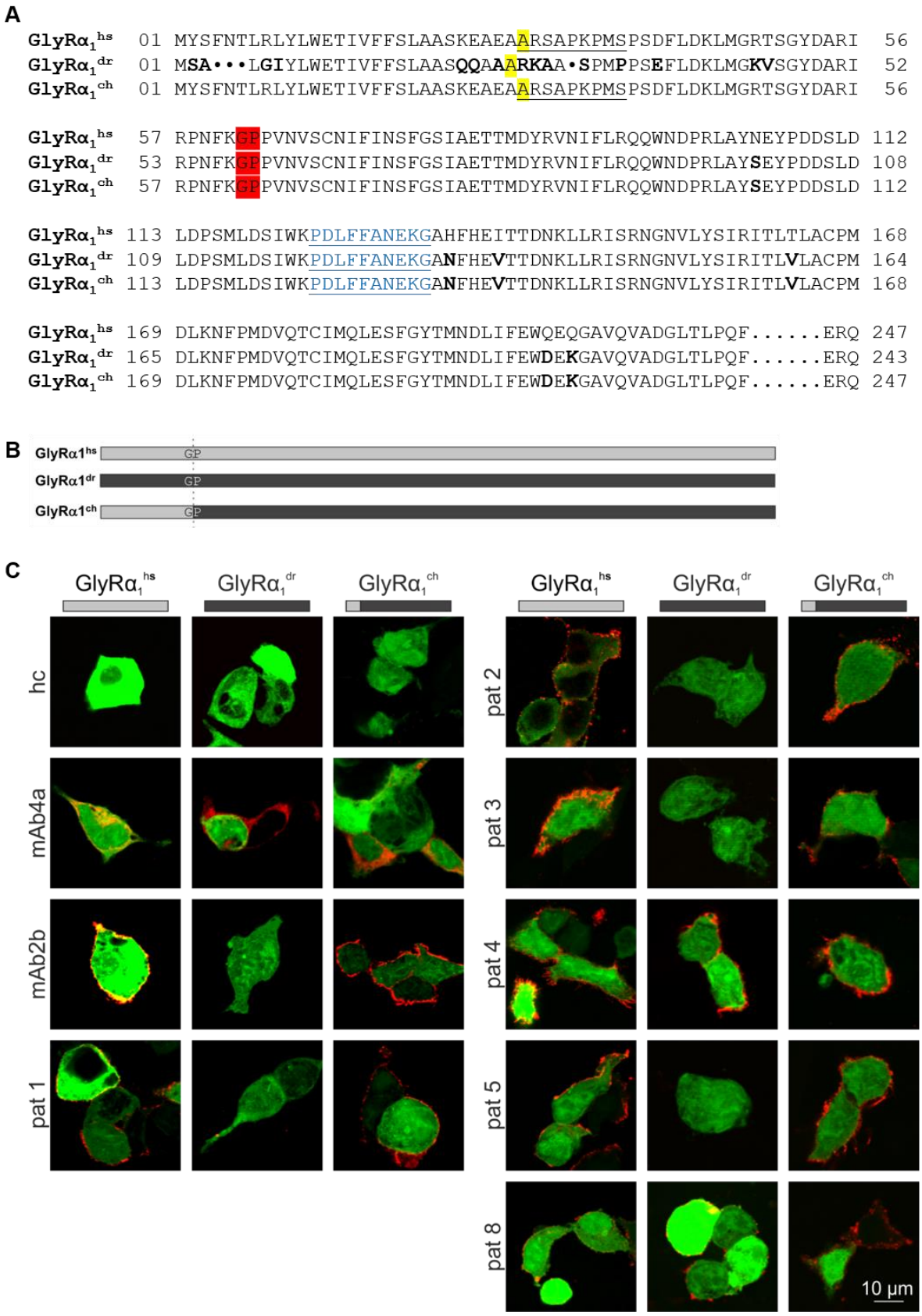

Fig. 16: Autoantibody epitope characterization in the N-terminal region of the GlyRα1. (**A**) Alignment of human (GlyRα1^{hs}) and zebrafish GlyRα1 (GlyRα1^{dr}) as well as a chimera (GlyRα1^{ch}) containing the human protein in the N-terminus followed by the zebrafish GlyRα1 sequence (edge is shown by red mark). Start of mature protein is displayed by yellow marked amino acids. Amino acid deviations were indicated by bold letters. The epitope of

mAb2b is underlined, the epitope of mAb4a is shown in blue and underlined. (**B**) Scheme of amino acid seqence. Human GlyRα1 is presented in light grey (top), zebrafish GlyRα1 in dark grey (middle) and chimera consists of GlyRα1^{hs} in N-terminus followed by GlyRα1^{dr} (bottom). (**C**) Immunocytochemical stainings of HEK293 cells that were transfected with GlyRα1^{hs}, GlyRα1^{dr} or GlyRα1^{ch} in combination with GFP (green). Cells were incubated with patient serum, healthy control or with controls mAb2b and mAb4a (red). ch = chimera; dr = *danio rerio*; hc = healthy control; hs = *homo sapiens*; pat = patient.

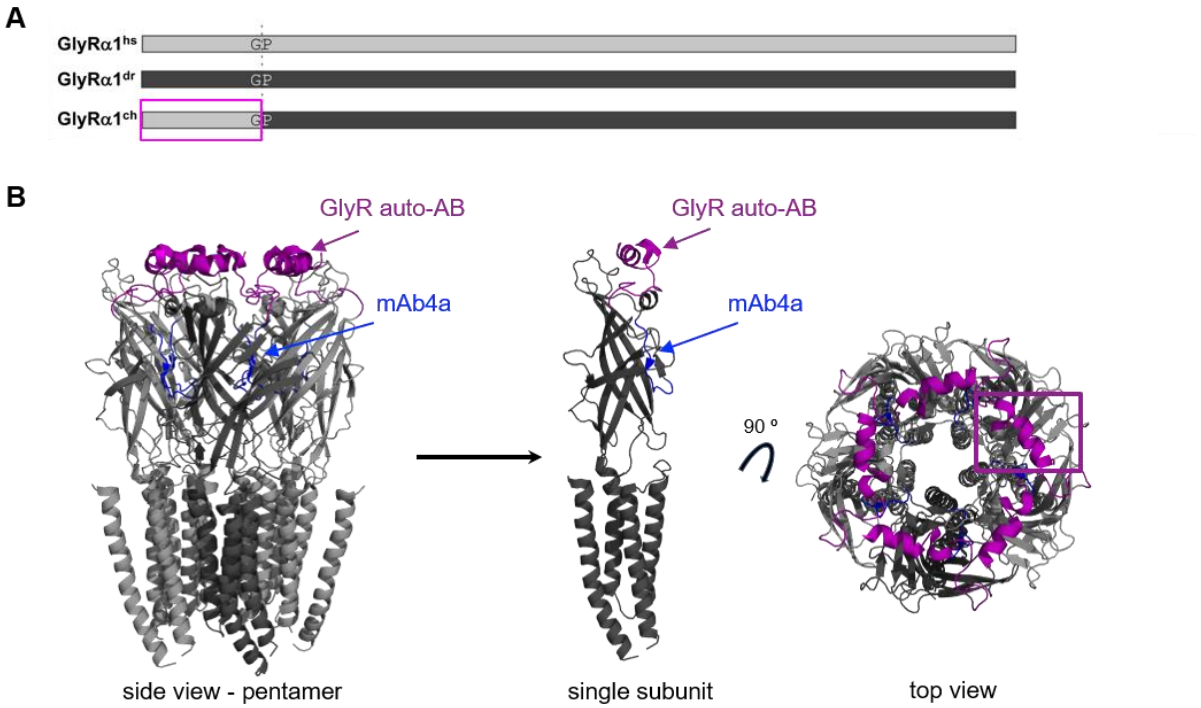

Fig. 17: Structural model of the GlyRα1 autoantibody epitope. (**A**) Schematic composition of human GlyRα1^{hs} (top, light grey), zebrafish GlyRα1^{dr} (middle, dark grey) and chimeric GlyRα1^{ch} (bottom, N-terminal part human and C-terminal part zebrafish). Cutting edge is shown by the dotted line. Magenta box indicates autoantibody binding site. (**B**) Strucutral model of GlyRα1 pentamer (left) and one single subunit (middle) according to Du et al. (2015). The top view is shown on the right. N-terminal autoantibody binding site is indicated in magenta and mAb4a binding site is presented in blue. The structural models were made and kindly provided by Dr. Natascha Schäfer (Institute for Clinical Neurobiology, Würzburg) by using the software PyMOL (DeLano Scientific, San Carlos, CA, USA). ch = chimera; dr = *danio rerio*; hs = *homo sapiens*.

In summary, the far N-terminal region in the GlyRα1 covering amino acids A^{1}-G^{34} was identified as part of the autoantibody epitope. Other amino acid mutations behind glycine at position 34 (from mature GlyRα1) were not bound by patient 1 autoantibodies but patient 4 and 8 autoantibodies targeted GlyRα1^{dr}, thus indicating the existence of further epitopes. Additionally, L132I and S137A mutation in GlyRα3 seem to play an important role in autoantibody binding as patient 1 was able to bind to this mutated variant whereas GlyRα3^{WT} was not bound. These stainings have to be repeated with other patient sera to verify the results.

3.2 GlyRα1 autoantibody binding and receptor glycosylation

3.2.1 Glycosylation prevention by tunicamycin treatment

Autoantibody binding might be influenced by the glycosylation state of the target protein. There are several studies discussing the necessity of glycosylation for binding of different kinds of autoantibodies (Labasque et al., 2014; Miura et al., 2015; Olsen et al., 2015). Here, the influence of glycosylation for GlyRα1 autoantibody binding was analyzed. First, glycosylation was prevented by tunicamycin treatment 24 h after HEK293 cell transfection with GlyRα1 and GFP. For characterization, patient 1 serum was used since enough material was available. In live stainings, patient 1 autoantibodies were not able to bind tunicamycin treated cells whereas a fluorescent signal was detected when the solvent of tunicamycin (DMSO) was used (Fig. 18A). In an incubation with the healthy control serum, no fluorescent signal was visible neither in tunicamycin nor in DMSO treated cells. MAb2b staining showed a weaker signal in tunicamycin treated cells compared to DMSO treated cells but binding of the antibody was possible in both conditions. In fixed and permeabilized HEK293 cells that were treated with tunicamycin and incubated with patient 1 serum, a weak fluorescent signal was detectable whereas no signal was visible in the DMSO control (Fig. 18B). No fluorescent signal was observed in both tunicamycin and DMSO treatment when cells were incubated with healthy control. In comparison, the mAb4a antibody was able to bind fixed and permeabilized cells with and without tunicamycin treatment.

In summary, patient 1 autoantibodies are no more able to bind GlyRα1 transfected HEK293 cells in which glycosylation was prevented by tunicamycin treatment in a live staining. Contrarily, in fixed and permeabilized cells, weak binding of patient 1 autoantibodies was possible under tunicamycin treatment. Tunicamycin was thought to completely block glycosylation. Since tunicamycin treatment was used 24 h after transfection, the observed staining pattern might result from GlyRs that were already synthesized and transported to the cellular membrane. The half-life of GlyRs under normal experimental conditions was estimated between 24 and 48 h (Hoch et al., 1989; Villmann et al., 2009a).

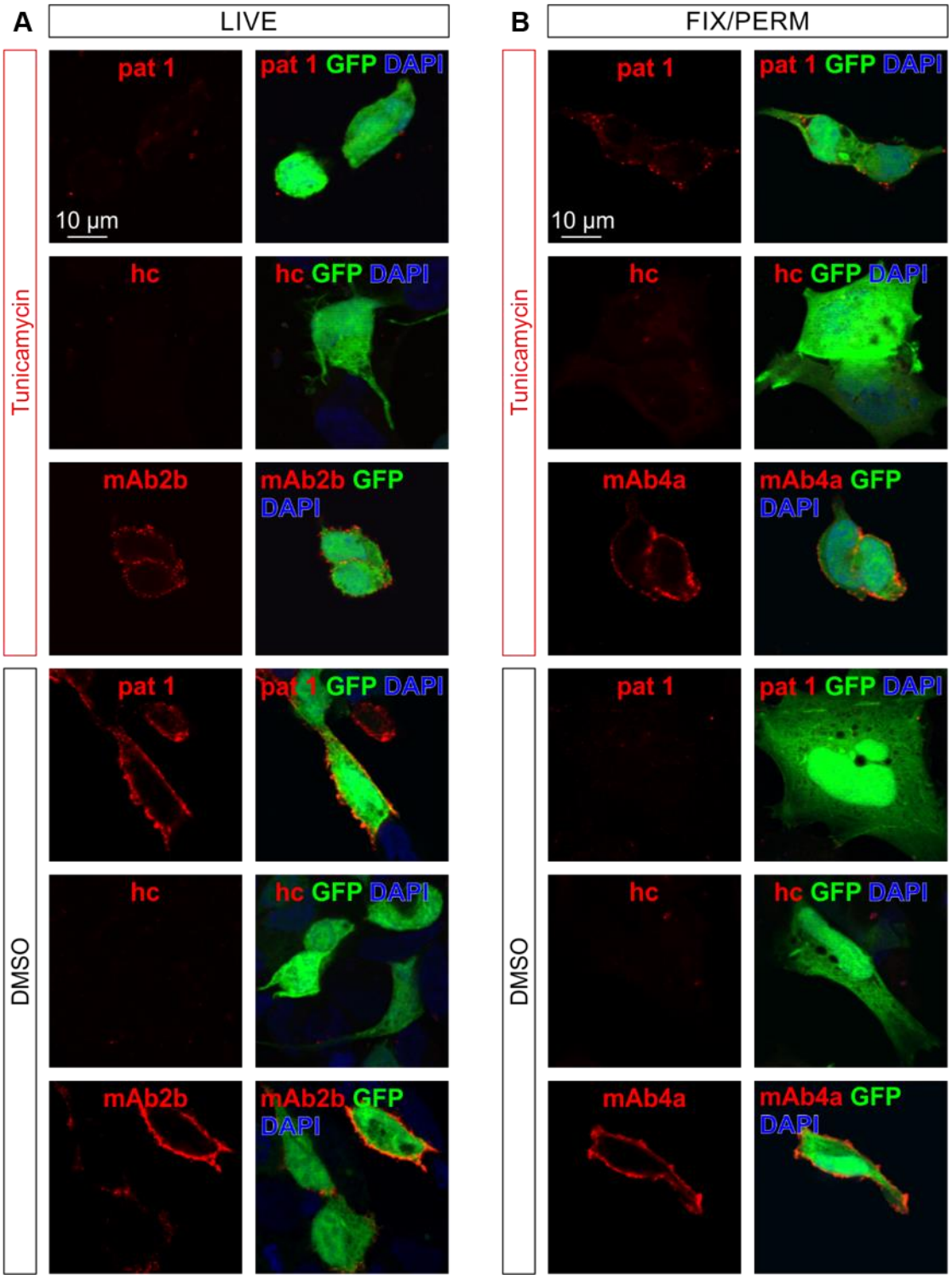

Fig. 18: Binding pattern of autoantibodies to tunicamycin treated HEK293 cells transfected with GlyRα1. (**A**) GlyRα1 and GFP (green) co-transfected HEK293 cells were treated with tunicamycin to prevent N-glycosylation. DMSO (solvent of tunicymycin) treated cells served as negative control. After, cells were incubated with patient 1 serum, healthy control and mAb2b (red) in live staining. DAPI staining (blue) is depicted in merged picture. (**B**) same like in (**A**) but staining of fix/permeabilized cells. MAb4a was used instead of mAb2b because mAb2b can not detect its epitope in fixed cells. hc = healthy control; pat = patient.

3.2.2 Prevention of glycosylation by generation of the de-glycosylation mutant N38Q

For further analyses of the requirement of glycosylation for autoantibody binding, a de-glycosylation mutant was created. The use of the mutant also circumvents side effects of tunicamycin and DMSO to the treated cells e.g. cytotoxicity. Therefore, the existing glycosylation site in GlyRα1 at asparagine 38 (number refers to mature protein) was exchanged to a glutamine (Fig. 19A). Complete de-glycosylation was verified by treating GlyRα1^{WT} or GlyRα1^{N38Q} transfected HEK293 cell lysates with glycosidases PNGaseF and EndoH and comparing the molecular weights of the resulting GlyRα1 subunits by Western blot analysis. PNGaseF treatment of GlyRα1^{WT} transfected cells resulted in a lower molecular weight compared to control samples (untreated GlyRα1^{WT} or GlyRα1^{WT} transfected HEK293 cell lysates incubated with same buffers like PNGaseF or EndoH treatment but excluding glycosidases) (Fig. 19B left). EndoH treatment resulted in a double band representing digested and undigested proteins. Both forms can occur because glycans are cleaved off by EndoH as long as the proteins are not localized in the Golgi apparatus. In the Golgi apparatus, proteins become EndoH resistant due to further processing of the sugar chains (Schaefer et al., 2018a). Untransfected HEK293 cells showed no detectable protein band. PNGaseF and EndoH treatment of the mutated α1 variant GlyRα1^{N38Q} demonstrated a reduced molecular weight compared to GlyRα1^{WT} but at the same molecular weight as undigested GlyRα1^{N38Q} confirming complete de-glycosylation (Fig. 19B right).

Before testing patient autoantibodies for their ability to bind to the de-glycosylation mutant GlyRα1^{N38Q}, this mutant receptor variant was structurally and functionally characterized in more detail. To do so, structural modeling, functional analysis as well as expression level determination within the cell were performed.

First, structural analyses and 3D reconstructions of GlyRα1^{N38Q} were performed to visualize possible structural changes due to the mutation. The mutation is located in the extracellular domain of the GlyRα1 (Fig. 19C, D). The sugar chains are directed to the outside of the receptor (Fig. 19D). Insertion of N38Q mutation resulted in a loss of a hydrogen bond between proline 36 and asparagine 31 (Fig. 19E). No further obvious structural changes were visible. Thus, one might assume that the GlyRα1^{N38Q} should be expressed. If, however, the functionality of the mutated GlyRα1^{N38Q} variant is affected, needs to be investigated using electrophysiological recordings.

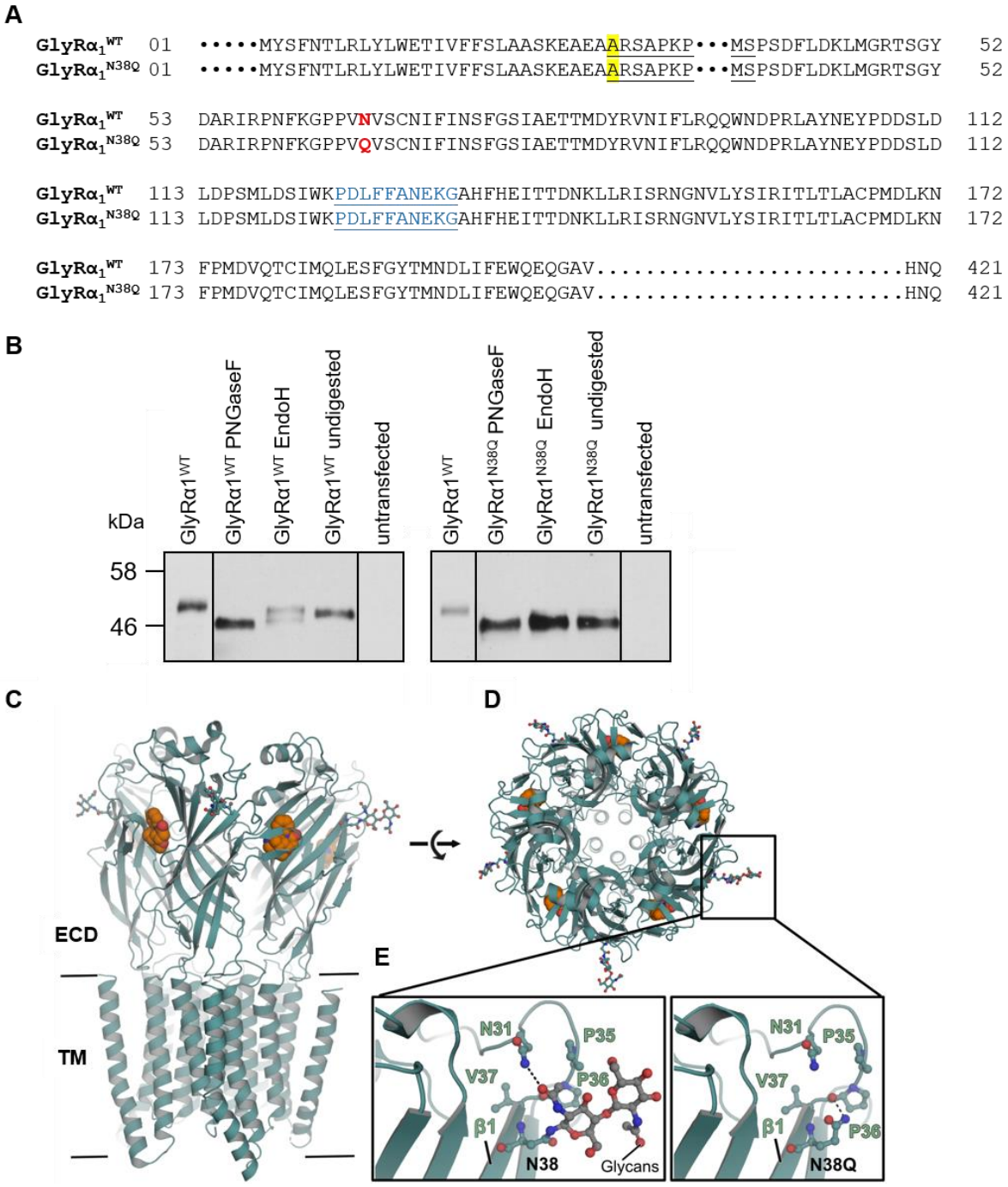

Fig. 19: General and structural analysis of de-glycosylation mutant GlyRα1^{N38Q}. (**A**) Alignment of GlyRα1^{WT} and GlyRα1^{N38Q}. Mutation is shown by a red mark (N38Q, number refers to mature protein). Amino acids contributing to the mAb2b epitope are underlined, mAb4a epitope is presented in blue, underlined letters. (**B**) Western blot of PNGaseF and EndoH treated lysates of HEK293 cells that were transfected with GlyRα1^{WT} (left) or with GlyRα1^{N38Q} (right). (**C**) Structural model of GlyRα3 in pentameric conformation according to Huang et al. (2015) (PDB: 5CFB). Note that asparagine residue at position 38 is present in all GlyRα subunits. Strychnine is displayed in orange and glycans in dark turquoise. (**D**) Top view of GlyRα3 structure shown in (**C**). (**E**) Zoom in at position N38 in wildtype situation (left) and mutated N38Q (right). A hydrogen bond between proline 36 and asparagine 31 is lost in GlyRα1^{N38Q}. ECD = extracellular domain; TM = transmembrane domain; WT = wildtype. The structural models were made and kindly provided by Dr. Vikram Kasaragod (Rudolf Virchow Center, Würzburg) by using the software PyMOL (DeLano Scientific, San Carlos, CA, USA).

Dose-response curve of HEK293 cells transfected with GlyRα1^{N38Q} that were analyzed from electrophysiological recordings showed a rightward shift compared to the curve of cells transfected with GlyRα1^{WT}, providing evidence for a reduced glycine potency (Fig. 20A). Analyses of maximal currents recorded from HEK293 cells by application of 100 µM glycine revealed a significant decrease which is about 0.3 times less in cells transfected with GlyRα1^{N38Q} compared to GlyRα1^{WT} (t-test: p = 0.0006; Fig. 20B, Tab. 23). In comparison, when glycine is applied at a saturating concentration (1 mM), the recorded maximal currents were not significantly different in cells transfected with GlyRα1^{WT} and GlyRα1^{N38Q} (t-test: p = 0.398, Tab. 23). Furthermore, the EC_{50} values analyzed from dose-response curves revealed that EC_{50} values of GlyRα1^{N38Q} transfected HEK293 cells were more than twofold increased compared to GlyRα1^{WT} (t-test: p = 0.00029; Fig. 20, Tab. 23). These results indicate that the glycine potency is affected in GlyRα1^{N38Q}, but the receptor is still functional.

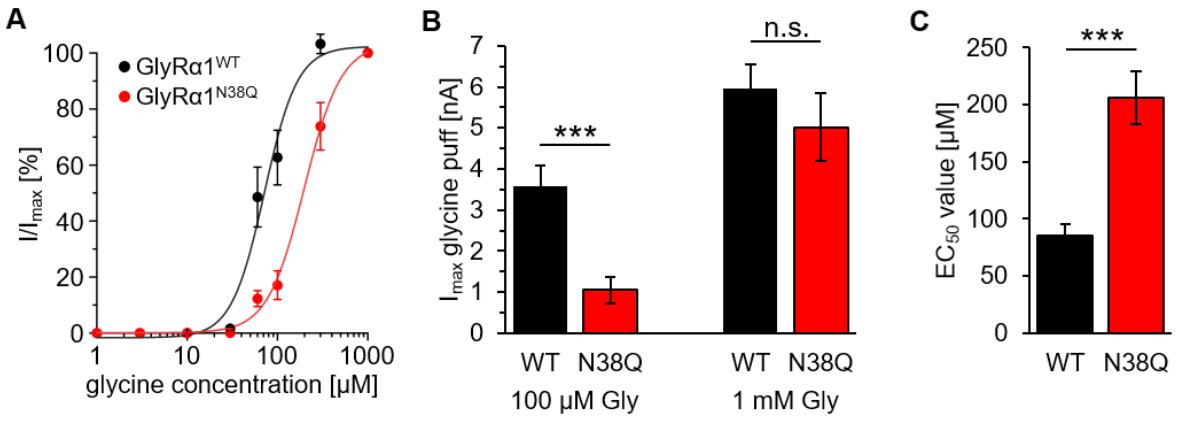

Fig. 20: Functional effects of de-glycosylation of GlyRα1. (**A**) Dose-response curve of HEK293 cells transfected with GlyRα1^{WT} (black) and GlyRα1^{N38Q} (red). (**B**) Maximal currents recorded from GlyRα1^{WT} (black) and GlyRα1^{N38Q} (red) transfected HEK293 cells when 100 µM or 1 mM glycine were applied. (**C**) EC_{50} values determined from dose-response curves. WT = wildtype.

Tab. 23: Physiological properties of GlyRα1^{WT} and GlyRα1^{N38Q} transfected HEK293 cells.

condition	n	$I_{100\ µM}$ [nA]	I_{sat} [nA]	EC_{50} [µM]
GlyRα1^{WT}	12	3.6 ± 0.5	6.0 ± 0.6	85 ± 11
GlyRα1^{N38Q}	13	1.0 ± 0.3	5.0 ± 0.8	206 ± 23

I_{sat} refers to the currents obtained at saturating glycine concentrations of 1 mM; n = number of cells recorded from three independent experiments.

Insertion of point mutations may influence the expression pattern of the GlyR proteins. The electrophysiological recordings indicated that GlyRα1^{N38Q} was expressed at the cell surface otherwise no currents would be recordable. To differentiate between whole cell, intracellular and surface GlyRs, biotinylation assays were performed to get deeper insights in the expression levels of GlyRα1^{N38Q}. Biotin was coupled to proteins present in the cellular membrane that are exposed to the extracellular space, like receptors (Fig. 21A). Cell lysis allowed harvesting of the whole cell pool of proteins. After adding streptavidin beads that bind tightly to biotin, the intracellular pool (supernatant) and surface pool (pellet) were separated by centrifugation. The three different pools were used for quantitative protein analysis from Western blots by normalization of the determined GlyR protein amount to pan-cadherin expression as a membrane marker and in this case housekeeping protein. Afterwards, GlyRα1^{WT} expression was set to 1. Both GlyRα1^{WT} and GlyRα1^{N38Q} were expressed in whole cell, intracellular and surface pool (Fig. 21B). The reduction of the molecular weight of the GlyRα1^{N38Q} mutant was obvious. Untransfected HEK293 cells were used as negative control. Gephyrin was used as control protein for the biotinylation assay which was detected in the whole cell and intracellular pool but not in the surface pool (Fig. 21C). Quantifying the whole cell expression level of the GlyRα1^{N38Q} mutant indicated that the expression level of GlyRα1^{N38Q} was significantly reduced of about 40% compared to GlyRα1^{WT} (t-test: $p = 0.042$; Fig. 21D, Tab. 24). A similar reduction was detectable in the surface expression (t-test: $p = 0.0997$). The intracellular expression level of GlyRα1^{WT} and GlyRα1^{N38Q} were indistinguishable (t-test: $p = 0.884$). In whole cell, intracellular and surface pool, there was no expression of GlyRs in untransfected cells.

These results indicate that the mutant GlyRα1^{N38Q} is expressed in the whole cell, intracellularly and at the cell surface and therefore forms functional chloride-gated ion channels. Thus, the mutant is suitable for testing the involvement of glycosylation for autoantibody binding. HEK293 cells were transfected with GlyRα1^{N38Q} and GFP and incubated with patient sera. All tested patient sera (patient 1 and 6-9) as well as GlyRα1 specific antibody mAb2b were able to bind to de-glycosylated GlyRα1^{N38Q} (Fig. 22). Healthy and disease control sera showed no fluorescent signal when incubated with GlyRα1^{N38Q} transfected HEK293 cells.

In summary, the de-glycosylation mutant GlyRα1^{N38Q} is functionally expressed in HEK293 cells but the loss of glycosylation does not influence autoantibody binding.

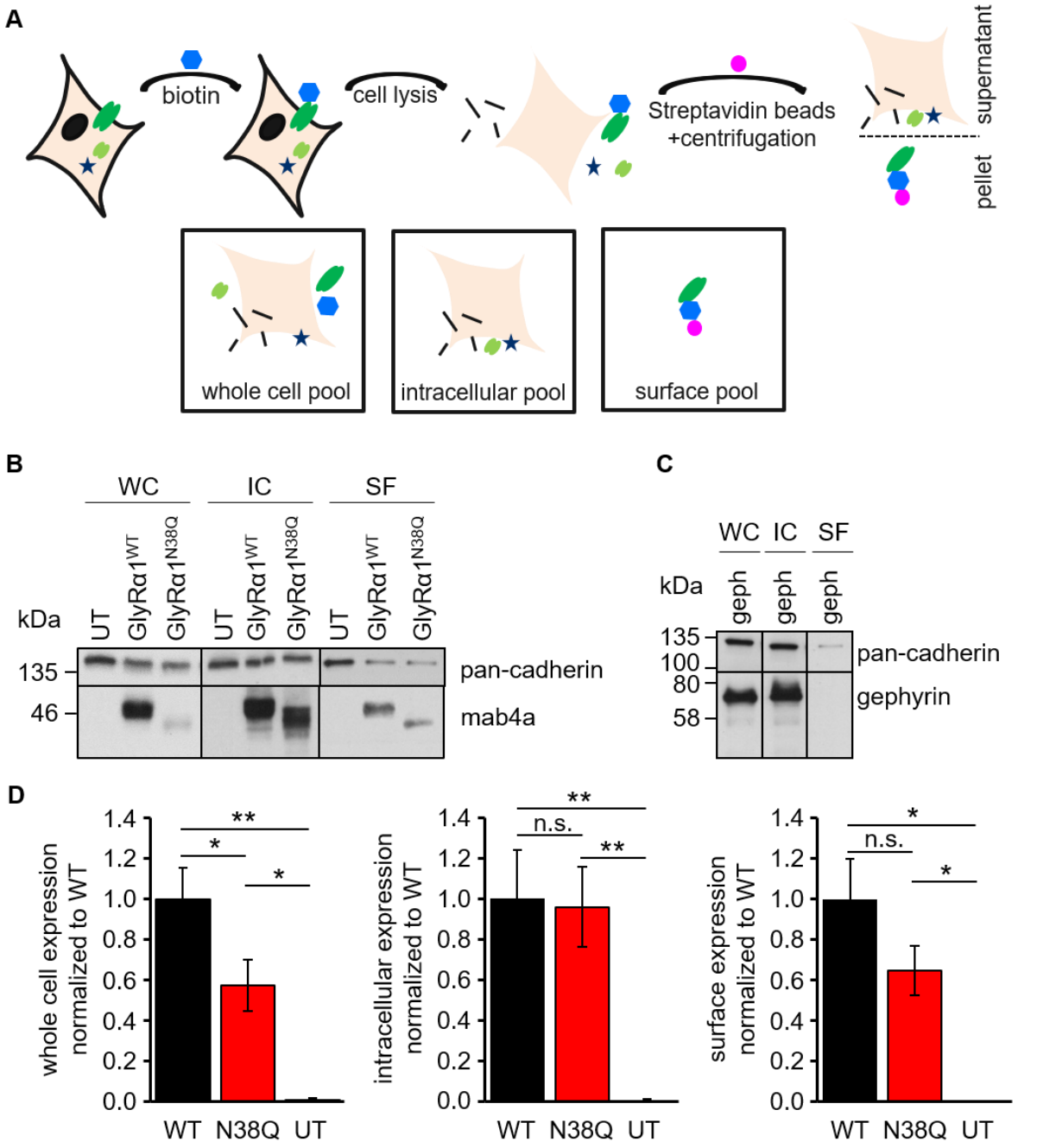

Fig. 21: Expression of GlyRα1^{N38Q} in whole cell, intracellular and surface pool compared to GlyRα1^{WT}. (**A**) Scheme of biotinylation assay. From left to right: in transfected HEK293 cells, receptors are expressed in the outer membrane (dark green) but there are also intracellular receptors (light green) in the maturation process from the ER towards the cellular membrane and further intracellular proteins (black star). Biotin (blue) is added to the cells and binds to membrane bound proteins. Cells are lysed (whole cell pool), streptavidin beads (magenta) are added and sample is centrifuged. Thereby the sample is divided into two fractions, a complex of streptavidin beads, biotin and membrane proteins in the pellet (surface pool) and all other cell components in the supernatant (intracellular pool). (**B**) Western blot of whole cell (WC), intracellular (IC) and surface (SF) pool of both GlyRα1^{WT} and GlyRα1^{N38Q} transfected HEK293 cells. Untransfected HEK293 cells (UT) were used as negative control. Western blots were stained with mAb4a and with pan-cadherin as loading control. (**C**) Gephyrin (geph) was used as positive control for the biotinylation assay. (**D**) Quantification of whole cell (left), intracellular (middle) and surface expression (right) of GlyRα1^{WT} (black), GlyRα1^{N38Q} (red) and untransfected cells (white with black edge). Values were normalized to pan-cadherin signal and GlyRα1^{WT} expression was set to 1. UT = untransfected; WT = wildtype.

Tab. 24: Expression levels of GlyRα1^{WT} and GlyRα1^{N38Q} in whole cell, intracellular and at cell surface in relation to GlyRα1^{WT}.

	n WT/N38Q/UT	GlyRα1^{WT}	GlyRα1^{N38Q}	UT
whole cell expression normalized to WT	5/5/5	1.0 ± 0.2	0.6 ± 0.1	0.0 ± 0.0
intracellular expression normalized to WT	5/5/5	1.0 ± 0.2	1.0 ± 0.2	0.0 ± 0.0
surface expression normalized to WT	6/5/6	1.0 ± 0.2	0.6 ± 0.1	0.0 ± 0.0

WT = wildtype; UT = untransfected. N38Q: number refers to mature protein.

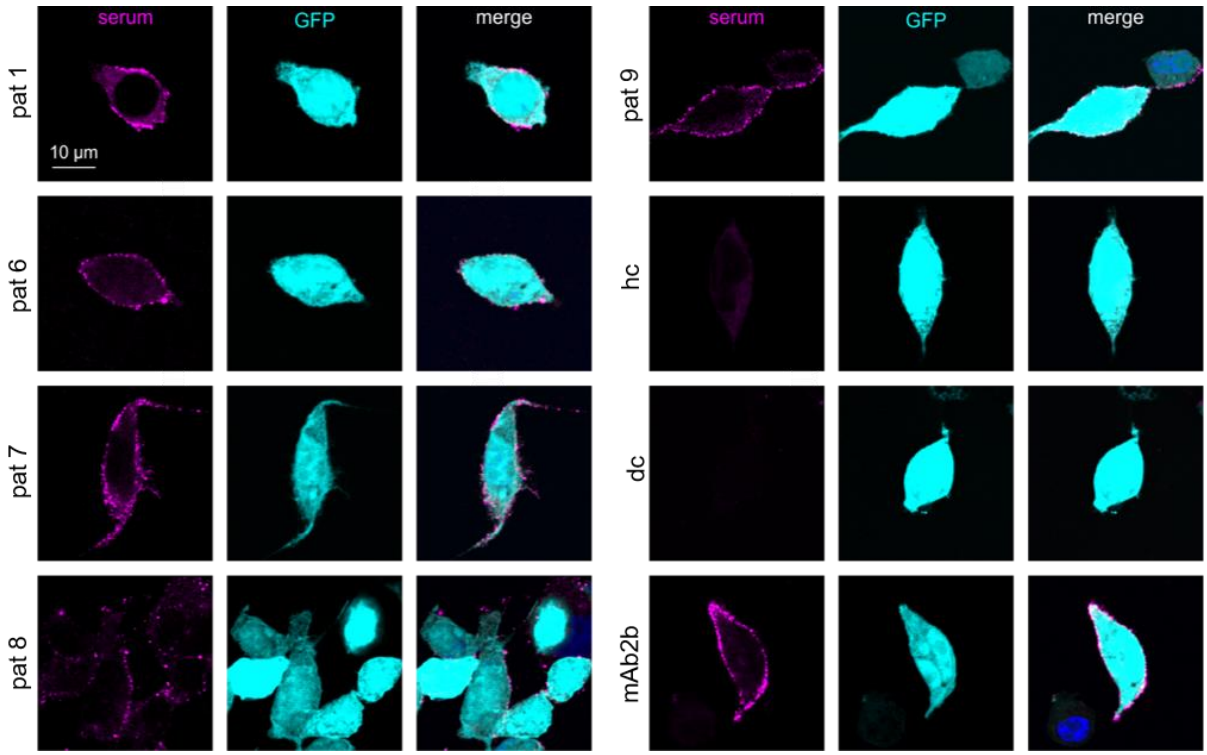

Fig. 22: Autoantibody binding to GlyRα1^{N38Q}. Immunocytochemical stainings of GlyRα1^{N38Q} transfected HEK293 cells with patient serum, healthy control, disease control and mAb2b (magenta). Cells were co-transfected with GFP (cyan) as transfection control. DAPI staining (blue) is shown in merged picture. dc = disease control; hc = healthy control; pat = patient.

3.3 Functional changes of GlyRα1 upon autoantibody binding

For more insights in the pathology of autoantibodies, it is necessary to find out downstream pathophysiological mechanisms beyond binding. Receptor internalization and degradation upon GlyR autoantibody binding were already demonstrated (Carvajal-Gonzalez et al., 2014). However, binding of the GlyR autoantibodies to the protein might acutely interfere with its function as an ion channel. Furthermore, it should be noted that in patients the autoantibodies are sometimes present over a long period of time until people are diagnosed, and therapy is started. Hence, GlyR homeostasis most probably counteracts receptor internalization.

Ion channel opening occurs following glycine binding to the glycine binding site localized deep in the adjacent structure of two neighboring subunits. Following binding of the agonist, the structure undergoes several structural transitions within the ECD which finally results in ion channel opening (Du et al., 2015).

So far, it was not investigated whether autoantibody binding to GlyRα1 influences receptor functionality. Here, GlyRα1 transfected HEK293 cells were used for electrophysiological recordings following 1 h pre-incubation with patient GlyR autoantibodies. The dose-response curves of HEK293 cells that were pre-incubated with patient sera (patient 1-5) were shifted to the right compared to healthy control and mAb2b incubated cells, indicating a reduced glycine potency (Fig. 23A_1). The same rightward shift was visible when HEK293 cells were pre-incubated with patient IgG (patient 1, 2 and 8) compared to healthy control serum (Fig. 23A_2). These data show a decrease in glycine potency as well. However, the maximal currents from patient serum or mAb2b incubated HEK293 cells at a saturating glycine concentration of 1 mM were not significantly altered from incubation with healthy control serum, pointing towards an unchanged glycine efficacy (t-test: $p_{pat1} = 0.36$, $p_{pat2} = 0.16$, $p_{pat3} = 0.11$, $p_{pat4} = 0.36$, $p_{mAb2b} = 0.43$; Fig. 23B_1, Tab. 25). The only exception is patient 5 serum which led to reduced maximal currents (t-test: $p = 0.029$). In contrast, in HEK293 cells pre-incubated with patient IgG instead of serum, patient 1 and 2 IgG resulted in a significant higher maximal current at 1 mM glycine whereas patient 8 IgG was not significantly different from healthy control serum (t-test: $p_{pat1} = 0.039$, $p_{pat2} = 0.034$, $p_{pat8} = 0.965$; Fig. 23B_2, Tab. 25). However, at a lower glycine concentration of 30 µM, I_{max} currents were significantly reduced in HEK293 cells incubated with all patient sera and IgG compared to cells incubated with healthy control serum (t-test serum: $p_{pat1} = 0.00065$, $p_{pat2} = 5.7xE^{-07,}$ $p_{pat3} = 0.04$, $p_{pat4} = 0.0002$, $p_{pat5} = 5.17xE^{-07}$; t-test IgG: $p_{pat1} = 0.00014$, $p_{pat2} = 3.32xE^{-05}$, $p_{pat8} = 3.08xE^{-05}$; Fig. 23C_1, C_2, Tab. 25). MAb2b incubated HEK293 cells exhibited unchanged maximal currents in comparison to healthy control serum pre-incubated cells (t-test: $p_{mAb2b} = 0.248$). These data at 30 µM glycine also reflect the distribution of the EC_{50} values. MAb2b incubation does not change the EC_{50} value compared to healthy control serum. Incubation with all patient sera and patient IgGs resulted

in significant increased EC_{50} values which were up to 3 fold higher for GlyRs incubated with serum and 4 fold higher for GlyRs incubated with purified patient IgG compared to EC_{50} values of healthy control serum (t-test serum: $p_{mAb2b} = 0.462$, $p_{pat1} = 0.0012$, $p_{pat2} = 0.0027$, $p_{pat3} = 0.014$, $p_{pat4} = 0.0039$, $p_{pat5} = 0.00034$; t-test IgG: $p_{pat1} = 0.00017$, $p_{pat2} = 0.00017$, $p_{pat8} = 8.53xE^{-06}$; Fig. 23D, Tab. 25).

Following the recordings, immunocytochemical stainings of HEK293 cells were conducted to determine binding of autoantibodies during the whole cell recording experiment. Healthy control serum incubated HEK293 cells showed no fluorescent signal after electrophysiological recordings because there were no autoantibodies present that could bind to the cells (Fig. 24). HEK293 cells pre-incubated with mAb2b, patient 1-5 serum and patient 1,2, and 8 IgG exhibited bright signals in immunohistochemical stainings after electrophysiological experiments, indicating stable autoantibody binding during functional recordings.

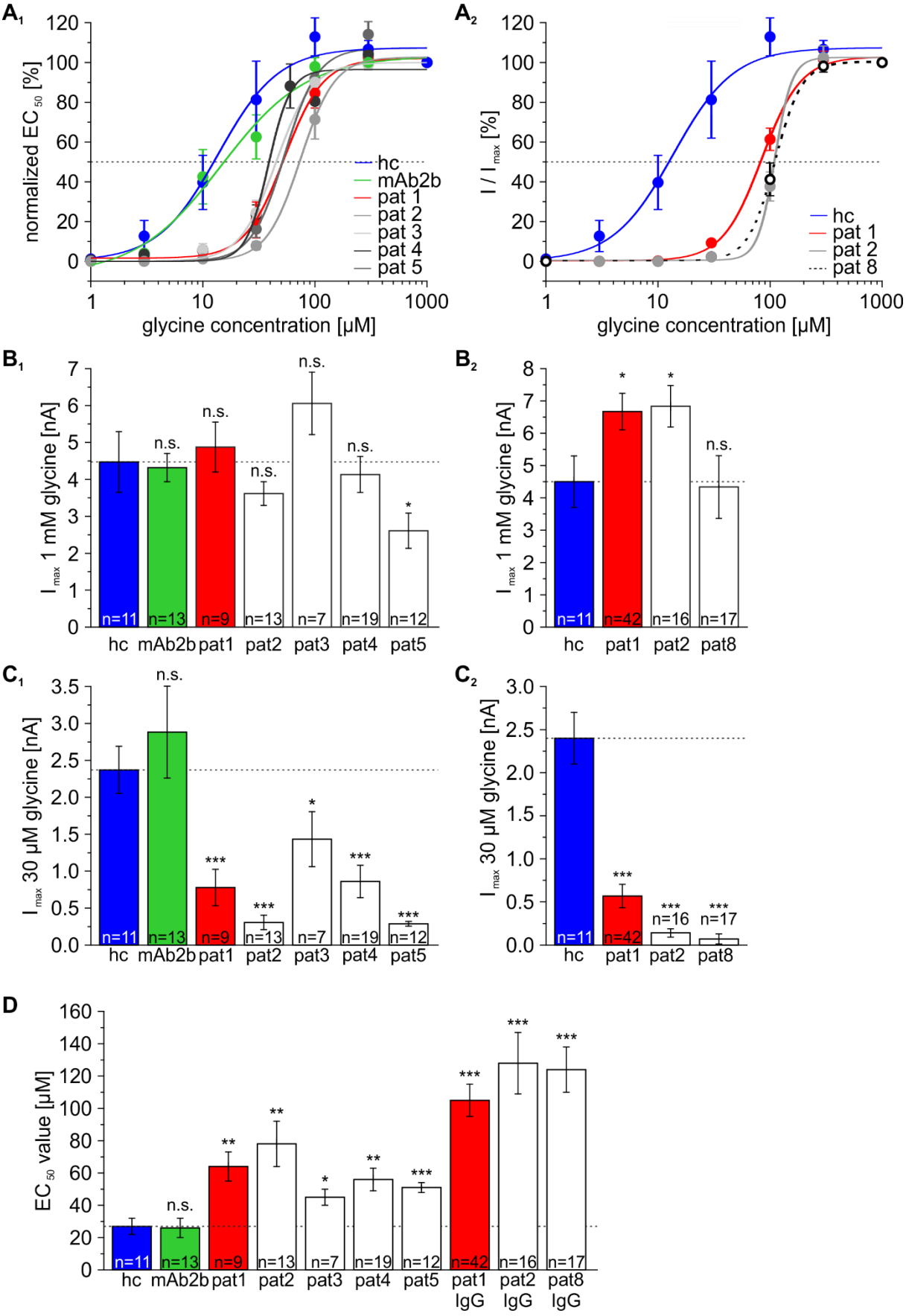

Fig. 23: Functional effects of autoantibody binding to GlyRα1. (**A1**) Dose-resonse curves of HEK293 cells that were transfected with GlyRα1 and pre-incubated with patient serum, healthy control or mAb2b. (**A2**) Same like in (**A1**) but cells were pre-incubated with patient IgG. (**B1**) Saturating currents of GlyRα1 transfected HEK293 cells

pre-incubated with patient serum, healthy control or mAb2b by application of 1 mM glycine. (**B_2**) Same like in (**B_1**) but cells were pre-incubated with patient IgG. (**C_1**) Currents of GlyRα1 transfected HEK293 cells pre-incubated with patient serum, healthy control or mAb2b by application of 30 µM glycine. (**C_2**) Same like in (**C_1**) but cells were pre-incubated with patient IgG. (**D**) EC_{50} values analyzed from dose-response curves of HEK293 cells transfected with GlyRα1 and incubated with patient serum, healthy control, patient IgG and mAb2b. hc = healthy control; pat = patient.

Tab. 25: Summarized values of electrophysiological recordings including dose-response currents and EC_{50} values.

condition	dilution	n	$I_{30µm}$ [nA]	I_{sat} [nA]	EC_{50} [µM]
hc	1:10	11	2.4 ± 0.3	4.5 ± 0.8	27 ± 5
mAb2b	1:500	13	2.9 ± 0.6	4.3 ± 0.4	26 ± 6
patient 1	1:10	9	0.8 ± 0.2	4.9 ± 0.7	64 ± 9
patient 1 IgG	1:50	42	0.5 ± 0.1	6.7 ± 0.6	105 ± 10
patient 2	1:10	13	0.3± 0.1	3.6 ± 0.3	78 ± 14
patient 2 IgG	1:50	16	0.14 ± 0.05	6.8 ± 0.6	128 ± 19
patient 3	1:10	7	1.4 ± 0.4	6.1 ± 0.8	45 ± 5
patient 4	1:10	19	0.9 ± 0.2	4.1 ± 0.5	56 ± 7
patient 5	1:10	12	0.3± 0.1	2.6 ± 0.5*	51 ± 3
patient 8 IgG	1:50	17	0.11 ± 0.04	4.5 ± 0.5	124 ± 14

I_{sat} refers to the currents obtained at saturating glycine concentration of 1 mM; n = number of cells recorded from three independent experiments. hc = healthy control.

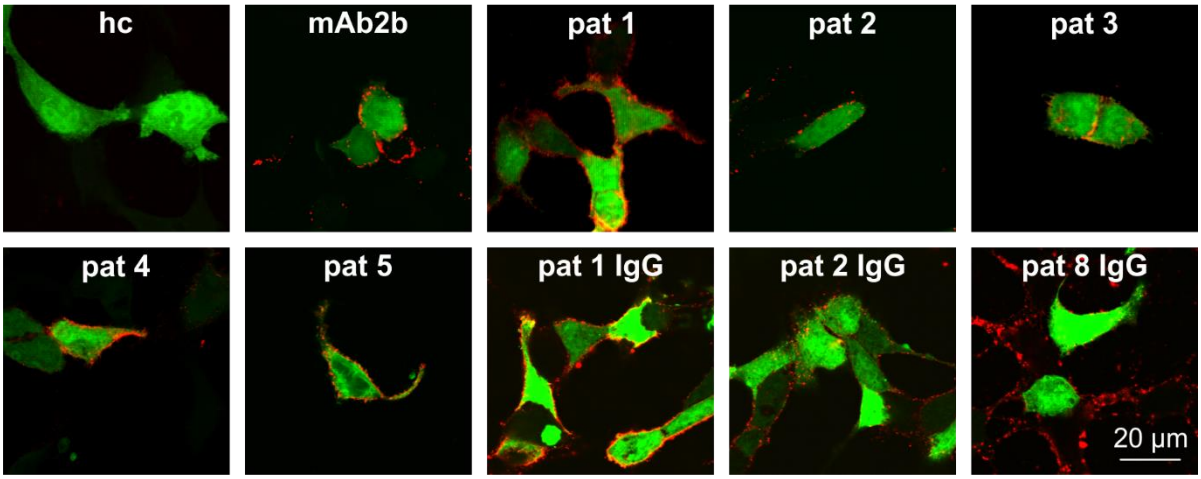

Fig. 24: Staining after electrophysiological recordings. HEK293 cells that were recorded in electrophysiological experiments were stained with anti-human Cy3 antibody (red) afterwards to verify stable antibody binding to transfected HEK293 cells. Cells were co-transfected with GFP (green). hc = healthy control; pat = patient.

Additionally to dose-dependent analysis of maximal currents, the receptor kinetics including time constants like rise time, desensitization or receptor deactivation can be analyzed from recorded traces. The desensitization of an ion channel in persisting presence of ligands plays an important role in receptor functionality due to a different structure of the whole receptor in its desensitized form compared to the open and closed conformation (Raltschev et al., 2016). Thereby, the fast synaptic transmission is sustained and modulated (Jones and Westbrook, 1996; Raltschev et al., 2016). In GlyRs, the desensitization can be determined by whole-cell recordings, thus showing relatively slow desensitization times of 0.5 - 11 s compared to $GABA_A$Rs (in ms range), which are dependent on the expression system used (Nikolic et al., 1998; Legendre, 2001; Gielen et al., 2015). Furthermore, it was demonstrated that the desensitization state of a receptor is influenced by substances, like the allosteric analgesic potentiator AM3607 (Huang et al., 2017). Thus, AM3607 bound to R^{29}-F^{32} in GlyRα3 led to a prolonged desensitization phase. As this potentiator binds in the same GlyR domain like the patient autoantibodies, analysis of changes in receptor desensitization upon autoantibody binding may provide additional information on GlyR autoantibody pathophysiology in SPS patients. Here, the fraction of desensitization was analyzed in electrophysiological recordings of GlyRα1 transfected HEK293 cells which were pre-incubated with patient sera. In HEK293 cells incubated with patient 1 and 5 serum as well as mAb2b, the fraction of desensitizing current was significantly reduced compared to incubation with healthy control serum (t-test fraction desensitization: $p_{mAb2b} = 0.04$, $p_{pat1} = 0.046$, $p_{pat2} = 0.36$, $p_{pat3} = 0.34$, $p_{pat4} = 0.41$, $p_{pat5} = 0.04$; Fig. 25A, Tab. 26). In contrast, patient 2-4 did not influence the fraction of desensitization. The tau value, which represents a time constant for receptor desensitization, pointed towards different subgroups of patients. Patients 1, 4 and 5 showed 0.8 fold shorter tau values compared to healthy control, indicating faster desensitization, whereas patient 2 and 3 led to 1.5 fold higher tau values suggesting slower channel desensitization (t-test tau: $p_{mAb2b} = 0.44$, $p_{pat1} = 0.16$, $p_{pat2} = 0.08$, $p_{pat3} = 0.30$, $p_{pat4} = 0.27$, $p_{pat5} = 0.29$; Fig. 25B, C, Tab. 26). The observed differences were, however, rather small and did not reach significance.

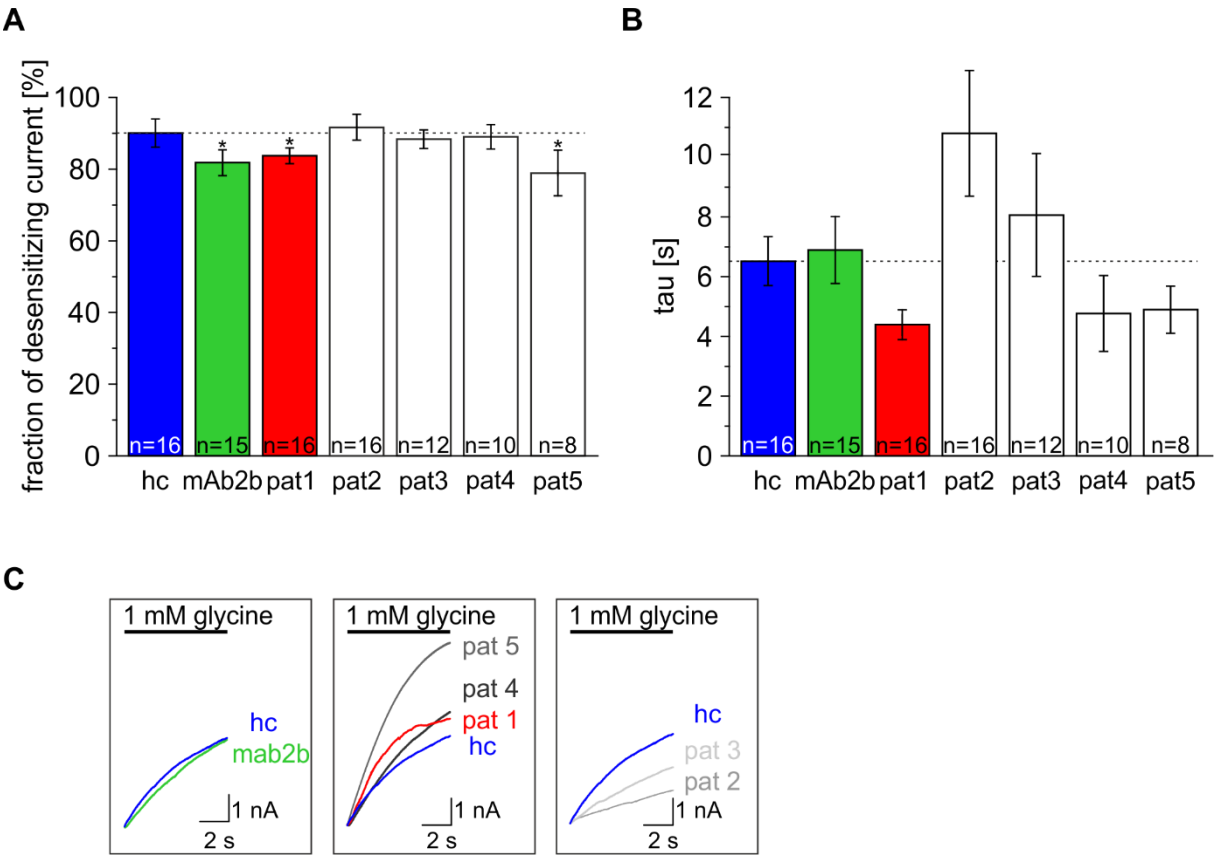

Fig. 25: GlyRα1 desensitization after autoantibody binding. (**A**) Fraction of desensitizing current in GlyRα1 transfected HEK293 cells that were pre-incubated with patient serum (red and white), healthy control (blue) or mAb2b (green). (**B**) Desensitization time constant tau analyzed during 10 s application of glycine. Values were determined from same recorded cells like in (**A**). (**C**) Representative traces of desensitization phase grouped in controls (left), faster desensitization compared to healthy control (middle) and slower desensitization compared to healthy control (right). hc = healthy control; pat = patient.

Tab. 26: Summary of values from desensitization experiments.

condition	dilution	n	fraction of desensitizing current [%]	tau [s]
hc	1:10	16	90.1 ± 2.9	6.5 ± 2.0
mAb2b	1:500	15	81.8 ± 3.6	6.9 ± 1.1
patient 1	1:10	16	83.7 ± 2.2	4.4 ± 0.5
patient 2	1:10	16	91.7 ± 3.6	10.8 ± 2.1
patient 3	1:10	12	88.3 ± 2.6	8.1 ± 2.1
patient 4	1:10	10	89.0 ± 3.4	4.8 ± 1.3
patient 5	1:10	8	78.9 ± 6.3	4.9 ± 0.8

n = number of cells recorded from three independent experiments; tau = time constant.

Functional analysis revealed that glycine binds to GlyRα1 in the presence of autoantibodies and allows chloride ion influx. If, however, glycine binds with the same affinity to the GlyRα1 as it does for GlyRs not targeted by autoantibodies, is not known. Assuming the correctness of the hypothesis, that GlyRα1 autoantibodies bind to the far N-terminus, then the affinity to the glycine binding site localized deeper in the channel at the interface between two adjacent subunits might be unaffected (Lynch, 2004; Betz and Laube, 2006). To test this, radioligand binding assays were performed by applying a saturating glycine concentration of 30 mM to GlyRα1 transfected HEK293 cells that were pre-incubated with patient serum. After, glycine was replaced by an increasing concentration series of the high-affinity antagonist [^{3}H] strychnine. Strychnine binds with an affinity between 32 and 64 nM to the GlyRα1 (Langosch et al., 1994; Grudzinska et al., 2005; Becker et al., 2008). No differences were detectable in dose-inhibition curves of untreated, mAb2b, healthy control and patient 1 incubated cells (Fig. 26A). The IC_{50} values, determined from dose-inhibition curves, were also not significantly different between mAb2b, healthy control and patient 1 treated cells compared to untreated cells (t-test: $p_{mAb2b} = 0.57$, $p_{hc} = 0.27$, $p_{pat1} = 0.75$; Fig. 26B, Tab. 27). These results are in accordance with previous data that showed no difference between autoantibody treated cells and controls when cells were first incubated with cold strychnine followed by competition with [^{3}H] strychnine (unpublished). These data together indicate that autoantibodies do not influence the binding affinity of the neurotransmitter glycine to GlyRs.

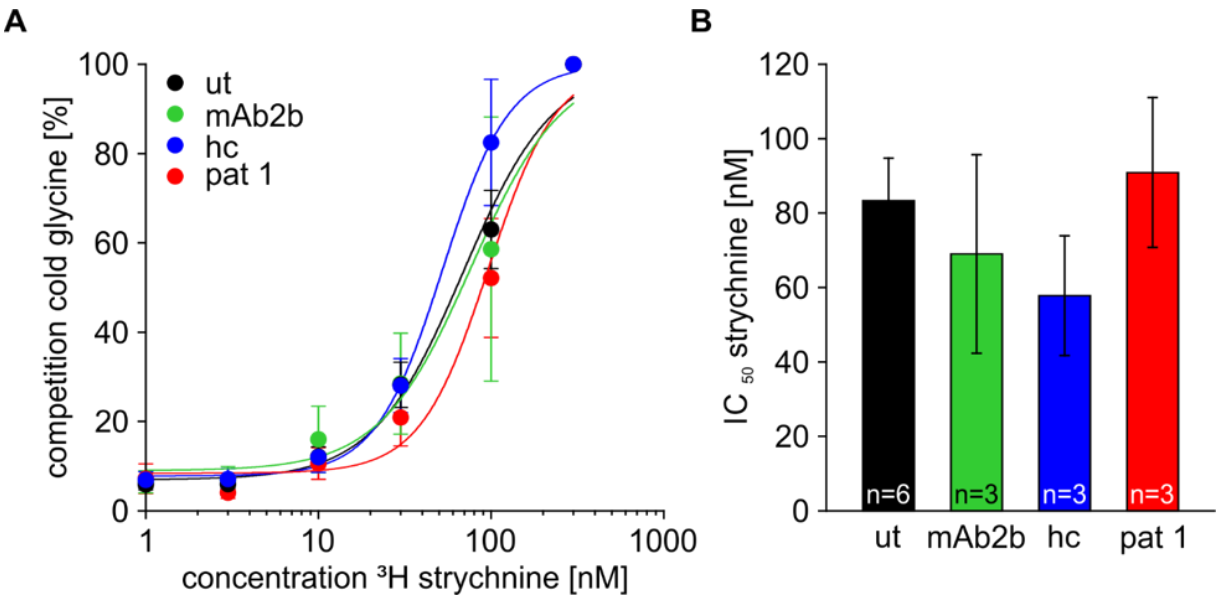

Fig. 26: Effects of autoantibody binding to ligand affinity. (**A**) Dose-response curve of radioligand binding assay. GlyRα1 transfected HEK293 cells were pre-incubated with patient 1 serum (red), healthy control (blue) or mAb2b (green) and incubated with cold glycine. After, glycine was replaced by increasing concentrations of ^{3}H strychnine (0, 1, 3, 10, 30, 100, 300 nM). Untreated HEK293 cells (ut) were used as negative control (black). (**B**) Analysis of IC_{50} values from dose-response-curves in (**A**). n number refers to independent experiments. hc = healthy control, pat = patient; ut = untreated.

Tab. 27: IC_{50} values of radioligand binding assay.

condition	n	IC_{50} strychnine [nM] glycine-strychnine competition
untreated	6	83.3 ± 11.4
patient 1	3	90.9 ± 20.1
healthy control	3	57.8 ± 16.1
mAb2b	3	69.0 ± 26.7

n number refers to independent experiments.

In summary, GlyRα1 autoantibodies influence receptor function by decreasing the glycine potency which was shown by increased EC_{50} values. However, maximal currents from saturating glycine concentrations and IC_{50} values of radioligand binding assays are unchanged, arguing for no influence of autoantibodies to glycine efficacy and affinity, respectively. The desensitization of GlyRα1 is altered by autoantibody binding to the N-terminal domain of the receptor arguing that the receptor in its partially open state is influenced by GlyR autoantibody binding. In sum, the alterations in receptor desensitization are rather small and are unable to explain but might at least contribute to the severity of the symptoms observed in SPS patients.

3.4 Neutralization of GlyRα1 autoantibodies

Plasmapheresis is one of the common treatments in SPS therapy. Besides the positive effects by reduced autoantibody concentrations, healthy material is removed from blood as well (Nydegger and Sturzenegger, 2001). Here, *in vitro* alternatives have been tried out to more precisely reduce the autoantibody concentration in the suspension by offering their specific target. Therefore, the autoantibody-containing solution was incubated for 1 h with transfected HEK293 cells and three times transferred to fresh GlyRα1 transfected HEK293 cells. All patient autoantibodies were completely reduced within three transfers, indicated by a decrease in fluorescent signal (Fig. 27). However, the amount of transfers that were sufficient for complete depletion varied. Patient 1, 6 and 9 autoantibodies were reduced after three transfers whereas patient 7 and 8 autoantibodies were depleted after one transfer. This could be due to different autoantibody titers in patients. In healthy and disease control, no fluorescent signal was detectable. In comparison, mAb2b was not reduced within three solution transfers which was possibly caused by the high antibody concentration used. The ratio of mean signal intensity from patient serum to mean intensity of GFP signal was used to quantify the autoantibody reduction (pictures of GFP signal not shown here). Thereby, the GFP signal was used as

reference. Positive GFP signals document successfully transfected cells. The calculated ratio demonstrated that the reduction from first to second coverslip was the highest for all patient sera tested, ranging from 30% to 85% (Fig. 28, Tab. 28). In patient 1 and 9, the ratio was gradually decreasing from coverslip 2 to 4 whereas in patient 6-8 the values did not differ that much. The ratio of patient serum signal to GFP signal was significantly decreased from first to second, third and fourth coverslip in all patients (except coverslip 1 to 2 in patient 9) (p-values of t-test summarized in Tab. 29). There was no significant difference between coverslip 1 and 2-4 in mAb2b, disease and healthy control. The ratio of the mAb2b signal to GFP signal stayed at a high level around 0.3 in all four coverslips whereas the ratio of healthy and disease control was in the range of 0.2 regardless of the coverslip number.

Another concept for specific targeting of antibodies and thereby neutralizing them includes the usage of the GlyRα1 extracellular domain (ECD) which was shown to harbor the estimated amino acid sequence determined as part of the autoantibody epitope (Fig. 16). There were GlyR constructs available that contain the extracellular domain which was coupled to a 6x his-tag (Fig. 29A). The original signal peptide, transmembrane domains 1-4 and intracellular loop of the GlyRs were removed. These ECD constructs were purified and refolded following a procedure described in Breitinger et al. (2004) and kindly provided by Christoph Kluck (Institute of Biochemistry, FAU Erlangen-Nürnberg) and Daniela Schneeberger (Rudolf-Virchow Center, Würzburg). First, three GlyRα1 and one GlyRα2 ECD constructs were tested for applicability by using Western blot analysis. Therefore, the ECD constructs were loaded on a gel and stained with Coomassie Blue, pan-α antibody mAb4a or an anti-his-tag antibody. The Coomassie staining of GlyRα2 ECD exhibited a bright but clear band although there was some background in the lower part of the lane (Fig. 29B left). In contrast, all three tested GlyRα1 ECDs provided clear, strong bands without any background. Staining of Western blot membranes with mAb4a resulted in two stronger bands at the GlyRα2 ECD sample whereas the higher band was also appearing in the Coomassie stain (Fig. 29B middle). GlyRα1 ECD 1 and 2 showed a strong band at around 29 kDa in line with the expected molecular weight of the constructs and a second band at around 58 kDa representing dimer formation. In contrast, for GlyRα1 ECD 3 many protein bands in the mAb4a staining were visible, probably including unspecific or degradation bands. The anti-his-tag staining revealed no signal for the GlyRα2 ECD because of lack of a his-tag in this construct (Fig. 29B right). GlyRα1 ECDs 1-3 exhibit strong, specific bands at around 29 kDa and a second band at around 58 kDa in the anti-his-tag staining. In conclusion, the GlyRα1 ECD 2 was selected for further experiments. For simplification, the GlyRα1 ECD 2 is called GlyRα1 ECD from now on.

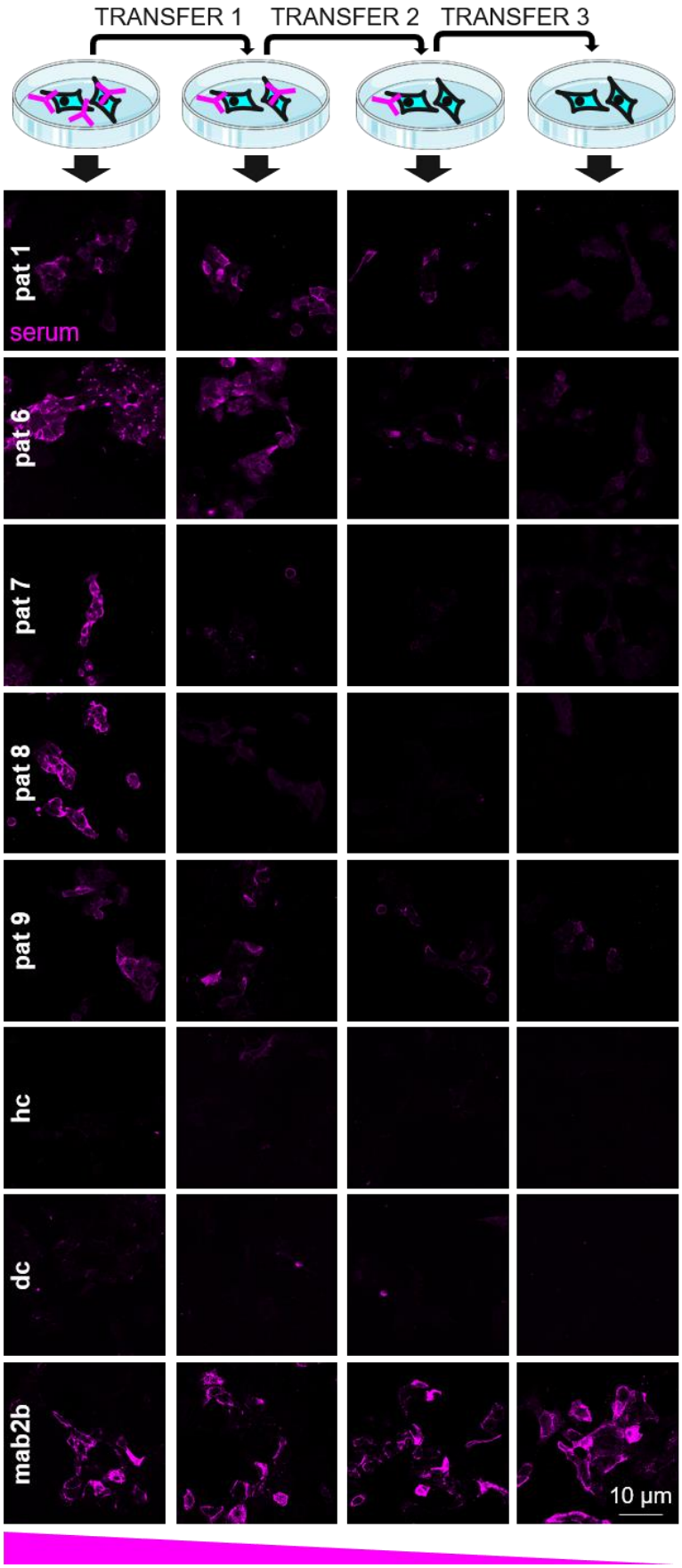

Fig. 27: Neutralization of autoantibodies by solution transfer using transfected HEK293 cells. Patient autoantibody containing solutions were transferred three times to new GlyRα1 transfected HEK293 cells. Healthy control, disease control and mAb2b were used as controls. dc = disease control; hc = healthy control; pat = patient.

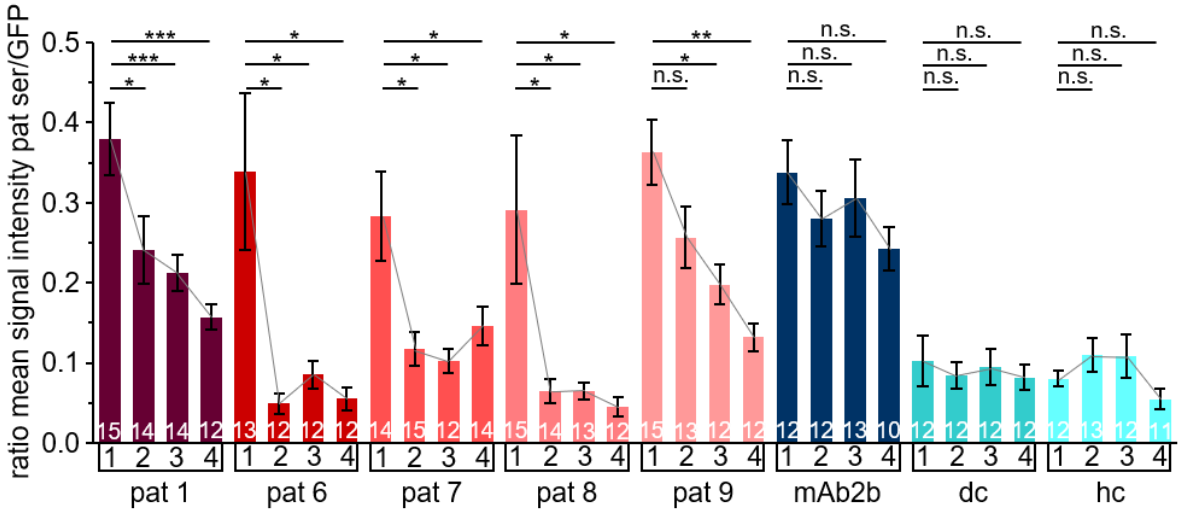

Fig. 28: Quantification of autoantibody neutralization by solution transfer. The ratio from the mean signal intensity of patient serum signal to mean signal intensity of GFP was calculated. White numbers in bars refer to number of analyzed pictures in four independent experiments. Black numbers 1-4 indicate the coverslip where HEK293 cells were attached to. dc = disease control; hc = healthy control; pat = patient.

Tab. 28: Calculated ratio of mean signal intensity patient serum to GFP signal from each coverslip.

	ratio mean signal intensity pat ser/GFP **coverslip 1**	ratio mean signal intensity pat ser/GFP **coverslip 2**	ratio mean signal intensity pat ser/GFP **coverslip 3**	ratio mean signal intensity pat ser/GFP **coverslip 4**
pat 1	0.38 ± 0.05	0.24 ± 0.04	0.21 ± 0.02	0.16 ± 0.02
pat 6	0.34 ± 0.10	0.05 ± 0.01	0.09 ± 0.02	0.06 ± 0.01
pat 7	0.28 ± 0.06	0.12 ± 0.02	0.10 ± 0.01	0.15 ± 0.02
pat 8	0.29 ± 0.09	0.06 ± 0.01	0.06 ± 0.01	0.05 ± 0.01
pat 9	0.36 ± 0.04	0.26 ± 0.04	0.20 ± 0.03	0.13 ± 0.02
mab2b	0.34 ± 0.04	0.28 ± 0.03	0.31 ± 0.05	0.24 ± 0.03
dc	0.10 ± 0.02	0.08 ± 0.02	0.09 ± 0.02	0.08 ± 0.02
hc	0.08 ± 0.01	0.11 ± 0.02	0.11 ± 0.03	0.05 ± 0.01

dc = disease control; hc = healthy control; pat = patient; ser = serum.

Tab. 29: Calculated p-values of mean signal intensity patient serum to GFP signal.

	p-value **coverslip 1 to 2**	p-value **coverslip 1 to 3**	p-value **coverslip 1 to 4**
pat 1	0.021 (*)	$6.2xE^{-04}$ (***)	0.0007 (***)
pat 6	0.018 (*)	0.028 (*)	0.023 (*)
pat 7	0.013 (*)	0.030 (*)	0.018 (*)
pat 8	0.026 (*)	0.033 (*)	0.040 (*)
pat 9	0.119	0.018 (*)	0.004 (**)
mab2b	0.155	0.236	0.279
dc	0.502	0.791	0.476
hc	0.273	0.310	0.159

dc = disease control; hc = healthy control; pat = patient. P-values were calculated by using the t-test. Stars in brackets indicate significance level, other p-values exhibit no significance.

In addition, the binding ability of patient autoantibodies to GlyRα1 ECD was tested by Western blot analysis. Therefore, the GlyRα1 ECD was loaded on a gel, then blotted on a nitrocellulose membrane which was incubated with patient 1 serum and IgG, followed by secondary anti-human antibody. Incubation with both patient 1 serum and IgG resulted in a clear band at around 29 kDa (Fig. 29C). The GlyRα1 ECD was also detected by mAb4a, shown by a strong band. The negative control, incubation with disease control serum, led to no detectable signal. These results enabled the usage of GlyRα1 ECD to specifically target autoantibodies.

As a first approach to neutralize autoantibodies from a suspension, the GlyRα1 ECD was coupled to ELISA plates. The plates were incubated with autoantibody containing sera and the supernatants from the wells were transferred to GlyRα1 transfected HEK293 cells followed by immunocytochemical staining to visualize remaining autoantibodies. In patient 6 and 8, this procedure resulted in no fluorescent signal, indicating no remaining autoantibodies and successful neutralization (Fig. 30 left). However, patient 1, 7 and 9 led to fluorescent signals after staining, suggesting an incomplete autoantibody reduction. To circumvent this problem that might occur from different autoantibody titers of the used patient samples, the autoantibody containing solution was transferred three times to new GlyRα1 ECD coated wells followed by transfer to GlyRα1 transfected HEK293 cells. Indeed, with this procedure no fluorescent signal was visible for all patient sera tested (Fig. 30 right). No fluorescent signal was detected in the disease and healthy control as well as in the mAb4a incubation regardless if only one or four suspension transfers were conducted (Fig. 31).

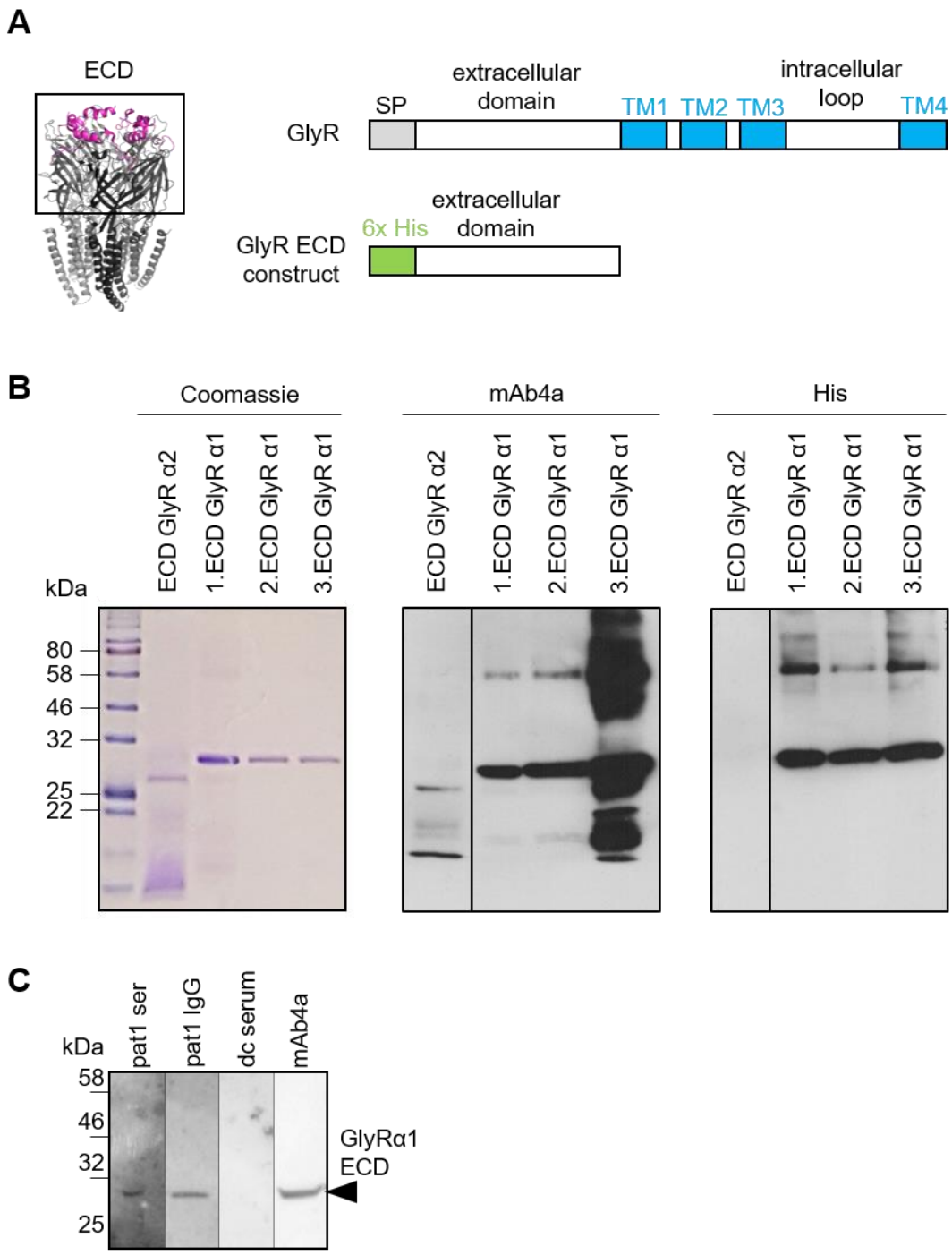

Fig. 29: Characterization of GlyRα1 extracellular domain construct. (**A**) Structural scheme of GlyR (left) with box showing the extracellular domain. Composition of one GlyR subunit (right top) including signal peptide (SP, grey), extracellular domain (white), transmembrane domains 1-4 (TM1-4, blue) and intracellular loop (white). Composition of GlyR ECD constructs (right bottom) harboring 6 his-tags (green) at the N-terminus followed by the extracellular domain (white). (**B**) Western blot analysis of ECD construct from GlyRα2 and three different ECD constructs of GlyRα1. Coomassie staining (left) and Western blots stained with mAb4a (middle) as well as anti-his-tag antibody (right) are shown. (**C**) GlyRα1 ECD 2 construct was stained with patient 1 serum, patient 1 IgG, disease control serum and mAb4a. dc = disease control; pat = patient; ser = serum.

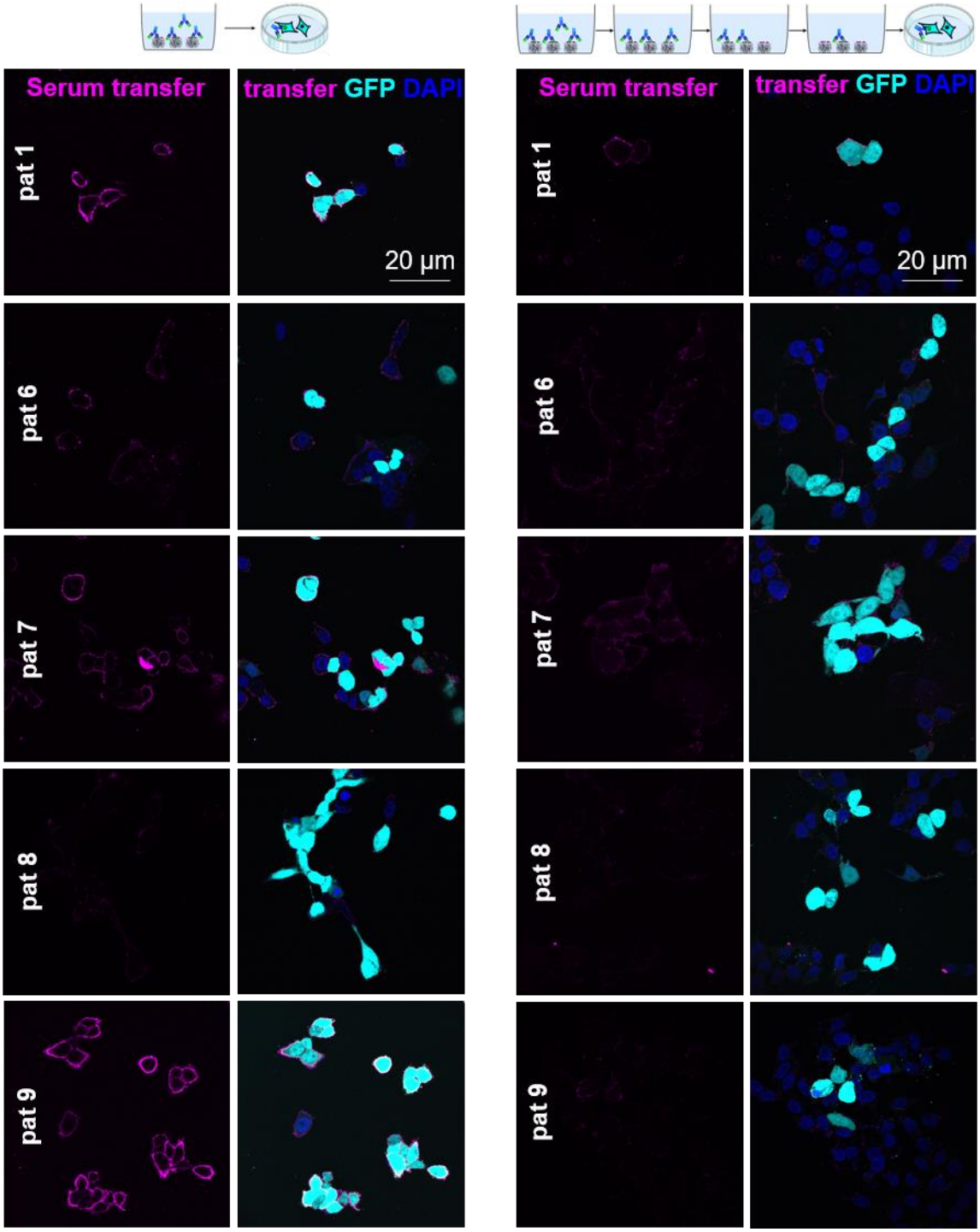

Fig. 30: Autoantibody neutralization with GlyRα1 ECD constructs bound to ELISA plates. Patient sera (magenta) were diluted 1:100 and applied to an ELISA plate coated with GlyRα1 ECD. After, solution was either transferred directly to GlyRα1 and GFP (cyan) co-transfected HEK293 cells (left) or transferred three times to new wells coated with GlyRα1 ECD followed by transfer to GlyRα1 and GFP co-transfected HEK293 cells (right). DAPI staining (blue) is shown in merged picture. pat = patient.

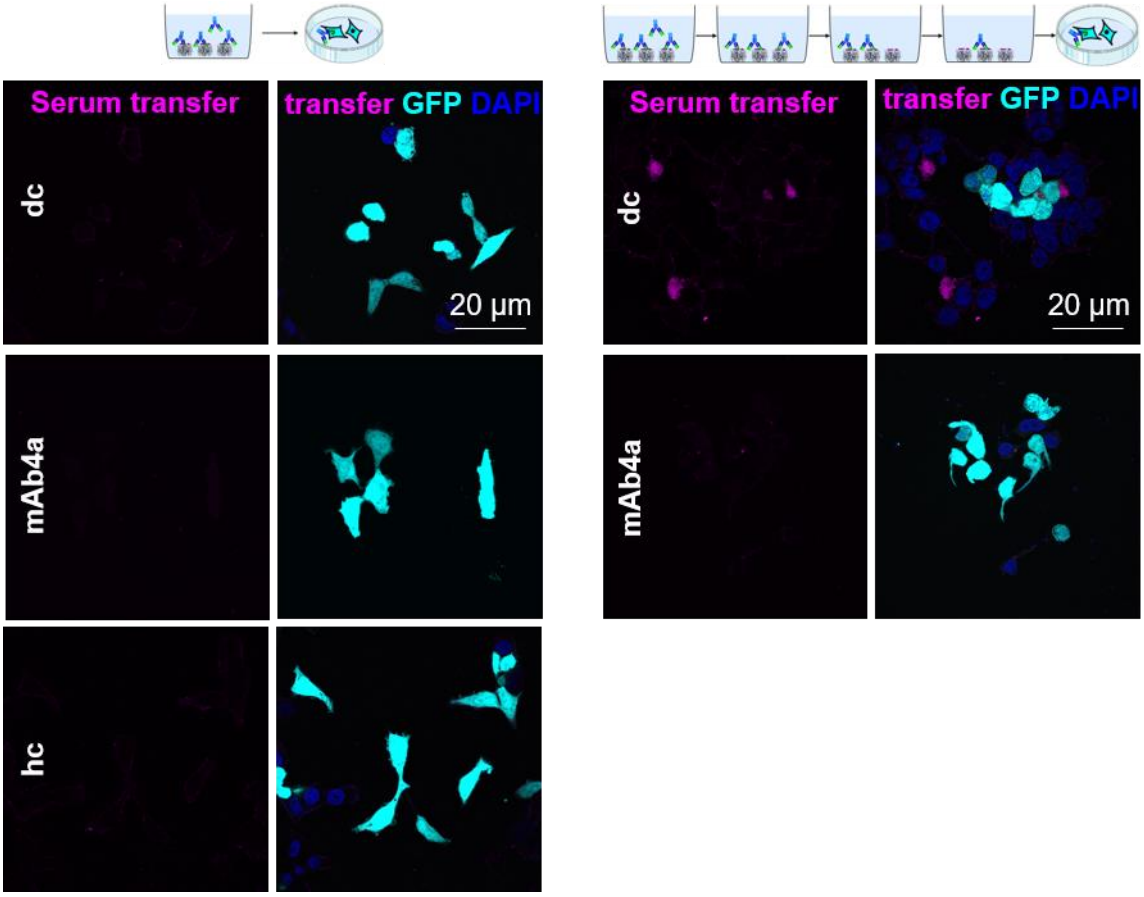

Fig. 31: Controls for autoantibody neutralization with GlyRα1 ECD constructs bound to ELISA plates. Disease and healthy control were diluted 1:100 and mAb4a 1:500 (magenta) and applied to well-plates coated with GlyRα1 ECD followed by either direct transfer to GlyRα1 and GFP (cyan) co-transfected HEK293 cells (left) or three transfers to new wells coated with GlyRα1 ECD followed by transfer to GlyRα1 and GFP co-transfected HEK293 cells (right). dc = disease control; hc = healthy control.

As a next step, the ELISA plates were used concerning the patient autoantibody binding to the GlyRα1 ECD. In brief, ELISA plates were coated with GlyRα1 ECD, and patient autoantibodies were incubated followed by application of secondary HRP-labelled antibodies (Fig. 32A). Finally, TMB substrate reacts with the HRP and this reaction was stopped with the application of acid resulting in a color change from blue to yellow (Fig. 32A, B). For analysis, the absorbance of the samples was measured with an ELISA reader at 450 nm. The highest absorbance of 2.4, which was significantly higher than disease and healthy control, showed the mAb4a because of high antibody concentration (Fig. 32, Tab. 30, Tab. 31). In contrast, the patient autoantibodies exhibited low absorbance values. Patient 1 and 7 showed the highest absorbance among the patient sera with values around 0.1 and 0.08, respectively, which were significantly higher than the disease control. Autoantibodies of patient 6 and 9 seemed to bind with lower intensity with absorbance levels of about 0.05 similar to values observed for the healthy control serum. Incubation with disease control serum elicited an absorbance of 0.03. The lowest absorbance of 0.02 was measured from patient 8 autoantibodies. Thus, all patient

autoantibodies bind to the GlyRα1 ECD coated ELISA plates but with much lower affinities than the commercial antibody mAb4a.

In summary, it is possible to specifically reduce and neutralize GlyRα1 autoantibodies from solutions by using GlyRα1 transfected HEK293 cells or purified and refolded GlyRα1 ECD constructs. Thereby, several neutralizing steps have to be performed.

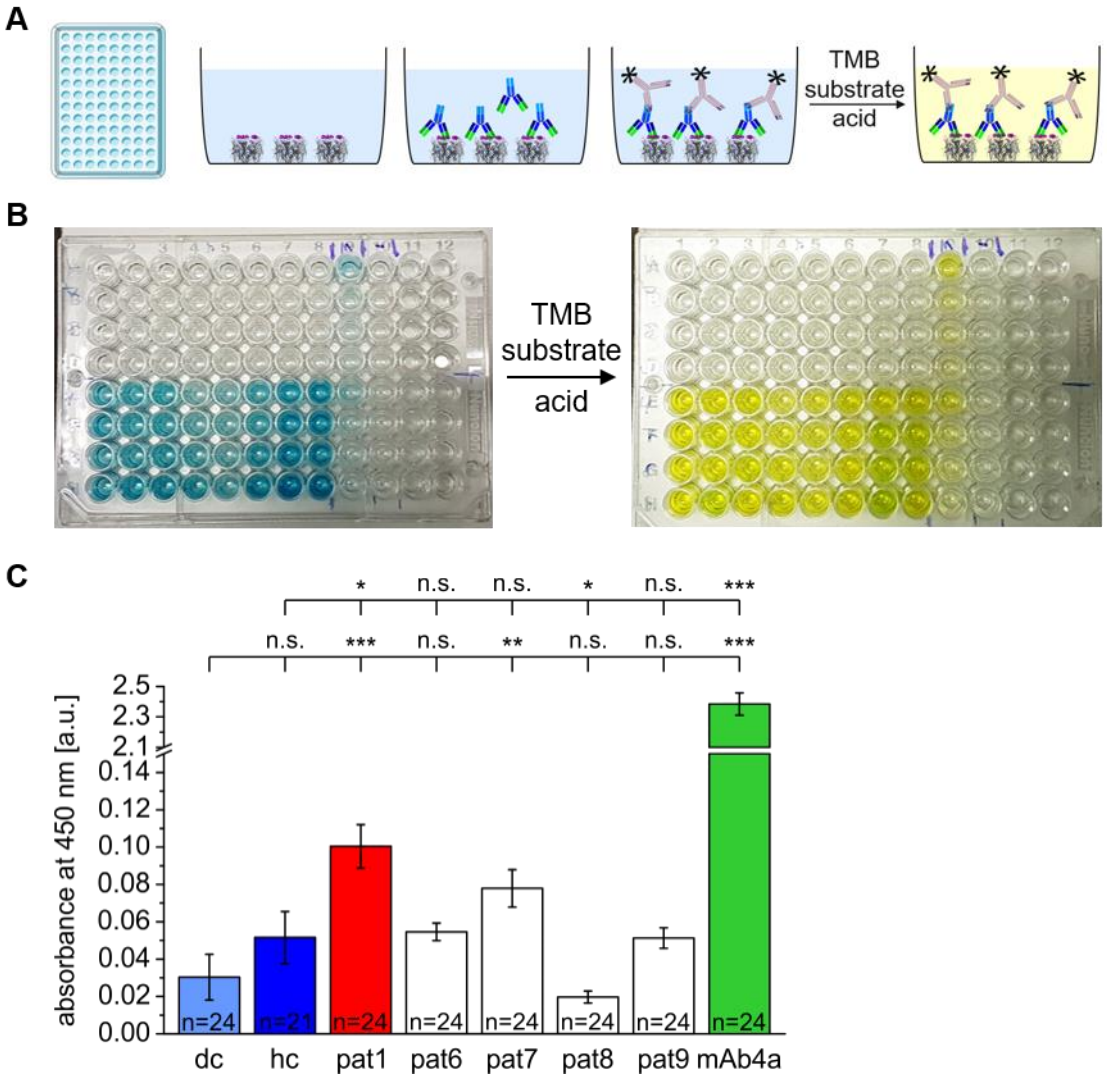

Fig. 32: ELISA of autoantibodies binding to extracellular domain. (**A**) Scheme of ELISA experiment. From left to right: ELISA plate was coated with GlyRα1 ECD construct (grey) and autoantibodies (blue) were added. After, secondary HRP labelled antibody (rose) was applied, TMB substrate was added to wells and reaction stopped with acid, thereby a color change from blue to yellow became visible. (**B**) Color change from blue to yellow by adding acid to TMB substrate. (**C**) Absorbance of samples recorded at 450 nm. ELISA plate was incubated with patient sera, disease control and healthy control in a 1:100 dilution. Dilution of mAb4a was 1:500. n number refers to analyzed wells of 6 independent experiments. dc = disease control; hc = healthy control; pat = patient.

Tab. 30: ELISA read-outs from plates incubated with patient autoantibodies.

condition	dilution	n	absorbance at 450 nm [a.u.]
patient 1	1:100	24	0.10 ± 0.01
patient 6	1:100	24	0.05 ± 0.00
patient 7	1:100	24	0.08 ± 0.01
patient 8	1:100	24	0.02 ± 0.00
patient 9	1:100	24	0.05 ± 0.01
dc	1:100	24	0.03 ± 0.01
hc	1:100	21	0.05 ± 0.01
mAb2b	1:500	24	2.38 ± 0.07

dc = disease control; hc = healthy control.

Tab. 31: Calculated p-values from t-test of ELISA read outs.

	p-value tested against **dc**	p-value tested against **hc**
disease control	-	0.275
healthy control	0.275	-
patient 1	0.0001 (***)	0.011 (*)
patient 6	0.075	0.843
patient 7	0.004 (**)	0.129
patient 8	0.414	0.039 (*)
patient 9	0.130	0.983
mab2b	$2.3 \times E^{-26}$ (***)	$1.9 \times E^{-26}$ (***)

P-values were calculated by using the t-test. Stars in brackets indicate significance level, other p-values exhibit no significance. dc = disease control; hc = healthy control.

3.5 *In vivo* animal models

3.5.1 Passive transfer of GlyRα1 autoantibodies into zebrafish larvae

For better understanding of autoantibodies and their disease pathology as well as to demonstrate a causal relation that autoantibodies harbor pathological potential, it is necessary to passively transfer the autoantibodies into animals thereby creating an animal model that can be used in further experiments and studies. If the injected animals develop similar symptoms to that observed in human patients suffering from SPS, the autoantibodies themselves can be determined pathologic. Additionally, using these animal models, the signaling pathways after autoantibody binding can be analyzed *in vivo*. First, zebrafish larvae as passive transfer model for autoantibodies were chosen because disturbed glycinergic neurotransmission can be easily and reliably tested by analyzing the touch-evoked escape responses. This method was previously used to examine effects of GlyR knockouts or point mutations e.g. in the

hyperekplexia model *bandoneon* which led to strong motor dysfunction and bilateral muscle contractions (Hirata et al., 2005; Ganser et al., 2013; Samarut et al., 2019).

Before starting the passive transfer into zebrafish larvae, it was necessary to analyze binding properties of patient autoantibodies to the different zebrafish GlyR subunits α1^{dr}, α2^{dr}, α3^{dr}, α4a^{dr}, α4b^{dr}, βa^{dr} and βb^{dr}. In the epitope characterization, most of the patient sera showed no binding to GlyRα1^{dr} but detected the chimera GlyRα1^{ch} (Fig. 16). Thus, the ability of autoantibodies to bind the other zebrafish subunits needs to be figured out as basis for successful usage of zebrafish larvae as passive transfer model. Aligning the zebrafish GlyR subunits indicated that they differ from human GlyRα1 mainly in far N-terminal region although there are also identical parts including the mAb4a epitope (Fig. 33). Immunocytochemical stainings indicated that only patient 4, 5 and 8 autoantibodies were able to bind the GlyRα1^{dr} whereas patient 1, 2 and 3 did not (Fig. 34). GlyRα2^{dr} was bound by autoantibodies from patient 2, 4 and 5 whereas patient 1, 3 and 8 autoantibodies exhibited no fluorescent signal. In contrast, all patient samples used containing GlyR autoantibodies, except patient 1 autoantibodies, were able to bind GlyRα3^{dr}. In GlyRα4a^{dr} transfected HEK293 cells, patient 1, 4 and 5 autoantibodies showed strong fluorescent signal, whereas patient 8 autoantibodies displayed weak binding and patient 2 and 3 yielded no binding. Autoantibodies from patient 1, 2, 4 and 5 indicated weak binding to GlyRα4b^{dr} whereas patient 3 and 8 were not able to bind to this subunit. MAb4a as positive control bound to all zebrafish GlyRα subunits. Analyzing the binding ability of patient autoantibodies to the zebrafish GlyRβ subunits revealed that none of the tested patient autoantibodies detected GlyRβa^{dr} or GlyRβb^{dr}, except patient 1 autoantibodies which marginally bound to GlyRβa^{dr} and patient 8 autoantibodies marginally to GlyRβb^{dr} (Fig. 35). MAb4a exhibited only weak binding to GlyRβb^{dr}. These results showed that patient autoantibodies target different zebrafish GlyR subunits which indicates that zebrafish larvae can be used in passive transfer experiments.

Passive transfer of patient autoantibodies into zebrafish occurred with two different methods. Either autoantibodies were directly injected into the 4th ventricle with a glass needle or the skin above the 4th ventricle was opened followed by treatment with autoantibodies in the swimming medium. 20 h later, touch-evoked escape responses were tested, and three different phenotypes were differentiated as described earlier (Hirata et al., 2013; Schaefer et al., 2018b). The zebrafish larvae had normal escape responses when they could swim very fast out of the camera view field after they were poked with a needle (Fig. 36A_1-A_3). A mild phenotype was characterized by the larvae's ability to move and swim away but it was a slow escape response and the zebrafish larvae did not swim out of the camera field of view (Fig. 36B_1-B_3). The severe phenotype existed when the zebrafish larvae was not able to swim away although it could move the tail (Fig. 36C_1-C_3).

Fig. 33: Alignment of zebrafish GlyR subunits with human GlyRα1. Comparison of amino acid sequence of GlyR α and β subunits of zebrafish to human GlyRα1. Amino acid deviations between zebrafish GlyR subunits and GlyRα1^{hs} are depicted in bold letters. Epitope of mAb2b is indicated by underlined amino acids and mAb4a epitope is shown in blue underlined letters. dr = *danio rerio*; hs = *homo sapiens*.

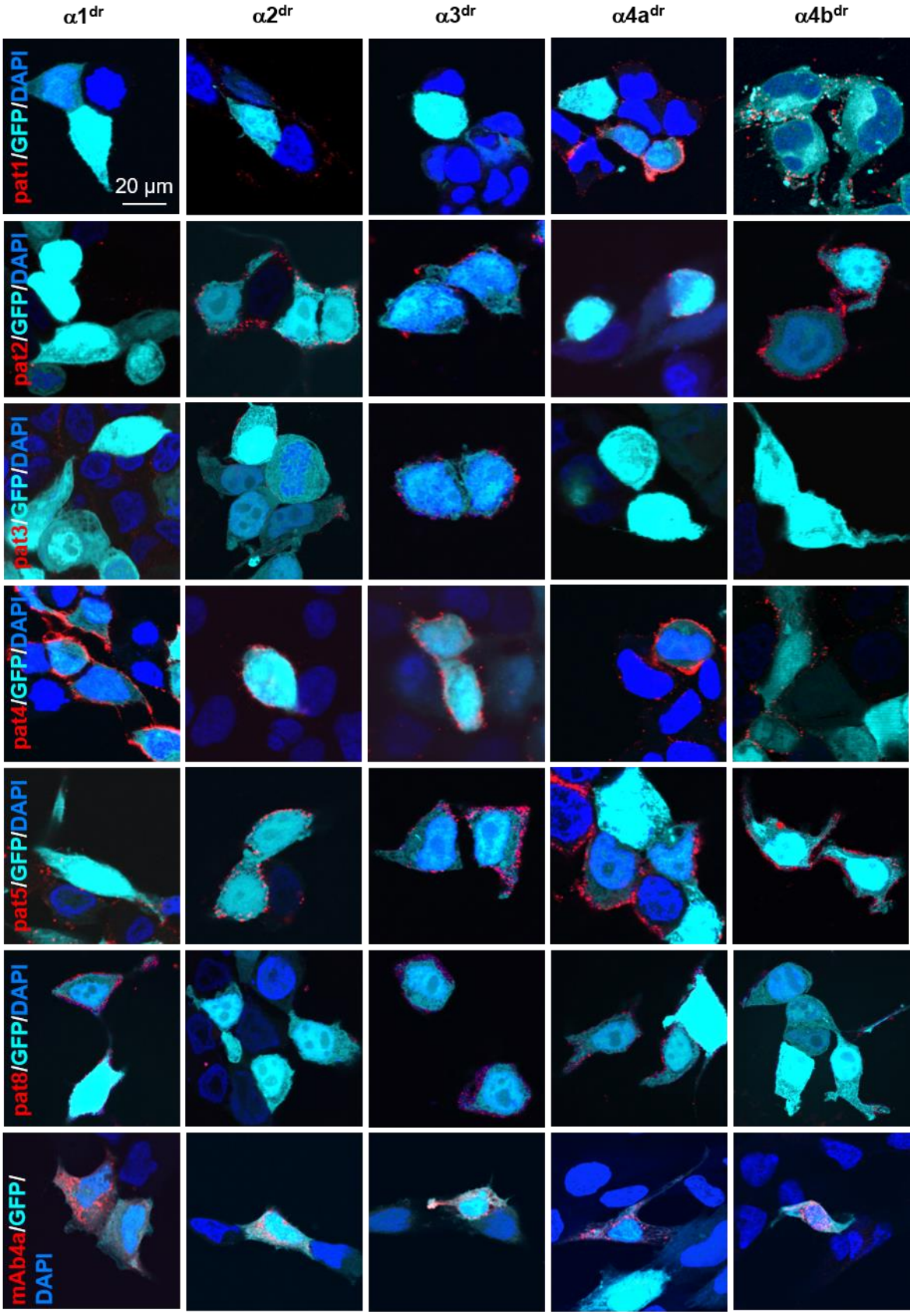

Fig. 34: Binding pattern of patient autoantibodies to different zebrafish GlyRα^{dr} subunits. HEK293 cells were transfected with GlyR α1^{dr}, α2^{dr}, α3^{dr}, α4a^{dr} or α4b^{dr} together with GFP (cyan) and stained with patient serum or mAb4a (red). DAPI staining (blue) was included. dr = *danio rerio*; pat = patient.

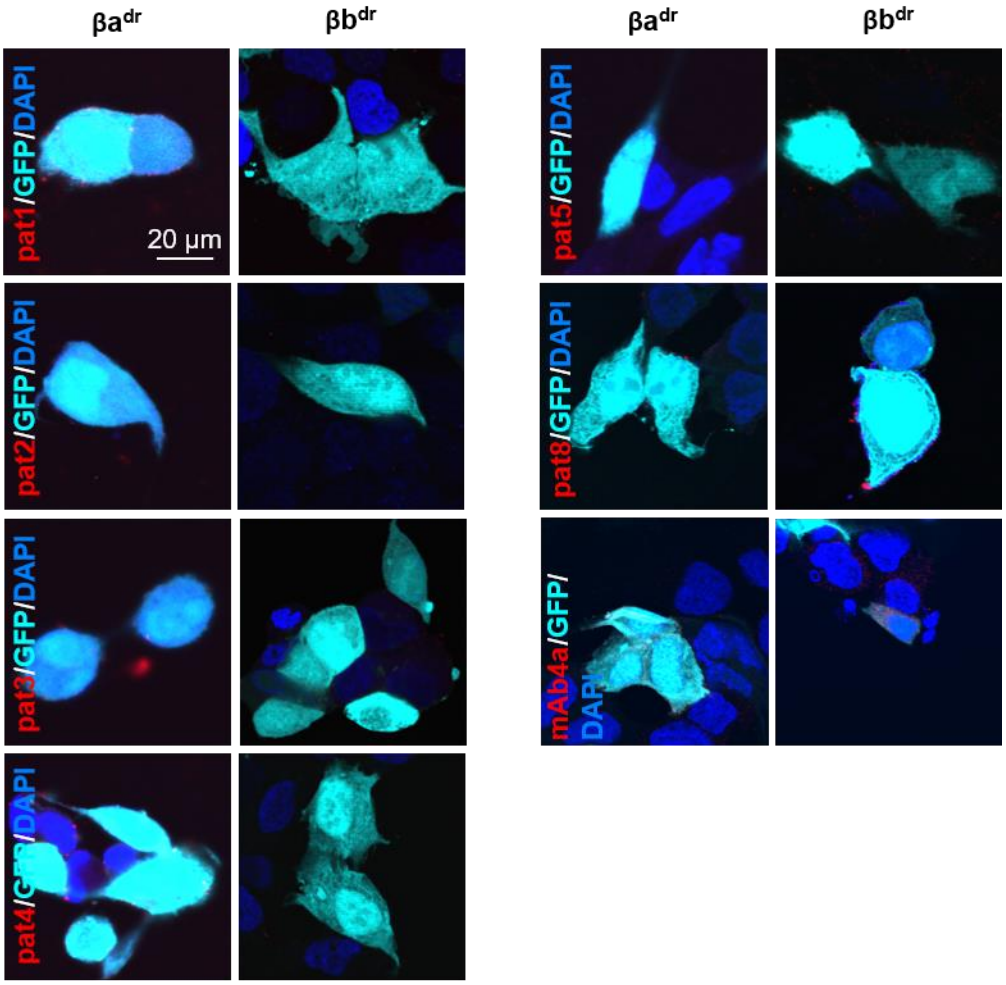

Fig. 35: Binding pattern of patient autoantibodies to different zebrafish GlyRβ^{dr} subunits. Immunocytochemical stainings of GlyRβa^{dr} or βb^{dr} transfected HEK293 cells (co-transfected with GFP, cyan) incubated with patient serum or mAb4a (red). DAPI staining (blue) was added. dr = *danio rerio*; pat = patient.

First, phenotypical differences in zebrafish larvae that were directly injected with patient autoantibodies were analyzed. In larvae injected with healthy control serum, 84.7% exhibited a normal phenotype whereas 14.3% showed a severe phenotype which was probably related to the transfer procedure (Fig. 36D, Tab. 32, statistical analysis in Supplementary tab. 1). Additionally to the healthy control, a disease control of a patient with only GAD autoantibodies was used because GAD autoantibodies also trigger SPS (Alexopoulos et al., 2013; McKeon et al., 2013) and one patient sample was used carrying GlyRα1 as well as GAD autoantibodies as it was shown for 15% of the SPS patients. All GAD positive serum injected zebrafish larvae presented a normal phenotype. In patient 1 serum injected larvae, the percentage of larvae with normal phenotype was decreased to 50% and severe as well as mild phenotype occurrence was increased to 25%.

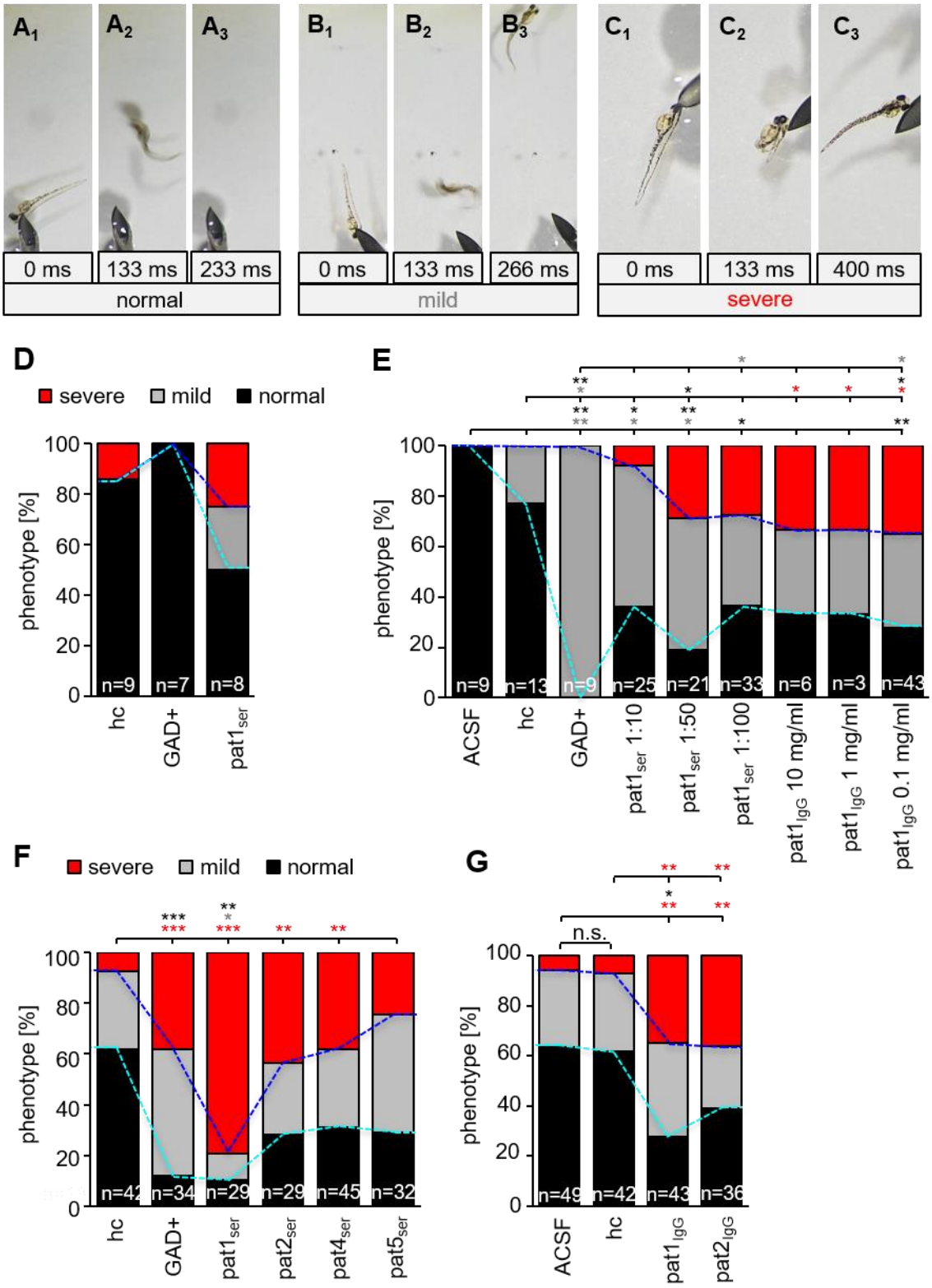

Fig. 36: Escape response of zebrafish larvae treated with patient autoantibodies. Autoantibodies were passively transferred either directly into the 4th ventricle or via diffusion through a lesion in the skin above the 4th ventricle. (**A1-A3**) Normal escape response of zebrafish larvae. Upon touch, zebrafish larvae swam quickly away out of the camera area. (**B1-B3**) Mild phenotype of zebrafish larvae. Touching the larvae resulted in an escape response but more slowly than normal phenotype and the zebrafish stops within the camera field of view. (**C1-C3**) Severe phenotype in zebrafish larvae. The zebrafish larvae were still able to move but touch evoked escape was missing. (**D**) Percentage of severe (red), mild (grey) and normal phenotype (black) in zebrafish larvae that were

injected with healthy control, GAD positive serum or patient 1 serum directly into the 4th ventricle. Blue line indicates changes in severe phenotype whereas cyan line shows differences in normal phenotype. (**E**) Phenotypical changes in larvae with skin lesions above the 4th ventricle treated with ACSF, healthy control, GAD positive serum as well as patient 1 serum and purified IgG in different dilutions/concentrations stated in the figure. (**F**) Phenotypical diversity of zebrafish larvae with skin lesions and treatment with healthy control, GAD positive serum and four different patient sera (dilution 1:100). (**G**) Percentage of normal, mild and severe phenotype in zebrafish larvae with skin lesions and patient IgG treatment (0.1 mg/ml) compared to ACSF and healthy control serum (1:100). ACSF = artificial cerebrospinal fluid; GAD = glutamate decarboxylase; hc = healthy control; pat = patient.

Tab. 32: Distribution of normal, mild and severe phenotype in zebrafish larvae that were injected with patient autoantibodies.

	dilution	n	normal phenotype [%]	mild phenotype [%]	severe phenotype [%]
hc	1:100	9	85.7	0.0	14.3
GAD$^+$	1:100	7	100.0	0.0	0.0
pat 1	1:100	8	50.0	25.0	25.0

n refers to number of injected zebrafish larvae. GAD$^+$ means patient serum containing only GAD autoantibodies. GAD = glutamate decarboxylase; hc = healthy control; pat = patient.

Tab. 33: Distribution of normal, mild and severe phenotype in zebrafish larvae with skin lesion above 4th ventricle and treatment with different dilutions/concentrations of patient 1 serum and IgG.

	dilution/ concentration	n	normal phenotype [%]	mild phenotype [%]	severe phenotype [%]
ACSF	-	9	100.0	0.0	0.0
hc	1:100	13	76.9	23.1	0.0
GAD$^+$	1:100	9	0.0	100.0	0.0
pat 1	1:10	25	36.0	56.0	8.0
pat 1	1:50	21	19.0	52.4	28.6
pat 1	1:100	33	36.4	36.4	27.2
pat 1 IgG	10 mg/ml	6	33.3	33.3	33.3
pat 1 IgG	1 mg/ml	3	33.3	33.3	33.3
pat 1 IgG	0.1 mg/ml	43	27.9	37.2	34.9

n refers to number of injected zebrafish larvae. GAD$^+$ means patient serum containing only GAD autoantibodies. ACSF = artificial cerebrospinal fluid; GAD = glutamate decarboxylase; hc = healthy control; pat = patient.

Tab. 34: Percentage of normal, mild and severe phenotype of zebrafish larvae with skin lesion above 4th ventricle and treatment with patient sera and IgG.

	dilution/ concentration	n	normal phenotype [%]	mild phenotype [%]	severe phenotype [%]
ACSF	-	49	63.3	30.6	6.1
hc	1:100	42	61.9	30.9	7.2
GAD$^+$	1:100	34	11.8	50	38.2
pat 1	1:100	29	10.3	10.3	79.4
pat 1 IgG	0.1 mg/ml	43	27.9	37.2	34.9
pat 2	1:100	32	28.1	28.1	43.8
pat 2 IgG	0.1 mg/ml	36	38.9	25.0	36.1
pat 4	1:100	29	31.0	31.0	38.0
pat 5	1:100	45	28.9	46.7	25.4

n refers to number of injected zebrafish larvae. GAD$^+$ means patient serum containing only GAD autoantibodies. ACSF = artificial cerebrospinal fluid; hc = healthy control; GAD = glutamate decarboxylase; pat = patient.

Afterwards, different concentrations of patient 1 serum and IgG were tested in zebrafish larvae with skin lesions above the 4th ventricle. ACSF and healthy control serum treated larvae elicited 100% and 76.9% normal phenotype, respectively, whereas 23.1% of healthy control group showed a mild phenotype (Fig. 36E, Tab. 33, statistical analysis in Supplementary tab. 2). All GAD positive serum treated larvae showed a mild phenotype. Compared to the controls ACSF, healthy control and GAD positive serum, in all groups of patient serum and IgG treatment, the severe phenotype was present between 8 and 33.3%. Furthermore, the percentage of mild phenotype was also increased in all treatments with patient GlyRα autoantibodies to a range of 33.3% to 56% regardless of the serum dilution or IgG concentration, while the amount of normal phenotype was reduced to 19-36.4%.

Due to low amounts of patient samples and the equal effects in the tested dilutions, patient serum was used in a dilution of 1:100 and IgG in a concentration of 0.1 mg/ml for the following experiments. It seems that at these concentrations, the maximal effect was already reached probably because of a good accessibility of the antibodies to their target through the lesion.

Next, the different patient sera were tested with larvae possessing skin lesions. The percentage of severe phenotype was significantly increased in all patient sera reaching a maximal level in patient 1 serum treated larvae of 79.4% (Fig. 36F, Tab. 34, statistical analysis in Supplementary tab. 3). Thus, patient 1 treated zebrafish larvae showed significantly reduced amounts of normal and mild phenotype. In contrast, the amounts of larvae representing the mild phenotype in patient serum 2, 4 and 5 treatment were almost equally compared to healthy

control serum. However, the normal phenotype was reduced when treated with patient samples 2, 4 and 5.
Purified IgG was available from patient 1 and 2 and was also tested in zebrafish larvae with skin lesions. The dramatic increase in severe phenotype reaching around 35% and reduction in normal phenotype to 27.9-38.9% compared to ACSF or healthy control was also detected in patient 1 and 2 IgG treated larvae (Fig. 36G, Tab. 34, statistical analysis in Supplementary tab. 3).

In summary, patient autoantibodies recognize different subunits of zebrafish GlyR which was a prerequisite to use the zebrafish as animal model to investigate GlyR autoantibody pathology. Passive transfer of autoantibodies verified this assumption because both patient serum and patient IgG treated larvae showed increased levels of the severity in the escape response and decreased amounts of normal escape response.

3.5.2 Passive transfer of GlyRα1 autoantibodies into mice

After successful transfer of autoantibodies into zebrafish, the transfer can be performed in higher, eukaryotic animals. Here, the patient autoantibodies were passively transferred into mice. Six mice were used for an initial test and 22 for behavioral experiments (Tab. 35, Tab. 36). The two groups of mice differed in the way of applying the patient autoantibodies. One group of test mice received manual injections and the other group received autoantibodies automatically via an osmotic pump. In the following paragraph, results of the behavioral experiments from mice with osmotic pumps are described.

Muscle stiffness is a major characteristic of SPS patients with GlyR autoantibodies. As a correlate in mice, phenotypical disturbances in locomotion were analyzed. Therefore, Rotarod performance using accelerated wheel speed was investigated on a daily basis and the times the mice spend on the rod were analyzed. As a baseline, the mice underwent the Rotarod two days before the surgery. A mixture of patient 1 and 8 IgG was made to combine the effects of autoantibodies and to create a brought spectrum of phenotypical characteristics (Geis et al., 2010). NaCl, disease control IgG and patient MIX IgG (mixture of patient 1 and 8 IgG) were injected intrathecally into mice. All mice, independent of the injected sample, performed well in the Rotarod test at every single day tested (Fig. 37A, Tab. 37, p-values summarized in Tab. 39). Regardless of the treatment, the mice stayed longer on the rod the more often the test was performed.

Afterwards, the von Frey test was conducted to estimate the sensitivity upon mechanic stimuli and pain. It is known that some SPS patients with GlyR autoantibodies feel pain but others not. Moreover, the patient autoantibodies have been shown to bind to GlyRα3 which is involved

in pain sensitization (Harvey et al., 2004; Hosl et al., 2006; Lynch and Callister, 2006; Acuna et al., 2016). Here, a significant lower paw withdrawal threshold was visible in patient MIX IgG treated mice compared to NaCl and disease control IgG injected mice at day 8 (Fig. 37B, Tab. 38, p-values are summarized in Tab. 40). Additionally, the same tendency for a decreased paw withdrawal threshold in patient MIX IgG treated mice compared to the NaCl and disease control IgG group was identified at day 3-11 albeit not reaching significance. Furthermore, the threshold decreased with increasing days after surgery in all mouse groups.

Tab. 35: Overview of test mice having an intrathecal catheter but no osmotic pump. Instead they were injected manually.

test animals (without osmotic pump)	total amount	survived
disease control	2	0
patient 1 IgG	2	2
patient 8 IgG	2	2
total	6	4

Patient MIX IgG is a mixture of patient 1 and 8 IgG.

Tab. 36: Overview of mice used in behavioral experiments. Animals were treated via a transplanted osmotic pump automatically.

experimental animals (osmotic pump)	total amount	survived
NaCl	6	5
disease control IgG	8	8
pat MIX IgG	8	6
total	22	19

Patient MIX IgG is a mixture of patient 1 and 8 IgG.

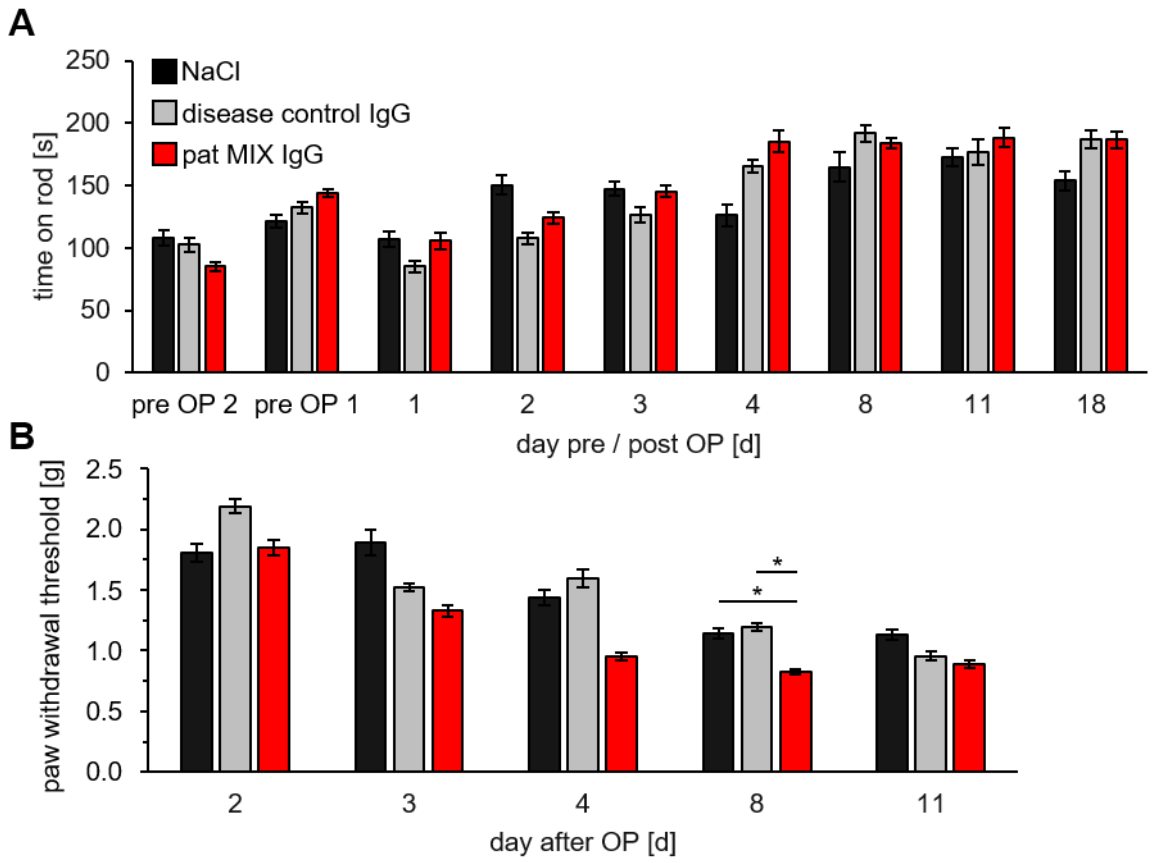

Fig. 37: Behavior of mice with passively transferred autoantibodies in Rotarod and von Frey test. (**A**) Time on rod of mice with passively transferred NaCl (black), disease control IgG (grey) and patient mix IgG (mixture of patient 1 and 8 IgG, red) at two days before operation and within 18 days after the surgery. (**B**) Paw withdrawal threshold of mice treated with NaCl (black), disease control IgG (grey) and patient MIX IgG (red) determined in von Frey test from 2 to 11 days after operation. Day of operation was defined as day 0. OP = operation; pat = patient.

Tab. 37: Rotarod analysis of NaCl, disease control IgG and pat MIX IgG treated mice.

	NaCl (n=6)	disease control IgG (n=8)	pat MIX IgG (n=8)
pre OP 2	108.1 ± 5.9	102.6 ± 5.6	85.2 ± 3.4
pre OP 1	121.4 ± 5.0	132.2 ± 4.7	143.7 ± 3.1
day 1	107.3 ± 6.3	85.2 ± 4.4	105.5 ± 6.3
day 2	150.2 ± 7.7	107.9 ± 4.7	124.0 ± 4.9
day 3	147.5 ± 5.4	126.5 ± 5.8	145.3 ± 4.8
day 4	126.3 ± 8.5	165.7 ± 4.9	185.1 ± 8.7
day 8	164.8 ± 11.7	191.6 ± 6.6	184.4 ± 4.1
day 11	172.4 ± 7.3	176.7 ± 10.2	188.5 ± 7.6
day 18	153.8 ± 7.5	186.7 ± 7.1	186.6 ± 7.0

n = number of mice; pat = patient. Day of operation was defined as day 0. Patient MIX IgG is a mixture of patient 1 and 8 IgG.

Tab. 38: Summary of calculated paw withdrawal threshold in von Frey experiments.

	NaCl (n=6)	disease control IgG (n=8)	pat MIX IgG (n=8)
day 2	1.81 ± 0.07	2.19 ± 0.06	1.85 ± 0.07
day 3	1.89 ± 0.10	1.52 ± 0.03	1.33 ± 0.05
day 4	1.44 ± 0.06	1.60 ± 0.07	0.95 ± 0.03
day 8	1.15 ±0.04	1.19 ± 0.03	0.82 ± 0.02
day 11	1.14 ± 0.04	0.95 ± 0.04	0.89 ± 0.03

n = number of mice; pat = patient. For each mouse, values for right and left paw were included. Day of operation was defined as day 0. Patient MIX IgG is a mixture of patient 1 and 8 IgG.

Tab. 39: P-values of Rotarod comparing NaCl, disease control IgG and patient MIX IgG by using the t-test.

	p-value **NaCl** against dc IgG	p-value **NaCl** against **pat MIX IgG**	p-value dc IgG against **pat MIX IgG**
pre OP 2	0.822	0.226	0.391
pre OP 1	0.599	0.188	0.511
day 1	0.318	0.947	0.399
day 2	0.106	0.309	0.442
day 3	0.402	0.919	0.427
day 4	0.144	0.147	0.532
day 8	0.449	0.491	0.762
day 11	0.896	0.561	0.721
day 18	0.314	0.252	0.997

dc = disease control; pat = patient. Day of operation was defined as day 0. Patient MIX IgG is a mixture of patient 1 and 8 IgG. All p-values indicate no significance.

Tab. 40: P-values of t-test comparing NaCl, disease control IgG and pat MIX IgG in von Frey experiment.

	p-value **NaCl** against dc IgG	p-value **NaCl** against **pat MIX IgG**	p-value dc IgG against **pat MIX IgG**
day 2	0.298	0.909	0.359
day 3	0.305	0.160	0.419
day 4	0.687	0.058	0.061
day 8	0.825	0.041 (*)	0.026 (*)
day 11	0.425	0.257	0.759

dc = disease control; pat = patient. Day of operation was defined as day 0. Patient MIX IgG is a mixture of patient 1 and 8 IgG. Stars in brackets indicate significance level, other p-values exhibit no significance.

Additionally, the Open Field test and Elevated Plus Maze were performed to analyze the exploratory behavior, locomotion performance and anxiousness level of the mice treated with patient autoantibodies. Due to hints that hyperekplexia and SPS patients are more anxious of for example sudden falls, also patient autoantibody treated mice could elicit a similar behavior (Mine et al., 2015; Hinson et al., 2018). Furthermore, the GlyRβ subunit, which could also represent a potential target for autoantibodies due to sequence similarities, was identified to be associated with increased anxiety behavior (Deckert et al., 2017). In the Open Field experiment, the total distance the mice moved was not significantly different comparing the NaCl, disease control IgG and patient MIX IgG group (Fig. 38, Tab. 41, p-values are summarized in Tab. 42). In addition, the time the mice spent in the periphery and in the center was also unchanged when mice were treated with patient MIX IgG or control mice injected with NaCl or disease control IgG. Within the recording time of 300 s, all groups of mice spent longer time in the periphery than in the center of around 250 s and 45 s, respectively.

The Elevated Plus Maze, yielded similar results like the Open Field with no significant behavioral alterations between the different groups. The total distance the mice moved was not significantly different comparing the NaCl, disease control IgG and patient MIX IgG group (Fig. 38, Tab. 43, p-values are summarized in Tab. 44). The same proportion of the total distance, like in the Open Field experiment, was detectable. Thus, the mice treated with NaCl moved least, followed by the patient MIX IgG treated mice and the disease control IgG injected mice. Furthermore, the mice spent about 220 s in the closed arm and about 70 s in the open arm regardless of the treatment.

In summary, the behavioral experiments yielded no obvious differences and thus no effect of autoantibody treated mice. At this point it was questionable if the autoantibodies indeed reached their target in the injected mice. For verification that the autoantibodies targeted GlyRs and for confirmation of the applicability of the passive transfer method in mice, immunohistochemical stainings of spinal cord and brain slices were performed. Here, samples from both groups the test mice with injections and the group with osmotic pumps were investigated.

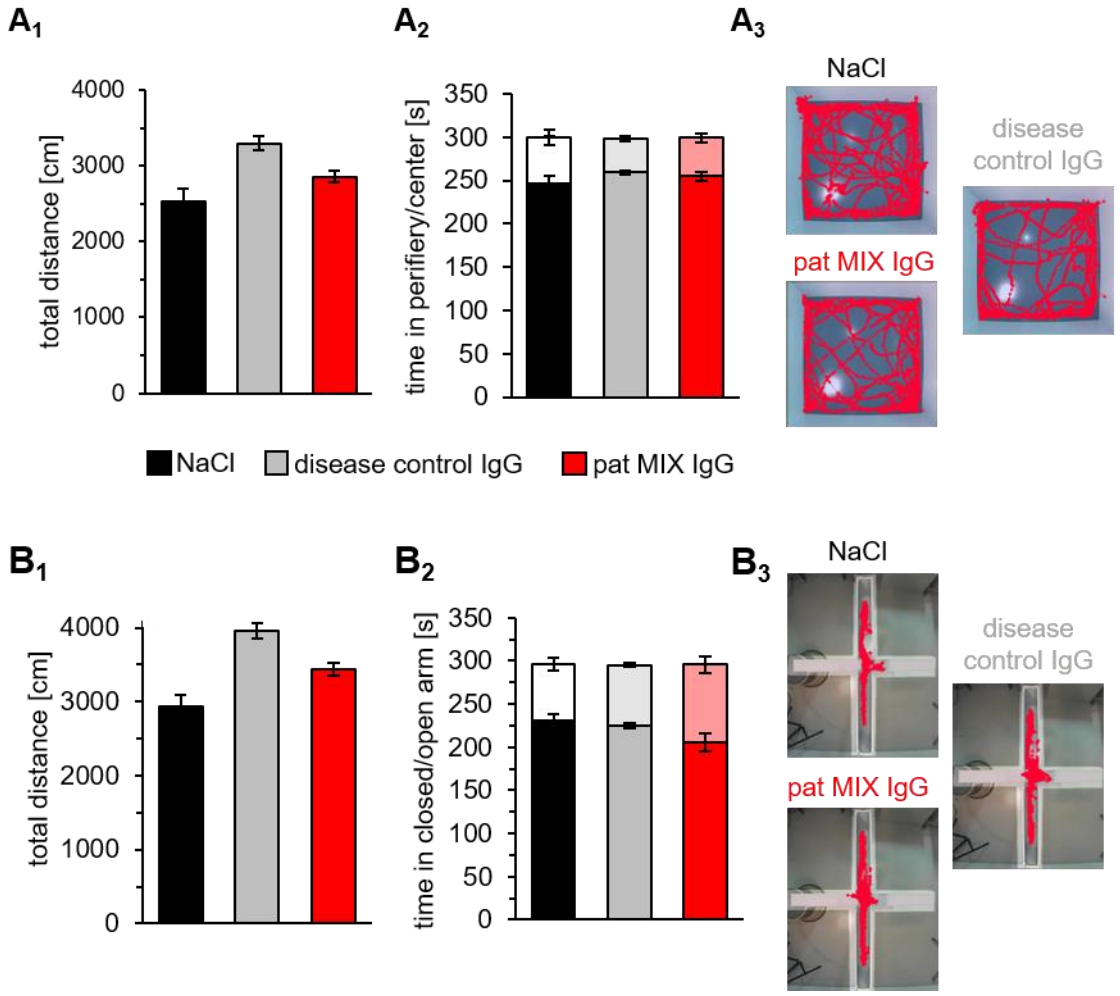

Fig. 38: Behavior of mice with passively transferred autoantibodies in Open Field and Elevated Plus Maze. (**A1-A3**) Open Field of NaCl (black), disease control IgG (grey) and mixture of IgG from patient 1 and 8 (red). Total distance (**A1**) and time in periphery (black, grey, red; **A2**) as well as time in center (white, light grey, light red; **A2**) were determined. (**A3**) Exemplary trackings of a NaCl, disease control IgG or patient mix IgG treated mice. (**B1-B3**) Analysis of Elevated Plus Maze regarding total distance (**B1**), time in closed arms (black, grey, red; **B2**) and time in open arms (white, light grey, light red; **B2**). (**B3**) Exemplary trackings of mice treated with NaCl, disease control IgG and patient MIX IgG pass through Elevated Plus Maze experiment. pat = patient.

Tab. 41: Summarized values of Open Field experiments including total distance, time in periphery and time spent in center.

	total distance [cm]	time in periphery [s]	time in center [s]
NaCl	2526.1 ± 166.2	246.8 ± 9.2	53.1 ± 9.3
disease control IgG	3295.7 ± 91.3	259.2 ± 2.8	39.2 ± 2.8
pat MIX IgG	2856.2 ± 70.7	255.0 ± 5.0	44.1 ± 5.0

pat = patient. Patient MIX IgG is a mixture of patient 1 and 8 IgG.

Tab. 42: P-values calculated from t-test comparing results from NaCl, disease control IgG and patient MIX IgG treated mice in Open Field.

	p-value **NaCl** against dc IgG	p-value **NaCl** against **pat MIX IgG**	p-value dc IgG against **pat MIX IgG**
total distance	0.135	0.450	0.229
time in periphery	0.561	0.762	0.810
time in center	0.520	0.737	0.786

dc = disease control; pat = patient. All p-values indicate no significant changes.

Tab. 43: Values analyzed from Elevated Plus Maze including total distance, time in open and in closed arm.

	total distance [cm]	**time in closed arm [s]**	**time in open arm [s]**
NaCl	2939.6 ± 153.1	231.2 ± 7.6	65.7 ± 7.5
disease control IgG	3963.3 ± 107.3	225.0 ± 2.8	70.5 ± 2.6
pat MIX IgG	3438.5 ± 94.3	205.8 ± 10.2	89.8 ± 9.9

pat = patient. Patient MIX IgG is a mixture of patient 1 and 8 IgG.

Tab. 44: P-values determined from t-test comparing the NaCl, disease control IgG and pat MIX IgG group in Elevated Plus Maze experiment.

	p-value **NaCl** against dc IgG	p-value **NaCl** against **pat MIX IgG**	p-value dc IgG against **pat MIX IgG**
total distance	0.070	0.311	0.244
time in closed arm	0.740	0.560	0.557
time in open arm	0.786	0.567	0.541

dc = disease control; pat = patient. All p-values indicate no significance.

Immunohistochemical stainings of spinal cord slices from disease control IgG injected test mice (without osmotic pumps) revealed no fluorescent signal when incubated with anti-human secondary antibody (Fig. 39A). Signals of mAb4a as a control for all GlyRα subunits and synaptophysin as a synaptic marker were bright. Following the passive transfer of patient 1 and 8 IgG, bright fluorescence signals were detectable in higher magnifications in addition to stainings with mAb2b/mAb4a antibodies and VGAT/synaptophysin (Fig. 39B, C, Supplementary fig. 2B). The fluorescent signal of patient MIX IgG in mice with transplanted osmotic pumps was visible in higher magnifications as well but it was weaker than the signal

in the test mice directly injected with the patient GlyR autoantibody IgGs (Fig. 40C, Supplementary fig. 2A). In contrast, no signal was detectable in mice with osmotic pumps that were treated with NaCl or disease control IgG (Fig. 40A, B).

In addition to the spinal cord, different brain regions that were shown to be rich in glycine receptors were also immunohistochemically analyzed. Due to the higher signal intensity in mice injected manually with patient IgG (without osmotic pumps), the focus in the analysis of the brain region was on those mice. No fluorescent signal or only background signal was detectable in brain slices of a mouse treated with disease control IgG in regions including hypoglossal nucleus, pre Bötzinger complex, lateral superior olive, superior paraolivary nucleus and inferior colliculus (Fig. 41, Fig. 42). In contrast, mAb2b/mAb4a and synaptophysin/VGAT staining resulted in a bright signal in these brain areas. In the hypoglossal nucleus and pre Bötzinger complex of a mouse injected with patient 1 IgG, no fluorescent signal was visible although mAb2b/mAb4a and synaptophysin/VGAT staining was detectable (Fig. 43A). However, in the cochlear nucleus, lateral superior olive, superior paraolivary nucleus and inferior colliculus, some bright dots were identified in patient 1 IgG treated mouse (Fig. 43B, Fig. 44). In patient 8 IgG injected mice, a very faint signal was detectable in all tested areas (Fig. 45, Fig. 46). In total, the patient IgG fluorescent signals in the brain regions seem to be weaker compared to the spinal cord which can be explained by the distance between the injection site and the localization of the brain area.

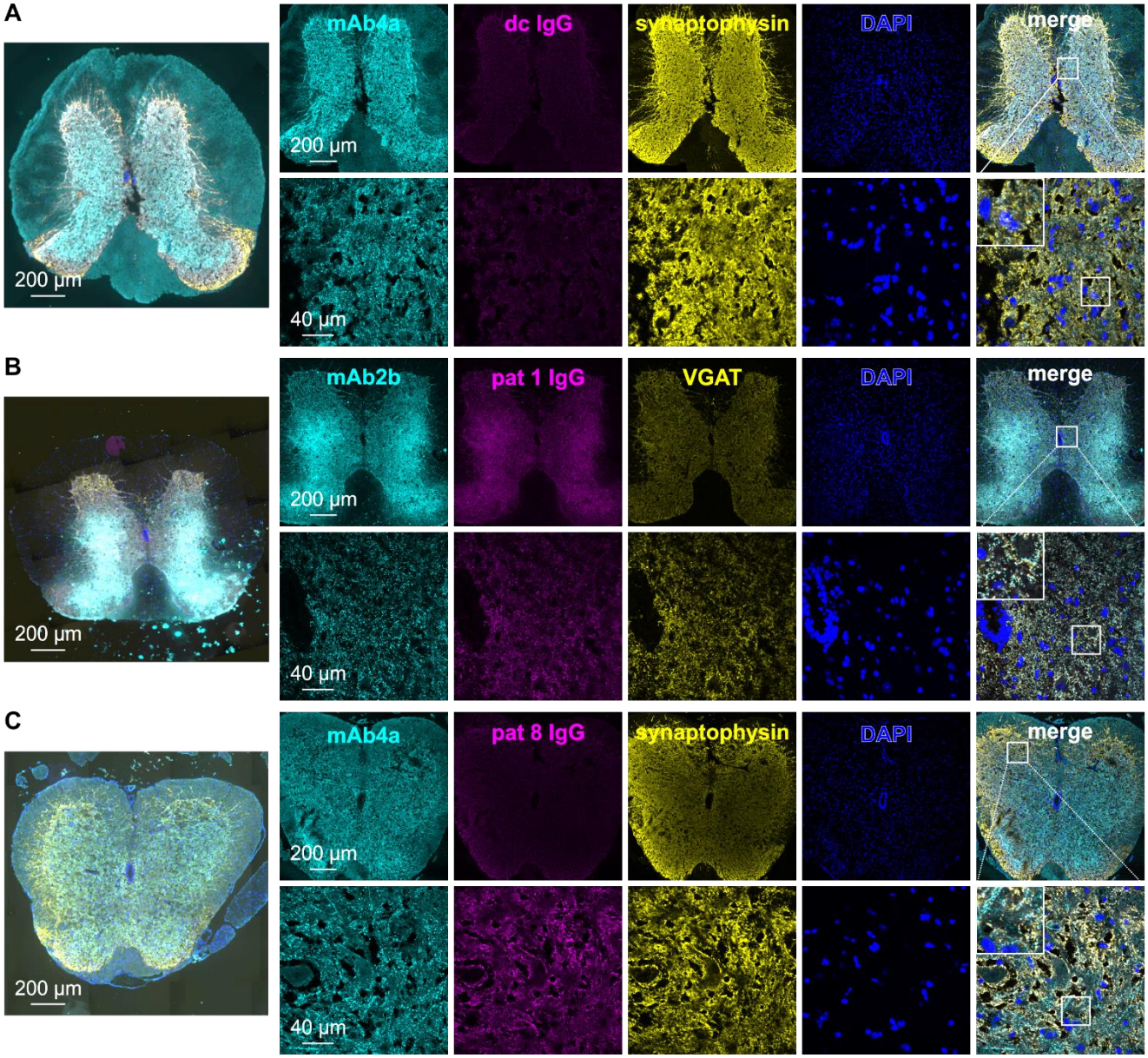

Fig. 39: Spinal cord immunohistochemical stainings of test mice without osmotic pump treated with disease control or patient IgG. (**A**) Immunohistochemical stainings of a mouse treated with disease control IgG (magenta) co-stained with mAb4a (cyan), synaptophysin (yellow) and DAPI (blue). (**B**) MAb2b (cyan), VGAT (yellow) and DAPI staining (blue) of mouse with patient 1 IgG that were passively transferred into the animal. (**C**) Staining of patient 8 IgG (magenta) treated mouse co-stained with mAb4a (cyan), synaptophysin (yellow) and DAPI (blue). dc = disease control; pat = patient. Overview (left), slight magnification (right top) and high magnification of top raw (right bottom) are presented.

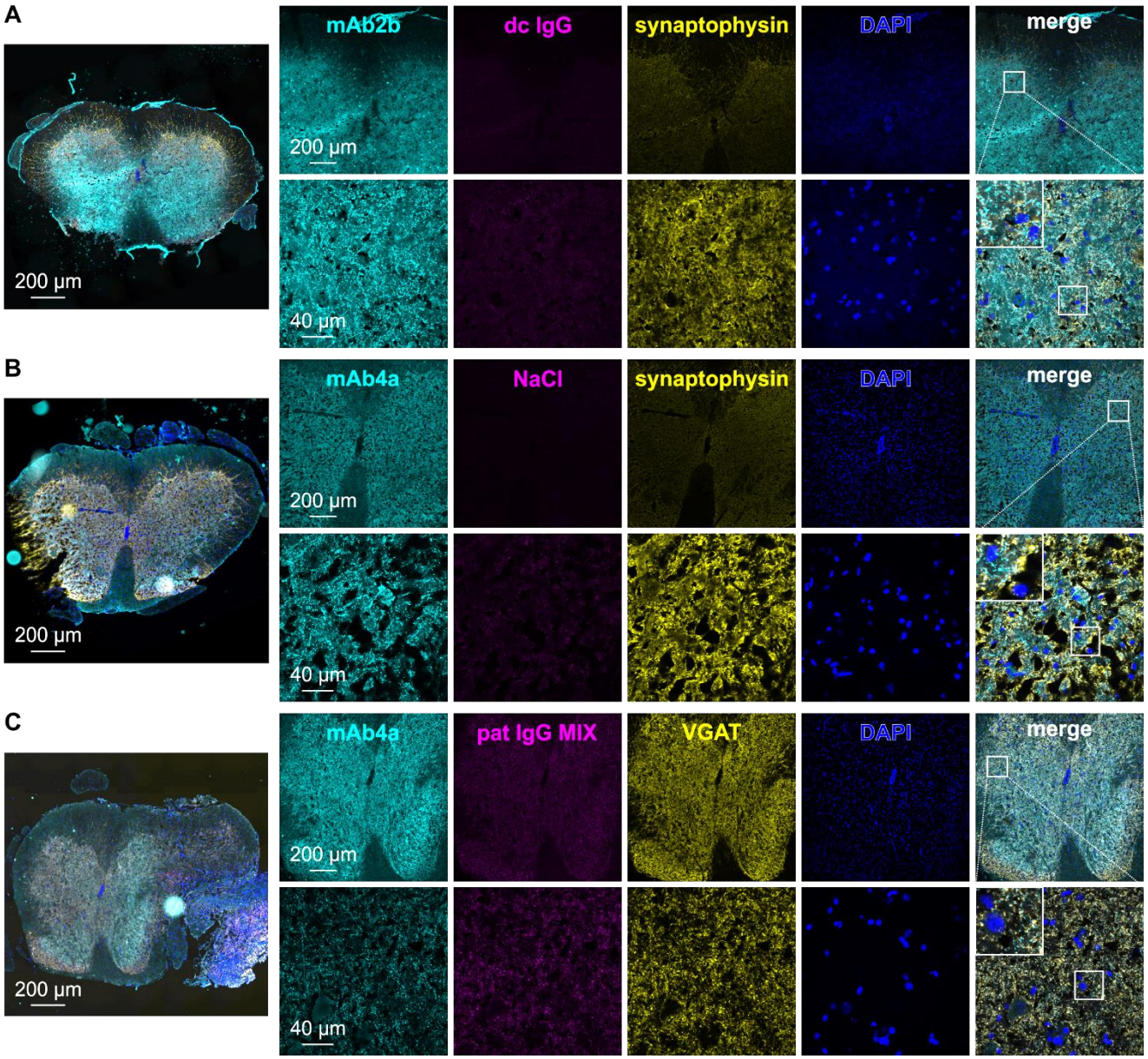

Fig. 40: Spinal cord immunohistochemical stainings of experimental mice with osmotic pumps treated with disease control IgG, NaCl or patient MIX IgG. (**A**) Immunohistochemical stainings of a mouse treated with disease control IgG (magenta) co-stained with mAb2b (cyan), synaptophysin (yellow) and DAPI (blue). (**B**) MAb4a (cyan), synaptophysin (yellow) and DAPI (blue) staining of a mouse with NaCl treatment. (**C**) Staining of patient MIX IgG (patient 1 and patient 8 IgG, magenta) treated mouse co-stained with mAb4a (cyan), VGAT (yellow) and DAPI (blue). dc = disease control; pat = patient. Overview (left), slight magnification (right top) and high magnification of white square in top raw (right bottom) are presented.

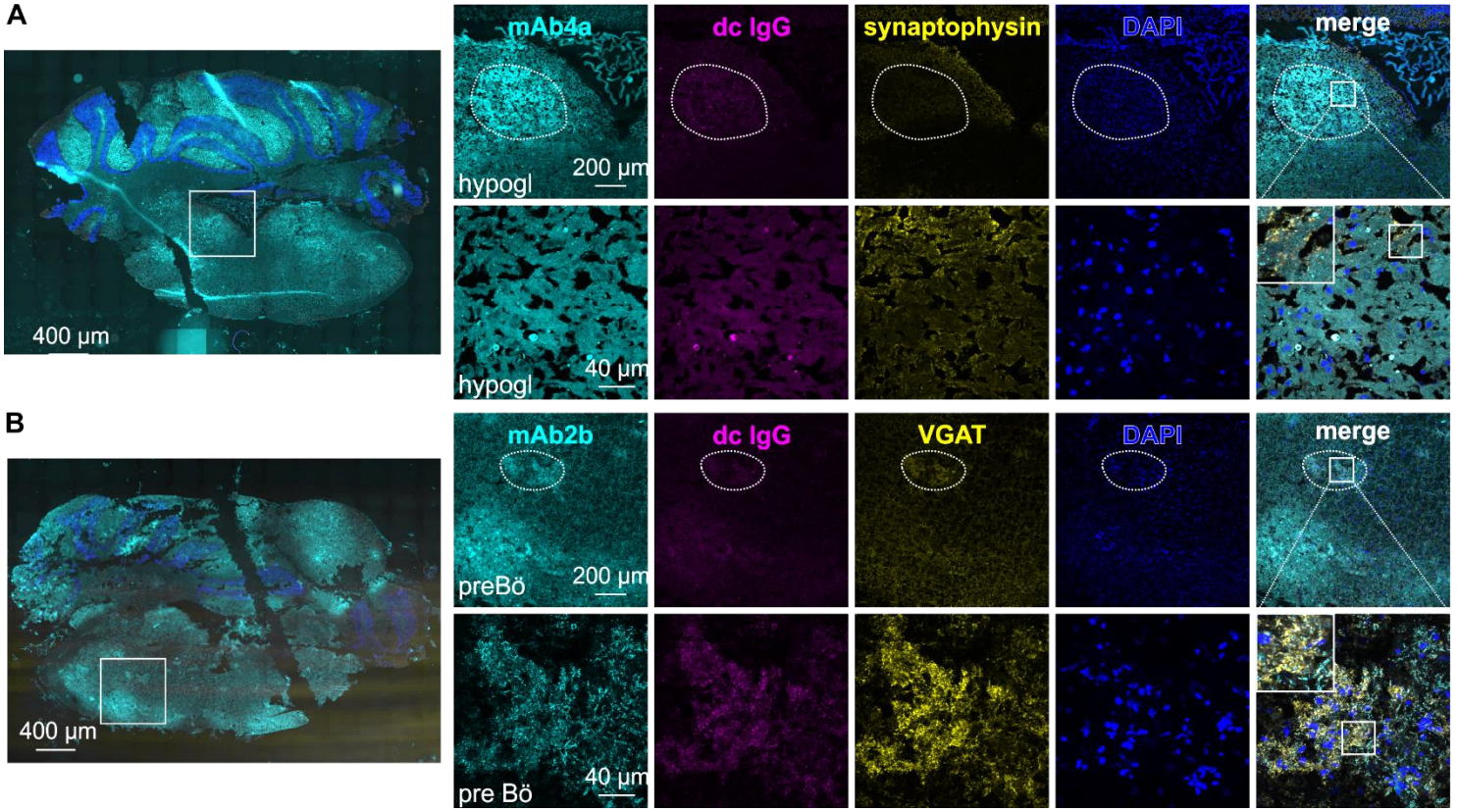

Fig. 41: Immunohistochemical stainings showing hypoglossal nucleus and pre Bötzinger complex of test mouse without osmotic pump treated with disease control IgG. (**A**) Immunohistochemical stainings showing the hypoglossal nucleus (hypogl) of a mouse treated with disease control IgG (magenta) co-stained with mAb4a (cyan), synaptophysin (yellow) and DAPI (blue). (**B**) MAb2b (cyan), VGAT (yellow) and DAPI staining (blue) of pre Bötzinger complex (pre Bö) of mouse treated with disease control IgG (magenta). dc = disease control. Overview (left), slight magnification (right top) and high magnification of white square in top raw (right bottom) are presented.

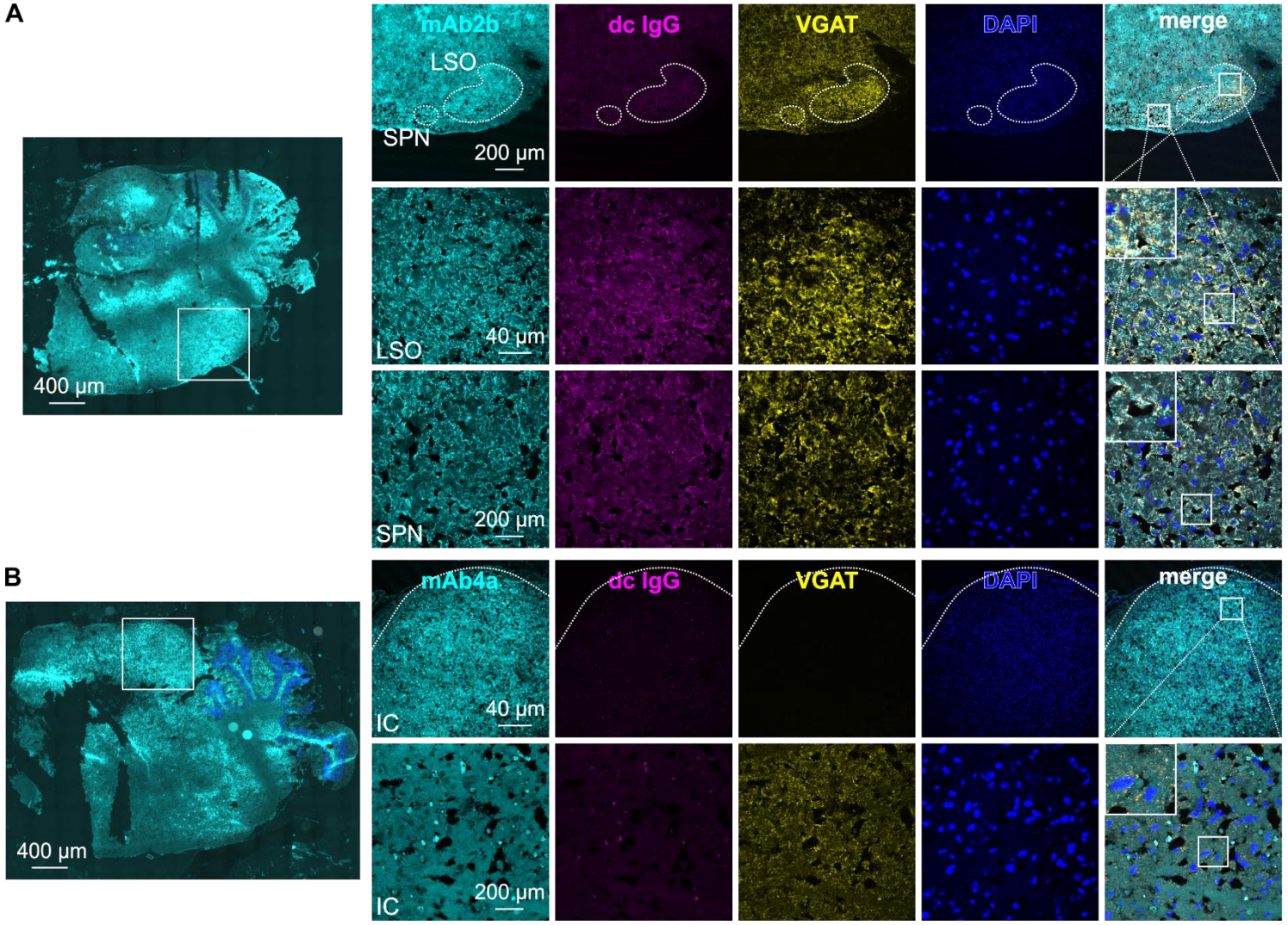

Fig. 42: Immunohistochemical stainings showing lateral superior olive, superior paraolivary nucleus and inferior colliculus of test mouse without osmotic pump treated with disease control IgG. (**A**) Immunohistochemical stainings showing the lateral superior olive (LSO) and superior paraolivary nucleus (SPN) of a mouse treated with disease control IgG (magenta) co-stained with mAb2b (cyan), VGAT (yellow) and DAPI (blue). (**B**) MAb4a (cyan), VGAT (yellow) and DAPI staining (blue) of inferior colliculus (IC) of mouse treated with disease control IgG (magenta). dc = disease control. Overview (left), slight magnification (right top) and high magnification of white squats in top raw (right middle and bottom) are presented.

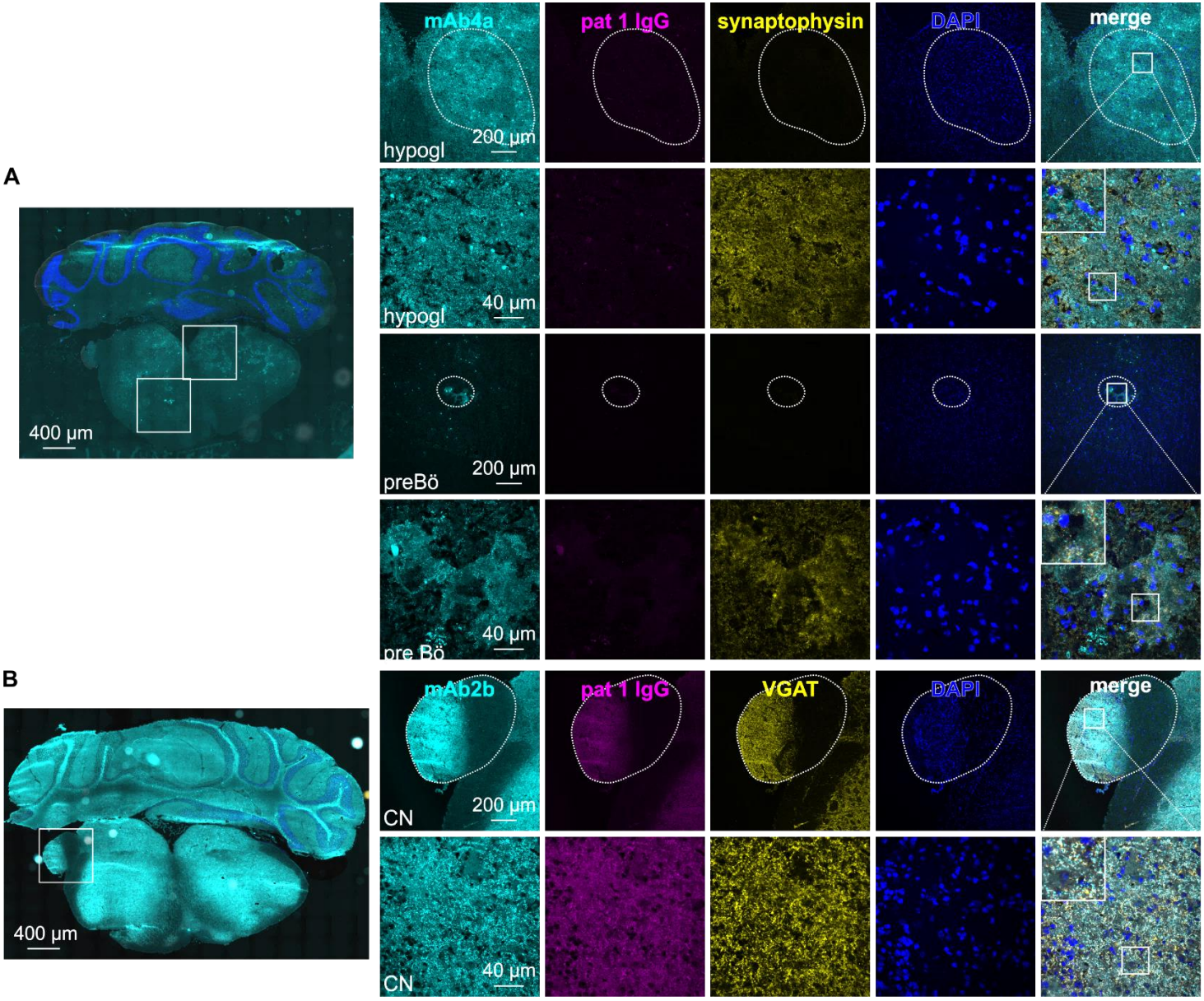

Fig. 43: Immunohistochemical stainings showing hypoglossal nucleus, pre Bötzinger complex and cochlear nucleus of test mouse without osmotic pump treated with patient 1 IgG. (**A**) Immunohistochemical stainings showing the hypoglossal nucleus (hypogl) and pre Bötzinger complex (pre Bö) of a mouse treated with patient 1 IgG (magenta) co-stained with mAb4a (cyan), synaptophysin (yellow) and DAPI (blue). (**B**) MAb2b (cyan), VGAT (yellow) and DAPI staining (blue) of cochlear nucleus (CN) of mouse treated with patient 1 IgG (magenta). pat = patient. Overview (left), slight magnification (right top) and high magnification of top raw (right bottom) are presented.

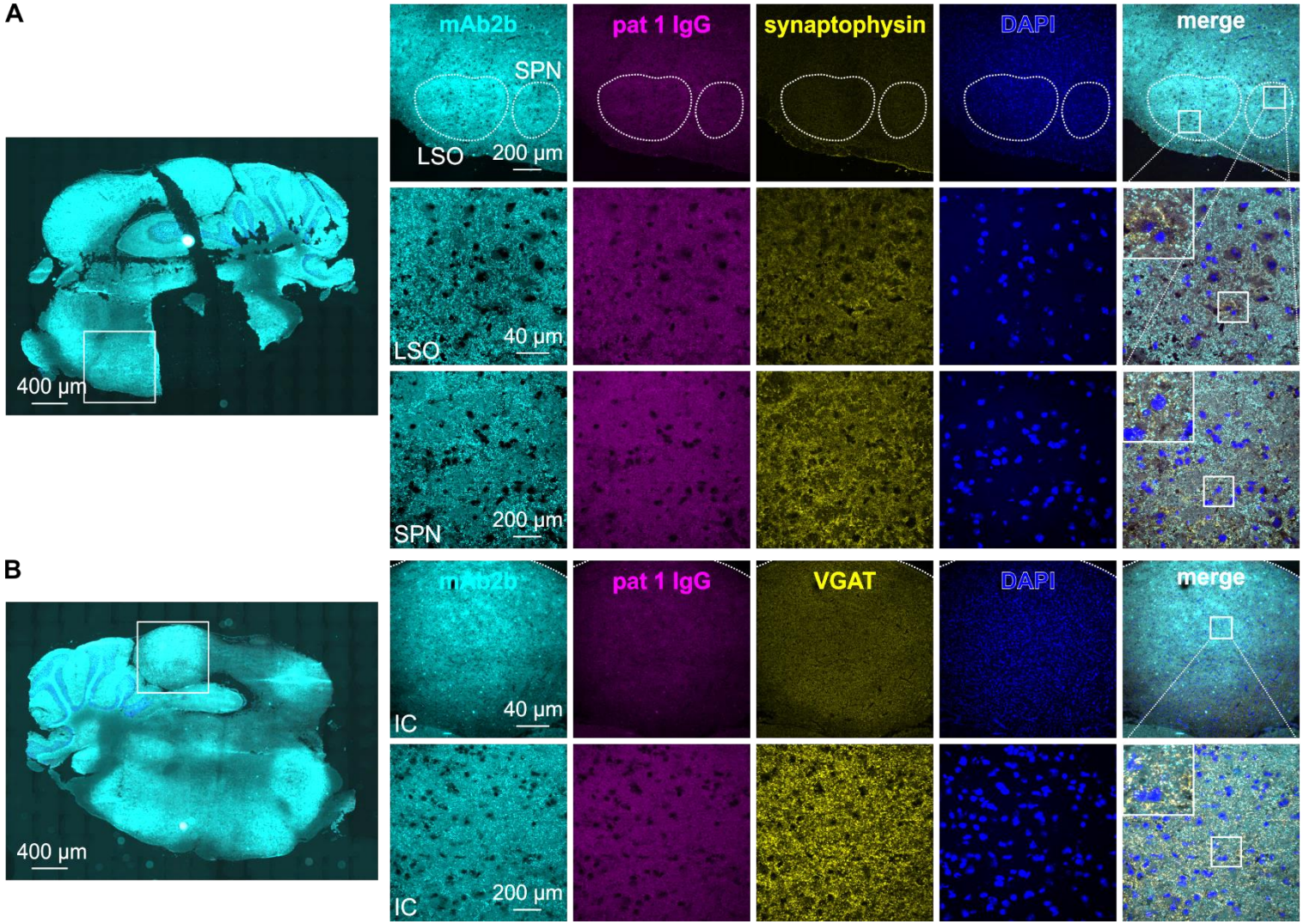

Fig. 44: Immunohistochemical stainings showing lateral superior olive, superior paraolivary nucleus and inferior colliculus of test mouse without osmotic pump treated with patient 1 IgG. (**A**) Immunohistochemical stainings showing the lateral superior olive (LSO) and superior paraolivary nucleus (SPN) of a mouse treated with patient 1 IgG (magenta) co-stained with mAb2b (cyan), synaptophysin (yellow) and DAPI (blue). (**B**) MAb2b (cyan), VGAT (yellow) and DAPI staining (blue) of inferior colliculus (IC) of mouse treated with patient 1 IgG (magenta). pat = patient. Overview (left), slight magnification (right top) and high magnification of white squares in top raw (right middle and bottom) are presented.

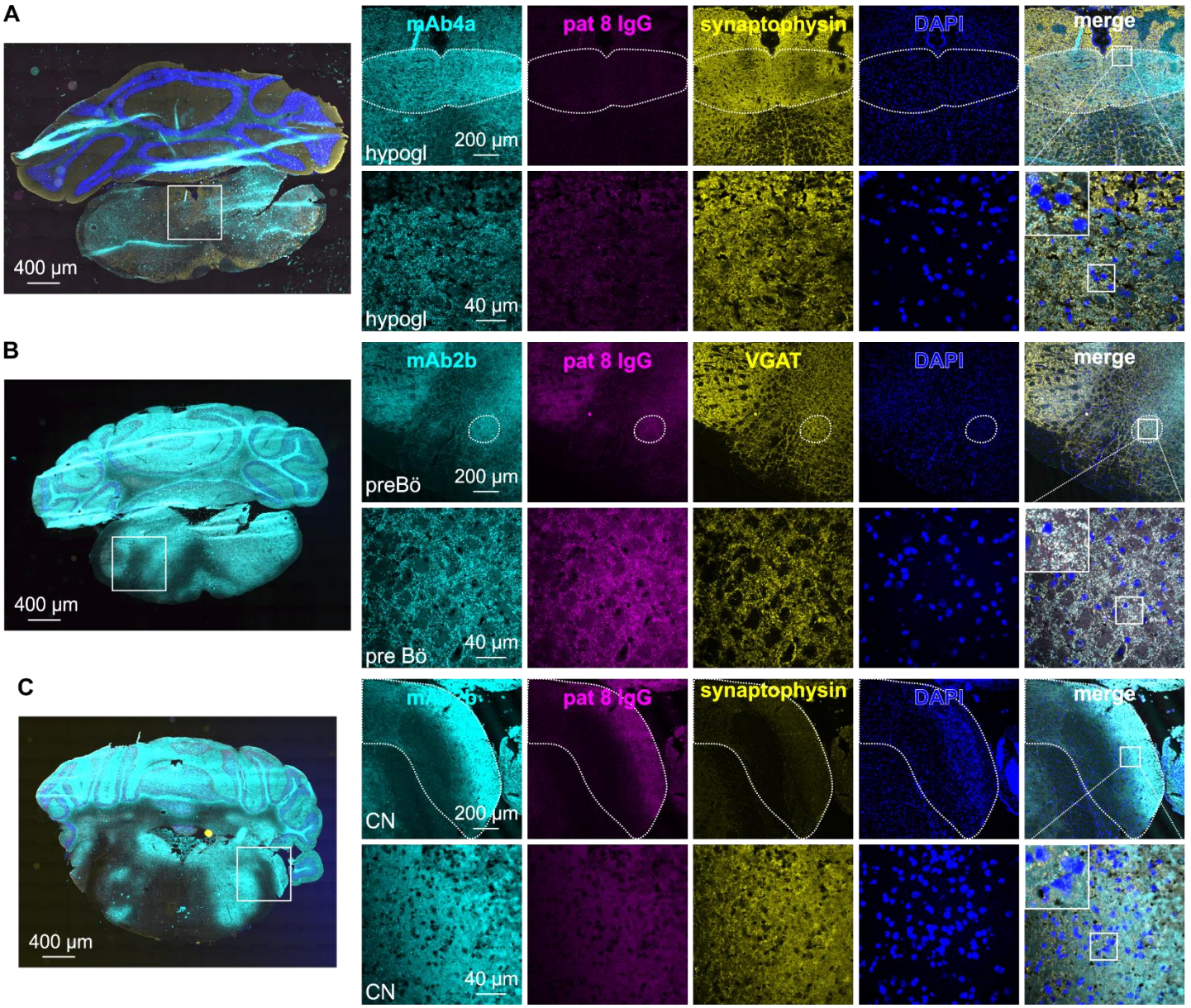

Fig. 45: Immunohistochemical stainings showing hypoglossal nucleus, pre Bötzinger complex and cochlear nucleus of test mouse without osmotic pump treated with patient 8 IgG. (**A**) Immunohistochemical stainings showing the hypoglossal nucleus (hypogl) of a mouse treated with patient 8 IgG (magenta) co-stained with mAb4a (cyan), synaptophysin (yellow) and DAPI (blue). (**B**) MAb2b (cyan), VGAT (yellow) and DAPI staining (blue) of pre Bötzinger complex (pre Bö) of mouse treated with patient 8 IgG (magenta). (**C**) MAb2b (cyan), synaptophysin (yellow) and DAPI staining (blue) of cochlear nucleus (CN) of mouse injected with patient 8 IgG (magenta). pat = patient. Overview (left), slight magnification (right top) and high magnification of white square in top raw (right bottom) are presented.

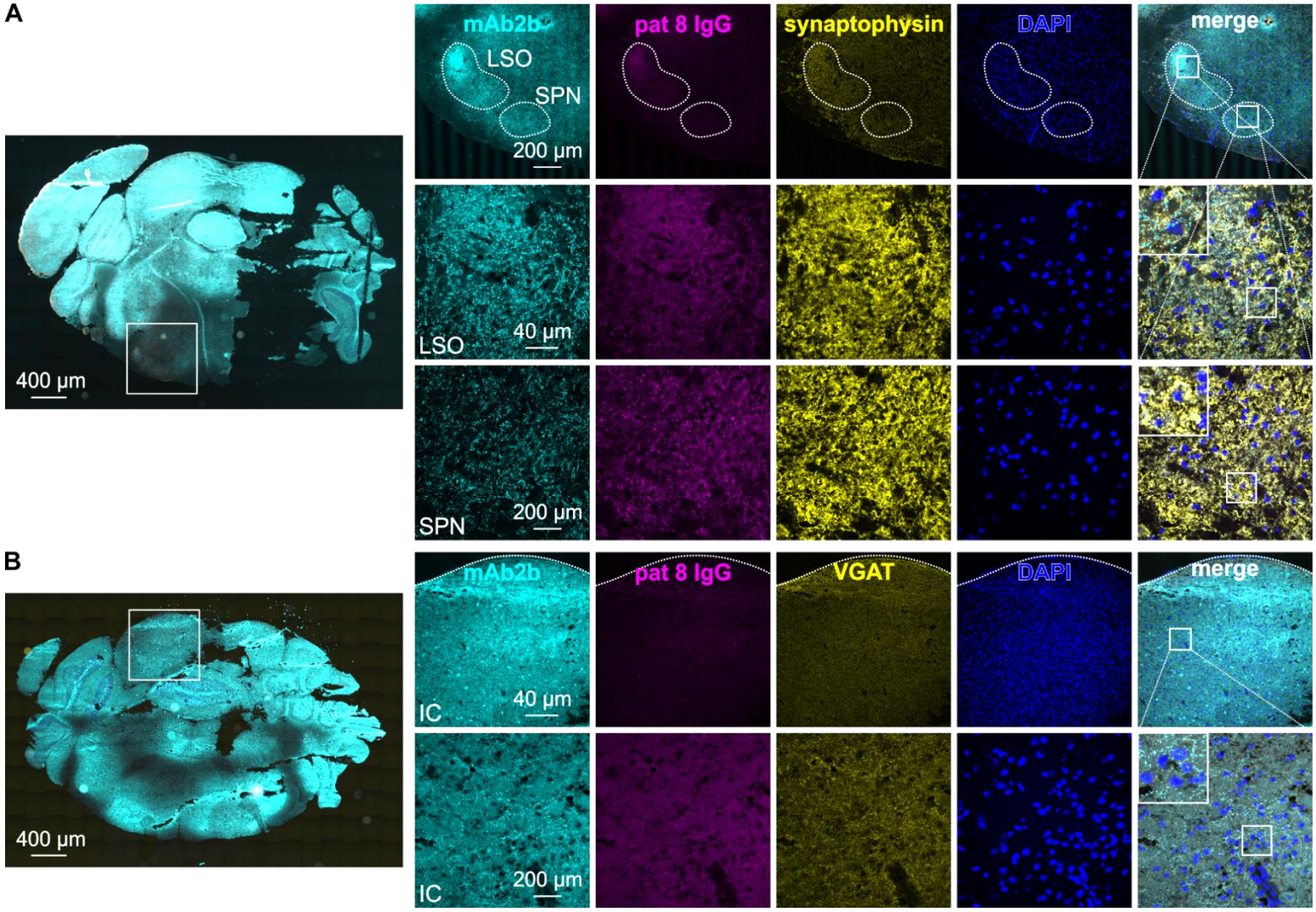

Fig. 46: Immunohistochemical stainings showing lateral superior olive, superior paraolivary nucleus and inferior colliculus of test mouse without osmotic pump treated with patient 8 IgG. (**A**) Immunohistochemical stainings showing the lateral superior olive (LSO) and superior paraolivary nucleus (SPN) of a mouse treated with patient 8 IgG (magenta) co-stained with mAb2b (cyan), synaptophysin (yellow) and DAPI (blue). (**B**) MAb2b (cyan), VGAT (yellow) and DAPI staining (blue) of inferior colliculus (IC) of mouse treated with patient 8 IgG (magenta). pat = patient. Overview (left), slight magnification (right top) and high magnification of white squares in top raw (right middle and bottom) are presented.

In summary, the immunohistochemical stainings confirmed that the patient autoantibodies reached the GlyRs in various tissues of the brain and spinal cord. Furthermore, the verification of autoantibodies in the spinal cord was also investigated by Western blot analyses. First, as proof of detectability of patient IgG in Western blots, patient 1 IgG was loaded in ascending concentration series (50-350 ng) on a PAA gel and stained with secondary anti-human antibody (Fig. 47A). Thus, the IgG band at around 110 kD was detected in all concentrations. Next, membrane preparations of murine spinal cords were prepared, and protein samples were loaded on a PAA gel. For comparison, pure patient 1 IgG (50 ng) was additionally loaded. In patient 1 IgG treated mice, a band at the same height like the pure patient 1 IgG at around 100 kDa was detected (Fig. 47B). Similarly, spinal cord membrane preparations of mice injected with patient 8 IgG without osmotic pumps resulted in a strong signal. An equal band was detectable in membrane preparations of mice treated with patient MIX IgG via osmotic pumps (Fig. 47C). In samples of spinal cord tissue from mice with NaCl and disease control IgG application, no band was detectable in staining with anti-human antibody. These results suggested that autoantibodies can be detected in spinal cord tissues via Western blot analysis.

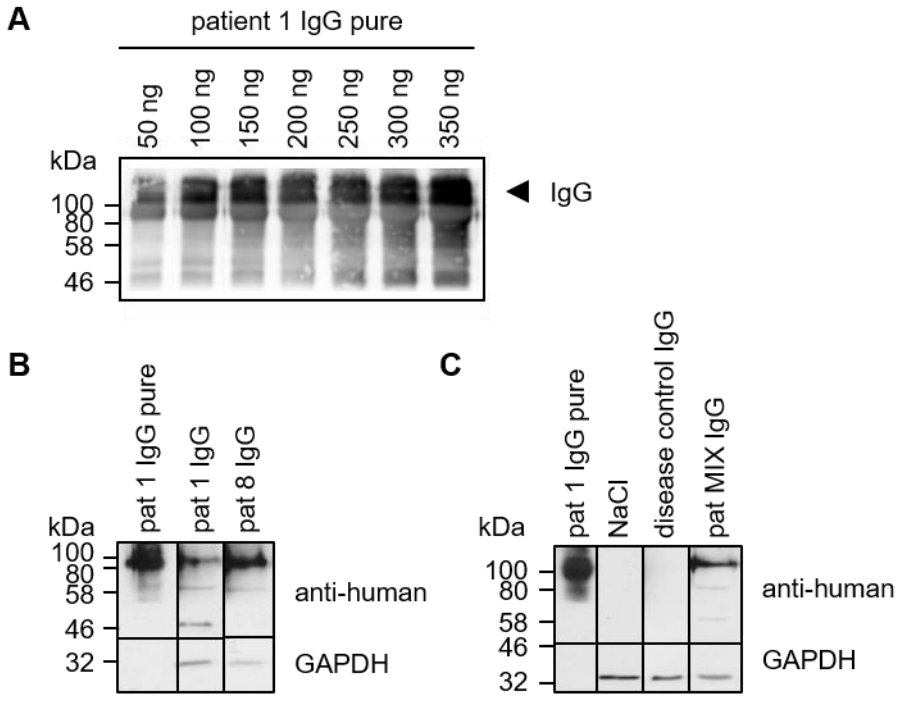

Fig. 47: Western blot analysis of spinal cord membrane preparations from mice treated with patient autoantibodies. (**A**) Series of ascending patient 1 IgG concentrations (50-350 ng) loaded on a Western blot gel as proof of detection by secondary anti-human antibody. (**B**) Spinal cord membrane preparations of mice without an osmotic pump treated with patient 1 IgG or patient 8 IgG. For comparison, 50 ng pure IgG was loaded. As loading control, GAPDH was additionally stained. (**C**) Spinal cord membrane preparations of mice treated with NaCl, disease control IgG or patient MIX IgG (containing patient 1 and 8 IgG) via osmotic pumps. Pure IgG (50 ng) was loaded for comparison and GAPDH was stained as loading control. pat = patient.

In summary, patient autoantibodies were successfully transferred into mice and binding of the target GlyR was confirmed by immunohistochemical stainings. Autoantibodies were detectable in spinal cord and brain regions including hypoglossal nucleus, pre Bötzinger complex, lateral superior olive, superior paraolivary nucleus, cochlear nucleus and inferior colliculus. Additionally, membrane preparations analyzed in Western blots verified the detectability of patient IgGs in the murine spinal cord.

4. Discussion

The rare autoimmune disease SPS is elicited by autoantibodies against different synaptic proteins such as GAD65 and amphiphysin (Solimena and De Camilli, 1991; De Camilli et al., 1993; Wessig et al., 2003; Koerner et al., 2004; Raju et al., 2006). The pathomechanisms for the intracellular proteins GAD65 and amphiphysin have been elucidated (Shupliakov et al., 1997; Di Paolo et al., 2002; Raju et al., 2005) whereas for autoantibodies against the glycine receptor the pathology is less intensively investigated. GAD65 autoantibodies inhibit the enzymatic activity of GAD, or amphiphysin autoantibodies cause an endocytic dysfunction as a consequence of the disabled interaction of amphiphysin with dynamin (Shupliakov et al., 1997; Di Paolo et al., 2002; Raju et al., 2005).

Autoantibodies against membrane proteins such as ion channels share other common pathophysiological mechanisms. These autoantibodies activate complement, modulate the antigen by cross-linking of receptors, and/or block receptor function (Hughes et al., 2004; Hughes et al., 2010; Carvajal-Gonzalez et al., 2014; Castillo-Gomez et al., 2017). Complement activation as well as receptor cross-linking depends on the IgG subclass of autoantibodies. IgG1 and IgG3 are able to activate complement, whereas IgG4 is not binding the C1q protein (Carvajal-Gonzalez et al., 2014; Balint and Bhatia, 2016).

Receptor internalization has been demonstrated for nicotinic acetylcholine receptors (nAchRs), NMDARs and GlyRs mainly due to high abundance of autoantibodies of the IgG1 subclass (Drachman, 1994; Dalmau et al., 2008; Hughes et al., 2010; Carvajal-Gonzalez et al., 2014; Moscato et al., 2014; Planaguma et al., 2015; Castillo-Gomez et al., 2017; Dalmau et al., 2017; Huang et al., 2017; Pan et al., 2019). Additionally, GlyRα1 autoantibodies activate complement (Carvajal-Gonzalez et al., 2014). In contrast, NMDAR autoantibodies do not lead to complement-mediated damage although they are predominantly IgG1 antibodies (Dalmau et al., 2007; Dalmau et al., 2008; Tuzun et al., 2009; Hughes et al., 2010; Irani et al., 2010; Martinez-Hernandez et al., 2011; Planaguma et al., 2015). An impairment in ion channel functionality was exhibited for autoantibodies against the GluN1 receptors and recently also shown for GlyR autoantibodies (Gleichman et al., 2012; Castillo-Gomez et al., 2017; Crisp et al., 2019). A detailed functional analysis on GluN1 demonstrated that the autoantibodies are able to initiate structural transitions in the receptor leading to a disability to switch back from the open to the closed conformation (Gleichman et al., 2012). Similar studies have not yet been performed on GlyR autoantibodies.

The mapping of the epitope(s) where autoantibodies bind to their target protein is crucial to understand the autoantibody pathology but also helps for further development of novel therapeutic options. In *Myasthenia gravis*, an extracellular localized N-terminal domain was identified as the major immunogenic region of the autoantibodies against the acetylcholine

receptor (Tzartos et al., 1991b; Tzartos et al., 1991a). Common epitopes have also been mapped for GluN1 autoantibodies but there are also other receptor domains which are only targeted by autoantibodies from single patients (Gleichman et al., 2012). Thus, most patient sera harbor polyclonal autoantibodies. For GlyR autoantibodies, a binding epitope was not characterized yet. With the knowledge of the epitope, predictions of structural or functional alterations can be drawn. In sum, disease pathomechanisms vary among different autoantibody types and targets.

At the beginning of the present thesis, it was known that GlyRα1 autoantibodies (i) are mainly of the IgG1 subtype, (ii) are able to activate complement, (iii) cross-link receptors, (iv) lead to subsequent internalization and receptor degradation, and (v) bind to the target in its native configuration (Carvajal-Gonzalez et al., 2014). Very recently, a blockade in GlyR function due to autoantibody binding was stated (Crisp et al., 2019). This thesis broadly expands the current knowledge about the pathomechanisms of GlyR autoantibody binding. Thereby, the most important findings are listed below and will be discussed in separate chapters afterwards (Fig. 48):

1) The GlyRα1 autoantibody epitope is located in the far N-terminus covering amino acids A^{1}-G^{34} (numbers refer to mature protein).
2) GlyRα1 de-glycosylation (at N^{38}) does not influence autoantibody binding.
3) GlyRα1 function is influenced by autoantibody binding shown by decreased potency and alterations in desensitization.
4) Specific GlyRα1 autoantibody reduction is possible by using GlyRα1 transfected HEK293 cells and GlyRα1 ECD constructs.
5) Passive transfer of GlyRα1 autoantibodies into zebrafish larvae and mice demonstrated successful targeting of GlyRs in CNS tissue. Phenotypically, the escape response in zebrafish is impaired in autoantibody treated larvae.

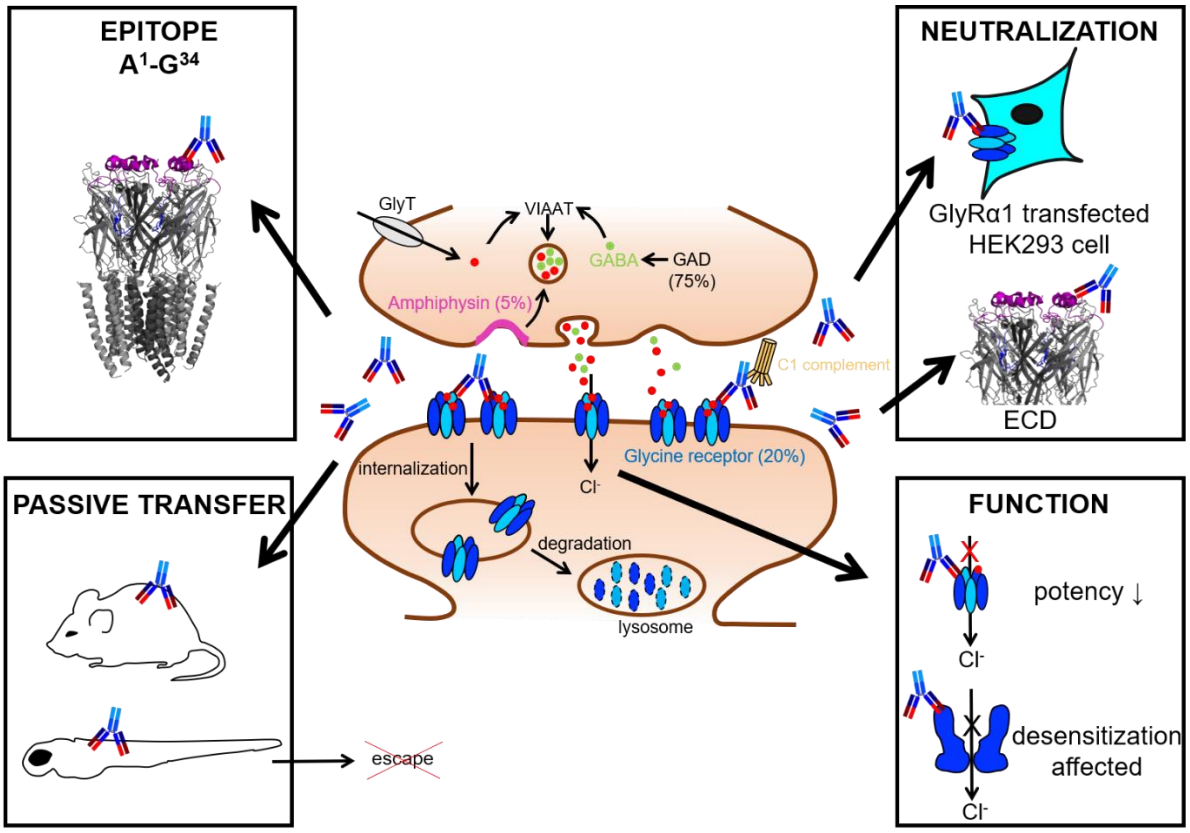

Fig. 48: Summary of most important findings in this study. Autoantibodies against glycine receptors (GlyR) located at postsynaptic membranes of inhibitory neurons cross-link GlyRs followed by internalization and degradation in lysosomes (middle). Additionally, these autoantibodies activate the C1 complement system. Novel findings of the present study include the epitope localization of autoantibodies at the GlyRα1 covering amino acids in the very far N-terminus of the protein (A^1-G^{34}, numbers refer to mature protein) (top left). Furthermore, GlyRα1 autoantibodies can be neutralized from the solution by specifically targeting GlyRα1 expressed in HEK293 cells or GlyRα1 ECD constructs (top right). In addition, GlyRα1 autoantibodies decrease glycine potency and affect the desensitization state of the receptor (bottom right). Lastly, GlyRα1 autoantibodies were successfully transferred into zebrafish larvae and mice resulting in an impaired escape behavior in zebrafish larvae (bottom left). ECD = extracellular domain; GAD = glutamate decarboxylase; GlyT = glycine transporter; VIAAT = vesicular inhibitory amino acid transporter.

4.1 GlyR autoantibodies bind to the N-terminal receptor domain

Knowledge about the localization of the autoantibody epitope provides further information about the pathophysiological effects of autoantibodies. Using live cell stainings, GlyR autoantibodies were reported to bind GlyRα1, α2 and α3 subunits in a native receptor configuration (Carvajal-Gonzalez et al., 2014; Doppler et al., 2016). Live stainings have been shown to provide more reliable results for autoantibody binding possibly due to the correct fold of the protein in its native conformation (Vincent et al., 2012). Thus, the epitope is accessible from the extracellular site of the cellular membrane. Therefore, in the present study live cell stainings were used for epitope characterization.

The GlyR is assembled of five subunits that consist of a large N-terminal ECD, four transmembrane domains connected via intra-or extracellular loops, and a short extracellular C-terminus (Du et al., 2015; Huang et al., 2015; Huang et al., 2017; Langlhofer and Villmann, 2017). Structures pointing toward the extracellular space presenting the potential target sequence for autoantibodies include the N-terminal ECD, the short loop between transmembrane domains 2 and 3, and the C-terminus. The structure of the GlyR N-terminus is highly determined by the fold of 10 β-sheets connected by short loops and a short α-helical element at the beginning of the structure (Du et al., 2015). Single point mutations as present in genetic variants of the GlyR associated with the motor disorder hyperekplexia are able to disrupt this structural organization and impair inhibitory neurotransmission (Chung et al., 2010; Schaefer et al., 2015). Moreover, the ECD binds the agonist glycine but also antagonists and allosteric modulators (e.g. analgesic potentiators) at defined domains between adjacent subunits in the pentameric receptor complex (Huang et al., 2017). The GlyR ECD determines the open, closed or desensitized receptor conformation upon binding of agonists and antagonists (Du et al., 2015; Huang et al., 2017).

Besides the importance of the structural fold of the GlyR ECD, the N-terminus plays a major role during receptor maturation and trafficking (Griffon et al., 1999; Breitinger and Becker, 2002; Schaefer et al., 2018a). As prerequisite for receptor assembly, receptor glycosylation at the amino acid motif N-X-S/T present in the GlyR N-terminus is required (Griffon et al., 1999; Schaefer et al., 2018a). After successful N-glycosylation, GlyRs can exit the ER and are further transported to the cell surface via the Golgi apparatus.

Commercially available antibodies also target the GlyR N-terminus. The GlyRα1 specific antibody mAb2b binds to amino acids A^{1}-S^{9} (numbers refer to mature protein) and the pan-α antibody mAb4a binds to P^{96}-G^{105} (numbers refer to mature GlyRα1 but sequence is conserved among all GlyRα subunits). In this study, the commercially antibodies binding to the GlyRα ECD have been used in combination with patient sera to characterize the autoantibody epitope(s). GlyRα1 autoantibodies from nine different patients have been investigated (summarized in Tab. 45). All patient sera tested bound GlyRα1. 6 of 9 patient autoantibodies showed strong binding, 2 of 9 weak binding and one patient serum no binding to GlyRα2 (Tab. 45). Additionally, 3 of 5 tested patient sera were positive against GlyRα3. The ability of autoantibodies to target GlyRα1, α2 and α3 are in accordance with previously published studies (Carvajal-Gonzalez et al., 2014; Doppler et al., 2016) and suggests that the GlyR autoantibodies are polyclonal.

Besides the ability to bind the GlyR in its native confirmation, the present study tested binding to GlyRs following fixation and permeabilization of the cells. Autoantibodies of 4 out of 5 patient sera recognized GlyRα1 in this experimental setup indicating that the autoantibodies are able

to detect both native and denatured GlyRα1 (Tab. 45). These results do not necessarily mean that also intracellular epitopes are targeted. Intracellular receptors are present in vesicular membranes, membrane of the ER and Golgi compartments during trafficking to the outer membrane and thus also expose their ECD to the cellular space depending on the compartment (Schaefer et al., 2018a). This is the first study demonstrating that at least some patient autoantibodies against the GlyR additionally recognize denatured epitopes. As commercially available tests for autoantibodies use denatured conditions, it should be pointed out that these tests provide a good prescreening but should be confirmed using native staining conditions as some sera might otherwise result in false negative results.

Using native conditions, this study detected autoantibody binding to GlyRα1 from patient serum, CSF and purified IgG from serum. Similar findings have been previously reported (Carvajal-Gonzalez et al., 2014).

So far, data have suggested the extracellular domain as binding site for the autoantibodies. A closer constriction analysis of the autoantibody binding epitope was performed using point mutations of GlyRα1 and α3. Not all patient sera have recognized both subunits. Moreover, both subunits share a high sequence homology in their N-terminal region with only some exceptions. Following expression in HEK293 cells, 10 mutants were stained with one patient serum that demonstrated binding to GlyRα1 but non-binding to α3. As control, mAb4a a pan-α antibody (epitope P^{96}-G^{105} identical in α1 and α3) was used and detected all constructs. The α1-specific antibody mAb2b (epitope A^{1}-S^{9}) recognized GlyRα1 variants only. Interestingly, there were two constructs (clone 1 and 8) that revealed binding to α3 in addition to α1. Thus, residues 132 (α1: I, α3:L) and 137 (α1:A, α3:S) might underly the specific targeting of GlyR autoantibodies to both α1 and α3 at least in the patient investigated.

Genetic variants associated with the neuromotor disorder hyperekplexia have been described in the GlyRα1 N-terminus. However, several of those mutations are nonsense or deletion/frameshift mutations which are not expressed at the cell surface and therefore not suitable for autoantibody binding tests (Bode et al., 2013; Bode and Lynch, 2014). Two murine mutations that are normally expressed but result in functional defects are the *spasmodic* mutation A52S and *shaky* Q177K (Ryan et al., 1994; Saul et al., 1994; Schaefer et al., 2017; Schaefer et al., 2018b). These mutations underlie either functional deficits such as decreased glycine affinity of the GlyR or reduced synaptic localization of GlyRα1. Both GlyR mutants were bound by the patient serum arguing that residues A^{52} and Q^{177} are rather not localized in a sequence important for epitope formation of GlyR autoantibodies.

So far, human and murine GlyRα1 were used for testing the ability of autoantibody binding. Besides the high homology between human and murine sequence, the sequence alignment of

GlyRs from different species demonstrated large sequence variations in the far N-terminus between the human and the zebrafish (*danio rerio* = dr) α1 variants including the binding site of the α1-specific mAb2b antibody.

The zebrafish expresses five GlyRα and two GlyRβ subunits (Hirata et al., 2009). Moreover, zebrafish larvae with disabled glycinergic inhibition show massive motor contraction when touched resulting in inability to swim away from a stimulus (Hirata et al., 2005; Ganser et al., 2013; Hirata et al., 2013; Samarut et al., 2019). This phenotype is in line with symptoms described for hyperekplexia but also comparable to the SPS phenotype in humans. GlyRα1^{dr} was not detected by 4 of 6 patient sera although all bound the GlyRα1^{hs} (Tab. 45). Moreover, mAb2b detected GlyRα1^{hs} but not GlyRα1^{dr}. These data provided first evidences that the N-terminus might represent an immunogenic region for specific binding of human GlyR autoantibodies. To verify this, a chimera consisting of the human N-terminal region (till amino acid G^{34}) followed by the zebrafish sequence was created (Niels v. Wardenburg, unpublished). The chimera was bound again by autoantibodies. These results indicated that the region between residues A^{1}-G^{34} harbors at least part of the autoantibody epitope.

To follow this line, the far N-terminus was further investigated. The N-terminal region of the GlyRα1 between residues A^{1}-G^{34} includes the binding epitope for the commercial antibody mAb2b. It was tested if the human autoantibodies are able to compete with the commercial antibody mAb2b. Competition experiments of a dilution series showed that the patient autoantibodies and the GlyRα1 specific antibody mAb2b are not competing for the same epitope but both antibodies colocalize and thus might both bind to the same receptor region or an overlapping epitope.

Interestingly, autoantibodies against the acetylcholine receptor in *Myasthenia gravis* exhibited also the main immunogenic region in the far N-terminal region of the receptor (Tzartos et al., 1991b; Tzartos et al., 1991a). Both receptor types, the nAchR and the GlyR belong to the same receptor superfamily and share common structural elements in the N-terminus (Nemecz et al., 2016).

The location of the GlyR autoantibody epitope in this particular region between residues A^{1}-G^{34} explains the observed binding of autoantibodies to the murine hyperekplexia mutants (A52S and Q177K) as the amino acid exchanges are located downstream of the identified epitope sequence. A structural analysis of GlyRα1 revealed that the region A^{1}-G^{34} is located in the outermost part of the ECD at the protein surface, thus easily accessible for autoantibodies.

This region has also been demonstrated to bind allosteric modulators in GlyRs and nAchRs (Huang et al., 2017). The allosteric analgesic potentiator AM-3607 binds to residues R^{29}-F^{32} in the pre-β1 region. This sequence overlaps with the identified GlyR autoantibody epitope region

and is determined by an α-helical fold. As soon as the analgesic potentiator AM-3607 together with the agonist glycine binds to the GlyRα3 receptor, the receptor turns into a desensitized receptor state. Therefore, binding of autoantibodies in the same region might induce similar structural transitions of the GlyR protein and influence ion channel function. Structurally, the α-helical fold of this region has additionally been shown to modulate the open, closed and desensitized receptor stages (Du et al., 2015). Thus, autoantibody binding to the α1-helix might interfere in the transition of the three stages, thereby probably altering inhibitory neurotransmission in human patients suffering from SPS.

In summary, our data identified a common GlyR autoantibody binding epitope at the N-terminus of GlyRα1. The binding of the patient sera to other GlyRα subunits however suggests that other so far non-identified epitopes exist that contribute to GlyR autoantibody binding. The use of microarrays spotted with different peptide parts of the expected protein represents a high throughput technique that might provide additional results for further autoantibody epitope tests in a short time window (Li et al., 2018; Sachse et al., 2018). A disadvantage of peptide approaches is however that peptides do not represent the correct structure of the sequence present in the native receptor configuration. Therefore, such approaches have to be combined with functional analyses.

Tab. 45: Binding abilities of patient autoantibodies against different GlyR subunits as well as changes in desensitization.

	α1^{hs}	α2^{mm}	α3^{hs}	α1^{hs} fix/perm	N38Q	α1^{dr}	α1^{ch}	tau	desens	α1^{dr}	α2^{dr}	α3^{dr}	α4a^{dr}	α4b^{dr}	βa^{dr}	βb^{dr}
pat 1	✓	✓	×	×	✓	×	✓	↓	↓	×	×	×	✓	✓	±	×
pat 2	✓	✓	✓	✓	n.d.	×	✓	↓	↔	×	✓	✓	×	✓	×	×
pat 3	✓	✓	✓	✓	n.d.	×	✓	↓	↓	×	×	✓	×	×	×	×
pat 4	✓	✓	✓	✓	n.d.	✓	✓	↑	↔	✓	✓	✓	✓	✓	×	×
pat 5	✓	×	×	✓	n.d.	×	✓	n.d.	n.d.	✓	✓	✓	✓	✓	×	×
pat 6	✓	±	n.d.	n.d.	✓	n.d.	n.d.	↑	↔	n.d.	n.d.	n.d.	n.d.	n.d.	n.d.	n.d.
pat 7	✓	✓	n.d.	n.d.	✓	n.d.	n.d.	n.d.	n.d.	n.d.	n.d.	n.d.	n.d.	n.d.	n.d.	n.d.
pat 8	✓	±	n.d.	n.d.	✓	±	✓	n.d.	n.d.	✓	×	✓	±	×	×	±
pat 9	✓	✓	n.d.	n.d.	✓	n.d.	n.d.	n.d.	n.d.	n.d.	n.d.	n.d.	n.d.	n.d.	n.d.	n.d.

α and β are related to GlyR. N38Q is a mutant of human GlyRα1 (number refers to mature protein). Here, only patient sera are listed. Symbol meanings: ✓ binding, × no binding, ± low binding, ↑ increase, ↓ decrease, ↔ unchanged. ch = chimera; desens = fraction of desensitizing currents; dr = *danio rerio*; fix/perm = fixed and permeabilized cells; ; hs = *homo sapiens*; mm = *mus musculus*; n.d. = not determined; pat = patient; tau = desensitization time constant.

4.2 Autoantibody binding is independent of GlyR glycosylation

Another property that is speculated to influence autoantibody binding is the glycosylation state of the target protein. N-glycosylation as posttranslational modification of GlyRs is a prerequisite for receptor assembly and takes place in the ER during protein maturation (Griffon et al., 1999; Schaefer et al., 2018a). After successful glycosylation, the GlyR can exit the ER and is further transported to the cellular membrane, thereby passing the Golgi apparatus. For N-glycosylation, glycans are attached to asparagine residues within the amino acid motif N-X-S/T. In the GlyRα1 and α3, one site for N-glycosylation is known whereas in GlyRα2 and β, two sites are present (α1: ^{38}NVS^{40}; α2: ^{45}NVT^{47}, ^{76}NDS^{78}; α3: ^{38}NVT^{40}; β: ^{32}NST^{34}, ^{220}NCT^{222}, numbers refer to mature protein) (Pult et al., 2011; Schaefer et al., 2018a).

The importance of the glycosylation status has been investigated for various antigens targeted by autoantibodies such as contactin-1, NMDAR-1 and Caspr2 (Gleichman et al., 2012; Labasque et al., 2014; Miura et al., 2015; Olsen et al., 2015). All three targets were analyzed in the un-glycosylated form or in partially de-glycosylated forms. For Contactin-1 the glycosylation seems to be necessary for autoantibody binding (Labasque et al., 2014). Common methods to analyze the influence of glycosylation include tunicamycin treatment of cells to prevent N-glycosylation during protein maturation. Another approach is to remove glycosylation sites with the recognition sequence N-X-S/T by mutation of the asparagine. The only glycosylation site present in GlyRα1 is located at asparagine 38 (N^{38}). This asparagine is localized in very close proximity to the region identified as part of the autoantibody epitope (A^{1}-G^{34}). Therefore, glycosylation might indeed influence the binding of GlyR autoantibodies.

We used tunicamycin treatment of GlyRα1 expressing HEK293 cells which revealed no binding of autoantibodies to the cells. In contrast, in fixed and permeabilized cells patient autoantibodies targeted the GlyRα1. It was demonstrated earlier that GlyRs expressed at the cell surface are glycosylated but glycosylation is also a prerequisite for ER exit and transport to the cellular surface (Griffon et al., 1999). Therefore, the non-binding of the autoantibodies is possibly due to an absence of GlyRs at the cellular surface resulted by a lack of transport of non-glycosylated GlyRs from the ER upon tunicamycin treatment. The binding of GlyR autoantibodies to intracellular localized GlyRs might either be a result of incomplete tunicamycin treatment and presence of intracellular glycosylated receptors or binding of GlyR autoantibodies to un-glycosylated GlyR protein. Thus, live staining procedures were probably hindered due to a lack of GlyRα1 at the cell surface following tunicamycin treatment.

Tunicamycin treatment bears also the disadvantage that longer treatment is toxic for cells. To circumvent that the observed effects result from cell cytotoxicity, a de-glycosylation mutant GlyRα1^{N38Q} was generated to investigate the status of glycosylation of the GlyR for

autoantibody binding. Patient autoantibodies were able to bind GlyRα1^{N38Q} in transfected HEK293 cells (Tab. 45). These data further support that glycosylation of the GlyR is not required for the autoantibody binding to the GlyR target.

The de-glycosylation mutant GlyRα1^{N38Q} was analyzed focusing on expression levels, possible structural changes and receptor functionality. De-glycosylation can be verified with PNGaseF and EndoH digest of GlyRs (Oertel et al., 2007; Schaefer et al., 2015). The mutant GlyRα1^{N38Q} was proven for lack of glycosylation shown by a reduction in molecular weight of the GlyR protein.

Using the GlyRα3 structure (Huang et al., 2015) for homology modeling (done in collaboration with the group of H. Schindelin, RVZ, Würzburg, Germany), no gross changes have been observed for GlyRα1^{N38Q} in comparison to the non-mutated receptor. The mutant resulted in a loss of a hydrogen bond between proline 36 and asparagine 31 which does not lead to structural rearrangements. It was therefore assumed that GlyRα1^{N38Q} is most probably transported towards the cellular surface. Electrophysiological recordings of HEK293 cells expressing GlyRα1^{N38Q} demonstrated functional receptors with a rightward shift in the dose-response curve following glycine application, thus indicating a reduced glycine potency. The reduction in glycine potency is comparable to the hyperekplexia mutant *spasmodic* (GlyRα1^{A52S}) which carries a mutation nearby the glycosylation site but is normally expressed (Ryan et al., 1994; Saul et al., 1994). Examining the currents at saturating glycine concentrations, the de-glycosylation mutant GlyRα1^{N38Q} revealed no significant difference compared to GlyRα1^{WT} suggesting unchanged glycine efficacy. The close localization of N38 and A52 in the GlyR structure points to a functional important determinant. From the X-ray analysis of the different receptor states open, closed and desensitized (Du et al., 2015), the region around residue A52 is known to be involved in structural transitions following ligand binding and their translation into ion channel opening rather than in direct agonist binding.

The observed functional receptor expression of the mutant GlyRα1^{N38Q} at the cell surface argues against earlier reports that the glycosylation is a prerequisite for surface expression (Griffon et al., 1999). Therefore, the expression levels of GlyRα1^{N38Q} within the cell and at the cellular surface have been compared. The GlyRα1^{N38Q} whole cell expression and subsequently the surface expression levels were reduced about 40%. The reduced whole cell and surface GlyR expression indicates that the trafficking to the cell surface is affected but not abolished by the de-glycosylation. However, the expression levels of 60% at the surface are high compared to some hyperekplexia mutants in the loop D/β2-3 nearby the glycosylation site. These hyperekplexia mutants GlyRα1^{W68C}, GlyRα1^{D70N} and GlyRα1^{R72H} result in 8-15% surface expression (Schaefer et al., 2015). No functional receptors have been recorded from those mutants. The data on the expression level of the de-glycosylation mutant indicate that mutation

of residue N38 affects expression but the resulting surface receptors are still sufficient to enable chloride ion influx to the mutated channels.

In conclusion, GlyRα1 autoantibodies are able to bind to the GlyR independent of the glycosylation state. Similar observations were taken from GluN1 autoantibodies which bind in regions surrounding the glycosylation site irrespective of the glycosylation status of the NMDA receptor (Gleichman et al., 2012; Castillo-Gomez et al., 2017). Gleichman et al. (2012) showed that both, tunicamycin treatment and de-glycosylation mutants, abolished autoantibody binding. However, further amino acid mutations nearby the glycosylation site also decreased binding of autoantibodies. Therefore, the authors stated that the region neighboring the glycosylation site N368 is important for autoantibody binding rather than the glycosylation itself. The sequence around the observed residues N368 and G369 in NMDA receptors was found to be involved in the control of the receptor physiology (Gielen et al., 2009; Yuan et al., 2009; Hansen et al., 2010; Gleichman et al., 2012). Hence, structural and thus functional changes upon autoantibody binding are more likely rather than effects of the glycosylation at these positions. As stated above, also autoantibodies against the nodal proteins Caspr2 and Contactin-1 detect their target in the absence of protein glycosylation (Miura et al., 2015; Olsen et al., 2015). Similar results have been obtained for GlyRα1 autoantibodies in the present study. Taken together, GlyRα1 autoantibodies do not necessarily need a glycosylated GlyR to target the protein.

4.3 Autoantibody binding alters GlyR function

Autoantibodies that target ion channels or associated proteins have been demonstrated to influence receptor function. Impairment in neuronal excitability by autoantibodies against NMDARs or LG1, which is associated with Kv1.1 and AMPA receptors, has been shown as well as receptor reorganization and memory dysfunction (Castillo-Gomez et al., 2017; Haselmann et al., 2018; Petit-Pedrol et al., 2018; Wenke et al., 2019). The observed changes in the channel physiology are due to autoantibody binding to receptor domains that are involved in structural transitions required for ion channel opening and/or closing. Finally, neurotransmission of signals is disrupted and results in different symptoms in patients depending on the autoantibody type.

Therefore, it was important to study and understand the pathophysiological effects of GlyR autoantibodies which are essential to draw conclusions for better therapeutic options for SPS patients.

To circumvent interference with receptor internalization, a pre-incubation with GlyR autoantibodies for one hour was used with subsequent whole cell recordings of transfected cell lines with the GlyRα1. We found a rightward shift in the glycine dose-response curves accompanied with an increased EC_{50} value of cells that were pre-incubated with patient autoantibodies compared to healthy controls. These results suggest a reduced glycine potency arguing that *in vivo* 2-5 fold higher glycine levels during neurotransmission are required to activate the same number of receptors as in the absence of GlyR autoantibodies. Similar changes in glycine potency were described as underlying the pathological mechanism in hyperekplexia mutants of the GlyRα1, e.g. the *spasmodic* (GlyRα1^{A52S}) or *shaky* mutation (GlyRα1^{Q177K}) (Ryan et al., 1994; Saul et al., 1994; Saul et al., 1999; Chung et al., 2010; Bode et al., 2013; Schaefer et al., 2015). Glycine efficacy, shown by currents at saturating glycine concentrations, was however unaltered in 4 of 5 patient sera containing GlyR autoantibodies investigated in the present study. The above mentioned influence of autoantibodies to glycine potency is in accordance with a study of autoantibodies in NMDAR encephalitis showing a functional inhibition determined by the area under curve after glutamate application (Castillo-Gomez et al., 2017). This effect was already detected after 6 min of pre-incubation with patient serum and was still identified after 16 min incubation time. A very recent study analyzed the effect of GlyR autoantibodies on miniature inhibitory postsynaptic currents (mIPSCs) recorded from cultured motoneurons (Crisp et al., 2019). The amplitudes of mIPSCs were significantly reduced only after 4 h and 16 h pre-incubation with the autoantibodies. Unfortunately, the authors did not show if the resulting decreased currents were due to enhanced receptor internalization after these long periods of autoantibody presence or if they result from pure interaction of the autoantibodies with the target protein. In our results using shorter incubation times, the observed reductions in glycine-evoked amplitudes using glycine concentrations around EC_{50} were much larger (ranging from 41-94%) and do not result from receptor internalization. In hyperekplexia mutants, it was shown that the amplitudes of maximal currents upon glycine application persisted although 30-50% of cell surface receptors were lost (Villmann et al., 2009a; Atak et al., 2015; Schaefer et al., 2015). First changes in maximal currents occurred at 85% reduction of surface receptors. Due to the fact that during 1 h incubation time with the GlyR autoantibodies the amount of surface GlyRs is reduced only about 32% (Niels v Wardenburg, unpublished data), the decreased maximal currents can be explained as pure effect of autoantibody binding. Additionally, detachment of autoantibodies during longer recording times was excluded by immunocytochemical stainings that confirmed stable autoantibody binding at the end of the recording session.

Ion channels have different functional states, the open, closed and desensitized conformation (Du et al., 2015). We identified a common binding epitope for GlyR autoantibodies that is

important for the transitions between the functional states. When this region is occupied in the GlyRα3 by the allosteric analgesic potentiator AM-3607, the receptor changes its desensitization (Huang et al., 2017). So far, there are reports on changes of GlyR desensitization determined by sequence variations in the large intracellular loop between transmembrane domains 3 and 4 (Breitinger et al., 2009; Villmann et al., 2009a; Melzer et al., 2010; Papke and Grosman, 2014; Langlhofer et al., 2015). In contrast, binding of the allosteric modulator AM-3607 to GlyRα3 stabilizes the receptor conformation and hence enhances glycine affinity of GlyRα3. Prolonged glycine binding further leads to a longer receptor desensitization. Therefore, binding of autoantibodies in the same region might induce similar structural transitions of the GlyR protein or influence ion channel desensitization.

In the present study, desensitization was investigated by application of glycine for 10 s as the receptor desensitizes slowly. The desensitization analysis revealed that patient autoantibodies influence the desensitization state of the receptor. The results argue that two subgroups of autoantibodies exist because some sera increased the fraction of receptor desensitization whereas others decreased desensitization (Tab. 45). In addition to the determination of the fraction of receptors which are desensitized, the decay time of desensitization was estimated. Here again, some sera showed fast desensitization, other sera desensitized slow. These data suggest that possibly different receptor domains are targeted by the patient polyclonal autoantibodies. Similarly, differences in decay kinetics were also previously shown in hyperekplexia mutants. Some mutations enhanced desensitization and others increased tau values (Saul et al., 1999; Graham et al., 2006; Graham et al., 2011; Zhang et al., 2016; Schaefer et al., 2017; Wang et al., 2018). Hyperekplexia mutations in close proximity to the identified autoantibody epitope, GlyRα1^{I143F} and GlyRα1^{W179S}, lead to prolonged desensitization due to changes in the intrinsic channel gating properties (Zhang et al., 2016). On the other hand, faster desensitization was observed for GlyRα1^{Q177K} and GlyRα1^{A52S} (Graham et al., 2006; Graham et al., 2011; Schaefer et al., 2018b). These mutations are thought to cause defects in the signal transduction pathway which modulates the receptors transition from ligand-bound into the closed formation (Schaefer et al., 2017).

In NMDAR encephalitis, patient autoantibody binding also results in an altered receptor desensitization (Gleichman et al., 2012). These autoantibodies attach to their target located in the N-terminus of NMDARs, a region that forms a clamshell-like structure which interacts with the other subunits and which modulates the dynamics for an open or closed conformation. Upon NMDAR autoantibody binding, the receptor is stabilized in the open conformation, thereby the open time and desensitization of the receptor is prolonged.

As a last step to characterize receptor functionality, binding of the agonist glycine was investigated. The glycine binding site is localized at the inner cavity between two adjacent GlyR subunits (Lynch, 2004; Huang et al., 2017). Although the identified autoantibody epitope in the GlyR N-terminus is localized far away from the ligand binding site, binding of autoantibodies might block the entrance of the neurotransmitter to its binding site. Binding of the allosteric potentiator AM-3607 to GlyRα3 stabilized glycine binding resulting in an increased glycine affinity (Huang et al., 2017). AM-3607 binds in close proximity to the proposed GlyRα1 autoantibody epitope, thus a modulation of the glycine affinity due to autoantibody binding could be possible. The ligand binding affinity was however unchanged in the presence of GlyR autoantibodies. These data are in line with previous results showing no differences in the obtained inhibitory constant values for the high-affinity antagonist strychnine in the presence and absence of GlyR autoantibodies (unpublished). Together, GlyR autoantibodies are unable to displace glycine or strychnine from the orthosteric binding sites. However, autoantibody binding has an impact on receptor conformation, thus affecting receptor transitions between the open, closed and desensitized state.

4.4 Autoantibodies can be specifically neutralized

Plasma exchange is commonly used to reduce autoantibody titers and although it is well tolerated in some patients, 150 g healthy material is removed together with 1-2 g offending material (Pineda, 1999; Pagano et al., 2014; Albahra et al., 2019). To reduce the removal of healthy material, more specific approaches are required to specifically target the autoantibodies. Here, HEK293 cells expressing the GlyRα1 were used to bind autoantibodies leading step by step to a reduction or depletion of GlyR autoantibodies from the patient serum. Similar methods have been used for autoantibodies targeting neurofascin-155 at the paranodes in patients suffering from immune neuropathies (Stengel et al., 2019). Pre-incubation of patient autoantibodies with neurofascin-155 transfected cells resulted in autoantibody depletion and a loss of paranodal binding in murine teased fibers tested afterwards. Here, three transfers of patient serum between cover slips with GlyRα1 transfected HEK293 cells were sufficient to completely neutralize GlyRα1 autoantibodies from the solution.

Another approach more suitable to neutralize patient autoantibodies from serum samples is to use purified proteins. GlyR autoantibodies have been shown to bind to the ECD of the GlyR. An ECD construct expressed and purified from *Escherichia coli* was previously characterized (Breitinger and Becker, 2002; Breitinger et al., 2004). The GlyRα1 ECD construct consists of about 50% of the entire subunit sequence including the ligand binding and receptor assembly domains. The purified GlyR ECD construct had a proper fold and hence, was able to bind the

agonist glycine and the antagonist strychnine. Again, three transfers of autoantibody containing solution in ELISA plates coated with the GlyRα1 ECD were sufficient to completely neutralize the autoantibodies, thus verifying the applicability of this method. Coating of ELISA plates with GlyR ECD can therefore be used for two applications: (i) to neutralize GlyR autoantibodies from patient serum and (ii) to determine the autoantibody titers in patient samples. In a previous study, anti-neurofascin-155 autoantibody pre-absorption of neurofascin-155 coated ELISA plates, resulted in a reduced immunoreactivity in a coated ELISA plate (Doppler et al., 2018). Thus, a reduction of immunoreactivity following incubation of patient samples with ELISA plates coated with the target is in line with the reduction of GlyRα1 autoantibodies obtained here. However, the detected absorbance values of anti-neurofascin-155 autoantibodies were between 1.25 and 2.25. In contrast, the absorbance values of GlyR autoantibodies were lower than 0.1 possibly due to the use of medium binding ELISA plates in the present study. Another option for low absorbance values can be low GlyRα1 autoantibody titers.

Taken together, GlyRα1 autoantibodies can be specifically reduced and neutralized from solutions by using GlyRα1 expressing HEK293 cells or purified and refolded GlyRα1 ECD. For the future, it would be advantageous if the full-length GlyRα1 could be purified and refolded. Coating the ELISA plates with full-length protein will allow binding of all GlyR autoantibodies assuming that there are other epitopes besides the common identified GlyR epitope.

4.5 Passive transfer models for GlyRα autoantibodies

4.5.1 Passive transfer of GlyRα autoantibodies into zebrafish larvae alters motor behavior

In 1990, five criteria that evaluate the presence of an autoantibody-mediated disease were established (Drachman, 1990). Beside the criteria that autoantibodies are present in patients or that the autoantibody interacts with the target antigen, one important evidence for an autoimmunity is the reproducibility of disease features by passive transfer. Mostly, passive transfer experiments were performed in rodents to enable deeper insights into the disease pathology and to identify the pathological potential of autoantibodies. Here, zebrafish larvae were used as first passive transfer model. The zebrafish was chosen as mutations in zebrafish genes encoding GlyR subunits result in an altered escape behavior due to muscle stiffness and disturbed motor coordination in affected animals (Hirata et al., 2005; Ganser et al., 2013; Leacock et al., 2018). Additionally, knockout experiments of GlyR subunits in the zebrafish resulted in disturbed motor coordination as well (Samarut et al., 2019). As we demonstrated no binding of GlyR autoantibodies to the GlyRα1^{dr} subunit of the zebrafish, other zebrafish

GlyR subunits were investigated using stainings with patient samples. Immunocytochemical stainings revealed that the patient autoantibodies are able to bind all GlyRα^{dr} subunits (α2^{dr}, α3^{dr}, α4a^{dr}, α4b^{dr}) in 3 of 6 of the tested patient sera (Tab. 45). The GlyRβ^{dr} subunits (βa^{dr}, βb^{dr}) were marginally bound by 1 of 6 patient sera (Tab. 45). These results were a prerequisite for the passive transfer experiment into zebrafish larvae.

Here, touch-evoked escape responses were used as a readout for the observed effects of autoantibodies to the motor behavior following injection or transfer of GlyR autoantibodies via a lesion into the zebrafish larvae. Thereby, the escape responses were categorized into normal, mild and severe phenotype as reported before (Hirata et al., 2013; Schaefer et al., 2018b). Passive transfer of GlyRα1 autoantibodies (serum and purified IgG) into zebrafish larvae indeed led to an increase in severe phenotype and a decrease in normal phenotype, whereas the mild phenotype was nearly unchanged. Thus, we provide first evidence that GlyR autoantibodies are able to impair the nerve-muscle circuit.

Although a significant increase in the severe escape response was obtained, also larvae which appeared quite normal persisted. This might be due to compensatory effects of the other GlyR subunits as not all GlyR subunits of the zebrafish are targeted by patient autoantibodies. For example, the β subunits were almost not targeted by the patient autoantibodies but they are important for bilateral muscle contractions. This was shown by mutations in the gene encoding the GlyRβ which led to behavioral defects in the hyperekplexia model *bandoneon* (Ganser et al., 2013). Thus, the GlyRβ subunits can sustain the inhibition although other GlyR subunits are blocked by autoantibodies.

As negative controls, larvae treated with ACSF and healthy control serum were used. Some of the control larvae developed mild and severe phenotypes. These phenotypes result from the skin lesions or injection procedures. Therefore, the application techniques during passive transfer per se cause some motor deficits that have to be stated as inevitable background effect.

In conclusion, the present study shows for the first time, that a passive transfer of GlyR autoantibodies into zebrafish changes the motor phenotype of the zebrafish. Following a touch, the larvae are unable to swim away due to enhanced muscle tone and stiffness. The observed phenotype is thus compatible with abnormal startle response in SPS or PERM patients.

4.5.2 Passively transferred GlyRα autoantibodies target GlyRs in murine spinal cord and brain

For passive transfer into mice, intrathecal applications either by injections or osmotic pumps have been utilized. This procedure has been used earlier for transfer of human amphiphysin or GAD65 autoantibodies from SPS patients into rats (Sommer et al., 2005; Geis et al., 2010; Geis et al., 2011; Manto et al., 2011; Hampe et al., 2013; Hansen et al., 2013; Manto et al., 2015; Werner et al., 2016). Here, mice were chosen instead of rats as there are numerous reports on GlyR mutant mice inducing severe neuromotor deficits similar to symptoms observed in human patients suffering from hyperekplexia (Kingsmore et al., 1994; Ryan et al., 1994; Saul et al., 1994; Schaefer et al., 2017; Schaefer et al., 2018b). Following a passive transfer of human GlyR autoantibodies into mice, GlyRα1 autoantibody binding was observed to GlyRs located in spinal cord, the hypoglossal nucleus, the preBötzinger complex, the cochlear nucleus, lateral superior olive, superior paraolivary nucleus and the inferior colliculus. Binding was demonstrated by immunohistochemical stainings and protein analyses from membrane preparations of murine tissues. We concluded that intrathecal applications seem to be also applicable for passive transfer of GlyRα1 autoantibodies.

Further observations that have to be taken into account for follow up the experiments are described in the next paragraph. The fluorescent signal intensities in mice with manual injections via intrathecal catheter were brighter, especially in the spinal cord, in comparison to the use of osmotic pumps. We used a concentration of injected IgG from patients with GlyR autoantibodies or control samples of 1 mg/ml. Other studies with GAD65 or amphiphysin autoantibodies used an 10 fold or 100 fold higher IgG concentration of about 10-100 mg/ml (Sommer et al., 2005; Geis et al., 2010; Geis et al., 2011; Manto et al., 2011; Hansen et al., 2013). In contrast to the GlyR, GAD65 and amphiphysin are intracellular proteins and thus possibly require higher IgG dose to reach the target. The use of a higher concentration in the passive transfer of GlyR autoantibodies might improve the phenotypical readout as a neuromotor phenotype following injection of patient IgG was almost absent. The correct positioning of the catheter in the vertebral canal was controlled and did not underlie the observed lack of alterations in the motor behavior of injected animals.

The passive transfer of amphiphysin autoantibodies successfully elicited patient symptoms like stiffness and muscle spasms in rats which was a result of a reduction in GABAergic transmission (Geis et al., 2010). Equally, intrathecal application of GAD65 autoantibodies into rats resulted in an anxious phenotype with impaired locomotor function, muscle stiffness, increased spinal cord excitability, impaired GABAergic neurotransmission and deteriorated cognitive functions (Geis et al., 2011; Hansen et al., 2013). This phenotypical expression after autoantibody treatment in rats is highly comparable to behavior observed in SPS patients.

We expected that a passive transfer of GlyRα1 autoantibodies into mice lead to an altered locomotor activity compatible to symptoms described for SPS patients and similar to genetic variants of the GlyR in humans and mice (Hutchinson et al., 2008; McKeon et al., 2013; Carvajal-Gonzalez et al., 2014; Mine et al., 2015; Hinson et al., 2018). Locomotion of mice treated with patient MIX IgG (mix from two patients) in comparison to mice injected with control IgG from a healthy individual and NaCl (vehicle) was investigated using the Rotarod. The time mice treated with patient MIX IgG spent on the Rotarod was indistinguishable from control mice. Further measurements of the distance traveled in other tests for anxiety, such as the Open Field and Elevated Plus Maze test, did also not display differences between mice treated with patient MIX IgG compared to control individuals.

SPS and hyperekplexia patients were described as being anxious of sudden falls due to unexpected noise or touch (Mine et al., 2015; Hinson et al., 2018). Additionally, increased anxiety was described for an allelic variation of the GlyRβ subunit, which might also represent a feasible target for GlyR autoantibodies (Deckert et al., 2017). There were no differences in the time spent in the periphery or in the center of the Open Field test as well as no differences of time spent in the open or closed arms of the Elevated Plus Maze between the control groups and mice treated with patient MIX IgG.

As a test for pain sensitization, the von Frey test was included using mechanic stimuli. This test was included as patient GlyR autoantibodies also target the GlyRα3 subunit, which plays a role in pain sensitization (Harvey et al., 2004; Hosl et al., 2006; Lynch and Callister, 2006; Acuna et al., 2016). Mice treated with patient MIX IgG mice exhibited a lower paw withdrawal threshold compared to control mice although only at one time point of the experimental series.

In sum, although the GlyR autoantibodies reached their target following passive transfer into animals, the phenotypic impairment such as neuromotor deficits related to the symptoms observed in human patients could not be observed with the behavioral tests used. A further observation was that some motor deficiency was seen within the first 30 min after patient IgG application of the mice that were manually injected (data not shown). The behavior tests mentioned above have been performed daily (Rotarod and von Frey) but application occurred continuously slowly via osmotic pumps. It was, however, difficult to discriminate the effects in manually injected mice from an impairment of locomotion due to the anesthesia used. A fast degradation of injected IgG and the low concentration used might also underlie the lack of a neuromotor phenotype and should be further investigated. Another typical symptom of human patients with SPS or with genetic variants of the GlyR is an increased startle response (Graham et al., 2006; Schaefer et al., 2012; Damasio et al., 2013; Schaefer et al., 2017; Hinson et al., 2018; Schaefer et al., 2018b). Startle responses can be measured in mice (Plappert et al.,

2001) and should be included into the behavioral characterization of mice used for passive transfer of human GlyR autoantibodies as the enhanced startle reaction represents one of the major symptoms in human patients with SPS.

In conclusion, human GlyRα1 autoantibodies were able to bind GlyRs in spinal cord and brain after passive transfer. Possibly, a higher concentration of autoantibodies is required to elicit an impaired neuromotor phenotype in mice.

5. Outlook

The results examined in this study identified a common GlyRα1 autoantibody epitope within the N-terminus covering amino acids A^{1}-G^{34}. However, further autoantibody epitopes might exist as not all patient samples target the same receptor subunits except GlyRα1. Microarrays spotted with different GlyR peptides could effectively support the epitope identification in a time-saving manner. Complete neutralization of autoantibodies was proven with two independent methods (expression of GlyRα1 in HEK293 cells and GlyRα1 ECD coated to ELISA plates). Specific neutralization in a personalized manner might be a suitable approach for future development of therapeutic options.

Further, the present study revealed an influence of GlyR autoantibodies on receptor functionality. Autoantibodies led to a decreased glycine potency as well as to an altered desensitization. This broadens the knowledge about SPS disease pathology beyond the so far published mechanisms of internalization and complement system activation (Carvajal-Gonzalez et al., 2014).

This study shows for the first time that a transfer of GlyR autoantibodies to zebrafish and mice results in successful targeting of the receptors in the spinal cord and brain. Moreover, zebrafish larvae showed impaired escape response. This behavioral output in the very simple animal model of the zebrafish is compatible with the enhanced startle response observed in SPS patients. Therefore, the direct pathological potential of GlyR autoantibodies has been clearly proven.

Additional therapeutic approaches to identify the autoantibody producing cells will also be helpful to develop more personalized therapies. So far, self-reactive B cells and long-lived plasma cells are discussed to play a role in autoantibody production (Wardemann et al., 2003; Hale et al., 2018). Nevertheless, it is not clarified yet why the B cell depleting drug rituximab improves the symptoms in some patients and in others not. SPS therapies would be more successful if autoantibody production would be prevented instead of depleting high numbers of already produced autoantibodies.

6. References

Acuna MA, Yevenes GE, Ralvenius WT, Benke D, Di Lio A, Lara CO, Munoz B, Burgos CF, Moraga-Cid G, Corringer PJ, Zeilhofer HU (2016). Phosphorylation state-dependent modulation of spinal glycine receptors alleviates inflammatory pain. J Clin Invest 126:2547-2560.

Albahra S, Yates SG, Joseph D, De Simone N, Burner JD, Sarode R (2019). Role of plasma exchange in stiff person syndrome. Transfus Apher Sci 58:310-312.

Alexopoulos H, Akrivou S, Dalakas MC (2013). Glycine receptor antibodies in stiff-person syndrome and other GAD-positive CNS disorders. Neurology 81:1962-1964.

Atak S, Langlhofer G, Schaefer N, Kessler D, Meiselbach H, Delto C, Schindelin H, Villmann C (2015). Disturbances of ligand potency and enhanced degradation of the human glycine receptor at affected positions G160 and T162 originally identified in patients suffering from hyperekplexia. Front Mol Neurosci 8:79.

Baer K, Waldvogel HJ, During MJ, Snell RG, Faull RL, Rees MI (2003). Association of gephyrin and glycine receptors in the human brainstem and spinal cord: an immunohistochemical analysis. Neuroscience 122:773-784.

Baizabal-Carvallo JF, Jankovic J (2015). Stiff-person syndrome: insights into a complex autoimmune disorder. J Neurol Neurosurg Psychiatry 86:840-848.

Balint B, Bhatia KP (2016). Stiff person syndrome and other immune-mediated movement disorders - new insights. Curr Opin Neurol 29:496-506.

Becker K, Breitinger HG, Humeny A, Meinck HM, Dietz B, Aksu F, Becker CM (2008). The novel hyperekplexia allele GLRA1(S267N) affects the ethanol site of the glycine receptor. Eur J Hum Genet 16:223-228.

Becker K, Braune M, Benderska N, Buratti E, Baralle F, Villmann C, Stamm S, Eulenburg V, Becker CM (2012). A retroelement modifies pre-mRNA splicing: the murine Glrb(spa) allele is a splicing signal polymorphism amplified by long interspersed nuclear element insertion. J Biol Chem 287:31185-31194.

Betz H, Laube B (2006). Glycine receptors: recent insights into their structural organization and functional diversity. J Neurochem 97:1600-1610.

Birnboim HC, Doly J (1979). A rapid alkaline extraction procedure for screening recombinant plasmid DNA. Nucleic Acids Res 7:1513-1523.

Blednov YA, Benavidez JM, Black M, Leiter CR, Osterndorff-Kahanek E, Harris RA (2015). Glycine receptors containing alpha2 or alpha3 subunits regulate specific ethanol-mediated behaviors. J Pharmacol Exp Ther 353:181-191.

Bode A, Lynch JW (2014). The impact of human hyperekplexia mutations on glycine receptor structure and function. Mol Brain 7:2.

Bode A et al. (2013). New hyperekplexia mutations provide insight into glycine receptor assembly, trafficking, and activation mechanisms. J Biol Chem 288:33745-33759.

Bormann J, Hamill OP, Sakmann B (1987). Mechanism of anion permeation through channels gated by glycine and gamma-aminobutyric acid in mouse cultured spinal neurones. J Physiol 385:243-286.

Breitinger HG, Becker CM (2002). The inhibitory glycine receptor-simple views of a complicated channel. Chembiochem 3:1042-1052.

Breitinger HG, Villmann C, Melzer N, Rennert J, Breitinger U, Schwarzinger S, Becker CM (2009). Novel regulatory site within the TM3-4 loop of human recombinant alpha3 glycine receptors determines channel gating and domain structure. J Biol Chem 284:28624-28633.

Breitinger U, Breitinger HG, Bauer F, Fahmy K, Glockenhammer D, Becker CM (2004). Conserved high affinity ligand binding and membrane association in the native and refolded extracellular domain of the human glycine receptor alpha1-subunit. J Biol Chem 279:1627-1636.

Brunso-Bechtold JK, Thompson GC, Masterton RB (1981). HRP study of the organization of auditory afferents ascending to central nucleus of inferior colliculus in cat. J Comp Neurol 197:705-722.

Buckwalter MS, Cook SA, Davisson MT, White WF, Camper SA (1994). A frameshift mutation in the mouse alpha 1 glycine receptor gene (Glra1) results in progressive neurological symptoms and juvenile death. Hum Mol Genet 3:2025-2030.

Busselberg D, Bischoff AM, Becker K, Becker CM, Richter DW (2001). The respiratory rhythm in mutant oscillator mice. Neurosci Lett 316:99-102.

Butler MH, Hayashi A, Ohkoshi N, Villmann C, Becker CM, Feng G, De Camilli P, Solimena M (2000). Autoimmunity to gephyrin in Stiff-Man syndrome. Neuron 26:307-312.

Carvajal-Gonzalez A, Leite MI, Waters P, Woodhall M, Coutinho E, Balint B, Lang B, Pettingill P, Carr A, Sheerin UM, Press R, Lunn MP, Lim M, Maddison P, Meinck HM, Vandenberghe W, Vincent A (2014). Glycine receptor antibodies in PERM and related syndromes: characteristics, clinical features and outcomes. Brain 137:2178-2192.

Castillo-Gomez E, Oliveira B, Tapken D, Bertrand S, Klein-Schmidt C, Pan H, Zafeiriou P, Steiner J, Jurek B, Trippe R, Pruss H, Zimmermann WH, Bertrand D, Ehrenreich H, Hollmann M (2017). All naturally occurring autoantibodies against the NMDA receptor subunit NR1 have pathogenic potential irrespective of epitope and immunoglobulin class. Mol Psychiatry 22:1776-1784.

Chaplan SR, Bach FW, Pogrel JW, Chung JM, Yaksh TL (1994). Quantitative assessment of tactile allodynia in the rat paw. J Neurosci Methods 53:55-63.

Chung SK et al. (2010). Pathophysiological mechanisms of dominant and recessive GLRA1 mutations in hyperekplexia. J Neurosci 30:9612-9620.

Crisp SJ, Dixon CL, Jacobson L, Chabrol E, Irani SR, Leite MI, Leschziner G, Slaght SJ, Vincent A, Kullmann DM (2019). Glycine receptor autoantibodies disrupt inhibitory neurotransmission. Brain 142:3398-3410.

Dalmau J, Geis C, Graus F (2017). Autoantibodies to synaptic receptors and neuronal cell surface proteins in autoimmune diseases of the central nervous system. Physiol Rev 97:839-887.

Dalmau J, Gleichman AJ, Hughes EG, Rossi JE, Peng X, Lai M, Dessain SK, Rosenfeld MR, Balice-Gordon R, Lynch DR (2008). Anti-NMDA-receptor encephalitis: case series and analysis of the effects of antibodies. Lancet Neurol 7:1091-1098.

Dalmau J, Tuzun E, Wu HY, Masjuan J, Rossi JE, Voloschin A, Baehring JM, Shimazaki H, Koide R, King D, Mason W, Sansing LH, Dichter MA, Rosenfeld MR, Lynch DR (2007). Paraneoplastic anti-N-methyl-D-aspartate receptor encephalitis associated with ovarian teratoma. Ann Neurol 61:25-36.

Damasio J, Leite MI, Coutinho E, Waters P, Woodhall M, Santos MA, Carrilho I, Vincent A (2013). Progressive encephalomyelitis with rigidity and myoclonus: the first pediatric case with glycine receptor antibodies. JAMA Neurol 70:498-501.

De Camilli P, Thomas A, Cofiell R, Folli F, Lichte B, Piccolo G, Meinck HM, Austoni M, Fassetta G, Bottazzo G, Bates D, Cartlidge N, Solimena M, Kilimann MW (1993). The synaptic vesicle-associated protein amphiphysin is the 128-kD autoantigen of Stiff-Man syndrome with breast cancer. J Exp Med 178:2219-2223.

Deckert J et al. (2017). GLRB allelic variation associated with agoraphobic cognitions, increased startle response and fear network activation: a potential neurogenetic pathway to panic disorder. Mol Psychiatry 22:1431-1439.

Devignot V, Prado de Carvalho L, Bregestovski P, Goblet C (2003). A novel glycine receptor alpha Z1 subunit variant in the zebrafish brain. Neuroscience 122:449-457.

Di Paolo G, Sankaranarayanan S, Wenk MR, Daniell L, Perucco E, Caldarone BJ, Flavell R, Picciotto MR, Ryan TA, Cremona O, De Camilli P (2002). Decreased synaptic vesicle recycling efficiency and cognitive deficits in amphiphysin 1 knockout mice. Neuron 33:789-804.

Doppler K, Schleyer B, Geis C, Grunewald B, Putz E, Villmann C, Sommer C (2016). Lockjaw in stiff-person syndrome with autoantibodies against glycine receptors. Neurol Neuroimmunol Neuroinflamm 3:e186.

Doppler K, Stengel H, Appeltshauser L, Grosskreutz J, Man Ng JK, Meinl E, Sommer C (2018). Neurofascin-155 IgM autoantibodies in patients with inflammatory neuropathies. J Neurol Neurosurg Psychiatry 89:1145-1151.

Drachman DB (1990). How to recognize an antibody-mediated autoimmune disease: criteria. Res Publ Assoc Res Nerv Ment Dis 68:183-186.

Drachman DB (1994). Myasthenia gravis. N Engl J Med 330:1797-1810.

Du J, Lu W, Wu S, Cheng Y, Gouaux E (2015). Glycine receptor mechanism elucidated by electron cryo-microscopy. Nature 526:224-229.

Durisic N, Godin AG, Wever CM, Heyes CD, Lakadamyali M, Dent JA (2012). Stoichiometry of the human glycine receptor revealed by direct subunit counting. J Neurosci 32:12915-12920.

Ganser LR, Yan Q, James VM, Kozol R, Topf M, Harvey RJ, Dallman JE (2013). Distinct phenotypes in zebrafish models of human startle disease. Neurobiol Dis 60:139-151.

Geis C, Beck M, Jablonka S, Weishaupt A, Toyka KV, Sendtner M, Sommer C (2009). Stiff person syndrome associated anti-amphiphysin antibodies reduce GABA associated [Ca(2+)]i rise in embryonic motoneurons. Neurobiol Dis 36:191-199.

Geis C, Weishaupt A, Grunewald B, Wultsch T, Reif A, Gerlach M, Dirkx R, Solimena M, Perani D, Heckmann M, Toyka KV, Folli F, Sommer C (2011). Human stiff-person syndrome IgG induces anxious behavior in rats. PLoS One 6:e16775.

Geis C, Weishaupt A, Hallermann S, Grunewald B, Wessig C, Wultsch T, Reif A, Byts N, Beck M, Jablonka S, Boettger MK, Uceyler N, Fouquet W, Gerlach M, Meinck HM, Siren AL, Sigrist SJ, Toyka KV, Heckmann M, Sommer C (2010). Stiff person syndrome-associated autoantibodies to amphiphysin mediate reduced GABAergic inhibition. Brain 133:3166-3180.

Gielen M, Thomas P, Smart TG (2015). The desensitization gate of inhibitory Cys-loop receptors. Nat Commun 6:6829.

Gielen M, Siegler Retchless B, Mony L, Johnson JW, Paoletti P (2009). Mechanism of differential control of NMDA receptor activity by NR2 subunits. Nature 459:703-707.

Gleichman AJ, Spruce LA, Dalmau J, Seeholzer SH, Lynch DR (2012). Anti-NMDA receptor encephalitis antibody binding is dependent on amino acid identity of a small region within the GluN1 amino terminal domain. J Neurosci 32:11082-11094.

Glendenning KK, Hutson KA, Nudo RJ, Masterton RB (1985). Acoustic chiasm II: Anatomical basis of binaurality in lateral superior olive of cat. J Comp Neurol 232:261-285.

Graham BA, Tadros MA, Schofield PR, Callister RJ (2011). Probing glycine receptor stoichiometry in superficial dorsal horn neurones using the spasmodic mouse. J Physiol 589:2459-2474.

Graham BA, Schofield PR, Sah P, Margrie TW, Callister RJ (2006). Distinct physiological mechanisms underlie altered glycinergic synaptic transmission in the murine mutants spastic, spasmodic, and oscillator. J Neurosci 26:4880-4890.

Griffon N, Buttner C, Nicke A, Kuhse J, Schmalzing G, Betz H (1999). Molecular determinants of glycine receptor subunit assembly. EMBO J 18:4711-4721.

Grothe B, Pecka M (2014). The natural history of sound localization in mammals--a story of neuronal inhibition. Front Neural Circuits 8:116.

Grothe B, Pecka M, McAlpine D (2010). Mechanisms of sound localization in mammals. Physiol Rev 90:983-1012.

Grudzinska J, Schemm R, Haeger S, Nicke A, Schmalzing G, Betz H, Laube B (2005). The beta subunit determines the ligand binding properties of synaptic glycine receptors. Neuron 45:727-739.

Hale M, Rawlings DJ, Jackson SW (2018). The long and the short of it: insights into the cellular source of autoantibodies as revealed by B cell depletion therapy. Curr Opin Immunol 55:81-88.

Hampe CS, Petrosini L, De Bartolo P, Caporali P, Cutuli D, Laricchiuta D, Foti F, Radtke JR, Vidova V, Honnorat J, Manto M (2013). Monoclonal antibodies to 65kDa glutamate decarboxylase induce epitope specific effects on motor and cognitive functions in rats. Orphanet J Rare Dis 8:82.

Hansen KB, Furukawa H, Traynelis SF (2010). Control of assembly and function of glutamate receptors by the amino-terminal domain. Mol Pharmacol 78:535-549.

Hansen N, Grunewald B, Weishaupt A, Colaco MN, Toyka KV, Sommer C, Geis C (2013). Human Stiff person syndrome IgG-containing high-titer anti-GAD65 autoantibodies induce motor dysfunction in rats. Exp Neurol 239:202-209.

Harvey RJ, Depner UB, Wassle H, Ahmadi S, Heindl C, Reinold H, Smart TG, Harvey K, Schutz B, Abo-Salem OM, Zimmer A, Poisbeau P, Welzl H, Wolfer DP, Betz H, Zeilhofer HU, Muller U (2004). GlyR alpha3: an essential target for spinal PGE2-mediated inflammatory pain sensitization. Science 304:884-887.

Haselmann H, Mannara F, Werner C, Planaguma J, Miguez-Cabello F, Schmidl L, Grunewald B, Petit-Pedrol M, Kirmse K, Classen J, Demir F, Klocker N, Soto D, Doose S, Dalmau J, Hallermann S, Geis C (2018). Human autoantibodies against the AMPA receptor subunit GluA2 induce receptor reorganization and memory dysfunction. Neuron 100:91-105 e109.

Hinson SR, Lopez-Chiriboga AS, Bower JH, Matsumoto JY, Hassan A, Basal E, Lennon VA, Pittock SJ, McKeon A (2018). Glycine receptor modulating antibody predicting treatable stiff-person spectrum disorders. Neurol Neuroimmunol Neuroinflamm 5:e438.

Hirata H, Carta E, Yamanaka I, Harvey RJ, Kuwada JY (2009). Defective glycinergic synaptic transmission in zebrafish motility mutants. Front Mol Neurosci 2:26.

Hirata H, Ogino K, Yamada K, Leacock S, Harvey RJ (2013). Defective escape behavior in DEAH-box RNA helicase mutants improved by restoring glycine receptor expression. J Neurosci 33:14638-14644.

Hirata H, Saint-Amant L, Downes GB, Cui WW, Zhou W, Granato M, Kuwada JY (2005). Zebrafish bandoneon mutants display behavioral defects due to a mutation in the glycine receptor beta-subunit. Proc Natl Acad Sci U S A 102:8345-8350.

Hirtz JJ (2012). Development of cytoarchitecture, microcircuitry and inhibitory transmission in the auditory brainstem: CaV 1.3 calcium channels and chloride regulation. In: Biology. Kaiserslautern: Technische Universität Kaiserslautern.

Hoch W, Betz H, Becker CM (1989). Primary cultures of mouse spinal cord express the neonatal isoform of the inhibitory glycine receptor. Neuron 3:339-348.

Hoftberger R, van Sonderen A, Leypoldt F, Houghton D, Geschwind M, Gelfand J, Paredes M, Sabater L, Saiz A, Titulaer MJ, Graus F, Dalmau J (2015). Encephalitis and AMPA receptor antibodies: Novel findings in a case series of 22 patients. Neurology 84:2403-2412.

Hosl K, Reinold H, Harvey RJ, Muller U, Narumiya S, Zeilhofer HU (2006). Spinal prostaglandin E receptors of the EP2 subtype and the glycine receptor alpha3 subunit, which mediate central inflammatory hyperalgesia, do not contribute to pain after peripheral nerve injury or formalin injection. Pain 126:46-53.

Howard FM, Jr. (1963). A new and effective drug in the treatment of the stiff-man syndrome: preliminary report. Proc Staff Meet Mayo Clin 38:203-212.

Huang X, Chen H, Michelsen K, Schneider S, Shaffer PL (2015). Crystal structure of human glycine receptor-alpha3 bound to antagonist strychnine. Nature 526:277-280.

Huang X, Shaffer PL, Ayube S, Bregman H, Chen H, Lehto SG, Luther JA, Matson DJ, McDonough SI, Michelsen K, Plant MH, Schneider S, Simard JR, Teffera Y, Yi S, Zhang M, DiMauro EF, Gingras J (2017). Crystal structures of human glycine receptor alpha3 bound to a novel class of analgesic potentiators. Nat Struct Mol Biol 24:108-113.

Hughes BW, Moro De Casillas ML, Kaminski HJ (2004). Pathophysiology of myasthenia gravis. Semin Neurol 24:21-30.

Hughes EG, Peng X, Gleichman AJ, Lai M, Zhou L, Tsou R, Parsons TD, Lynch DR, Dalmau J, Balice-Gordon RJ (2010). Cellular and synaptic mechanisms of anti-NMDA receptor encephalitis. J Neurosci 30:5866-5875.

Hutchinson M, Waters P, McHugh J, Gorman G, O'Riordan S, Connolly S, Hager H, Yu P, Becker CM, Vincent A (2008). Progressive encephalomyelitis, rigidity, and myoclonus: a novel glycine receptor antibody. Neurology 71:1291-1292.

Imboden M, Devignot V, Goblet C (2001). Phylogenetic relationships and chromosomal location of five distinct glycine receptor subunit genes in the teleost Danio rerio. Dev Genes Evol 211:415-422.

Irani SR, Alexander S, Waters P, Kleopa KA, Pettingill P, Zuliani L, Peles E, Buckley C, Lang B, Vincent A (2010). Antibodies to Kv1 potassium channel-complex proteins leucine-rich, glioma inactivated 1 protein and contactin-associated protein-2 in limbic encephalitis, Morvan's syndrome and acquired neuromyotonia. Brain 133:2734-2748.

Jin R, Singh SK, Gu S, Furukawa H, Sobolevsky AI, Zhou J, Jin Y, Gouaux E (2009). Crystal structure and association behaviour of the GluR2 amino-terminal domain. EMBO J 28:1812-1823.

Jones MV, Westbrook GL (1996). The impact of receptor desensitization on fast synaptic transmission. Trends Neurosci 19:96-101.

Jonsson S, Morud J, Pickering C, Adermark L, Ericson M, Soderpalm B (2012). Changes in glycine receptor subunit expression in forebrain regions of the Wistar rat over development. Brain Res 1446:12-21.

Karakas E, Simorowski N, Furukawa H (2009). Structure of the zinc-bound amino-terminal domain of the NMDA receptor NR2B subunit. EMBO J 28:3910-3920.

Kingsmore SF, Giros B, Suh D, Bieniarz M, Caron MG, Seldin MF (1994). Glycine receptor beta-subunit gene mutation in spastic mouse associated with LINE-1 element insertion. Nat Genet 7:136-141.

Kling C, Koch M, Saul B, Becker CM (1997). The frameshift mutation oscillator (Glra1(spd-ot)) produces a complete loss of glycine receptor alpha1-polypeptide in mouse central nervous system. Neuroscience 78:411-417.

Kneussel M, Betz H (2000). Clustering of inhibitory neurotransmitter receptors at developing postsynaptic sites: the membrane activation model. Trends Neurosci 23:429-435.

Koerner C, Wieland B, Richter W, Meinck HM (2004). Stiff-person syndromes: motor cortex hyperexcitability correlates with anti-GAD autoimmunity. Neurology 62:1357-1362.

Kotak VC, Korada S, Schwartz IR, Sanes DH (1998). A developmental shift from GABAergic to glycinergic transmission in the central auditory system. J Neurosci 18:4646-4655.

Kuhse J, Schmieden V, Betz H (1990). A single amino acid exchange alters the pharmacology of neonatal rat glycine receptor subunit. Neuron 5:867-873.

Kuhse J, Laube B, Magalei D, Betz H (1993). Assembly of the inhibitory glycine receptor: identification of amino acid sequence motifs governing subunit stoichiometry. Neuron 11:1049-1056.

Labasque M, Hivert B, Nogales-Gadea G, Querol L, Illa I, Faivre-Sarrailh C (2014). Specific contactin N-glycans are implicated in neurofascin binding and autoimmune targeting in peripheral neuropathies. J Biol Chem 289:7907-7918.

Lai M, Hughes EG, Peng X, Zhou L, Gleichman AJ, Shu H, Mata S, Kremens D, Vitaliani R, Geschwind MD, Bataller L, Kalb RG, Davis R, Graus F, Lynch DR, Balice-Gordon R, Dalmau J (2009). AMPA receptor antibodies in limbic encephalitis alter synaptic receptor location. Ann Neurol 65:424-434.

Langlhofer G, Villmann C (2017). The role of charged residues in independent glycine receptor folding domains for intermolecular interactions and ion channel function. J Neurochem 142:41-55.

Langlhofer G, Janzen D, Meiselbach H, Villmann C (2015). Length of the TM3-4 loop of the glycine receptor modulates receptor desensitization. Neurosci Lett 600:176-181.

Langosch D, Laube B, Rundstrom N, Schmieden V, Bormann J, Betz H (1994). Decreased agonist affinity and chloride conductance of mutant glycine receptors associated with human hereditary hyperekplexia. EMBO J 13:4223-4228.

Leacock S, Syed P, James VM, Bode A, Kawakami K, Keramidas A, Suster M, Lynch JW, Harvey RJ (2018). Structure/Function studies of the alpha4 subunit reveal evolutionary loss of a GlyR subtype involved in startle and escape responses. Front Mol Neurosci 11:23.

Legendre P (2001). The glycinergic inhibitory synapse. Cell Mol Life Sci 58:760-793.

Li X, Li H, Hu Q, Lin J, Zhang Q, Li Y, Li J, Chen T, Zhang Q, Qiu Y (2018). Detection of epitopes in systemic lupus erythematosus using peptide microarray. Mol Med Rep 17:6533-6541.

Lynch JW (2004). Molecular structure and function of the glycine receptor chloride channel. Physiol Rev 84:1051-1095.

Lynch JW, Callister RJ (2006). Glycine receptors: a new therapeutic target in pain pathways. Curr Opin Investig Drugs 7:48-53.

Malmierca M, Ryugo D (2012). The mouse nervous system. Amsterdam, Netherlands: Elsevier.

Malosio ML, Marqueze-Pouey B, Kuhse J, Betz H (1991). Widespread expression of glycine receptor subunit mRNAs in the adult and developing rat brain. EMBO J 10:2401-2409.

Mantegazza R, Cordiglieri C, Consonni A, Baggi F (2016). Animal models of myasthenia gravis: utility and limitations. Int J Gen Med 9:53-64.

Manto M, Honnorat J, Hampe CS, Guerra-Narbona R, Lopez-Ramos JC, Delgado-Garcia JM, Saitow F, Suzuki H, Yanagawa Y, Mizusawa H, Mitoma H (2015). Disease-specific monoclonal antibodies targeting glutamate decarboxylase impair GABAergic neurotransmission and affect motor learning and behavioral functions. Front Behav Neurosci 9:78.

Manto MU, Hampe CS, Rogemond V, Honnorat J (2011). Respective implications of glutamate decarboxylase antibodies in stiff person syndrome and cerebellar ataxia. Orphanet J Rare Dis 6:3.

Manzke T, Niebert M, Koch UR, Caley A, Vogelgesang S, Hulsmann S, Ponimaskin E, Muller U, Smart TG, Harvey RJ, Richter DW (2010). Serotonin receptor 1A-modulated phosphorylation of glycine receptor alpha3 controls breathing in mice. J Clin Invest 120:4118-4128.

Martinez-Hernandez E, Horvath J, Shiloh-Malawsky Y, Sangha N, Martinez-Lage M, Dalmau J (2011). Analysis of complement and plasma cells in the brain of patients with anti-NMDAR encephalitis. Neurology 77:589-593.

Martinez-Hernandez E, Arino H, McKeon A, Iizuka T, Titulaer MJ, Simabukuro MM, Lancaster E, Petit-Pedrol M, Planaguma J, Blanco Y, Harvey RJ, Saiz A, Graus F, Dalmau J (2016). Clinical and immunologic investigations in patients with stiff-serson spectrum disorder. JAMA Neurol 73:714-720.

McKeon A, Martinez-Hernandez E, Lancaster E, Matsumoto JY, Harvey RJ, McEvoy KM, Pittock SJ, Lennon VA, Dalmau J (2013). Glycine receptor autoimmune spectrum with stiff-man syndrome phenotype. JAMA Neurol 70:44-50.

Meddows E, Le Bourdelles B, Grimwood S, Wafford K, Sandhu S, Whiting P, McIlhinney RA (2001). Identification of molecular determinants that are important in the assembly of N-methyl-D-aspartate receptors. J Biol Chem 276:18795-18803.

Meinck HM, Thompson PD (2002). Stiff man syndrome and related conditions. Mov Disord 17:853-866.

Melzer N, Villmann C, Becker K, Harvey K, Harvey RJ, Vogel N, Kluck CJ, Kneussel M, Becker CM (2010). Multifunctional basic motif in the glycine receptor intracellular domain induces subunit-specific sorting. J Biol Chem 285:3730-3739.

Mine J, Taketani T, Yoshida K, Yokochi F, Kobayashi J, Maruyama K, Nanishi E, Ono M, Yokoyama A, Arai H, Tamaura S, Suzuki Y, Otsubo S, Hayashi T, Kimura M, Kishi K, Yamaguchi S (2015). Clinical and genetic investigation of 17 Japanese patients with hyperekplexia. Dev Med Child Neurol 57:372-377.

Miura Y, Devaux JJ, Fukami Y, Manso C, Belghazi M, Wong AH, Yuki N, Group CCS (2015). Contactin 1 IgG4 associates to chronic inflammatory demyelinating polyneuropathy with sensory ataxia. Brain 138:1484-1491.

Moersch FP, Woltman HW (1956). Progressive fluctuating muscular rigidity and spasm ("stiff-man" syndrome); report of a case and some observations in 13 other cases. Proc Staff Meet Mayo Clin 31:421-427.

Morest DK (1968). The growth of synaptic endings in the mammalian brain: a study of the calyces of the trapezoid body. Z Anat Entwicklungsgesch 127:201-220.

Moscato EH, Peng X, Jain A, Parsons TD, Dalmau J, Balice-Gordon RJ (2014). Acute mechanisms underlying antibody effects in anti-N-methyl-D-aspartate receptor encephalitis. Ann Neurol 76:108-119.

Mulhardt C, Fischer M, Gass P, Simon-Chazottes D, Guenet JL, Kuhse J, Betz H, Becker CM (1994). The spastic mouse: aberrant splicing of glycine receptor beta subunit mRNA caused by intronic insertion of L1 element. Neuron 13:1003-1015.

Nabekura J, Katsurabayashi S, Kakazu Y, Shibata S, Matsubara A, Jinno S, Mizoguchi Y, Sasaki A, Ishibashi H (2004). Developmental switch from GABA to glycine release in single central synaptic terminals. Nat Neurosci 7:17-23.

Nemecz A, Prevost MS, Menny A, Corringer PJ (2016). Emerging molecular mechanisms of signal transduction in pentameric ligand-gated ion channels. Neuron 90:452-470.

Nikolic Z, Laube B, Weber RG, Lichter P, Kioschis P, Poustka A, Mulhardt C, Becker CM (1998). The human glycine receptor subunit alpha3. Glra3 gene structure, chromosomal localization, and functional characterization of alternative transcripts. J Biol Chem 273:19708-19714.

Nydegger UE, Sturzenegger T (2001). Treatment of autoimmune disease: synergy between plasma exchange and intravenous immunoglobulins. Ther Apher 5:186-192.

Oertel J, Villmann C, Kettenmann H, Kirchhoff F, Becker CM (2007). A novel glycine receptor beta subunit splice variant predicts an unorthodox transmembrane topology. Assembly into heteromeric receptor complexes. J Biol Chem 282:2798-2807.

Ogino K, Hirata H (2016). Defects of the glycinergic synapse in zebrafish. Front Mol Neurosci 9:50.

Olsen AL, Lai Y, Dalmau J, Scherer SS, Lancaster E (2015). Caspr2 autoantibodies target multiple epitopes. Neurol Neuroimmunol Neuroinflamm 2:e127.

Pagano MB, Murinson BB, Tobian AA, King KE (2014). Efficacy of therapeutic plasma exchange for treatment of stiff-person syndrome. Transfusion 54:1851-1856.

Pan H et al. (2019). Uncoupling the widespread occurrence of anti-NMDAR1 autoantibodies from neuropsychiatric disease in a novel autoimmune model. Mol Psychiatry 24:1489-1501.

Paoletti P (2011). Molecular basis of NMDA receptor functional diversity. Eur J Neurosci 33:1351-1365.

Papke D, Grosman C (2014). The role of intracellular linkers in gating and desensitization of human pentameric ligand-gated ion channels. J Neurosci 34:7238-7252.

Patrizio A, Renner M, Pizzarelli R, Triller A, Specht CG (2017). Alpha subunit-dependent glycine receptor clustering and regulation of synaptic receptor numbers. Sci Rep 7:10899.

PDBe-KB Consortium (2020). PDBe-KB: a community-driven resource for structural and functional annotations. Nucleic Acids Research, Database Issue. In.

Petit-Pedrol M, Sell J, Planaguma J, Mannara F, Radosevic M, Haselmann H, Ceanga M, Sabater L, Spatola M, Soto D, Gasull X, Dalmau J, Geis C (2018). LGI1 antibodies alter Kv1.1 and AMPA receptors changing synaptic excitability, plasticity and memory. Brain 141:3144-3159.

Pineda AA (1999). Selective therapeutic extraction of plasma constituents, revisited. Transfusion 39:671-673.

Planaguma J, Leypoldt F, Mannara F, Gutierrez-Cuesta J, Martin-Garcia E, Aguilar E, Titulaer MJ, Petit-Pedrol M, Jain A, Balice-Gordon R, Lakadamyali M, Graus F, Maldonado R, Dalmau J (2015). Human N-methyl D-aspartate receptor antibodies alter memory and behaviour in mice. Brain 138:94-109.

Planaguma J, Haselmann H, Mannara F, Petit-Pedrol M, Grunewald B, Aguilar E, Ropke L, Martin-Garcia E, Titulaer MJ, Jercog P, Graus F, Maldonado R, Geis C, Dalmau J (2016). Ephrin-B2 prevents N-methyl-D-aspartate receptor antibody effects on memory and neuroplasticity. Ann Neurol 80:388-400.

Plappert CF, Pilz PK, Becker K, Becker CM, Schnitzler HU (2001). Increased sensitization of acoustic startle response in spasmodic mice with a mutation of the glycine receptor alpha1-subunit gene. Behav Brain Res 121:57-67.

Pult F, Fallah G, Braam U, Detro-Dassen S, Niculescu C, Laube B, Schmalzing G (2011). Robust post-translocational N-glycosylation at the extreme C-terminus of membrane and secreted proteins in Xenopus laevis oocytes and HEK293 cells. Glycobiology 21:1147-1160.

Raju R, Foote J, Banga JP, Hall TR, Padoa CJ, Dalakas MC, Ortqvist E, Hampe CS (2005). Analysis of GAD65 autoantibodies in Stiff-Person syndrome patients. J Immunol 175:7755-7762.

Raju R, Rakocevic G, Chen Z, Hoehn G, Semino-Mora C, Shi W, Olsen R, Dalakas MC (2006). Autoimmunity to GABAA-receptor-associated protein in stiff-person syndrome. Brain 129:3270-3276.

Raltschev C, Hetsch F, Winkelmann A, Meier JC, Semtner M (2016). Electrophysiological signature of homomeric and heteromeric glycine receptor channels. J Biol Chem 291:18030-18040.

Reuss S (2000). Introduction to the superior olivary complex. Microsc Res Tech 51:303-306.

Rineer S, Fretwell T (2017). Evaluation of treatment outcomes in patients with stiff person syndrome with rituximab vs. standard of care. Cureus 9:e1387.

Ryan SG, Buckwalter MS, Lynch JW, Handford CA, Segura L, Shiang R, Wasmuth JJ, Camper SA, Schofield P, O'Connell P (1994). A missense mutation in the gene encoding the alpha 1 subunit of the inhibitory glycine receptor in the spasmodic mouse. Nat Genet 7:131-135.

Sachse K, Rahman KS, Schnee C, Muller E, Peisker M, Schumacher T, Schubert E, Ruettger A, Kaltenboeck B, Ehricht R (2018). A novel synthetic peptide microarray assay detects Chlamydia species-specific antibodies in animal and human sera. Sci Rep 8:4701.

Samarut E, Chalopin D, Riche R, Allard M, Liao M, Drapeau P (2019). Individual knock out of glycine receptor alpha subunits identifies a specific requirement of glra1 for motor function in zebrafish. PLoS One 14:e0216159.

Saul B, Schmieden V, Kling C, Mulhardt C, Gass P, Kuhse J, Becker CM (1994). Point mutation of glycine receptor alpha 1 subunit in the spasmodic mouse affects agonist responses. FEBS Lett 350:71-76.

Saul B, Kuner T, Sobetzko D, Brune W, Hanefeld F, Meinck HM, Becker CM (1999). Novel GLRA1 missense mutation (P250T) in dominant hyperekplexia defines an intracellular determinant of glycine receptor channel gating. J Neurosci 19:869-877.

Schaefer N, Vogel N, Villmann C (2012). Glycine receptor mutants of the mouse: what are possible routes of inhibitory compensation? Front Mol Neurosci 5:98.

Schaefer N, Roemer V, Janzen D, Villmann C (2018a). Impaired glycine receptor trafficking in neurological diseases. Front Mol Neurosci 11:291.

Schaefer N, Zheng F, van Brederode J, Berger A, Leacock S, Hirata H, Paige CJ, Harvey RJ, Alzheimer C, Villmann C (2018b). Functional consequences of the postnatal switch from neonatal to mutant adult glycine receptor alpha1 subunits in the shaky mouse model of startle disease. Front Mol Neurosci 11:167.

Schaefer N, Kluck CJ, Price KL, Meiselbach H, Vornberger N, Schwarzinger S, Hartmann S, Langlhofer G, Schulz S, Schlegel N, Brockmann K, Lynch B, Becker CM, Lummis SC, Villmann C (2015). Disturbed neuronal ER-Golgi sorting of unassembled glycine receptors suggests altered subcellular processing is a cause of human hyperekplexia. J Neurosci 35:422-437.

Schaefer N, Berger A, van Brederode J, Zheng F, Zhang Y, Leacock S, Littau L, Jablonka S, Malhotra S, Topf M, Winter F, Davydova D, Lynch JW, Paige CJ, Alzheimer C, Harvey RJ, Villmann C (2017). Disruption of a structurally important extracellular element in the glycine receptor leads to decreased synaptic integration and signaling resulting in severe startle disease. J Neurosci 37:7948-7961.

Schindelin J, Arganda-Carreras I, Frise E, Kaynig V, Longair M, Pietzsch T, Preibisch S, Rueden C, Saalfeld S, Schmid B, Tinevez JY, White DJ, Hartenstein V, Eliceiri K, Tomancak P, Cardona A (2012). Fiji: an open-source platform for biological-image analysis. Nat Methods 9:676-682.

Shupliakov O, Low P, Grabs D, Gad H, Chen H, David C, Takei K, De Camilli P, Brodin L (1997). Synaptic vesicle endocytosis impaired by disruption of dynamin-SH3 domain interactions. Science 276:259-263.

Siembab VC, Smith CA, Zagoraiou L, Berrocal MC, Mentis GZ, Alvarez FJ (2010). Target selection of proprioceptive and motor axon synapses on neonatal V1-derived Ia inhibitory interneurons and Renshaw cells. J Comp Neurol 518:4675-4701.

Simon J, Wakimoto H, Fujita N, Lalande M, Barnard EA (2004). Analysis of the set of GABA(A) receptor genes in the human genome. J Biol Chem 279:41422-41435.

Singer JH, Talley EM, Bayliss DA, Berger AJ (1998). Development of glycinergic synaptic transmission to rat brain stem motoneurons. J Neurophysiol 80:2608-2620.

SMART (Servier Medical Art) licensed under a Creative Common Attribution 3.0 Unported License. http://smart.sevier.com. In.

Smith PH, Joris PX, Carney LH, Yin TC (1991). Projections of physiologically characterized globular bushy cell axons from the cochlear nucleus of the cat. J Comp Neurol 304:387-407.

Sobolevsky AI, Rosconi MP, Gouaux E (2009). X-ray structure, symmetry and mechanism of an AMPA-subtype glutamate receptor. Nature 462:745-756.

Solimena M, De Camilli P (1991). Autoimmunity to glutamic acid decarboxylase (GAD) in Stiff-Man syndrome and insulin-dependent diabetes mellitus. Trends Neurosci 14:452-457.

Sommer C, Weishaupt A, Brinkhoff J, Biko L, Wessig C, Gold R, Toyka KV (2005). Paraneoplastic stiff-person syndrome: passive transfer to rats by means of IgG antibodies to amphiphysin. Lancet 365:1406-1411.

Stengel H, Vural A, Brunder AM, Heinius A, Appeltshauser L, Fiebig B, Giese F, Dresel C, Papagianni A, Birklein F, Weis J, Huchtemann T, Schmidt C, Kortvelyessy P, Villmann C, Meinl E, Sommer C, Leypoldt F, Doppler K (2019). Anti-pan-neurofascin IgG3 as a marker of fulminant autoimmune neuropathy. Neurol Neuroimmunol Neuroinflamm 6.

Tolbert LP, Morest DK, Yurgelun-Todd DA (1982). The neuronal architecture of the anteroventral cochlear nucleus of the cat in the region of the cochlear nerve root: horseradish peroxidase labelling of identified cell types. Neuroscience 7:3031-3052.

Tollin DJ (2003). The lateral superior olive: a functional role in sound source localization. Neuroscientist 9:127-143.

Toyka KV, Brachman DB, Pestronk A, Kao I (1975). Myasthenia gravis: passive transfer from man to mouse. Science 190:397-399.

Toyka KV, Lowenadler B, Heininger K, Besinger UA, Birnberger KL, Fateh-Moghadam A, Heilbronn E (1980). Passively transferred myasthenia gravis: protection of mouse endplates by Fab fragments from human myasthenic IgG. J Neurol Neurosurg Psychiatry 43:836-842.

Tuzun E, Zhou L, Baehring JM, Bannykh S, Rosenfeld MR, Dalmau J (2009). Evidence for antibody-mediated pathogenesis in anti-NMDAR encephalitis associated with ovarian teratoma. Acta Neuropathol 118:737-743.

Tzartos SJ, Cung MT, Demange P, Loutrari H, Mamalaki A, Marraud M, Papadouli I, Sakarellos C, Tsikaris V (1991a). The main immunogenic region (MIR) of the nicotinic acetylcholine receptor and the anti-MIR antibodies. Mol Neurobiol 5:1-29.

Tzartos SJ, Barkas T, Cung MT, Kordossi A, Loutrari H, Marraud M, Papadouli I, Sakarellos C, Sophianos D, Tsikaris V (1991b). The main immunogenic region of the acetylcholine receptor. Structure and role in myasthenia gravis. Autoimmunity 8:259-270.

Vicari AM, Folli F, Pozza G, Comi GC, Comola M, Canal N, Besana C, Borri A, Tresoldi M, Solimena M, DeCamilli P, et al. (1989). Plasmapheresis in the treatment of stiff-man syndrome. N Engl J Med 320:1499.

Villmann C, Oertel J, Melzer N, Becker CM (2009a). Recessive hyperekplexia mutations of the glycine receptor alpha1 subunit affect cell surface integration and stability. J Neurochem 111:837-847.

Villmann C, Oertel J, Ma-Hogemeier ZL, Hollmann M, Sprengel R, Becker K, Breitinger HG, Becker CM (2009b). Functional complementation of Glra1(spd-ot), a glycine receptor subunit mutant, by independently expressed C-terminal domains. J Neurosci 29:2440-2452.

Vincent A, Waters P, Leite MI, Jacobson L, Koneczny I, Cossins J, Beeson D (2012). Antibodies identified by cell-based assays in myasthenia gravis and associated diseases. Ann N Y Acad Sci 1274:92-98.

Wang CH, Hernandez CC, Wu J, Zhou N, Hsu HY, Shen ML, Wang YC, Macdonald RL, Wu DC (2018). A missense mutation A384P associated with human hyperekplexia reveals a desensitization site of glycine receptors. J Neurosci 38:2818-2831.

Wardemann H, Yurasov S, Schaefer A, Young JW, Meffre E, Nussenzweig MC (2003). Predominant autoantibody production by early human B cell precursors. Science 301:1374-1377.

Warr WB (1972). Fiber degeneration following lesions in the multipolar and globular cell areas in the ventral cochlear nucleus of the cat. Brain Res 40:247-270.

Weltzien F, Puller C, O'Sullivan GA, Paarmann I, Betz H (2012). Distribution of the glycine receptor beta-subunit in the mouse CNS as revealed by a novel monoclonal antibody. J Comp Neurol 520:3962-3981.

Wenke NK, Kreye J, Andrzejak E, van Casteren A, Leubner J, Murgueitio MS, Reincke SM, Secker C, Schmidl L, Geis C, Ackermann F, Nikolaus M, Garner CC, Wardemann H, Wolber G, Pruss H (2019). N-methyl-D-aspartate receptor dysfunction by unmutated human antibodies against the NR1 subunit. Ann Neurol 85:771-776.

Werner C, Pauli M, Doose S, Weishaupt A, Haselmann H, Grunewald B, Sauer M, Heckmann M, Toyka KV, Asan E, Sommer C, Geis C (2016). Human autoantibodies to amphiphysin induce defective presynaptic vesicle dynamics and composition. Brain 139:365-379.

Wessig C, Klein R, Schneider MF, Toyka KV, Naumann M, Sommer C (2003). Neuropathology and binding studies in anti-amphiphysin-associated stiff-person syndrome. Neurology 61:195-198.

Wu WP, Xu XJ, Hao JX (2004). Chronic lumbar catheterization of the spinal subarachnoid space in mice. J Neurosci Methods 133:65-69.

Yang Z, Taran E, Webb TI, Lynch JW (2012). Stoichiometry and subunit arrangement of alpha1beta glycine receptors as determined by atomic force microscopy. Biochemistry 51:5229-5231.

Young TL, Cepko CL (2004). A role for ligand-gated ion channels in rod photoreceptor development. Neuron 41:867-879.

Yu WM, Goodrich LV (2014). Morphological and physiological development of auditory synapses. Hear Res 311:3-16.

Yuan H, Hansen KB, Vance KM, Ogden KK, Traynelis SF (2009). Control of NMDA receptor function by the NR2 subunit amino-terminal domain. J Neurosci 29:12045-12058.

Zeilhofer HU (2005). The glycinergic control of spinal pain processing. Cell Mol Life Sci 62:2027-2035.

Zhang Y, Bode A, Nguyen B, Keramidas A, Lynch JW (2016). Investigating the mechanism by which gain-of-function mutations to the alpha1 glycine receptor cause hyperekplexia. J Biol Chem 291:15332-15341.

7. Supplementary material

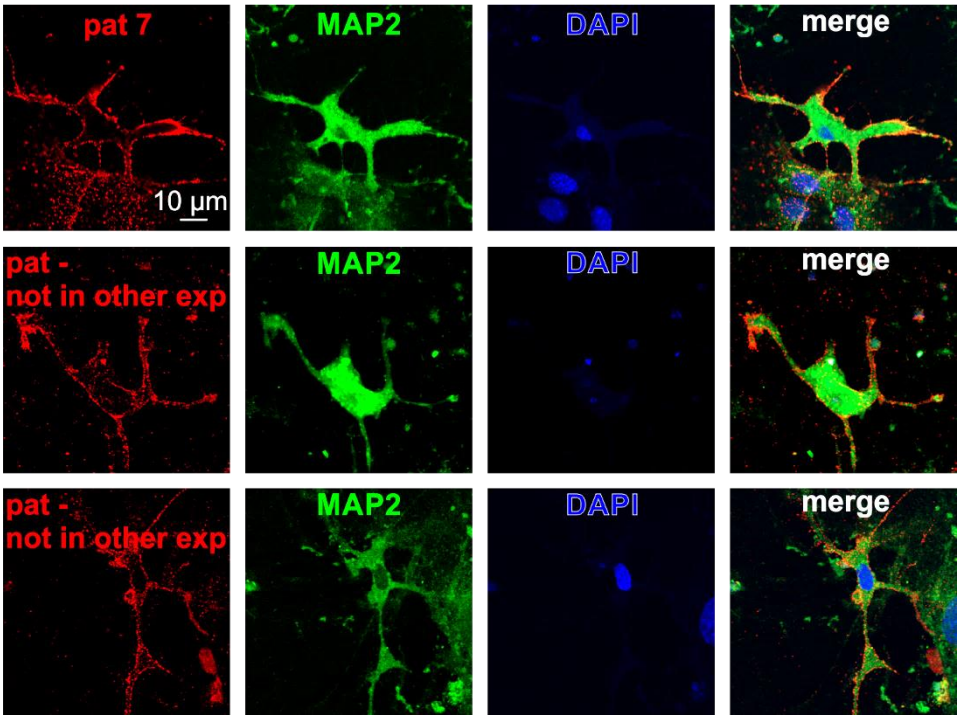

Supplementary fig. 1: Patient autoantibodies bind to cultured motoneurons. Cultivated motoneurons at an age of 21 days *in vitro* were stained with patient autoantibodies (red) and neuronal marker MAP2 (green). DAPI is shown in blue. In middle and lower raw, two patient sera are shown that are not included in other experiments of this study. exp = experiment; pat = patient.

Supplementary tab. 1: Statistical analysis of zebrafish with injections of healthy control serum, GAD positive serum and patient 1 serum.

		n	hc	GAD⁺	pat 1
NORMAL	hc	9		n.s.	n.s.
	GAD⁺	7	n.s.		n.s.
	pat 1	8	n.s.	n.s.	
		n	Hc	GAD⁺	pat 1
MILD	hc	9		n.s.	n.s.
	GAD⁺	7	n.s.		n.s.
	pat 1	8	n.s.	n.s.	
		n	hc	GAD⁺	pat 1
SEVERE	hc	9		n.s.	n.s.
	GAD⁺	7	n.s.		n.s.
	pat 1	8	n.s.	n.s.	

		n	hc	GAD⁺	pat 1
NORMAL	hc	9		0.789	0.398
	GAD⁺	7	0.789		0.273
	pat 1	8	0.398	0.273	
		n	hc	GAD⁺	pat 1
MILD	hc	9		n.d.	0.186
	GAD⁺	7	n.d.		0.221
	pat 1	8	0.186	0.221	
		n	hc	GAD⁺	pat 1
SEVERE	hc	9		0.355	0.643
	GAD⁺	7	0.355		0.221
	pat 1	8	0.643	0.221	

$\chi 2$ *test*, n.s. = not significant, n.d. = could not be determined (due to division by zero in calculation), *p<0.05; **p<0.01, ***p<0.001, colors refer to phenotype. GAD = glutamate decarboxylase; hc = healthy control; pat = patient.

Supplementary tab. 2: Statistical analysis of zebrafish with skin lesions and incubation with different dilutions of patient 1 serum compared to ACSF, healthy control serum and GAD positive serum.

		n	ACSF	hc	GAD⁺	pat 1 1:10	pat 1 1:50	pat 1 1:100	pat 1 IgG 10 mg/ml	pat 1 IgG 1 mg/ml	pat 1 IgG 0.1 mg/ml
NORMAL	ASCF	9		n.s.	**	*	**	*	n.s.	n.s.	**
	hc	13	n.s.		**	n.s.	*	n.s.	n.s.	n.s.	*
	GAD⁺	9	**	**		n.s.	n.s.	n.s.	n.s.	n.s.	n.s.
	pat 1, 1:10	25	*	n.s.	n.s.		n.s.	n.s.	n.s.	n.s.	n.s.
	pat 1, 1:50	21	**	*	n.s.	n.s.		n.s.	n.s.	n.s.	n.s.
	pat 1, 1:100	33	*	n.s.	n.s.	n.s.	n.s.		n.s.	n.s.	n.s.
	pat 1 IgG, 10 mg/ml	6	n.s.	n.s.	n.s.	n.s.	n.s.	n.s.		n.s.	n.s.
	pat 1 IgG, 1 mg/ml	3	n.s.	n.s.	n.s.	n.s.	n.s.	n.s.	n.s.		n.s.
	pat 1 IgG, 0.1 mg/ml	12	**	*	n.s.	n.s.	n.s.	n.s.	n.s.	n.s.	
MILD		n	ACSF	hc	GAD⁺	pat 1 1:10	pat 1 1:50	pat 1 1:100	pat 1 IgG 10 mg/ml	pat 1 IgG 1 mg/ml	pat 1 IgG 0.1 mg/ml
	ASCF	9		n.s.	**	*	*	n.s.	n.s.	n.s.	n.s.
	hc	13	n.s.		*	n.s.	n.s.	n.s.	n.s.	n.s.	n.s.
	GAD⁺	9	**	*		n.s.	n.s.	*	n.s.	n.s.	*
	pat 1, 1:10	25	*	n.s.	n.s.		n.s.	n.s.	n.s.	n.s.	n.s.
	pat 1, 1:50	21	*	n.s.	n.s.	n.s.		n.s.	n.s.	n.s.	n.s.
	pat 1, 1:100	33	n.s.	n.s.	*	n.s.	n.s.		n.s.	n.s.	n.s.
	pat 1 IgG, 10 mg/ml	6	n.s.	n.s.	n.s.	n.s.	n.s.	n.s.		n.s.	n.s.
	pat 1 IgG, 1 mg/ml	3	n.s.	n.s.	n.s.	n.s.	n.s.	n.s.	n.s.		n.s.
	pat 1 IgG, 0.1 mg/ml	16	n.s.	n.s.	*	n.s.	n.s.	n.s.	n.s.	n.s.	
SEVERE		n	ACSF	hc	GAD⁺	pat 1 1:10	pat 1 1:50	pat 1 1:100	pat 1 IgG 10 mg/ml	pat 1 IgG 1 mg/ml	pat 1 IgG 0.1 mg/ml
	ASCF	9		n.s.	n.s.	n.s.	n.s.	n.s.	n.s.	n.s.	n.s.
	hc	13	n.s.		n.s.	n.s.	n.s.	n.s.	*	*	*
	GAD⁺	9	n.s.	n.s.		n.s.	n.s.	n.s.	n.s.	n.s.	n.s.
	pat 1, 1:10	25	n.s.	n.s.	n.s.		n.s.	n.s.	n.s.	n.s.	*
	pat 1, 1:50	21	n.s.	n.s.	n.s.	n.s.		n.s.	n.s.	n.s.	n.s.
	pat 1, 1:100	33	n.s.	n.s.	n.s.	n.s.	n.s.		n.s.	n.s.	n.s.
	pat 1 IgG, 10 mg/ml	6	n.s.	*	n.s.	n.s.	n.s.	n.s.		n.s.	n.s.
	pat 1 IgG, 1 mg/ml	3	n.s.	*	n.s.	n.s.	n.s.	n.s.	n.s.		n.s.
	pat 1 IgG, 0.1 mg/ml	15	n.s.	*	n.s.	*	n.s.	n.s.	n.s.	n.s.	

		n	ACSF	hc	GAD⁺	pat 1 1:10	pat 1 1:50	pat 1 1:100	pat 1 IgG 10 mg/ml	pat 1 IgG 1 mg/ml	pat 1 IgG 0.1 mg/ml
NORMAL	ASCF	9		0.567	0.003	0.024	0.002	0.017	0.140	0.273	0.002
	hc	13	0.567		0.009	0.091	0.011	0.073	0.266	0.412	0.013
	GAD⁺	9	0.003	0.009		0.072	0.190	0.070	0.083	0.083	0.113
	pat 1, 1:10	25	0.024	0.091	0.072		0.281	0.982	0.922	0.942	0.563
	pat 1, 1:50	21	0.002	0.011	0.190	0.281		0.254	0.513	0.612	0.506
	pat 1, 1:100	33	0.017	0.073	0.070	0.982	0.254		0.909	0.933	0.516
	pat 1 IgG, 10 mg/ml	6	0.140	0.266	0.083	0.922	0.513	0.909		1.000	0.816
	pat 1 IgG, 1 mg/ml	3	0.273	0.412	0.083	0.942	0.612	0.933	1.000		0.864
	pat 1 IgG, 0.1 mg/ml	12	0.002	0.013	0.113	0.563	0.506	0.516	0.816	0.864	
MILD		n	ACSF	hc	GAD⁺	pat 1 1:10	pat 1 1:50	pat 1 1:100	pat 1 IgG 10 mg/ml	pat 1 IgG 1 mg/ml	pat 1 IgG 0.1 mg/ml
	ASCF	9		0.150	0.003	0.025	0.030	0.070	0.083	0.083	0.067
	hc	13	0.150		0.016	0.150	0.196	0.477	0.685	0.749	0.443
	GAD⁺	9	0.003	0.016		0.169	0.143	0.017	0.140	0.273	0.013
	pat 1, 1:10	25	0.025	0.150	0.169		0.868	0.269	0.488	0.612	0.261
	pat 1, 1:50	21	0.030	0.196	0.143	0.868		0.379	0.553	0.663	0.380
	pat 1, 1:100	33	0.070	0.477	0.017	0.269	0.379		0.909	0.933	0.952
	pat 1 IgG, 10 mg/ml	6	0.083	0.685	0.140	0.488	0.553	0.909		1.000	0.883
	pat 1 IgG, 1 mg/ml	3	0.083	0.749	0.273	0.612	0.663	0.933	1.000		0.915
	pat 1 IgG, 0.1 mg/ml	16	0.067	0.443	0.013	0.261	0.380	0.952	0.883	0.915	
SEVERE		n	ACSF	hc	GAD⁺	pat 1 1:10	pat 1 1:50	pat 1 1:100	pat 1 IgG 10 mg/ml	pat 1 IgG 1 mg/ml	pat 1 IgG 0.1 mg/ml
	ASCF	9		n.d.	n.d.	0.396	0.109	0.117	0.083	0.083	0.076
	hc	13	n.d.		n.d.	0.308	0.054	0.060	0.037	0.037	0.033
	GAD⁺	9	n.d.	n.d.		0.396	0.109	0.117	0.083	0.083	0.076
	pat 1, 1:10	25	0.396	0.308	0.396		0.096	0.095	0.121	0.205	0.033
	pat 1, 1:50	21	0.109	0.054	0.109	0.096		0.930	0.850	0.886	0.679
	pat 1, 1:100	33	0.117	0.060	0.117	0.095	0.930		0.797	0.849	0.558
	pat 1 IgG, 10 mg/ml	6	0.083	0.037	0.083	0.121	0.850	0.797		1.000	0.952
	pat 1 IgG, 1 mg/ml	3	0.083	0.037	0.083	0.205	0.886	0.849	1.000		0.965
	pat 1 IgG, 0.1 mg/ml	15	0.076	0.033	0.076	0.033	0.679	0.558	0.952	0.965	

$\chi 2$ *test*, n.s. = not significant, n.d. = could not be determined (due to division by zero in calculation), *p<0.05; **p<0.01, ***p<0.001, colors refer to phenotype. ACSF = artificial cerebrospinal fluid; GAD = glutamate decarboxylase; hc = healthy control; pat = patient.

Supplementary tab. 3: Statistical analysis of zebrafish with skin lesions and incubation with patient 1-5 serum and patient 1 and 2 IgG compared to ACSF, healthy control serum and GAD positive serum.

		n	ACSF	hc	GAD⁺	pat1	pat1 IgG	pat2	pat2 IgG	pat4	pat5
NORMAL	ASCF	49		n.s.	***	***	*	*	n.s.	n.s.	*
	hc	42	n.s.		***	**	n.s.	n.s.	n.s.	n.s.	n.s.
	GAD⁺	34	***	***		n.s.	*	n.s.	*	n.s.	n.s.
	pat 1	29	***	**	n.s.		n.s.	n.s.	*	n.s.	n.s.
	pat1 IgG	43	*	n.s.	*	n.s.		n.s.	n.s.	n.s.	n.s.
	pat 2	32	*	n.s.	n.s.	n.s.	n.s.		n.s.	n.s.	n.s.
	pat2 IgG	36	n.s.	n.s.	*	*	n.s.	n.s.		n.s.	n.s.
	pat 4	29	n.s.	n.s.	n.s.	n.s.	n.s.	n.s.	n.s.		n.s.
	pat 5	45	*	n.s.	n.s.	n.s.	n.s.	n.s.	n.s.	n.s.	
		n	ACSF	hc	GAD⁺	pat1	pat1 IgG	pat2	pat2 IgG	pat4	pat5
MILD	ASCF	49		n.s.	n.s.	n.s.	n.s.	n.s.	n.s.	n.s.	n.s.
	hc	42	n.s.		n.s.	*	n.s.	n.s.	n.s.	n.s.	n.s.
	GAD⁺	34	n.s.	n.s.		**	n.s.	n.s.	n.s.	n.s.	n.s.
	pat 1	29	n.s.	*	**		*	n.s.	n.s.	n.s.	**
	pat1 IgG	43	n.s.	n.s.	n.s.	*		*	n.s.	n.s.	n.s.
	pat 2	32	n.s.	n.s.	n.s.	n.s.	*		*	*	n.s.
	pat2 IgG	36	n.s.	n.s.	n.s.	n.s.	n.s.	*		n.s.	n.s.
	pat 4	29	n.s.	n.s.	n.s.	n.s.	n.s.	*	n.s.		n.s.
	pat 5	45	n.s.	n.s.	n.s.	**	n.s.	n.s.	n.s.	n.s.	
		n	ACSF	hc	GAD⁺	pat1	pat1 IgG	pat2	pat2 IgG	pat4	pat5
SEVERE	ASCF	49		n.s.	***	***	**	***	**	**	*
	hc	42	n.s.		***	***	*	**	**	**	n.s.
	GAD⁺	34	***	***		*	***	n.s.	n.s.	n.s.	n.s.
	pat 1	29	***	***	*		*	n.s.	*	***	***
	pat1 IgG	43	**	*	***	*		n.s.	n.s.	n.s.	n.s.
	pat 2	32	***	**	n.s.	n.s.	n.s.		n.s.	n.s.	*
	pat2 IgG	36	**	**	n.s.	*	n.s.	n.s.		n.s.	n.s.
	pat 4	29	**	**	n.s.	***	n.s.	n.s.	n.s.		n.s.
	pat 5	45	n.s.	n.s.	n.s.	***	n.s.	*	n.s.	n.s.	

		n	ACSF	hc	GAD⁺	pat1	pat1 IgG	pat2	pat2 IgG	pat4	pat5
NORMAL	ASCF	49		0.9348	0.0003	0.0006	0.0133	0.0277	0.1269	0.0547	0.0149
	hc	42	0.9348		0.00002	0.0034	0.0772	0.1125	0.3833	0.1830	0.0874
	GAD⁺	34	0.0003	0.00002		0.8662	0.0337	0.1344	0.0253	0.0933	0.1042
	pat 1	29	0.0006	0.0034	0.8662		0.1093	0.1179	0.0252	0.0833	0.0939
	pat1 IgG	43	0.0133	0.0772	0.0337	0.1093		0.3067	0.3967	0.8784	0.9174
	pat 2	32	0.0277	0.1125	0.1344	0.1179	0.3067		0.0982	0.3057	0.9359
	pat2 IgG	36	0.1269	0.3833	0.0253	0.0252	0.3967	0.0982		0.3967	0.4385
	pat 4	29	0.0547	0.1830	0.0933	0.0833	0.8784	0.3057	0.3967		0.8687
	pat 5	45	0.0149	0.0874	0.1042	0.0939	0.9174	0.9359	0.4385	0.8687	
MILD		n	ACSF	Hc	GAD⁺	pat1	pat1 IgG	pat2	pat2 IgG	pat4	pat5
	ASCF	49		0.9767	0.1618	0.0717	0.5865	0.8406	0.6304	0.9740	0.2089
	hc	42	0.9767		0.5448	0.0226	0.8694	0.4192	0.2745	0.5674	0.6200
	GAD⁺	34	0.1618	0.5448		0.0053	0.3945	0.1570	0.0862	0.2428	0.8324
	pat 1	29	0.0717	0.0226	0.0053		0.0295	0.1179	0.1716	0.0832	0.0073
	pat1 IgG	43	0.5865	0.8694	0.3945	0.0295		0.0193	0.3366	0.7819	0.4894
	pat 2	32	0.8406	0.4192	0.1570	0.1179	0.0193		0.0263	0.0221	0.1246
	pat2 IgG	36	0.6304	0.2745	0.0862	0.1716	0.3366	0.0263		0.3366	0.1113
	pat 4	29	0.9740	0.5674	0.2428	0.0832	0.7819	0.0221	0.3366		0.3025
	pat 5	45	0.2089	0.6200	0.8324	0.0073	0.4894	0.1246	0.1113	0.3025	
SEVERE		n	ACSF	Hc	GAD⁺	pat1	pat1 IgG	pat2	pat2 IgG	pat4	pat5
	ASCF	49		0.8501	$3.65 \times E^{-6}$	$6.27 \times E^{-08}$	0.0018	0.0003	0.0016	0.0013	0.0214
	hc	42	0.8501		$2.84 \times E^{-08}$	$7.76 \times E^{-06}$	0.0101	0.0024	0.0090	0.0077	0.0673
	GAD⁺	34	$3.65 \times E^{-6}$	$2.84 \times E^{-08}$		0.0315	0.0008	0.7262	0.8841	0.9844	0.2708
	pat 1	29	$6.27 \times E^{-08}$	$7.76 \times E^{-06}$	0.0315		0.0109	0.0749	0.0199	$1.33 \times E^{-12}$	0.0006
	pat1 IgG	43	0.0018	0.0101	0.0008	0.0109		0.5302	0.9272	0.8934	0.3039
	pat 2	32	0.0003	0.0024	0.7262	0.0749	0.5302		0.4474	0.3826	0.0271
	pat2 IgG	36	0.0016	0.0090	0.8841	0.0199	0.9272	0.4474		0.9272	0.2091
	pat 4	29	0.0013	0.0077	0.9844	$1.33 \times E^{-12}$	0.8934	0.3826	0.9272		0.2989
	pat 5	45	0.0214	0.0673	0.2708	0.0006	0.3039	0.0271	0.2091	0.2989	

$\chi 2$ *test*, n.s. = not significant, *p<0.05; **p<0.01, ***p<0.001, colors refer to phenotype. ACSF = artificial cerebrospinal fluid; GAD = glutamate decarboxylase; hc = healthy control; pat = patient.

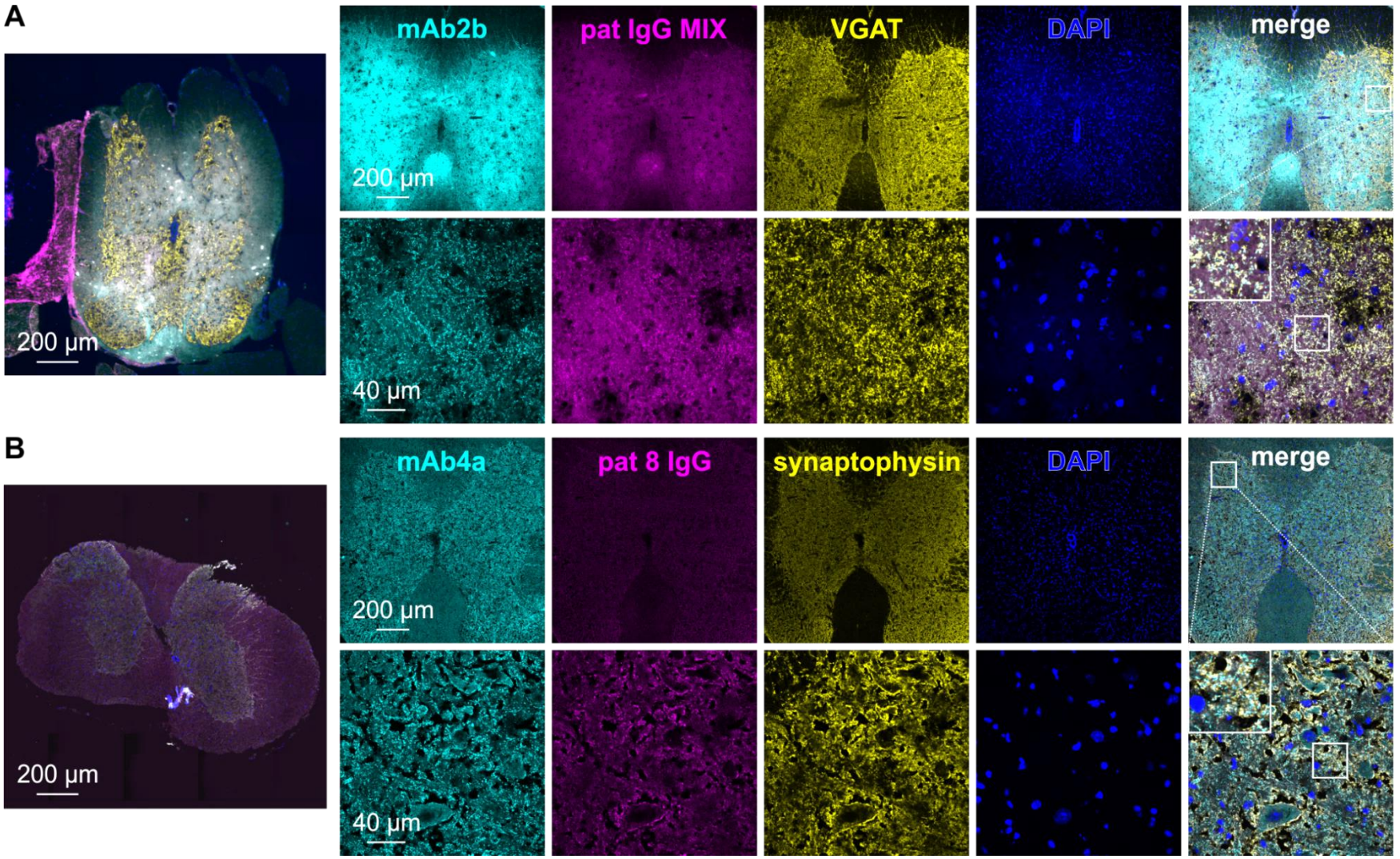

Supplementary fig. 2: Spinal cord immunohistochemical stainings of mice. (**A**) Immunohistochemical stainings of mouse with transplanted osmotic pump treated with patient MIX IgG (magenta) co-stained with mAb2b (cyan), VGAT (yellow) and DAPI (blue). (**B**) MAb4a (cyan), synaptophysin (yellow) and DAPI staining (blue) of mouse treated with patient 8 IgG that was passively transferred into the animal without an osmotic pump. pat = patient.

8. Index of abbreviations

ACSF	artificial cerebrospinal fluid
AMPAR	α-amino-3-hydroxy-5-methyl-4-isoxazolepropionic acid receptor
BSA	bovine serum albumin
c	caudal
Caspr2	contactin associated protein-like 2
ch	chimera
CN	cochlear nucleus
CSF	cerebrospinal fluid
d	dorsal
dc	disease control
desens	fraction of desensitizing currents
div	day(s) *in vitro*
DMSO	dimethyl sulfoxide
DNA	desoxyribonucleic acid
dNTP	desoxyribonucleotide triphosphate
dr	*danio rerio*
DTT	dithiothreitol
ECD	extracellular domain
EGFP	enhanced green fluorescent protein
ELISA	enzyme-linked immunosorbent assay
EndoH	endoglycosidase H
EPM	Elevated Plus Maze
ER	endoplasmic reticulum
exp	experiment
FBS	fetal bovine serum
GABA	gamma-aminobutyric acid
GAD	glutamate decarboxylase
GAD65	GAD isoform with a molecular weight of 65 kDa
GAPDH	glyceraldehyde-3-phosphate dehydrogenase
geph	gephyrin
GFP	green fluorescent protein
GlyR	glycine receptor
GlyT	glycine transporter
HBS	HEPES buffered saline
HBSS	Hank’s balanced salt solution

hc	healthy control
HEK	human embyonic kidney cell
hpf	hours post-fertilization
HRP	horseradish peroxidase
hs	*homo sapiens*
hypogl	hypoglossal nucleus
IC	inferior colliculus (in stainings of brain slices; stated in figure)
IC	intracellular (in biotinylation assay; stated in figure)
LSO	lateral superior olive
MAP2	microtubule associated protein 2
MEM	Minimum essential medium
mIPSC	miniature inhibitory postsynaptic currents
mm	*mus musculus*
MNTB	medial nucleus of the trapezoid body
nAchR	nicotinic acetylcholine receptors
NB medium	Neurobasal medium
NGS	normal goat serum
NMDAR	N-methyl-D-aspartate receptor
OP	operation
PAA	polyacrylamide
pat	patient
PBS	phosphate buffered saline
PCR	polymerase chain reaction
Pen/Strep	penicillin/streptomycin
PERM	progressive encephalomyelitis with rigidity and myoclonus
PFA	paraformaldehyde
PNGaseF	peptide N-glycosidase F
pre Bö	pre Bötzinger complex
sat	saturating
SDS	sodium dodecyl sulfate
SEM	standard error of the mean
ser	serum
SF	surface
SOC	superior olivary complex
SPN	superior paraolivary nucleus
SPS	stiff-person syndrome
Sulfo-NHS-LC-Biotin	sulfosuccinimidyl-6-[biotin-amido]hexanoate

TBS	Tris buffered saline
TM	transmembrane domain
ut	untransfected or untreated (as stated in the figures)
VGAT	vesicular GABA transporter
VIAAT	vesicular inhibitory amino acid transporter
WC	whole cell
wt	wildtype

9. Curriculum vitae

10. Affidavit

I hereby confirm that my thesis entitled “Stiff-person syndrome - Pathophysiological mechanisms of glycine receptor autoantibodies” is the result of my own work. I did not receive any help or support from commercial consultants. All sources and / or materials applied are listed and specified in the thesis.

Furthermore, I confirm that this thesis has not yet been submitted as part of another examination process neither in identical nor in similar form.

Place, Date Signature

11. Eidesstattliche Erklärung

Hiermit erkläre ich an Eides statt, die Dissertation „Stiff-Person Syndrom - Pathophysiologische Mechanismen von Glyzinrezeptor Autoantikörpern“ eigenständig, d.h. insbesondere selbstständig und ohne Hilfe eines kommerziellen Promotionsberaters, angefertigt und keine anderen als die von mir angegebenen Quellen und Hilfsmittel verwendet zu haben.

Ich erkläre außerdem, dass die Dissertation weder in gleicher noch in ähnlicher Form bereits in einem anderen Prüfungsverfahren vorgelegen hat.

Ort, Datum Unterschrift

12. Acknowledgements

Ich möchte mich ganz herzlich bei allen bedanken, die zum Gelingen meiner Dissertation beigetragen haben.

Zunächst bedanke ich mich in besonderem Maße bei Frau Prof. Dr. Carmen Villmann für das interessante Thema meiner Promotionsarbeit sowie für die wissenschaftlichen Anregungen, die während meiner Arbeit stets sehr hilfreich waren.

Ich danke ebenfalls Frau Prof. Dr. Claudia Sommer für die Zweitkorrektur meiner Dissertation. Der intensive Austausch während der Projektmeetings war eine große Bereicherung.

Bei Herrn Prof. Dr. Christian Geis bedanke ich mich dafür, dass er meine Arbeit als dritter Gutachter prüft. Außerdem möchte ich mich herzlich bedanken, dass mir die Möglichkeit geboten wurde, die *in vivo* Versuche in Jena durchzuführen. Die Unterstützung durch Herrn Prof. Christian Geis und seiner gesamten Arbeitsgruppe waren für meine Arbeit stets förderlich.

Außerdem gilt mein Dank Herrn Prof. Dr. Paul Pauli für die Übernahme des Vorsitzes des Promotionskomitees.

Ich danke Herrn Prof. Dr. Sendtner für Anregungen und Diskussionen während der Progress Reports.

Frau Dr. Christina Lillesaar hat mir die Möglichkeit geboten, die Zebrafisch-Experimente in der Abteilung für Physiologische Chemie des Biozentrums an der Universität in Würzburg durchzuführen. Vielen Dank dafür und für die wertvollen Ratschläge.

Herrn Dr. Vikram Kasaragod danke ich für die Erstellung des Strukturmodells meiner Mutante.

Ebenfalls bedanken möchte ich mich bei Christoph Kluck und Daniela Schneeberger für die Entwicklung des ECD Konstruktes, ohne das ich nicht diese aufschlussreichen Experimente hätte durchführen können.

Ein besonderer Dank gilt allen Mitarbeitern der AG Villmann, insbesondere Dr. Natascha Schäfer, Dieter Janzen, Dr. Alexandra Kitzenmaier, Nadine Vornberger, Christine Schmitt und

Dana Wegmann. Herzlichen Dank für eure Unterstützung und die äußerst angenehme Zusammenarbeit im Labor. Besonders danke ich Natascha für die Bereitstellung des von ihr perfektionierten Histo-Protokolls und für die Erstellung des Strukturmodells des Autoantikörper-Epitops.

Recht herzlich bedanke ich mich bei Regine Sendtner, Viktor Buterus, Franziska Wagner, Sebastian Rose und Susan Schellworth vom Team des Tierstalls in der Klinischen Neurobiologie in Würzburg für die gute und nette Zusammenarbeit.

Des Weiteren bedanke ich mich bei allen Mitarbeitern des Instituts für Klinische Neurobiologie für das angenehme Arbeitsklima und die freundliche Unterstützung.

Abschließend danke ich sehr herzlich meiner gesamten Familie für den emotionalen Rückhalt.